Analytical solutions for modeling soft soil consolidation by vertical drains

Rohan Walker
University of Wollongong

ANALYTICAL SOLUTIONS FOR MODELING SOFT SOIL CONSOLIDATION BY VERTICAL DRAINS

A thesis submitted in fulfillment of the

requirements for the award of the degree

Doctor of Philosophy

from

University of Wollongong, NSW Australia

by

Rohan Walker, B. Eng (Hons. I)

School of Civil, Mining and Environmental Engineering

2006

CERTIFICATION

I, Rohan Walker, declare that this thesis, submitted in fulfillment of the requirements for the award of Doctor of Philosophy, in the Department of Civil Engineering, University of Wollongong, is wholly my own work unless otherwise referenced or acknowledged. The document has not been submitted for qualifications at any other academic institution.

_____

Rohan Walker

2nd June 2006

ABSTRACT

Vertical drains increase the rate of soil consolidation by providing a short horizontal drainage path for pore water flow, and are used worldwide in many soft soil improvement projects. This thesis develops three new contributions to the solution of consolidation problems: (i) a more realistic representation of the smear zone where soil properties vary gradually with radial distance from the vertical drain; (ii) a nonlinear radial consolidation model incorporating void ratio dependant soil properties and non-Darcian flow; and (iii) a solution to multi-layered consolidation problems with vertical and horizontal drainage using the spectral method. Each model is verified against existing analytical solutions and laboratory experiments conducted at the University of Wollongong, NSW Australia. The nonlinear radial consolidation model and the spectral method are verified against two trial embankments involving surcharge and vacuum loading at the Second Bangkok International Airport, Thailand. The versatility of the spectral method model is further demonstrated by analysing ground subsidence associated with ground water pumping in the Saga Plain, Japan.

New expressions for the smear zone μ parameter, based on a linear and parabolic variation of soil properties in the radial direction, give a more realistic representation of the extent of smear and suggest that smear zones may overlap. Overlapping linear smear zones provide some explanation for the phenomena of a minimum drain spacing, below which no increase in the rate of consolidation is achieved. It appears this minimum influence radius is 0.6 times the size of the linear smear zone. The new smear zone parameters may be used with consolidation models (ii) and (iii), as mentioned above.

The analytical solution to nonlinear radial consolidation is valid for both Darcian and non-Darcian flow and can capture the behaviour of both overconsolidated and normally consolidated soils. For nonlinear material properties, consolidation may be faster or slower when compared to the cases with constant material properties. The difference depends on the compressibility/permeability ratios (C_c/C_k and C_r/C_k), the preconsolidation pressure and the stress increase. If $C_c/C_k < 1$ or $C_r/C_k < 1$ then the coefficient of consolidation increases as excess pore pressures dissipate and consolidation is faster.

The multi-layered consolidation model includes both vertical and radial drainage where permeability, compressibility and vertical drain parameters vary linearly with depth. The ability to include surcharge and vacuum loads that vary with depth and time allows for a large variety of consolidation problems to be analysed. The powerful model can also predict consolidation behaviour before and after vertical drains are installed and has potential for nonlinear consolidation analysis.

ACKNOWLEDGEMENTS

I would like to thank the following people for their help during my undergraduate and postgraduate studies at the University of Wollongong:

My thesis supervisor Prof. Buddhima Indraratna for his patience, enthusiasm, advice and constant source of ideas. Prof. Indraratna has always been available to answer my queries. His support in professional and personal matters has been invaluable.

Dr. Chamari Bamunawita, Dr. Cholachat Rujikiatkamjorn and Dr. Iyathurai Sathananthan. These three Doctors of Philosophy graduated during my postgraduate studies and provided excellent examples of quality research and friendly advice in the field of vertical drains. I would specifically like to thank them for use of their large-scale laboratory testing data.

Queensland Department of Main Roads (Australia), who through the Australian Research Council provided funds for my PhD scholarship. In particular I would like to thank Mr. Vasantha Wijeyakulasuriya who gave his advice on my research work.

The sponsor of my Undergraduate Foundation Cooperative Scholarship, ActewAGL (Canberra, Australia), without whose assistance I may never have come to the University of Wollongong.

The University Recreation and Aquatic Centre, and National Australia Bank for my University of Wollongong Sports Scholarship.

My track and field coach, Mr. Peter Lawler, whose selfless contribution to athletics in Australia, and my own personal development in the decathlon and 400m hurdles has been enormous.

And finally thank you to my family and friends for their humour and encouragement in times of stress. Their support, spoken or unspoken, has helped me negotiate the twists and turns, of my PhD research.

PUBLISHED WORK

The following publications are related to this PhD thesis:

Walker, R. and Indraratna, B. (2006). "Vertical drain consolidation with parabolic distribution of permeability in smear zone". *Journal of Geotechnical and Geoenvironmental Engineering, ASCE*, in press July, 2006.

In preparation:

Walker, R. and Indraratna, B. "Vertical drain consolidation with non-Darcian flow and void ratio dependent compressibility and permeability".

Walker, R. and Indraratna, B. "Consolidation of stratified soil with vertical and horizontal drainage under surcharge and vacuum loading".

Walker, R. and Indraratna, B. "Vertical drain consolidation with overlapping smear zones".

TABLE OF CONTENTS

CERTIFICATION ii
ABSTRACT iii
ACKNOWLEDGEMENTS v
PUBLISHED WORK vii
TABLE OF CONTENTS viii
LIST OF FIGURES xi
LIST OF TABLES xiv
LIST OF SYMBOLS xv
1 INTRODUCTION 1
1.1 General 1
1.2 Consolidation 1
1.2.1 Consolidation with Vertical Drains 3
1.3 Historical Development of Theory 5
1.4 Vacuum Loading and Electro-osmosis 11
1.5 Objectives and Scope of Present Study 13
1.6 Organisation of Dissertation 14
2 LITERATURE REVIEW 17
2.1 General 17
2.2 Installation and Monitoring of Vertical Drains 17
2.3 Vertical Drain Properties 19
2.3.1 Equivalent Drain Diameter for Band Shaped Drain 19
2.3.2 Filter and Apparent Opening Size (AOS) 21
2.3.3 Discharge Capacity 22
2.3.4 Smear Zone 27
2.3.5 Important Parameters 33
2.4 Influence Zone of Drains 34
2.5 Fundamentals of Soil Consolidation 35
2.5.1 Soil Settlement 35
2.5.2 Consolidation Settlement 37
2.5.3 Soil Permeability Characteristics 39
2.5.4 Increase in Shear Strength 40
2.6 Vertical Consolidation Theory 40
2.6.1 Terzaghi's One-dimensional Theory 40
2.7 Radial Consolidation Theory 43
2.7.1 Equal Strain Hypothesis 43
2.7.2 λ method (Hansbo, 1979, 1997, 2001) 45
2.7.3 Determination of Radial Coefficient of Consolidation 47
2.7.3.1 Log U vs t approach 47
2.7.3.2 Plotting Settlement Data (Asaoka, 1978) 47
2.7.4 Curve Fitting Method (Robinson and Allam, 1998) 48
2.8 Combined Vertical and Radial Consolidation Theory 49
2.8.1 Single Layer Consolidation 49
2.8.2 Multi-layered Consolidation 51
2.9 Application of Vacuum Preloading (Indraratna et al. 2005b) 55
2.10 Summary 56
3 THEORETICAL CONSIDERATIONS 58
3.1 General 58

3.2 Determination of μ Parameter Based on Smear Zone Characteristics and the Associated Soil Properties 60
3.2.1 General Approach to Equal Strain Radial Consolidation with Darcian Flow 60
3.2.2 Smear Zone with Linear Variation of Permeability 67
3.2.3 Smear Zone with Parabolic Variation of Permeability 71
3.2.4 Size of Constant, Parabolic, and Linear Smear Zones Producing Equivalent Rate of Consolidation 74
3.2.5 Relative Importance of Compressibility Variations in the Smear Zone ... 77
3.2.6 Overlapping Smear Zones 79
3.3 Nonlinear Radial Consolidation 85
3.3.1 Previous Attempts at Modeling Void Ratio Dependant Material Properties 85
3.3.2 Analytical Solution 87
3.3.3 Approximation for Vacuum Loading 91
3.3.4 Normally Consolidated Soil 93
3.3.4.1 Concise Notation 97
3.3.5 Overconsolidated Soil 98
3.3.6 Settlements 100
3.3.7 Degree of Consolidation 101
3.3.8 Approximation for Arbitrary Loading 103
3.3.9 Illustrative Example 106
3.4 Multi-layered Consolidation with the Spectral Method 108
3.4.1 Analytical Solution 108
3.4.2 Continuity Equation 109
3.4.3 Depth and Time Dependence of Parameters 114
3.4.4 Spectral Method 115
3.4.5 Explicit Equations 121
3.5 Verification of Spectral Method Model 125
3.5.1 Multi-Layered Free Strain With Thin Sand Layers (Nogami and Li, 2003) 125
3.5.2 Double Layered Ground With Vertical and Radial Drainage(Nogami and Li, 2003) 126
3.5.3 Linearly Varying Vacuum Loading (Indraratna et al., 2005b) 127
3.5.4 Multiple Ramp Loading (Tang and Onitsuka, 2001) 128
3.5.5 Partially Penetrating Vertical Drains (Runnesson et al., 1985) 129
3.5.6 Vertical Consolidation of Four Layers (Schiffman and Stein, 1970) 130
3.6 Shortcomings of Spectral Analysis 131
3.7 Vertical Drainage in a Single Layer with Constant c_v (Spectral Method) 133
3.8 Consolidation Before and After Drain Installation (Spectral Method) 140
3.9 Summary 142
4 LABORATORY VERIFICATION 145
4.1 General 145
4.2 Laboratory Testing of Vertical Drain Consolidation 145
4.3 The University of Wollongong Large-scale Consolidometer 146
4.3.1 General Testing Procedure 148
4.3.2 Verification of Smear Zone with Parabolic Variation of Permeability ... 151
4.3.3 Verification of Nonlinear Consolidation Model 156
4.3.4 Verification of Combined Surcharge and Vacuum Loading 159

4.4 Summary 162
5 CASE HISTORY VERIFICATION 163
5.1 General 163
5.2 Second Bangkok International Airport (Bergado et al., 1998) 163
5.2.1 Spectral Method Parameters 166
5.2.2 Nonlinear Radial Consolidation Model Parameters 171
5.2.3 Comparison of Settlement and Excess Pore Pressure 172
5.2.4 Comparison With Previous Finite Element Method Studies 176
5.3 Land Subsidence Due to Seasonal Pumping of Groundwater in Saga Plain, Japan (Sakai, 2001) 177
5.4 Summary 181
6 CONCLUSIONS AND RECOMMENDATIONS 182
6.1 General Summary 182
6.2 Representation of Smear Zone 182
6.3 Nonlinear Radial Consolidation Model 185
6.4 Multi-layered Spectral Method Model 187
6.5 Recommendations for Future Research 189
7 REFERENCE LIST 191
APPENDIX A: μ PARAMETER FOR PIECEWISE CONSTANT PROPERTIES 208
A.1 Multi-segment Smear Zone 208
A.2 Ideal Drain (No Smear) 210
A.3 Smear Zone with Constant Reduced Permeability 212
APPENDIX B: Nonlinear Spectral Method 214
B.1 General 214
B.2 Constitutive Model 214
B.3 Initial Effective Stress Distribution 217
B.4 Verification 218
B.5 Vertical Consolidation of Normally Consolidated Soil 219
B.6 Cyclic Loading 223
B.6.1 Illustrative Example 224

LIST OF FIGURES

Figure 1.1 Soil phase diagram 1
Figure 1.2 Primary consolidation 2
Figure 1.3 Typical oedometer settlement 3
Figure 1.4 Settlement damage 4
Figure 1.5 Drainage with and without drains 5
Figure 1.6 Settlements with and without drains 5
Figure 1.7 PVD installation a) crane mounted installation rig, b) drain delivery arrangement, c) cross section of mandrel and drain (after Koerner, 1987) 7
Figure 1.8 Examples of mandrel shapes (Saye, 2001) 8
Figure 1.9 Typical core shapes of strip drains (adapted from Hausmann, 1990) 8
Figure 1.10 Flow of water by electro-osmosis (Abeiera et al., 1999) 12
Figure 2.1 Basic instrumentation of embankment 18
Figure 2.2 Schematic diagram of embankment subjected to vacuum loading 19
Figure 2.3 Possible deformation modes of PVD as a result of ground settlement (adapted from Bergado et al., 1996) 23
Figure 2.4 Typical values of vertical discharge capacity (after Rixner et al., 1986) 24
Figure 2.5 Variation of horizontal permeability around circular sand drain (original data from Onoue et al., 1991) 29
Figure 2.6 Variation of horizontal permeability around a) PVD band drain and b) circular sand drain (original data from Indraratna and Redana, 1998a) 30
Figure 2.7 Variation of horizontal permeability around PVD band drain (original data from Indraratna and Sathananthan, 2005a) 31
Figure 2.8 Vertical drain installation patterns 35
Figure 2.9 Patterns of soft soil settlement under embankments (after Zhang, 1999) 37
Figure 2.10 One-dimensional compression and void ratio-permeability relationship 38
Figure 2.11 Consolidation curves for vertical drainage 42
Figure 2.12 Schematic of soil cylinder with vertical drain (after Hansbo,1979) 43
Figure 2.13 Radial consolidation curves for an ideal drain 45
Figure 2.14 Aboshi and Monden (1963) method for determining c_h 47
Figure 2.15 Asaoka (1978) method for determining c_h 48
Figure 2.16 Approximate pore pressure distribution for multi-layered soil (after Onoue, 1988b) 55
Figure 2.17 Linear variation of vacuum pressure with depth 55
Figure 3.1 Axisymmetric unit cell 60
Figure 3.2 Ramp loading 66
Figure 3.3 Linear distribution of permeability in the smear zone 68
Figure 3.4 Parabolic distribution of permeability in the smear zone 72
Figure 3.5 Extent of smear zones producing equivalent rate of consolidation (r_e/r_w = 40) 76
Figure 3.6 Shape of smear zones producing equivalent rate of consolidation (r_e/r_w = 40) with reference to a constant permeability smear zone size of r_s/r_w = a) 2, b) 3, c) 4 77
Figure 3.7 Effect of smear zone compressibility for smear zone with a) constant, b) linear, and c) parabolic compressibility 79
Figure 3.8 Schematic of overlapping smear zones 80
Figure 3.9 Time required for 90% consolidation for overlapping smear zones with linear variation of permeability 83

Figure 3.10 Unit cell 87
Figure 3.11 Consolidation curves depending on total change in consolidation coefficient 97
Figure 3.12 Void ratio-stress relationship for overconsolidated soil 98
Figure 3.13 Comparison between degree of consolidation based on settlement and pore pressure for normally consolidated soil 103
Figure 3.14 Comparison between degree of consolidation based on settlement and pore pressure for overconsolidated soil 103
Figure 3.15 Schematic of piecewise loading 104
Figure 3.16 Nonlinear radial consolidation for non-Darcian flow exponent a) $n = 1.001$ and b) $n = 1.3$ 107
Figure 3.17 Unit cell 109
Figure 3.18 Depth and time dependence of surcharge and vacuum loading 115
Figure 3.19 Model verification: multi-layer equal-strain vs free-strain 126
Figure 3.20 Model verification: double layered ground 127
Figure 3.21 Model verification: surcharge and vacuum loading 128
Figure 3.22 Model verification: multiple stage loading 129
Figure 3.23 Model verification: partially penetrating vertical drains 130
Figure 3.24 Model verification: 4 layer vertical drainage 131
Figure 3.25 Errors associated with series solution 133
Figure 3.26 Degree of consolidation for pervious top and impervious bottom 135
Figure 3.27 Degree of consolidation for pervious top and pervious bottom 136
Figure 3.28 Pore pressure isochrones for pervious top and impervious bottom 138
Figure 3.29 Pore pressure isochrones for pervious top and pervious bottom 139
Figure 4.1 Large-scale consolidometer 148
Figure 4.2 Schematic of large-scale consolidation apparatus 150
Figure 4.3 Horizontal permeability along radial distance from drain in large-scale consolidometer (original data from Indraratna and Redana, 1998a) 152
Figure 4.4 Ratio of horizontal to vertical permeability along radial distance from drain in large-scale consolidometer (original data from Indraratna and Redana, 1998a) 152
Figure 4.5 Predicted and measured settlement for large-scale consolidometer 155
Figure 4.6 Typical $e - \log(\sigma')$ and $e - \log(k_h)$ for Moruya Clay (Rujikiatkamjorn, 2006) 157
Figure 4.7 Comparison between proposed nonlinear model and Indraratna et al. (2005a) 158
Figure 4.8 Settlement of large-scale consolidation cell with vacuum and surcharge loading 161
Figure 5.1 Site plan for the test embankments at Second Bangkok International Airport (Bamunawita, 2004) 164
Figure 5.2 General soil properties for SBIA test embankments (after Sangmala, 1997) 165
Figure 5.3 Compression properties for SBIA test embankments (after Sangmala, 1997) 166
Figure 5.4 Variation of load with depth at embankment centerline 171
Figure 5.5 Centerline surface settlement plots for SBIA test embankments 173
Figure 5.6 Centerline settlement at various depths for embankment TV2 174
Figure 5.7 Excess pore pressure 3 m below centerline of embankment TV1 175
Figure 5.8 Excess pore pressure 3 m below centerline of embankment TV2 175

Figure 5.9 Centerline settlement for embankment TV2 including previous finite element models 177
Figure 5.10 Excess pore pressure below TV2 inclduing a prevous finite element model 177
Figure 5.11 Soil properties at Shiroishi (after Sakai, 2001) 179
Figure 5.12 Compression of 26 m of marine clay 181
Figure 6.1 Horizontal permeability along radial distance from drain in large-scale consolidometer (original data from Indraratna and Redana, 1998a) 183
Figure 6.2 Time required for 90% consolidation for overlapping smear zones with linear variation of permeability 185
Figure 6.3 Consolidation curves depending on total change in consolidation coefficient 186
Figure 6.4 Consolidation curves for constant c_v 189
Figure A.1 Discretised radial properties 208
Figure B.1 Void ratio-stress relationship for evolving maximum effective stress 215
Figure B.2 Verification of nonlinear spectral method 219
Figure B.3 Effect of varying soil depth 220
Figure B.4 Effect of varying initial surface stress 221
Figure B.5 Effect of varying initial surface void ratio 222
Figure B.6 Settlement under cyclic loading 225

LIST OF TABLES

Table 1.1 Details of some selected PVD (Hausmann, 1990) 9
Table 2.1 Percentage reduction in discharge capacity for deformed PVD (Bergado et al., 1996) 25
Table 2.2 Short-term discharge capacity, in m^3/year, of eight band drains measured in laboratory (Hansbo, 1981) 26
Table 2.3 Current recommended values for specification of discharge capacity (Suthananthan, 2005a) 27
Table 2.4 Proposed smear zone parameters (after Xiao, 2001) 32
Table 3.1 Parameters used to produce Figure 3.11 97
Table 3.2 Parameters for illustrative example 106
Table 3.3 Parameters for double layered ground 127
Table 3.4 Soil profile, four layer system 130
Table 4.1 Parameters used in analysis (Indraratna et al., 2005a) 158
Table 5.1 Modified Cam-clay parameters for SBIA test embankments (Indraratna et al., 2004) 166
Table 5.2 Soil properties for spectral method modeling of TV1 pore pressure 168
Table 5.3 Soil properties for spectral method modeling of TV2 pore pressure 168
Table 5.4 Soil properties for spectral method modeling of TV1 settlement 169
Table 5.5 Soil properties for spectral method modeling of TV2 settlement 170
Table 5.6 Soil properties for nonlinear radial consolidation modeling of embankment TV1 172
Table 5.7 Soil properties for settlement modeling of Shiroishi ground subsidence 180
Table B.1 Parameters for verification example 219
Table B.2 Default parameters for normally consolidated vertical consolidation parametric study 220
Table B.3 Soil properties for cyclic loading example 225

LIST OF SYMBOLS

a	PVD width
$\mathbf{A}$	vector of time dependant coefficients
A	smear zone permeability parameter; function; time dependant coefficient; cyclic load amplitude
A_η	smear zone compressibility parameter
b	PVD thickness
B	smear zone permeability parameter
B_η	smear zone compressibility parameter
C	smear zone permeability parameter; integration constant
$\mathbf{c}$	vector of constants
$\widetilde{c}_h$	horizontal coefficient of consolidation for non-Darcian flow
$\widetilde{c}_{h0}$	initial horizontal coefficient of consolidation for non-Darcian flow
C_c	compression index
c_h	horizontal coefficient of consolidation
c_{h0}	initial value of horizontal consolidation coefficient
c_{h1}, c_{h2}	horizontal consolidation coefficients for double layered ground
c_{he}	effective consolidation coefficient
c_{hf}	final value of horizontal consolidation coefficient
C_k	permeability change index
C_r	recompression index
CS	function
c_v	vertical coefficient of consolidation
$\bar{c}_v$	reference value of vertical consolidation coefficient
c_{v1}, c_{v2}	vertical consolidation coefficients for double layered ground
D_{85}	diameter of clay particles corresponding to 85% passing
d_e	diameter of influence area
dQ_1, dQ_2	infinitesimal volume flows
dT_h	reference horizontal time factor divided by time
dT_v	reference vertical time factor divided by time
d_w	drain diameter
e	void ratio
$\mathbf{E}$	matrix of eigenvalue exponential terms
e_0	initial void ratio
e_{00}	initial void ratio at soil surface
e_{0n}	void ratio at the depth below which soil is normally consolidated
e_f	final void ratio
e_r	error

F	function
f	source/sink term; function; cyclic load natural frequency
F_c	discharge capacity reduction factor due to bending
F_{fc}	discharge capacity reduction factor due to filtration and clogging
F_t	discharge capacity reduction factor due to lateral pressure
g	function
G_s	specific weight of soil solids
H	height of soil; drainage length
H_0	initial height of soil
H_1, H_2	layer depths for double layered ground
h_c	height of clay layer
h_s	height of sand layer
i	hydraulic gradient; integer
i_l	critical hydraulic gradient for non-Darcian flow
j	integer
J_0, Y_0	bessel functions
$\bar{k}$	reference value of permeability
$\tilde{k}$	non-Darcian coefficient of consolidation
$\tilde{k}_h$	undisturbed non-Darcian horizontal permeability
$\tilde{k}_s$	smear zone non-Darcian horizontal permeability
k_0	permeability at soil/drain interface; initial coefficient of permeability
k_1	ratio of vacuum pressure at drain bottom to drain top
k_{clay}	clay permeability
k_{filter}	PVD filter permeability
k_h	undisturbed horizontal coefficient of permeability
$\bar{k}_h$	reference value of horizontal permeability
k_{h1}, k_{h2}	horizontal permeability for double layered ground
k_s	smear zone permeability
k_{sand}	sand permeability
k_{soil}	soil permeability
$k_{\text{undisturbed}}$	coefficient of permeability for undisturbed soil
k_v	vertical coefficient of permeability
$\bar{k}_v$	reference value of vertical permeability
k_{v1}, k_{v2}	vertical permeability for double layered ground
k_{vB}	vertical permeability at bottom of soil layer
K_{ve}	equivalent vertical coefficient of permeability
k_{vT}	vertical permeability at top of soil layer
k_w	drain permeability
l	depth of vertical drain; integer

L	linear operator
$\#l$	number of soil layers
m	integer; overconsolidated shear strength index
M	summation term e.g. $M = (2m+1)\pi/2$ in Terzaghi theory
M^-	function
M^+	function
m_v	coefficient of volume compressibility
$\overline{m}_v$	reference value of volume compressibility
m_{v0}	initial value of volume compressibility; volume compressibility at soil/drain interface
m_{va}	average value of volume compressibility
m_{vB}	volume compressibility at bottom of soil layer
m_{vs}	smear zone volume compressibility
m_{vT}	volume compressibility at top of soil layer
m_{vX}	volume compressibility where interacting smear zones begin to overlap
n	ratio of influence radius to drain radius; non-Darcian flow index
N	ratio of influence radius to drain radius; integer
n'	ratio of influence radius to equivalent mandrel radius based on the mandrel perimeter
O_{95}	95% of filter openings are smaller than this opening
OCR	overconsolidation ratio
P	cyclic load wave period
p_0	vacuum pressure at soil surface
P_{av}	averaging factor to account for changing coefficient of consolidation
PTIB	pervious top impervious bottom boundary condition
PTPB	pervious top pervious bottom boundary condition
q_w	drain discharge capacity
$q_{w(\text{required})}$	required discharge capacity
$q_{w(\text{specified})}$	discharge capacity specified to manufacture
r	radial coordinate
r_e	radius of influence area
r_m	equivalent radius of mandrel
r_s	radius of smear zone
s	integration variable
$\overline{s}$	mean square distance of the flownet draining a circular area to a rectangular drain.
s_{constant}	smear zone size calculated with constant permeability smear zone
$s_{\text{equivalent}}$	smear zone size calculated with linear or parabolic permeability producing equivalent consolidation to smear zone calculated with constant permeability
SN	function
S_p	drain spacing interval

S_u	undrained shear strength
s_X	ratio of smear zone interaction radius to drain radius
t	time
$\widetilde{T}$	modified time factor
$\widetilde{T}_{Darcy}$	Darcian time factor
$\widetilde{T}_m$	modified time factor at application of mth instantaneous laod
$\widetilde{T}_p$	modified time factor at preconsolidation pressure
t_{90}	time required to reach 90% consolidation
T_c	construction time factor
t_f	end time for integration
T_h	time factor for horizontal consolidation
T_{h0}	horizontal time factor calculated from initial parameters
t_Ω	drain installation time; piecewise nonlinear time marker
t_s	starting time for integration
T_v	time factor for vertical consolidation
U	degree of consolidation
u	pore water pressure
$\overline{u}$	average excess pore pressure
$\overline{\overline{u}}$	depth averaged pore pressure
$\overline{u}_0$	initial excess pore pressure
$\Delta\overline{u}$	change in pore pressure
$\overline{u}_\delta$	fundamental pore pressure solution
U_h	average degree of consolidation in the horizontal direction
U_{hs}	degree of consolidation calculated with settlement data
u_m^-	pore pressure immediately before application of mth instantaneous load
u_m^+	pore pressure immediately after application of mth instantaneous load
u_s	smear zone pore pressure
U_z	average degree of consolidation in the vertical direction
$\mathbf{v}$	matrix of eigenvectors
w	pore pressure in the drain; vacuum pressure
W	normalised pore pressure
$\mathbf{w}$	matrix dependant on vacuum loading terms
W_p	nomalised pore pressure at preconsolidation pressure
$\mathbf{x}$	vector of unknown coefficients
x	integration variable
y	transformed integration variable
z	depth coordinate
Z	nomalised depth
z_n	depth below which all soil is normally consolidated

Greek symbols

α	non-Darcian radial consolidation parameter; function parameter; soil property parameter
λ	non-Darcian radial consolidation parameter; slope of Cam-clay consolidation line; spectral method eigenvalue
β	non-Darcian radial consolidation parameter; slope of Asaoka plot; function variable
$\boldsymbol{\chi}$	vector of constants
$\#\chi$	number of series term used in previous time step
Δ	change operator
δ	dirac delta function
ε	strain
$\partial\varepsilon/\partial t$	volumetric strain rate
η	lumped vertical drain parameter; ratio of undisturbed volume compressibility to drain/soil interface volume compressibility
$\overline{\eta}$	reference value of lumped drain parameter
η_X	ratio of interacting smear zone volume compressibility to drain/soil interface compressibility
$\boldsymbol{\Gamma}$	matrix dependant on compressibility and geometry parameters
γ_w	unit weight of water
κ	ratio of undisturbed permeability to permeability at the drain/soil interface; slope of Cam-clay swelling line
κ_X	ratio of interacting smear zone permeability to drain/soil interface permeability
$\boldsymbol{\Lambda}$	function
μ	smear zone parameter for Darcian flow
μ^*	composite smear zone parameter
μ_{m_v}	smear zone compressibility parameter
μ_w	well resistance parameter
μ_X	overlapping smear zone parameter
$\boldsymbol{\Omega}$	matrix dependant on non-zero initial condition
ω	cyclic load angular frequency
ϕ	basis function
$\boldsymbol{\Phi}$	vector of basis functions
$\overline{\phi}$	integrated basis function
$\overline{\boldsymbol{\Phi}}$	vector of integrated basis functions
φ	cyclic load phase
$\boldsymbol{\Psi}$	matrix dependant on permeability, and geometry parameters
ρ	settlement
ρ_c	consolidation or primary settlement
ρ_i	immediate or distortion settlement
ρ_∞	final settlement
ρ_l	settlement caused by lateral displacement
ρ_s	secondary compression
ρ_t	total settlement

σ	total stress
$\boldsymbol{\sigma}$	matrix dependant on surcharge loading terms
$\overline{\sigma}$	average total stress
$\overline{\sigma}'$	average effective stress
σ'	effective stress
σ'_0	initial effective stress
σ'_{00}	initial effective stress at soil surface
σ'_{0n}	this effective stress marks the depth below which soil is normally consolidated
σ'_{0z}	initial effective stress at depth z
$\sigma'_{\max}$	evolving maximum effective stress
σ'_p	preconsolidation stress
σ'_{v0}	vertical effective stress
$\Delta\sigma$	change in total stress
τ	time
θ	function parameter
$\boldsymbol{\Theta}$	matrix dependant on cyclic loading terms
υ	velocity of flow
υ_r	velocity of flow in radial direction
υ_v	velocity of flow in the vertical direction
Ξ	function
ζ	depth

1 INTRODUCTION

1.1 General

Throughout the world, due to rapid development and urbinisation, infrastructure projects are increasingly located on marginal soils. Untreated soils in their virgin state may be unsuitable for short or long term construction activities and so must be improved before use. In particular, many coastal areas contain thick layers of compressible clay originally deposited by sedimentation from rivers, lakes and seas. These soft soils have low bearing capacity and exhibit excessive settlements in response to loading. One of the most successful and widely used techniques to improve soft soils is preloading with vertical drains to consolidate the soil and hasten strength gain. This thesis mainly builds on the knowledge of consolidation by vertical drains developed in the past fifty years.

This chapter explains the concept of consolidation and how preloading with vertical drains can hasten the drainage process. The development of vertical drain theories is discussed and the chapter concludes with an outline of aims and content of this thesis.

1.2 Consolidation

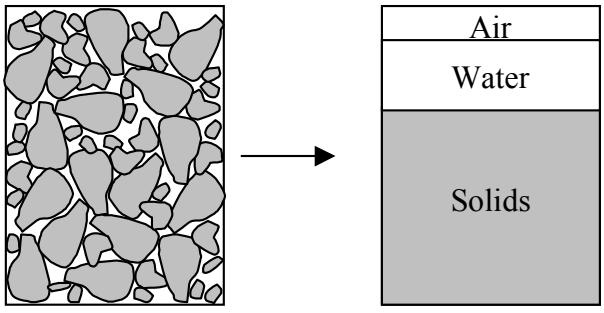

Figure 1.1 Soil phase diagram

Soil may be of two or three phase composition (see Figure 1.1). The voids between the soil solids are filled with water, air or a combination of both. Consolidation involves the reduction of voids under load. It occurs in three stages (see Figure 1.3). Immediate settlement occurs immediately after the application of load and occurs with zero volume change, i.e. shape change only. In saturated soil (i.e. no air) the increase in pressure arising from the load is immediately taken by the water which is incompressible. Such excess pore-water pressure gradually dissipates as water seeps out of the soil and the pressure is transferred to the soil skeleton. This is known as primary consolidation (see Figure 1.2). Primary consolidation may take years depending on the permeability of the soil. When all excess pore-water pressure has dissipated the soil continues to consolidate indefinitely as the soil skeleton rearranges under the load. This secondary settlement occurs at a much slower rate then primary consolidation.

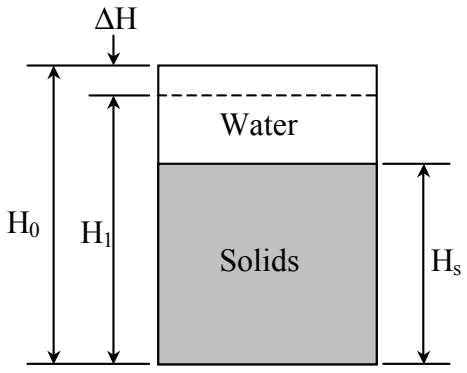

Figure 1.2 Primary consolidation

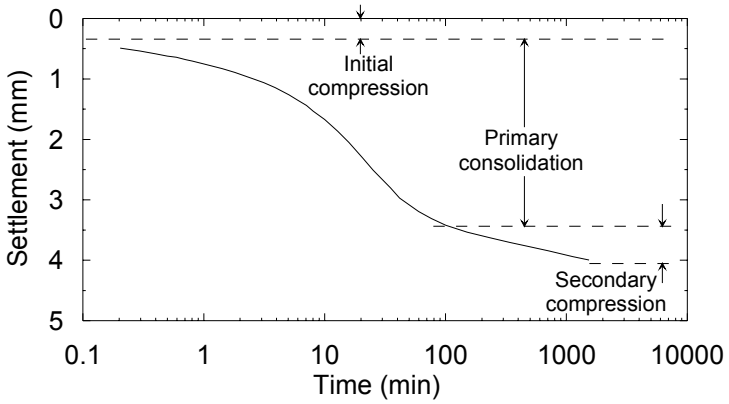

Figure 1.3 Typical oedometer settlement

Settlement of soils can cause serious problems for structures like embankments founded on them. If structures settle uniformly little damage is experienced except perhaps to services feeding it. However, settlement is rarely uniform. Varied loading and the heterogeneous nature of soil lead to differential settlement. This produces added loads that often create cracking in the structure. It may be difficult to build such structures in the first place if soils have insufficient strength to withstand the applied loads. Shear strength in soil is broadly dependant on soil density. The densification of soil due to consolidation thus results in significant strength gain, allowing larger loads to be placed on the soil.

1.2.1 Consolidation with Vertical Drains

Preconsolidation is a technique used to minimise the effect of settlements on structures and improve the strength of the soil. Basically a load is applied to the site, usually in the form of an embankment, where a structure is to be built. This embankment causes the foundation soil to consolidate. Once the required primary consolidation is achieved the preconsolidation load is removed and the structure built. Thus after construction the soil foundation is subject to the slow gradual

process of secondary compression. Differential settlements are reduced so the structure is less likely to crack or deform.

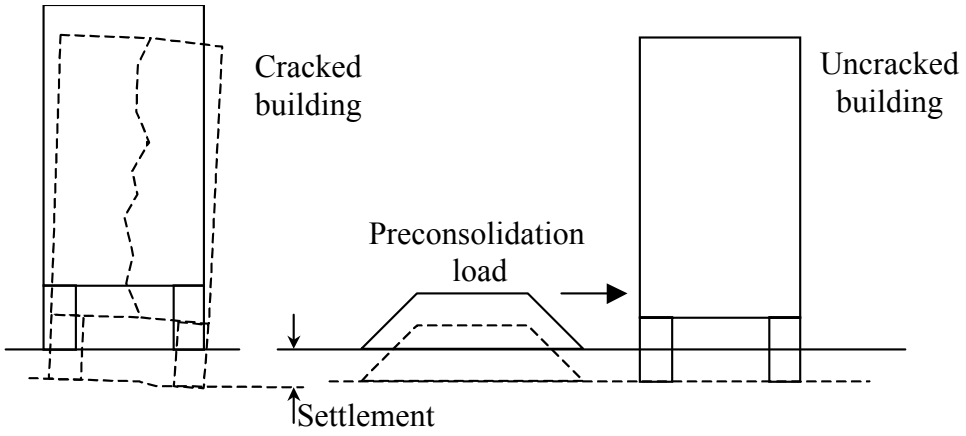

Figure 1.4 Settlement damage

The speed with which preloading achieves the required consolidation is hastened by increasing the magnitude of the preload. The magnitude of preload is limited by soil failure criteria. Thus preloading surcharges are increased in stages as the shear strength of soil improves and is able to resist increased loads without failure. To speed the consolidation process so preloads can be built up more quickly (or not built up as high in the first place), one must speed the egress of water from the soil body. This can be achieved by installation of vertical drains that shorten the drainage path for water to escape under the excess pore-water pressure (see Figure 1.5). In particular they provide a radial drainage path in addition to vertical drainage paths. Clays often have greater permeability in the horizontal direction than in the vertical direction. Usually water only flows in the vertical direction due to the large extent of the clay body. Vertical drains allow the increased horizontal permeability to be exploited.

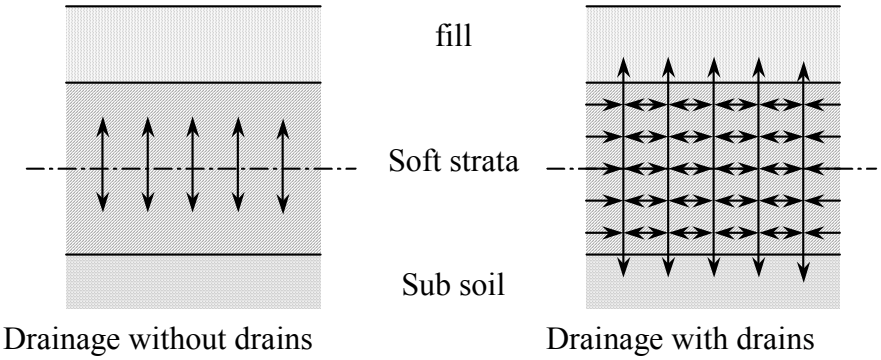

Figure 1.5 Drainage with and without drains

1.3 Historical Development of Theory

Vertical drains improve the shear strength of clays and reduce post construction settlements to tolerable levels (Johnson, 1970). While secondary settlement cannot be eliminated it is hoped that with vertical drains 100% of primary consolidation can be achieved quickly compared with non-modified ground. Consolidation times, though reduced from many years, still take months meaning adequate planning is essential to allow for these periods. Structures with high concentrated loads cannot be used with vertical drains as the uniform surcharge loading prior to construction does not replicate these loads.

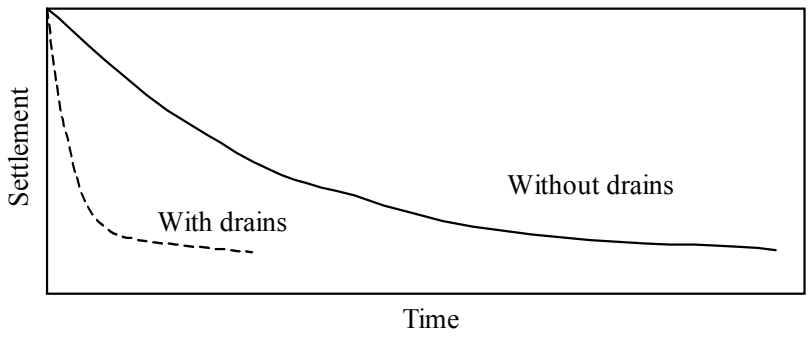

Figure 1.6 Settlements with and without drains

There are two classes of vertical drains: displacement and non-displacement. The non-displacement drains involve removal of in situ soil and backfilling with more permeable material, usually sand. Holes may be formed by driving, jetting, or auguring with typical diameters of 200 to 450 mm (Hausmann, 1990). Displacement type drains are prefabricated and are forced into the soil with a hollow mandrel (see Figures 1.7 and 1.8). The mandrel is then removed leaving the drain in place. Prefabricated vertical drains (PVD) consist of a core surrounded by a filter sleeve (see Figure 1.9). Dimensions of some PVD appear in Table 1.1.

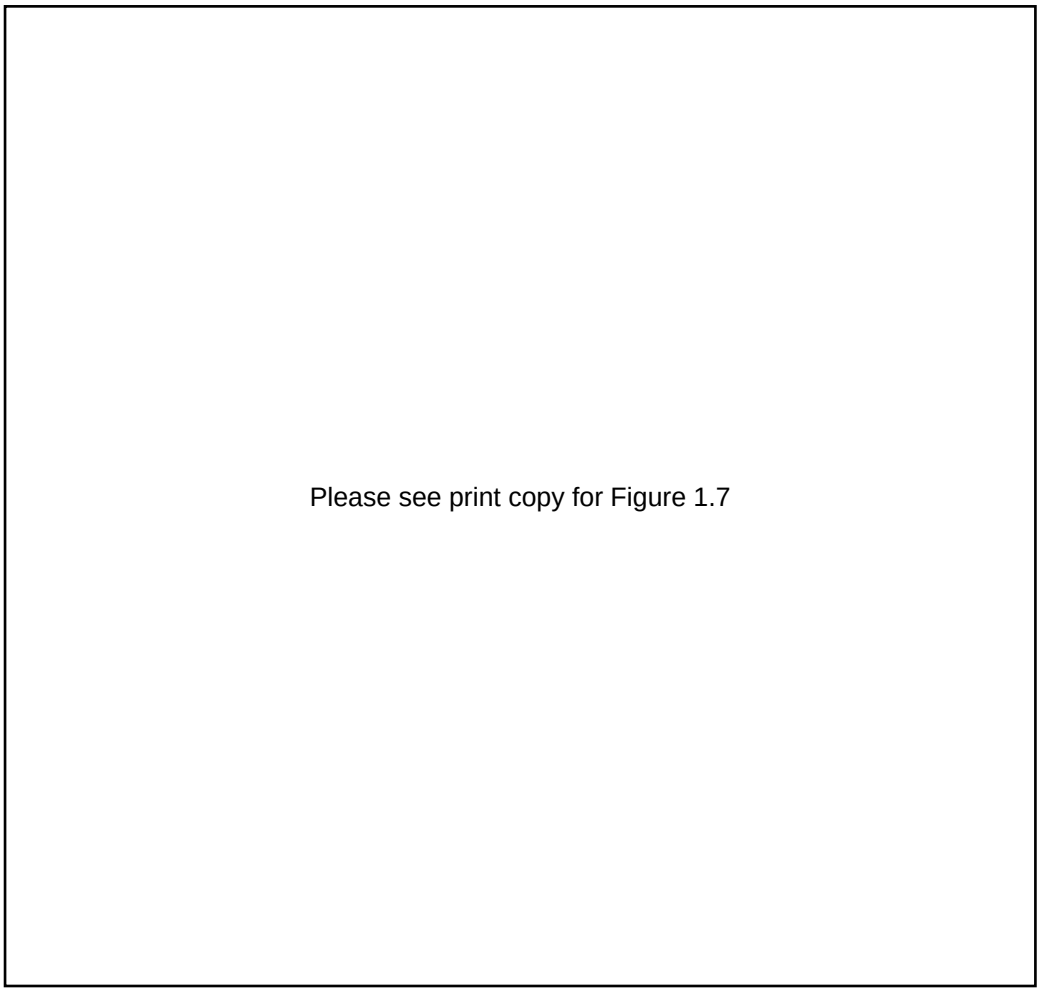

Figure 1.7 PVD installation a) crane mounted installation rig, b) drain delivery arrangement, c) cross section of mandrel and drain (after Koerner, 1987)

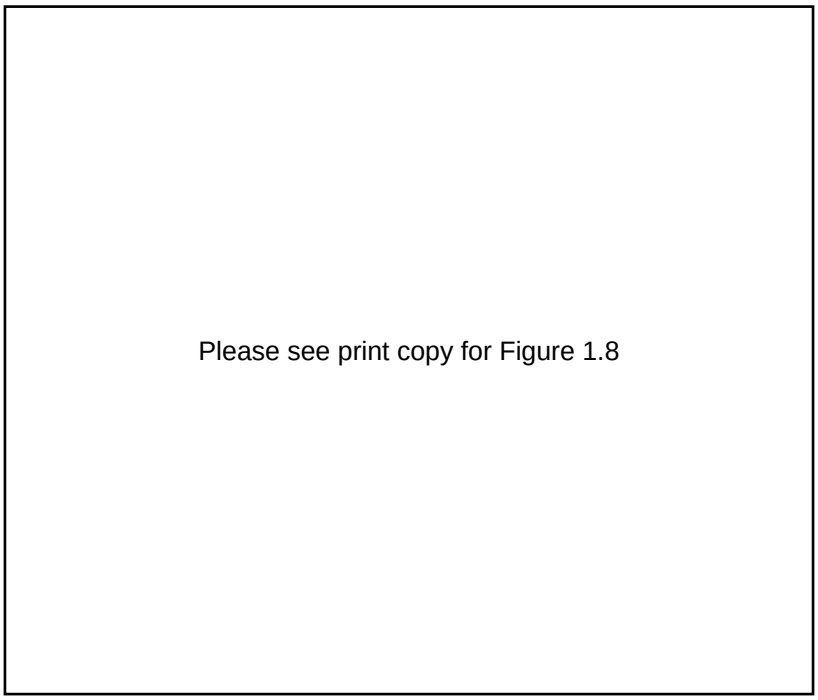

Figure 1.8 Examples of mandrel shapes (Saye, 2001)

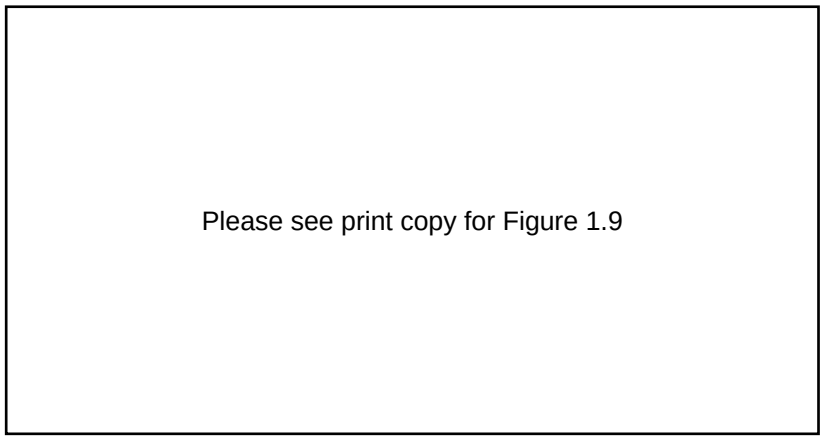

Figure 1.9 Typical core shapes of strip drains (adapted from Hausmann, 1990)

Table 1.1 Details of some selected PVD (Hausmann, 1990)

Please see print copy for Table 1.1

Barron (1948) was the first to undertake axisymmetric analysis of vertical sand drains. At the same time Kjellman (1948) was using cardboard wick drains (core surrounded by cardboard) instead of sand. This was the first of many prefabricated vertical drains (PVD) to be developed. Barron (1948) considered a single drainage cell assuming: saturated soil; uniform loads result in vertical compressive strain; the influence zone (area of soil that drains to a single drain) is circular; the permeability of the drain is infinite; and Darcy's law is valid. Barron developed rigorous solutions for the free strain case (no arching of soil) and approximate solutions for the equal strain case (horizontal sections remain horizontal throughout consolidation process). The difference between free and equal strain cases was found to be negligible so the equal strain case was used. Barron (1948) also included the effects of smear (for equal strain) and well resistance (for equal and free strain). Solutions involved Bessel functions and were time consuming to perform. As a result the effects of smear and well resistance were often ignored to simplify calculations (Hansbo, 1981). Others (Fellenius, 1981) believed inaccuracies in field measurement negated any benefit gained from including smear and well resistance in the analysis.

Vertical drain solutions were further developed by questioning Barron's assumptions for the following cases: rigorous solution including vertical and horizontal drainage for equal strain with well resistance (Yoshikuni and Nakanodo, 1974); as just mentioned including smear effects (Onoue et al., 1988a); Approximate solution assuming non-Darcian flow (Hansbo, 1997). Approximate solutions, (Zeng and Xie, 1989; Hansbo, 1981), have proved more popular due to less computational effort. In particular Hansbo's approximate solution including smear and well resistance is widely used. The method compares well to more rigorous solutions (Chai et al., 1995). Another reason approximate solutions were preferred was because even rigorous solutions to the unit cell problem were insufficient in completely predicting the behaviour of multiple drains.

Only under the centerline of embankments were unit cell solutions accurate in predicting results (Indraratna and Redana, 2000). Lateral deformations especially, were impossible to predict with unit cell theories. The finite element method (FEM) was used to consider multiple drain problems. Much of FEM work (Zeng et al., 1987, Hird et al., 1992) has centered on attempting to match axisymmetric properties to a two dimensional plane strain model that is faster to solve than a full three dimensional model. Paralleling the rigorous unit cell solutions, refinement of FEM methods were made by including well resistance and smear effects (Indraratna and Redana, 1997). FEM also allowed the use of critical state soil mechanics (Britto and Gunn, 1987) and other constitutive models that predict some aspects of clay behaviour with greater accuracy than simple soil models.

1.4 Vacuum Loading and Electro-osmosis

There are occasions when the use of surcharge loading alone is too slow or inappropriate for the site. Specified construction times may be very short, the required load would result in an embankment of unsafe height, space for embankment construction may be limited or there is no access to suitable fill material. In such cases in is necessary to use more refined techniques instead of, or in combination with surcharge loading.

Electro-osmosis is one way to hasten water flow in soil (Lefebvre and Burnotte, 2002; Mohamedelhassan and Shang, 2002; Shang, 1998; Su and Wang, 2003; Esrig, 1968; Karunaratne et al., 2004). Electrically conductive drains can be used to apply an electric potential to the soil. In fine-grained soils surface forces on particles dominate. Clay particles usually have a negative surface charge due to a double layer of adsorbed water. When electrical potential is applied (between vertical drains) cations move to the more negatively charged potential bringing their associated water with them (see Figure 1.10). Particles also 'drag' water with them. The electro-osmotic flow, as it is called, is larger than flow of hydration water alone, with electro-osmotic conductivity 200 to 1000 times greater than hydraulic conductivity (Abeiera et al., 1999). The 'pulling' action occurring when electro-conductive vertical drains are used can result in 2 to 3 times faster settlement than non-conductive drains that 'push' water out with a surcharge load.

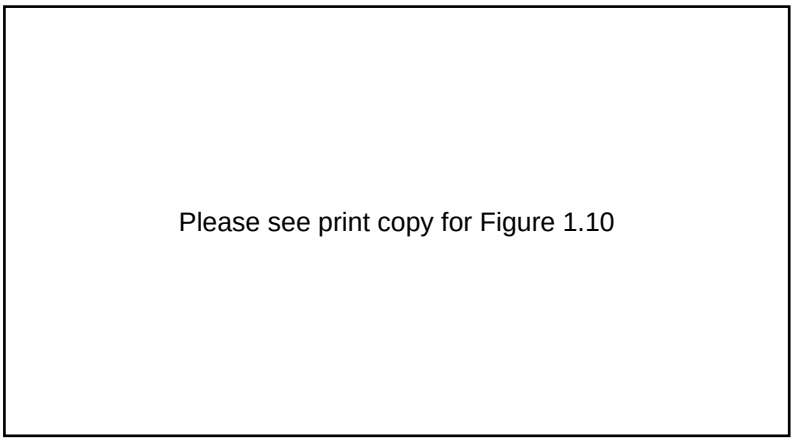

Figure 1.10 Flow of water by electro-osmosis (Abeiera et al., 1999)

More common than exploiting electro-osmosis is applying a vacuum to the soil surface and vertical drain tops. An external negative load is applied to the soil surface in the form of vacuum through a sealed membrane system (Choa, 1989). Higher effective stress is achieved by rapidly decreasing the pore water pressure, while the total stress remains unchanged. When vacuum preloading is affected via PVD, the surrounding soil tends to move radially inward (Chai et al., 2005), while the conventional surcharge loading causes outward lateral flow. The result is a reduction of the outward lateral displacements, thereby reducing the risk of damage to adjacent structures, piles etc. In the case of vacuum application, it is important to ensure that the site to be treated is totally sealed and isolated from any surrounding permeable soils to avoid air leakage that adversely affects the vacuum efficiency.

Vacuum loading or use of conductive drains can be used alone or in combination with surcharge loading. As both methods require electricity provision, costs may be inhibitive for large treatment areas. There may however be little alternative to using these advanced methods if specified construction times are very short.

1.5 Objectives and Scope of Present Study

The main objective of this study was to develop useful analytical tools for the analysis of soil consolidation problems involving vertical drains. Existing analytical solutions are often simplistic, involving numerous assumptions about the soil behaviour. In order to consider spatial and temporal variation of soil properties recourse is usually made to numerical methods. There is thus a knowledge gap between the simple methods and markedly more complicated numerical methods. This knowledge gap is filled somewhat by the three models presented in this thesis. The motivation for the three models is given below:

1. The smear effect is a significant factor in the retardation of consolidation by vertical drains. Traditionally modeled with a small zone of reduced permeability close to the drain, a greater understanding of smear effects is gained by considering more realistic representations of a smear zone with spatially varied properties. The larger smear zone sizes predicted with linear and parabolic variations in permeability (developed in this thesis) suggest the possibility of overlapping smear zones. Overlapping smear zones, not considered in existing theory, may give some insight into the phenomena that continually reducing drain spacing does not lead to reduced consolidation times.
2. Where existing analytical solution to radial drainage problems consider only average soil properties, the nonlinear radial consolidation model presented in this thesis explicitly captures the variation of permeability and compressibility described by semi-log void ratio relationships. Analytical

solutions to nonlinear problems are rare and can be used for verification of numerical models as well as more accurate prediction of consolidation behaviour.

3. The complexity involved with existing analytical solutions to multi-layered soil consolidation problems often precludes their use. Thus, use of analytical solutions is effectively limited to simple one or two layer problems with instantaneous loading. To more easily analyse realistic soil deposits exhibiting stratification, an analytical model is developed based on the spectral method, which produces a single expression describing the pore pressure profile across all layers. The solution is calculated with common matrix operations. Unlike existing solutions the model does not become unwieldy when the number of layers increases. With vacuum and surcharge loading that vary with depth and time, and dummy layers to apply pore pressure boundary conditions, the spectral method model provides a general tool for analyzing a wide variety of consolidation problems with flexibility usually associated with numerical methods.

The new analytical consolidation models are verified against existing analytical solutions, laboratory experiments, and case histories.

1.6 Organisation of Dissertation

Following this introductory chapter, Chapter 2 presents a comprehensive survey of the literature associated with vertical drains. Factors that affect the efficacy of consolidation by vertical drains, such as well resistance and smear effect, along with

the drain properties themselves are described in detail. Focus is directed towards existing analytical solutions to vertical drain consolidation problems.

Chapter 3 provides the main section of this thesis, presenting the new analytical soil consolidation models. A more realistic representation of smearing, where properties within the smear zone vary with radial distance from the drain, is presented. "μ" parameters for use in Hansbo's (1981) radial consolidation equations are derived for linear and parabolic variations in permeability. The possibility of overlapping smear zones is investigated with the new representations. Material nonlinearity is considered in a new equal strain radial consolidation model that explicitly captures the effect of: non-Darcian flow; semi-log void ratio-stress relationship; and semi-log void ratio-permeability relationship. The model can be used for overconsolidated or normally consolidated soil. Finally a powerful multi-layered consolidation model incorporating vertical and horizontal drainage is presented. Using the spectral method to solve the governing equation, a single expression calculated with common matrix operations describes the pore pressure distribution across all layers. Surcharge and vacuum loading that vary with both depth and time can be analysed. The model is verified against a number of existing specific analytical solutions and used to investigate some deviations from Terzaghi one-dimensional consolidation theory.

Chapter 4 uses the analytical methods developed in Chapter 3 to analyse large-scale laboratory consolidation experiments conducted at the University of Wollongong. Three laboratory experiments are studied: a smear zone with parabolic variation of

permeability; combined vacuum and surcharge loading; and consolidation considering soil compressibility and permeability indices.

Chapter 5 presents two case histories with which the new consolidation models are used to analyse. Two trial embankments for the second Bangkok International Airport including vacuum and surcharge loading are described. The measured values of pore pressure and settlement below the embankment centerlines are compared with values predicted by the spectral method model and the nonlinear radial consolidation model. The versatility of the spectral method model is then shown by accurately predicting the subsidence associated with groundwater pumping in the Saga Plain, Japan.

Chapter 6 draws conclusions from the current research and provides recommendations for future work. Following Chapter 6 are the reference list and two appendices.

2 LITERATURE REVIEW

2.1 General

This Chapter extends the introductory material of Chapter 1 by presenting a comprehensive survey of the literature associated with vertical drains. Factors that effect consolidation by vertical drains, such as well resistance and smear effect, along with the drain properties themselves are described in detail. Focus is directed towards existing analytical solutions to vertical drain consolidation problems.

2.2 Installation and Monitoring of Vertical Drains

A typical instrumented vertical drain scheme is shown in Figure 2.1. The site is first prepared by removing vegetation and surface debris, and grading the ground if necessary. This initial step is sometimes problematic especially with very soft soils as construction equipment can get bogged or cause severe rutting at the site. It is beneficial to minimize the disturbance to any weathered surface crust which may provide at least some strength to the soil and help prevent lateral spreading under embankment loading. Vertical drains are usually installed from a sand blanket. The sand blanket provides a sound working platform and allows water egress from the drains. The drainage function of the sand blanket may be facilitated by horizontal drains on the surface.

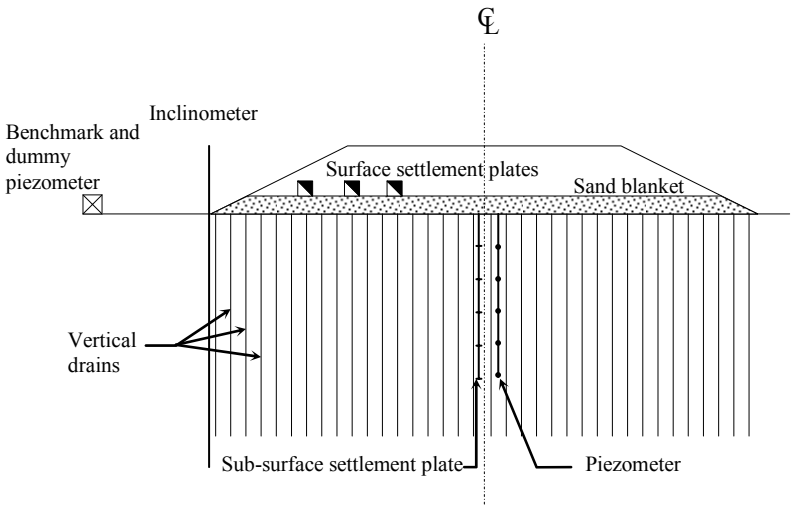

Figure 2.1 Basic instrumentation of embankment

Horizontal surface drains in both transverse and longitudinal directions are used extensively in vacuum preloading projects. They provide hydraulic connectivity to the vacuum pump. Figure 2.2 shows the pertinent features of a vacuum preloading scheme. To ensure only the area of interest is subjected to vacuum, the embankment is surrounded by a trench excavated approximately 0.5 m below groundwater level and filled with an impervious slurry (Bentonite). An impermeable geomembrane is placed across the entire preload area and sealed along the peripheral trench. The trenches are backfilled with water to improve the seal between the membrane and the Bentonite slurry. It is vital to maintain the geomembrane seal as any breaches will reduce the efficiency of the applied vacuum.

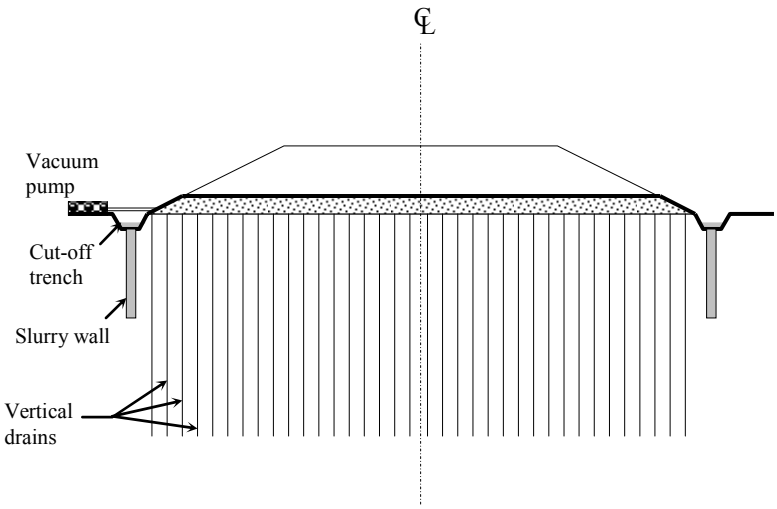

Figure 2.2 Schematic diagram of embankment subjected to vacuum loading

Field instrumentation for monitoring and evaluating the performance of the embankment is essential to prevent sudden failures, to record changes in the rate of settlement and to verify the design parameters. Several types of geotechnical instrumentation such as settlement gauges, piezometers and inclinometers are required to install at the construction site. Performance evaluation is important to improve settlement predictions and to provide sound guidelines for future design. For significant projects, well instrumented trial embankments may be constructed to gain a better understanding of the field conditions.

2.3 Vertical Drain Properties

2.3.1 Equivalent Drain Diameter for Band Shaped Drain

Most analytical solutions to vertical drain problems assume that pore water flows into a drain with circular cross-section. An example of an analytical solution that does not assume a circular drain is that of Wang and Jiao (2004) who model a polygonal influence area draining to a similarly shaped polygon of smaller size. If

band shaped drains are to be analysed with such solutions then the rectangular cross section needs to be converted to an equivalent circular one. The following conversion relationships have been proposed for a rectangular drain with width a and thickness b :

$$d_w = 2\frac{(a+b)}{\pi} \text{ (Hansbo, 1981)} \tag{2.1}$$

$$d_w = \frac{a+b}{2} \text{ (Atkinson and Eldred, 1981)} \tag{2.2}$$

$$d_w = \left(\frac{4ab}{\pi}\right)^{0.5} \text{ (Fellenius and Castonguay, 1985)} \tag{2.3}$$

$$d_w = 0.5a + 0.7b \text{ (Long and Corvo, 1994)} \tag{2.4}$$

$$d_w = d_e - 2\sqrt{(\bar{s}^2)} + b \text{ (Pradhan et al.,1993)} \tag{2.5a}$$

where,

$$\bar{s}^2 = \frac{1}{4}d_e^{\,2} + \frac{1}{12}a^2 - \frac{2a}{\pi^2}d_e \tag{2.5b}$$

Equation (2.1) and Equation (2.3) are based, respectively, on perimeter and area equivalence. Long and Corvo (1994) use an electrical analogy to determine an equivalent diameter. A rectangular 'drain' is painted on electrically conducting paper with silver paint. The resulting flownet is found with an analog field plotter. The size of equivalent circular drain cross section that best matches the flownet is described by Equation (2.4). Pradhan et al. (1993) produce Equation (2.5) by considering the mean square distance, $\bar{s}$, of the flownet draining a circular area to a rectangular drain. Equation (2.2) was developed to account for the throttle that occurs close to the drain.

As to which of the above equations is the best there is no definitive answer. Based on finite element studies Rixner et al. (1986) recommends Equation (2.2). Long and Corvo believe Equation (2.2) is better than Equation (2.1), but Equation (2.4) is better still. It should be noted that there is minimal difference in the consolidation rates calculated using any of the equations (Indraratna and Redana, 2000; Welker et al., 2000).

2.3.2 Filter and Apparent Opening Size (AOS)

The drain material (sand drain) and the filter jacket of PVD have to perform two basic but contrasting requirements: retaining the soil particles and at the same time allowing the passage of pore water. The general guideline for the drain permeability is given by:

$$k_{\text{filter}} > 2k_{\text{soil}} \tag{2.6}$$

Effective filtration can minimise soil particle movement through the filter. A commonly employed filtration requirement is:

$$\frac{O_{95}}{D_{85}} \leq 3 \tag{2.7}$$

where, apparent opening size (AOS) O_{95} indicates the approximate largest particle that would effectively pass through the filter. Sieving is done using glass beads of successively larger diameter until 5% passes through the filter; this size in millimeters defines the AOS, O_{95} based on ASTM D 4751 (ASTM, 1993). This apparent opening size is usually taken to be less than 90 μm based on Equation (2.7). D_{85} indicates the diameter of clay particles corresponding to 85% passing. The retention ability of the filter is described by:

$$\frac{O_{50}}{D_{50}} \leq 24 \tag{2.8}$$

Filter material may become clogged if the soil particles become trapped within the filter fabric. Clogging is prevented by ensuring that (Christopher and Holtz, 1985):

$$\frac{O_{95}}{D_{15}} \geq 3 \tag{2.9}$$

2.3.3 Discharge Capacity

Discharge capacity is an important parameter that controls the performance of prefabricated vertical drains. Only PVD with sufficient discharge capacity can function properly. There are two major uncertainties related to the discharge capacity of a vertical drain: the first is the determination of the required discharge capacity to be used in design (Holtz et al., 1991); the second is the measurement of drain discharge capacity in the laboratory and field. To measure discharge capacity it is necessary to simulate field conditions as closely as possible. According to Holtz et al. (1991), the discharge capacity depends primarily on the following factors:

(i) The area of the drain core available for flow (free volume);

(ii) The effect of lateral earth pressure (Figure 2.4);

(iii) Possible folding, bending, and crimping of the drain (Figure 2.3, Table 2.1); and

(iv) Infiltration of fine soil particles through the filter.

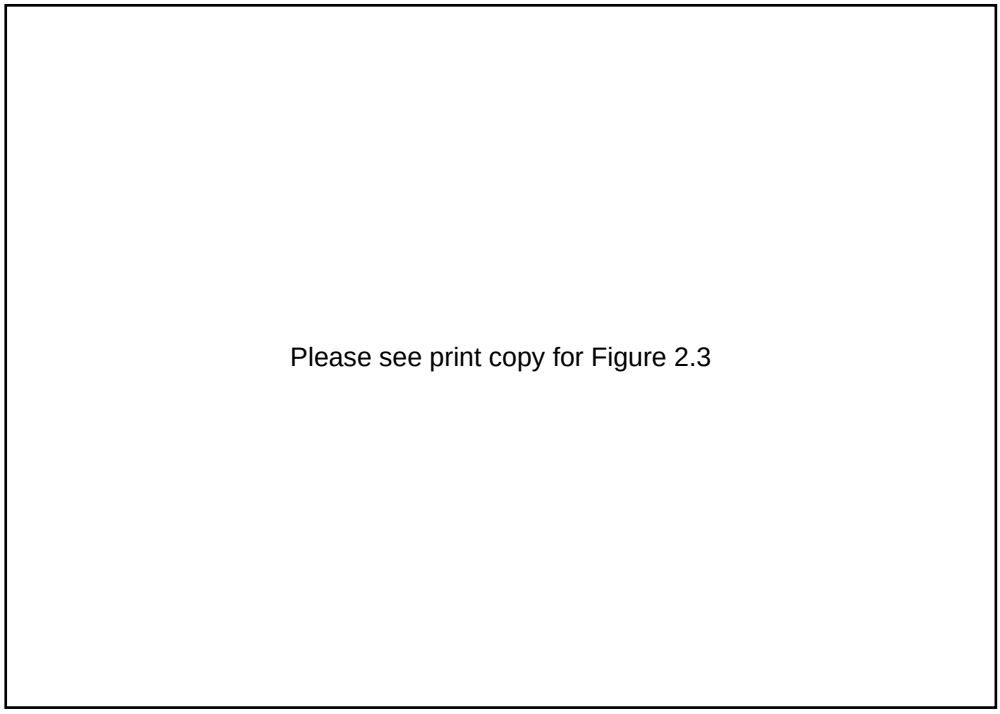

Figure 2.3 Possible deformation modes of PVD as a result of ground settlement (adapted from Bergado et al., 1996)

In design when specifying the discharge capacity q_w, Bergado et al. (1996) suggests that:

$$q_{w(\text{specified})} = F_c F_t F_{fc} q_{w(\text{required})} \tag{2.10}$$

where,

$F_c = 2$ is the reduction factor due to 20% bend and one clamp (Table 2.1)

$F_t = 1.25$ is the reduction factor due to lateral pressure

$F_{fc} = 3.5$ is the reduction factor due to filtration and clogging.

Thus,

$$q_{w(specified)} = 8.75 q_{w(required)} \tag{2.11}$$

$q_{w(required)}$ can be calculated from:

$$q_{w(required)} = \frac{\rho_\infty U_{10} l \pi c_h}{4 T_h} \tag{2.12}$$

where, ρ_∞ = final settlement, U_{10} = 10% degree of consolidation, l = depth of vertical drain, c_h = horizontal coefficient of consolidation and T_h = time factor for horizontal consolidation. The dependence of discharge capacity on lateral confining pressure for various drain types is shown in Figure 2.4 and Table 2.2.

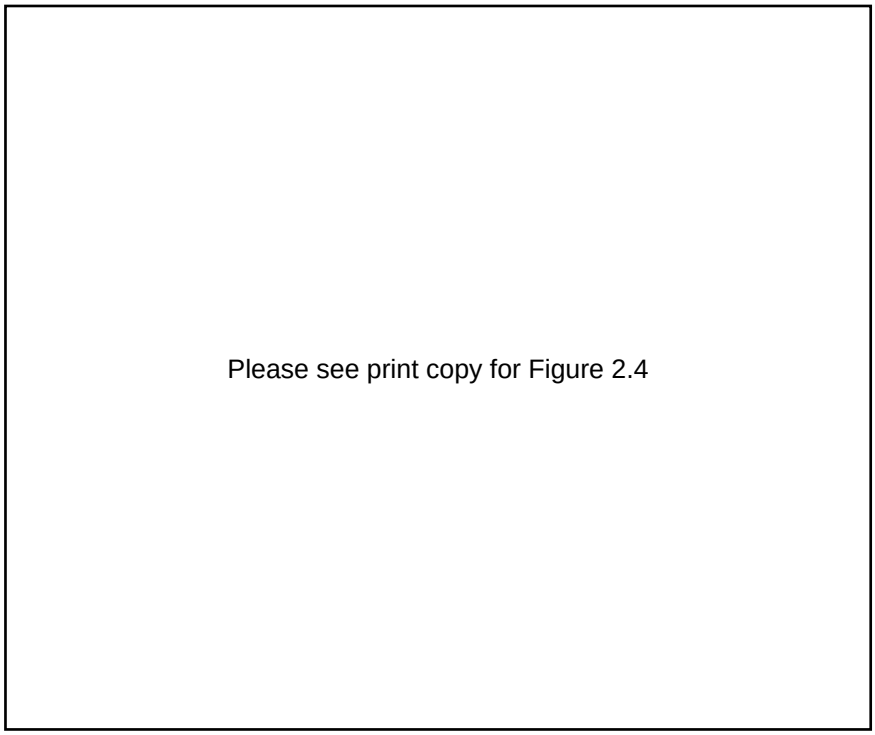

Figure 2.4 Typical values of vertical discharge capacity (after Rixner et al., 1986)

Table 2.1 Percentage reduction in discharge capacity for deformed PVD (Bergado et al., 1996)

Please see print copy for Table 2.1

Holtz et al. (1988) suggested that as long as the working discharge capacity of PVD exceeds 150 m^3/year after installation, the effect on consolidation of well resistance should not be significant. Indraratna and Redana (2000) stated that long term well resistance will be significant for PVD with q_w less than 40-60 m^3/year. However, discharge capacity can fall below this desired minimum value due to the reasons mentioned earlier. For certain types of PVD, affected by significant vertical compression and high lateral pressure, q_w values may be reduced to 25-100 m^3/year (Holtz et al., 1991). Clearly, the 'clogged' drains are associated with q_w values approaching zero.

Table 2.2 Short-term discharge capacity, in m^3/year, of eight band drains measured in laboratory (Hansbo, 1981)

Please see print copy for Table 2.2

Kremer et al. (1982) stated that the minimum vertical discharge capacity must be 160 m^3/year, under a hydraulic gradient of 0.625 applied across a 40 cm drain length, subjected to a 100 kPa confining pressure. Based on laboratory data and their experience Jamiolkowski et al. (1983) concluded that for an acceptable quality of drain q_w should be at least 10-15 m^3/year at a lateral stress range of 300-500 kPa, for drains that may be 20 m long. Hansbo (1987a) specified that q_w becomes a critical property for long drains if its capacity is less than 50-100 m^3/year. Holtz et al. (1991) reported that the q_w of PVD could vary from 100-800 m^3/year. For certain types of PVD affected by significant vertical compression and high lateral pressure, q_w values may be reduced to 25-100 m^3/year (Holtz et al., 1991). The current recommended values for discharge capacity are given in Table 2.3.

Table 2.3 Current recommended values for specification of discharge capacity (Suthananthan, 2005a)

Please see print copy for Table 2.3

2.3.4 Smear Zone

When vertical drains are installed in soft ground the soil surrounding the drain is disturbed as mandrels or augers/drills are inserted and withdrawn. The effects associated with this installation disturbance are termed smear effects, and are detrimental to radial consolidation. Compared to the undisturbed soil, permeability in the smear zone is reduced and compressibility is increased. Two processes are responsible for smear, remolding of the soil immediately adjacent to the drain, and consolidation of soil further away from the drain caused by dissipation of excess pore pressures created by cavity expansion when the mandrel is pushed into the soil (Sharma and Xiao, 2000). The extent of smearing depends on the mandrel size and soil type (Eriksson et al., 2000; Lo, 1998; Rowe, 1968). Highly sensitivity clays with prominent macro fabric generally exhibit the greatest smear effects. For clays with thin sand layers the smear effect is expected to be high as low permeable clay is smeared across high permeability sand (Hird and Moseley, 2000). Based on laboratory studies Hird and Sangtian (2002) report that the effect of smear on such

soils is only severe when $k_{\text{sand}}/k_{\text{clay}} > 100$. The shape of the smear zone is approximately elliptical around rectangular PVD (Indraratna and Redana, 1998a, Welker et al., 2000), and circular around sand drains.

A number of researchers have noted that the disturbance in the smear zone increases towards the drain (Chai and Miura, 1999; Hawlader et al., 2002; Sharma and Xiao, 2000; Hird and Moseley, 2000; Indraratna and Redana, 1998a; Madhav et al., 1993; Bergado et al., 1991). Laboratory studies on circular sand drains and rectangular PVD exhibit a parabolic decrease in horizontal permeability towards the drain as shown in Figures 2.5-2.7. The permeability close to the drain can be reduced by one order of magnitude (Bo et al., 2003) and is often assumed to be the same as the vertical permeability (Hansbo, 1981; Indraratna and Redana, 1998a). The vertical permeability remains relatively unchanged. The ratio of horizontal to vertical permeability (k_h/k_v) approaches unity at the drain soil interface (Indraratna and Redana, 1998a). For various undisturbed soils k_h/k_v varies between 1.36-2 (Tavenas et al., 1983; Shogaki et. al., 1995; Bergado et. al., 1991). Whereas in the smeared zone reduced values of 0.9-1.3 occur (Indraratna and Redana ,1998b).

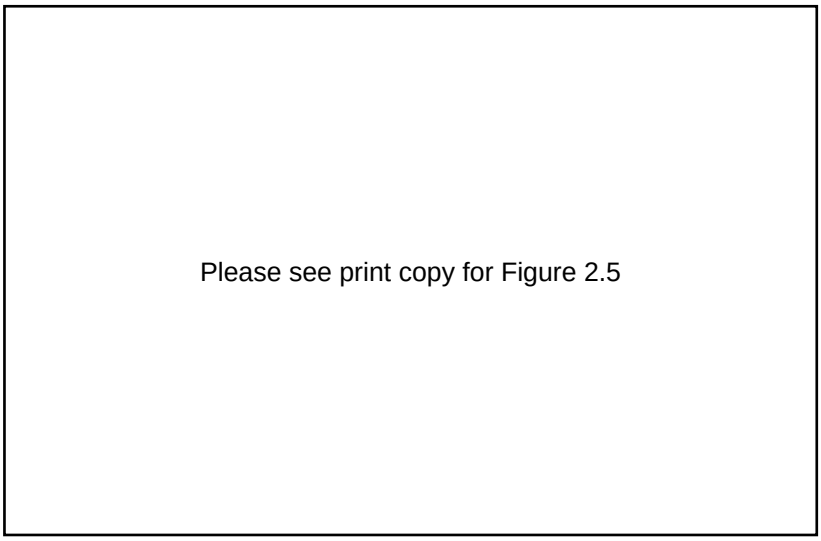

Figure 2.5 Variation of horizontal permeability around circular sand drain (original data from Onoue et al., 1991)

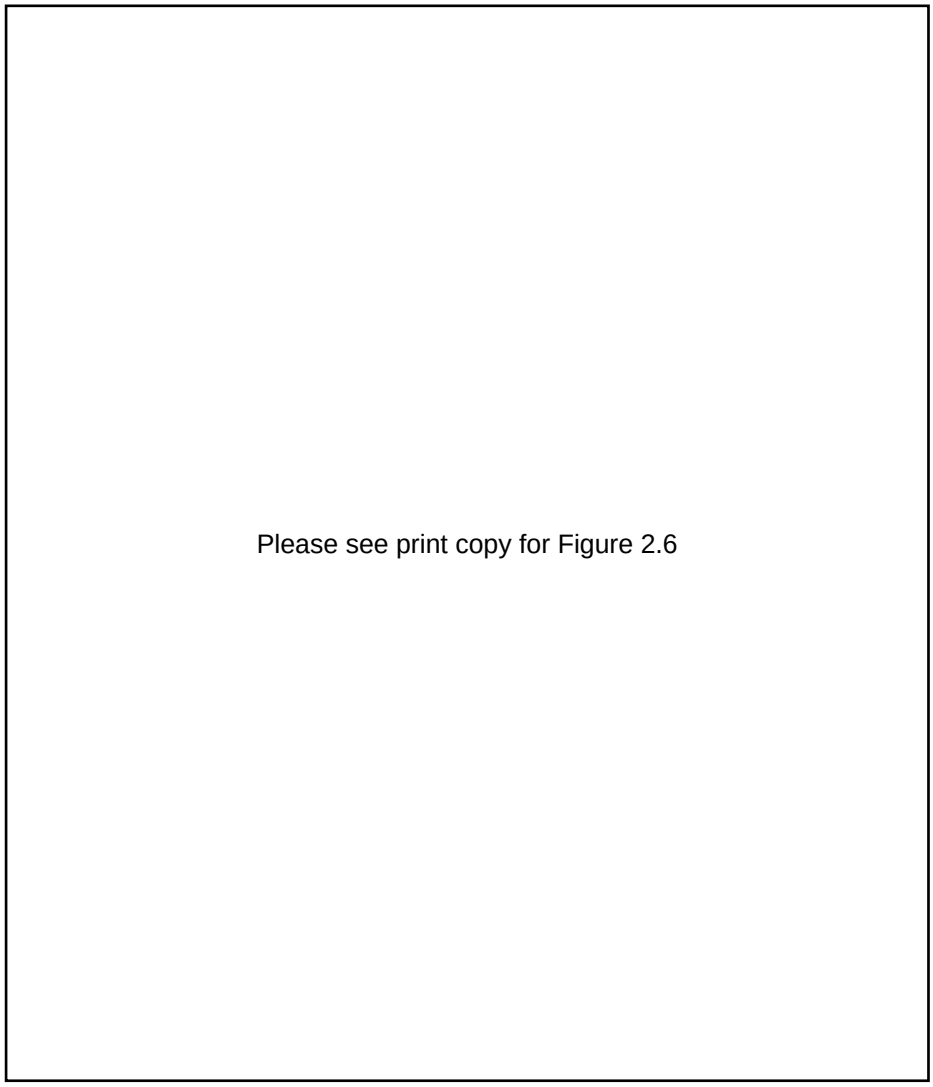

Figure 2.6 Variation of horizontal permeability around a) PVD band drain and b) circular sand drain (original data from Indraratna and Redana, 1998a)

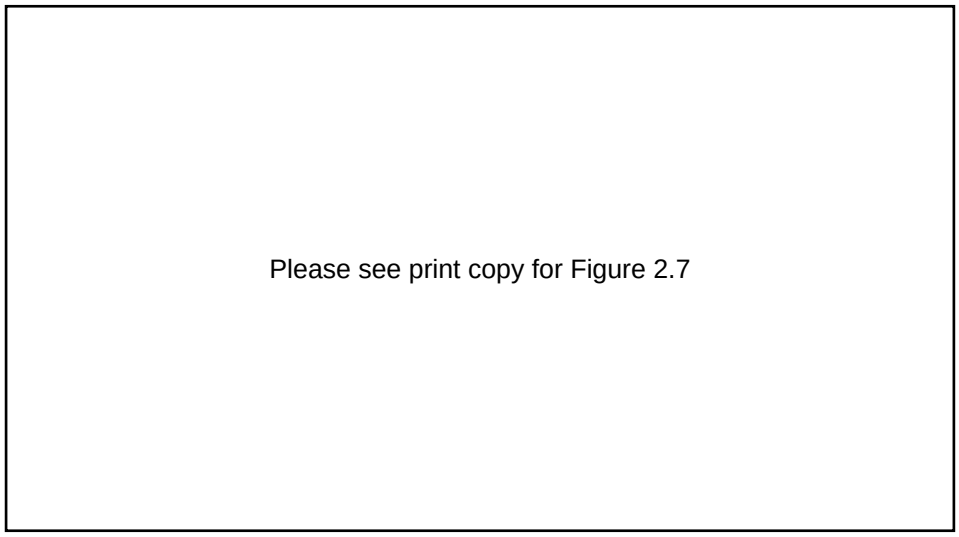

Figure 2.7 Variation of horizontal permeability around PVD band drain (original data from Indraratna and Sathananthan, 2005a)

Despite the observed variations in smear zone permeability the most common method of including smear effects in vertical drain analysis is to model smear as a zone of constant reduced permeability (Hansbo, 1981). This leads to ambiguity when considering the "size" of the smear zone. The outer radius of smear zone is typically designated r_s. But r_s can be defined as the point where the horizontal permeability begins to fall below the undisturbed permeability, or, the point at which a smear zone of constant reduced permeability exhibits equivalent effects to those associated with the actual permeability distribution. Values of r_s based on the later definition are smaller than those based on gradual variation of permeability, indicating that the permeability close to the drain has a greater effect on radial consolidation than permeability further from the drain (Chai and Miura, 1999; Hawlader et al., 2002; Sharma and Xiao, 2000; Hird and Moseley, 2000; Bergado et

al., 1991). Proposed smear zone parameters for a constant permeability smear zone are given in Table 2.4.

Table 2.4 Proposed smear zone parameters (after Xiao, 2001)

Please see print copy for Table 2.4

While a small zone of low permeability close to the drain will greatly effect radial consolidation rates (as all expelled water must pass through this zone), a small zone of increased compressibility, owing to its small volume, will not effect consolidation to a large extent. Perhaps this is why the soil compressibility in the smear zone is usually ignored. However, field trials of vertical drains at different spacing indicate that for smaller drain spacing, total settlement is higher and values of horizontal consolidation coefficient (back calculated ignoring smear zone compressibility

effects) are lower than for widely spaced drains (Saye, 2001; Arulrajah et al., 2004; Bergado et al., 2002). Both findings are consistent with smeared soil of increased compressibility making up a greater percentage of soil as drain spacing is decreased.

Also ignored in conventional analysis of smear is the possible variation of smear zone parameters with depth. Sathananthan (2005a) uses cavity expansion theory to predict excess pore pressures generated when a circular mandrel is inserted into the soft ground (using modified Cam-clay soil model). Sathananthan (2005a) proposes that the extent of smearing be the region in which the generated pore pressure is greater than the initial overburden stress (total stress). As the overburden stress and soil properties vary with depth so too would the smear zone parameters.

2.3.5 Important Parameters

There are many parameters that affect both the efficiency and the prediction accuracy of vertical drains. Though refinements are continually being made it is the gross properties of the system that are most influential. Even before analysis is performed an extensive knowledge of the preconsolidation history of the soil with depth should be known. Vertical drains are not effective unless the preconsolidation pressure is exceeded (Hansbo, 1981; Johnson, 1970; Indraratna et al., 1999). The drain spacing is very important. For doubling the well influence diameter it takes 6 times as long to reach 90% consolidation, while reducing the drain well diameter by a factor of 20 results in 4 times as long to reach 90% consolidation (Richart, 1957). Thus drain efficiency is influenced more by spacing than well diameter. Consolidation times can be reduced and smear and well resistance effects can be negated by decreasing the spacing between drains. The most important material parameter is the coefficient

of consolidation c_h (Zhou et al., 1999; Hong and Shang, 1998; Hansbo, 1987a). Accurate determination of c_h is often difficult. A probabilistic approach can be taken to account for possible variation in input parameters when calculating the degree of consolidation (Zhou et al., 1999; Hong and Shang, 1998). During the design process a sensitivity analysis should be conducted (Lau and Cowland, 2000).

Ideal drains are those not inhibited by well resistance or smear. Solutions modeled on such drains show the fastest dissipation of excess pore-water pressure. Ideal drains may be realistic for long term behaviour greater than 400 days (Indraratna et al., 1992), however, short-term settlements and pore pressure predictions are governed by drain efficiency. Ideal drains overpredict short-term settlement and pore pressure dissipation (Indraratna and Redana, 1998a). Inclusion of smear and well resistance improves prediction but still slightly over predicts settlement (Indraratna et al., 1999). When water is retarded from exiting the soil the increased duration of higher pore pressure allows greater mobilisation of shear strains. This leads to greater lateral deformation than if water escape was uninhibited. Thus ideal drains under predict lateral deformation (Indraratna and Redana, 2000). Lateral deformation can only be considered in multi-drain analysis.

2.4 Influence Zone of Drains

Vertical drains are commonly installed in square or triangular patterns (Figure 2.8). The area covered by pore water flowing to a single drain is known as the influence zone. To convert the square or hexagonal influence zones to equivalent circular zones for use in analytical solutions, a circle of equal area is calculated. The

corresponding influence radius, r_e, for triangular and square spacing arrangements depends on the drain spacing, S_p by:

$$r_e = 0.564 S_p \text{ (Square Pattern)} \tag{2.13}$$

$$r_e = 0.525 S_p \text{ (Triangular Pattern)} \tag{2.14}$$

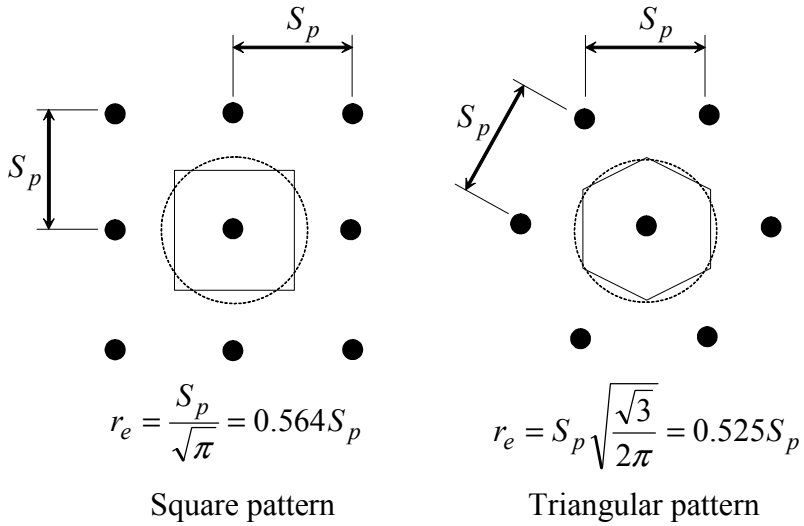

Figure 2.8 Vertical drain installation patterns

A square pattern of drains may be easier to lay out and control during installation in the field, however, a triangular pattern is usually preferred since it provides a more uniform consolidation between drains than the square pattern.

2.5 Fundamentals of Soil Consolidation

2.5.1 Soil Settlement

Conventionally, the deformation of embankments and the subsoil has four components (Athanasiu et al., 1999): immediate or distortion settlement (ρ_i), consolidation or primary settlement (ρ_c), secondary compression (ρ_s), and

settlement caused by lateral displacement (ρ_l). The total settlement (ρ_t) of a loaded soil is defined as:

$$\rho_t = \rho_i + \rho_c + \rho_s + \rho_l \tag{2.15}$$

Immediate settlement takes place immediately after the application of load and is occurs with zero volume change, i.e. shape change only. Primary compression is associated with pore water flow in the soil. When soil is loaded the incompressible pore water filling the voids initially takes the load. As the pore water gradually seeps out of the voids under a hydraulic gradient, pore water pressure dissipates, the load is transferred to the soil particles, and the void volume is reduced. The expulsion of water by dissipation of excess pore water pressure is called consolidation. Primary compression, the largest part of soft soil settlement, is the compression caused by consolidation. The secondary consolidation is due to effect of time-dependent stress-strain behaviour or soil structure viscosity. Two different approaches are commonly used. The first approach assumes that the secondary consolidation occurs after the end of primary consolidation (Mesri and Choi, 1985). For the other approach the creep behaviour is assumed during the entire primary consolidation process (Bjerrum, 1967; Tatsuoka et al., 2002). Lateral displacements are caused by the tendency of embankment loading to squeeze soil outwards. This creates a non-uniform settlement profile as shown in Figure 2.9. The settlement caused by lateral displacements will only be significant for large strains. The volume of settlements will equal the volume of lateral displacements. Lateral displacements are difficult to predict.

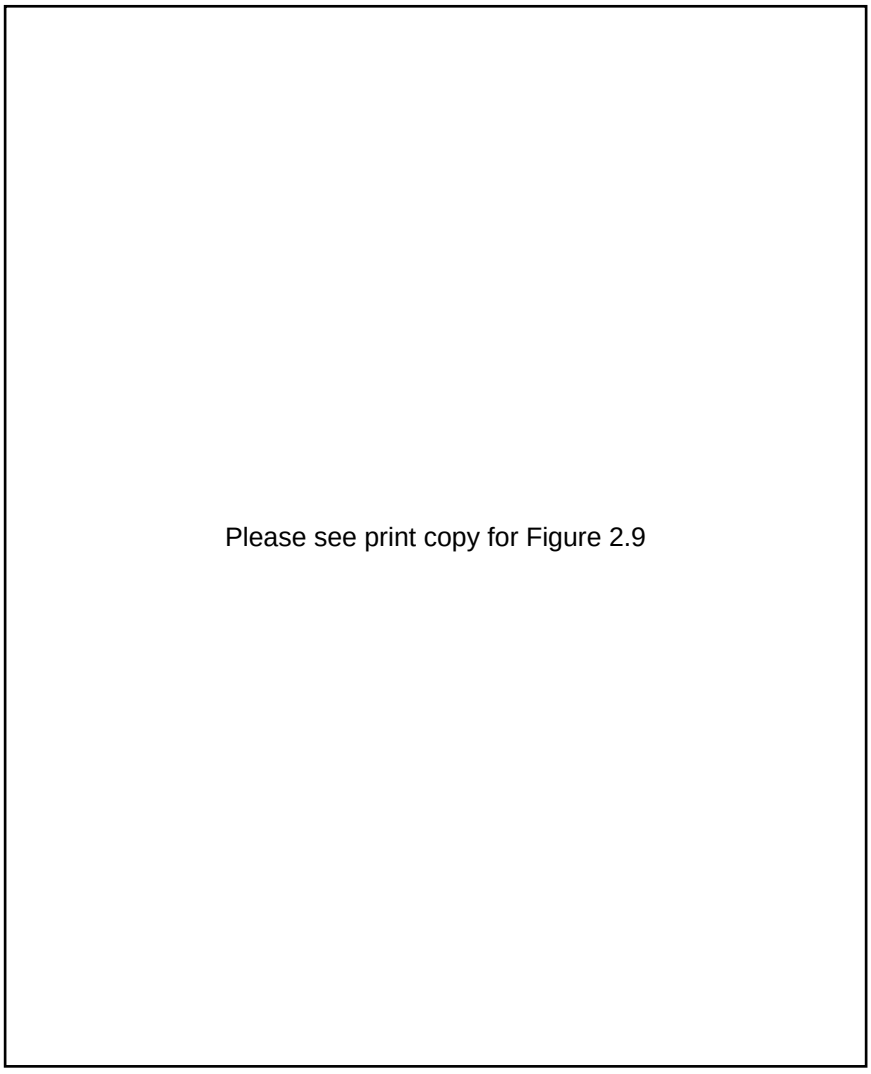

Figure 2.9 Patterns of soft soil settlement under embankments (after Zhang, 1999)

2.5.2 Consolidation Settlement

For soft soils of low permeability immediate settlement is negligible and consolidation settlement dominates. If the lateral deformations are negligible, then only Terzaghi type one-dimensional consolidation is expected. The process of consolidation is normally illustrated by Figure 2.10.

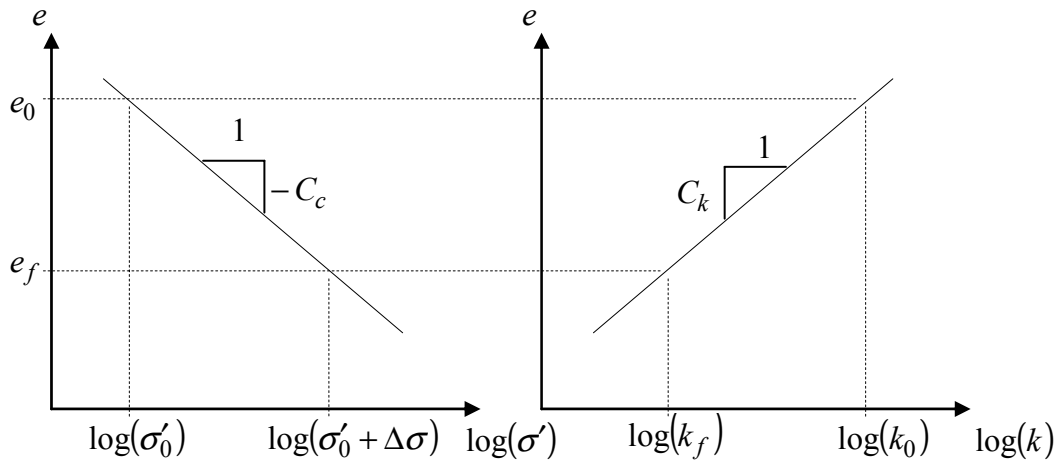

Figure 2.10 One-dimensional compression and void ratio-permeability relationship

To estimate consolidation settlement, the first step is to check whether the soil is normally consolidated or overconsolidated. The clay is called normally consolidated when the magnitude of preconsolidation pressure, σ'_p, determined from a laboratory test is equal to the present in-situ overburden pressure, σ'_0. When the preconsolidation pressure is larger than the present in-situ overburden pressure the clay is considered to be overconsolidated. If the initial and final effective stresses (σ'_0 and $\sigma'_0 + \Delta\sigma$) fall in the recompression zone then final settlements are calculated with:

$$\rho = \frac{HC_r}{1+e_0}\log\left(1+\frac{\Delta\sigma}{\sigma'_0}\right) \tag{2.16}$$

where, H = depth of soil, e_0 = initial void ratio. If the initial and final effective stresses fall in the compression zone then the final settlement is given by:

$$\rho = \frac{HC_c}{1+e_0}\log\left(1+\frac{\Delta\sigma}{\sigma'_0}\right) \tag{2.16b}$$

If the initial effective stress is less than the preconsolidation pressure, σ'_p, and the final effective stress is greater than the preconsolidation pressure then the final settlement is:

$$\rho = \frac{H}{1+e_0}\left((C_r - C_c)\log(OCR) + C_c \log\left(1+\frac{\Delta\sigma}{\sigma'_0}\right)\right) \tag{2.16c}$$

where, OCR is the overconsolidation ratio defined by:

$$OCR = \frac{\sigma'_p}{\sigma'_0} \tag{2.17}$$

2.5.3 Soil Permeability Characteristics

Permeability has a significant influence on the consolidation behaviour of soil. Figure 2.10, above, shows a semi-log relationship between permeability and void ratio. This is generally valid in the range of volumetric strains encountered in engineering practice. The relationship between coefficient of soil permeability and void ratio can be expressed by:

$$e = e_0 + C_k \log(k/k_0) \tag{2.18}$$

where, C_k = permeability change index, k_0 = initial permeability. Equation (2.18) is independent of the soil stress history (i.e., valid for over consolidated or normally consolidated clay) (Nagaraj et al., 1994). Tavenas et al. (1983) gave the following empirical relationship between permeability change index and initial void ratio:

$$C_k = 0.5e_0 \tag{2.19}$$

2.5.4 Increase in Shear Strength

For fine-grained soils when assessing the increase in shear strength due to consolidation, Mesri's (1975) empirical relation can be used:

$$S_u = 0.22\sigma' \tag{2.20}$$

where, $\sigma = \min(\text{effective vertical stress; preconsolidation pressure})$

For overconsolidated soil the shear strength is approximated by (Bergado et al., 2002):

$$\left(\frac{S_u}{\sigma'_{v0}}\right)_{\text{overconsolidated}} = \left(\frac{S_u}{\sigma'_{v0}}\right)_{\text{normal}} OCR^m \tag{2.21}$$

For Bangkok clays Bergado et al. (2002) found $S_u/\sigma'_{v0} = 0.22$ and $m = 0.8$. The normalization of undrained shear strength to vertical effective stress is known as the SHANSEP method (Ladd, 1991).

2.6 Vertical Consolidation Theory

2.6.1 Terzaghi's One-dimensional Theory

Terzaghi's theory of one-dimensional consolidation is widely used in engineering practice to predict compression rates and excess pore water dissipation in low permeability soils. The assumptions of the Terzaghi (1943) theory are:

a) Soils are homogeneous and fully saturated. Compressibility of soil and pore water is negligible;
b) Pore water flow is solely in the vertical direction;
c) The effect of geometry changes caused by soil compression is insignificant (i.e. small strain theory). The self-weight of soils is neglected.
d) Pore water flow is governed by Darcy's law;

e) There is a linear relationship between void ratio and effective stress that is independent of time and stress history;

f) The coefficient of soil permeability is assumed to be constant during the consolidation process; and

g) There is no creep occurring during soil settlements.

The governing equation based on the above assumptions is:

$$\frac{\partial^2 u}{\partial z^2} = c_v \frac{\partial u}{\partial t} \tag{2.22}$$

Equation (2.22) is a second order linear partial differential equation analogous to the heat equation. Solving Equation (2.22) for uniform instantaneous loading, Terzaghi gives the average degree of degree of consolidation (U_z) as a function the dimensionless time factor T_v:

$$U_z = 1 - \sum_{m=1}^{\infty} \frac{2}{M^2} \exp\left(-M^2 T_v\right) \tag{2.23a}$$

where

$$M = \pi(2m-1)/2\,,\ m = 1,2,3... \tag{2.23b}$$

$$T_v = \frac{c_v t}{H^2} \tag{2.23c}$$

H is the length of drainage path. Non-uniform pore pressure distributions can be used in the solution of Equation (2.22) (Singh, 2005). Figure 2.11 shows the consolidation curves for initial pore pressure distributions that vary in a linear fashion across the soil layer.

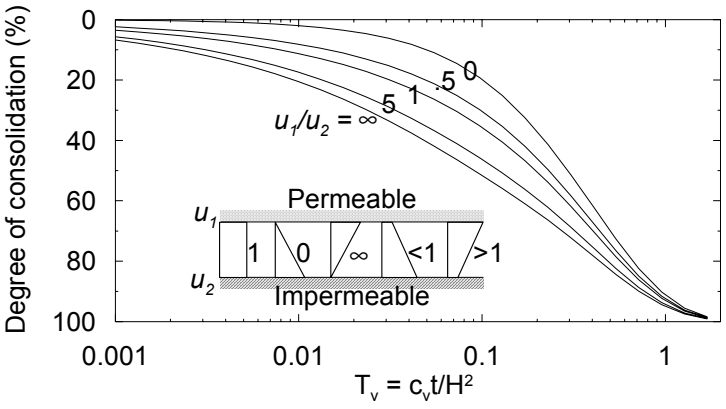

Figure 2.11 Consolidation curves for vertical drainage

Since Terzaghi's solution, developments in vertical consolidation have arisen by relaxing some of the assumptions in Terzaghi's theory. Morris (2005) developed analytical solutions to one-dimensional consolidation assuming finite strain. Fox and Berles (1997) use finite difference techniques with a piecewise linear formulation for large strain consolidation. Fox and Berles (1997) give correction factors for Terzaghi 1-D consolidation to account for change in drainage layer thickness. For a final strain (ρ_∞ / H_0) of 0.4, the decrease in time to reach a certain degree of consolidation is 30%. Fox and Qui (2004) use the finite difference method to include compressibile pore fluid. Xie and Leo (2004) consider one-dimensional large strain consolidation with variable compressibility and permeability. Small strain settlement prediction is larger than large strain prediction. Small strain pore pressure and settlement evolution is slower than large strain evolution. Yang et al. (2002) simulate the consolidation of lumpy dredged material by modeling inter-lump voids and intra-lump voids. Zhu and Yin (2005a) study the pore pressure dissipation after dredged material has ceased to be deposited. Zhu and Yin (1998) consider consolidation of soil under depth dependant ramp load. Vaziri and Christian (1994) allow for slightly unsaturated ground conditions.

2.7 Radial Consolidation Theory

2.7.1 Equal Strain Hypothesis

The first conventional procedure for predicting radial consolidation was introduced by Barron (1948). This approach was based on the consolidation theory of Terzaghi (1925). Barron (1948) developed the exact (rigorous) solution of vertical drain based on 'free strain hypothesis' and an approximate solution based on 'equal strain hypothesis'. For equal strain conditions horizontal sections remain horizontal throughout consolidation process. The difference between free and equal strain cases was found to be negligible so equal strain case was used. Barron also included the effects of smear (for equal strain) and well resistance (for equal and free strain). Solutions involved Bessel functions and were time consuming to perform. As a result the effects of smear and well resistance were often ignored to simplify calculations (Hansbo, 1981). Han and Ye (2002) produced equal strain solutions for radial drainage to a stone column which explicitly incorporated the stiffness of the stone column.

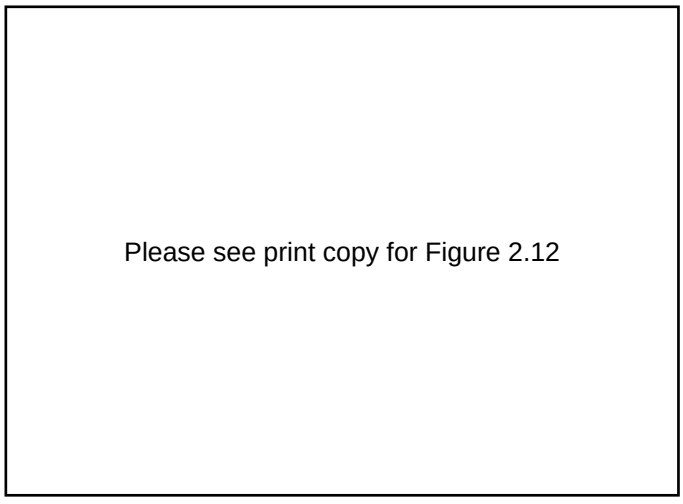

Figure 2.12 Schematic of soil cylinder with vertical drain (after Hansbo,1979)

Figure 2.12 shows the schematic illustration of a soil cylinder with a central vertical drain, where, r_w = drain radius, r_s = smear zone radius, r_e = soil cylinder radius and l = the length of the drain installed into the soft ground. The coefficient of permeability in the vertical and horizontal directions are k_v and k_h. k_s is the coefficient of permeability in the smear zone. By considering the flow into and out of an infinitesimal cylindrical element the governing equation for consolidation by radial drainage (Barron, 1948) is given by:

$$\frac{\partial u}{\partial t} = c_h\left(\frac{\partial^2 u}{\partial r^2} + \frac{1}{r}\frac{\partial u}{\partial r}\right) \tag{2.24}$$

where, t is the time elapsed after the load is applied, u is the excess pore water pressure at radius r and at depth z. Under equal strain conditions the left hand side of Equation (2.24) becomes dependant on the average excess pore pressure, $\bar{u}$. Hence:

$$\frac{\partial \bar{u}}{\partial t} = c_h\left(\frac{\partial^2 u}{\partial r^2} + \frac{1}{r}\frac{\partial u}{\partial r}\right) \tag{2.25}$$

Hansbo (1981) uses a different approach where by the volume of water flowing through the inner wall of an annulus of soil is assumed equal to the volume change in the annulus. Solution of the two equal strain equations by Barron (1948) and Hansbo (1981) result in similar expressions for pore water pressure. Hansbo's (1981) solution is:

$$\bar{u} = \Delta\sigma \exp\left(\frac{-8T_h}{\mu}\right) \tag{2.26}$$

where,

$$T_h = \frac{c_h t}{4r_e^2} \tag{2.27}$$

$$\mu = \ln\left(\frac{n}{s}\right) + \left(\frac{k_h}{k_s}\right)\ln(s) - 0.75 + \pi z(2l - z)\left(\frac{k_h}{q_w}\right) \tag{2.28a}$$

In the above equations $n = r_e / r_w$ is the drain spacing ratio and $s = r_s / r_w$ is the smear zone size ratio. When ignoring well resistance, the term with q_w in Equation (2.28) is omitted. For an ideal drain with no smear or well resistance:

$$\mu = \ln(n) - 0.75 \tag{2.28b}$$

Consolidation curves for an ideal drain are illustrated in Figure 2.13.

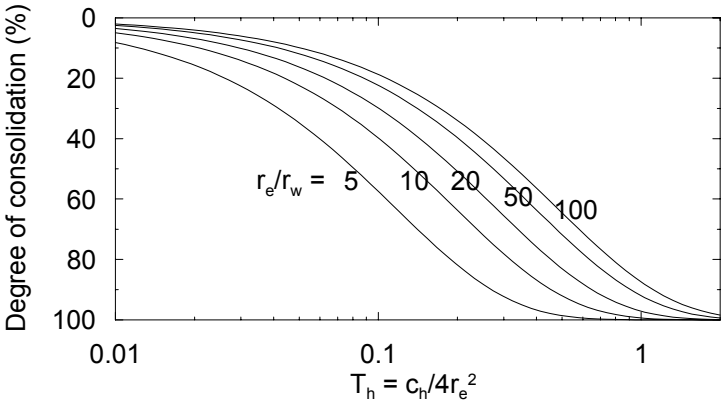

Figure 2.13 Radial consolidation curves for an ideal drain

2.7.2 λ method (Hansbo, 1979, 1997, 2001)

Hansbo (1979, 1997, 2001) developed alternate radial consolidation equations based on a non-Darcian flow law. The deviation from Darcy's law is supported by the full-scale field test at Ska-Edeby, Sweden. Below a critical hydraulic gradient pore water flow is non-Darcian exhibiting a power law flow relation. Hansbo (1979) proposes the following flow relationships:

$$v = \begin{cases} \widetilde{k} i^n & i \le i_l \\ k(i - i_0) & i \ge i_l \end{cases} \tag{2.29}$$

where, $i_l = \dfrac{ni_0}{n-1}$ is the critical hydraulic gradient, and $\widetilde{k} = \left(n^{-1} i^{1-n}\right) k$. The average pore water pressure for radial drainage incorporating the above non-Darcian flow relations are given by (Hansbo, 2001):

$$U_h = 1 - \left[1 + \frac{\lambda t}{\alpha d_e^2}\left(\frac{\Delta\sigma}{d_e \gamma_w}\right)^{n-1}\right]^{1/(n-1)} \tag{2.30a}$$

where,

$$\lambda = \frac{\widetilde{k}_h}{m_v \gamma_w} \tag{2.30b}$$

$$\alpha = \frac{n^{2n}\beta^n}{4(n-1)^{n+1}} \tag{2.30c}$$

$$\begin{aligned}\beta = {} & \frac{1}{3n-1} - \frac{n-1}{n(3n-1)(5n-1)} - \frac{(n-1)^2}{2n^2(5n-1)(7n-1)} \\ & + \frac{1}{2n}\left[\left(\frac{\widetilde{k}_h}{\widetilde{k}_s} - 1\right)\left(\frac{d_e}{d_w}\right)^{(1/n-1)} - \frac{\widetilde{k}_h}{\widetilde{k}_s}\left(\frac{d_e}{d_w}\right)^{(1/n-1)}\right] \\ & - \left(\frac{1}{2n} - \frac{1}{3n-1}\right)\left[\left(\frac{\widetilde{k}_h}{\widetilde{k}_s} - 1\right)\left(\frac{d_e}{d_w}\right)^{(1/n-3)} - \frac{\widetilde{k}_h}{\widetilde{k}_s}\left(\frac{d_e}{d_w}\right)^{(1/n-3)}\right] \\ & + \frac{\widetilde{k}_h}{2q_w}\pi z(2l - z)\left(1 - \frac{1}{n}\right)\left(\frac{d_e}{d_w}\right)^{(1/n-1)}\left(1 - \frac{d_w^2}{d_e^2}\right)^{1/n}\end{aligned} \tag{2.30d}$$

If $n = 1.0001$ is substituted into Equation (2.30) the resulting value of average pore pressure is the same as for the Darcian equations presented above.

2.7.3 Determination of Radial Coefficient of Consolidation

2.7.3.1 Log U vs t approach

Aboshi and Monden (1963) presented a curve fitting method using $\ln(U)$ and linear t. This method is developed by taking the natural 'log' on both sides of Barron or Hansbo's solution (Equation 2.26) and rearranging, to give the following expression:

$$\ln(1-U) = -\frac{8c_h t}{4r_e^2} \tag{2.31}$$

It follows from Equation (2.31) that the coefficient of radial consolidation c_h can be determined from the slope of the $\ln(1-U)$ vs T_h plot as shown in (Figure 2.14). The average degree of consolidated can be determined by settlement data or pore pressure data.

Please see print copy for Figure 2.14

Figure 2.14 Aboshi and Monden (1963) method for determining c_h

2.7.3.2 Plotting Settlement Data (Asaoka, 1978)

Asaoka (1978) developed a method where a series of settlement measurements ($\rho_1,...,\rho_{n-1},\rho_n$) observed at constant time intervals are plotted as shown in

Figure 2.15. The coefficient of radial drainage in this method is derived using Barron (1948) or Hansbo's (1981) solution, which is given by:

$$c_h = \frac{-r_e^2 \mu}{8} \frac{\ln(\beta)}{\Delta t} \tag{2.32}$$

where, β is the slope of the line formed by the observed displacement data, and Δt is the time interval between observations. The ultimate settlement can be found from incomplete settlement data by extrapolating the straight line Asoaka plot to the 45° line. Matyas and Rothenburg (1996) and Cao et al. (2001) observed that Asaoka plots exhibit two straight lines. Ultimate settlements determined from the first line (U = 25-45%) are under predicted by up to 30%. The second line (U >45%) gives correct values. Larger time intervals give better predicted values.

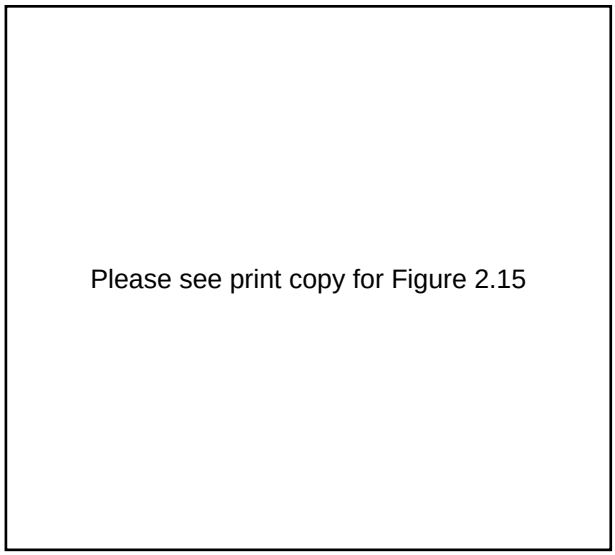

Figure 2.15 Asaoka (1978) method for determining c_h

2.7.4 Curve Fitting Method (Robinson and Allam, 1998)

Laboratory time-compression data can be divided into three parts:

1. Initial compression (ρ_i)

2. Primary consolidation (ρ_∞)

3. Secondary compression

Ignoring the later Robinson and Allam (1998) show that displacement δ for vertical consolidation is given by:

$$\rho = \rho_\infty \left[1 - \frac{8}{\pi^2} \sum_{m=0}^{\infty} \frac{1}{(2m+1)^2} \exp\left(-\frac{\pi^2}{4} (2m+1)^2 \frac{c_v t}{H^2} \right) \right] + \rho_i \qquad (2.33)$$

The three unknowns (ρ_i, ρ_∞, c_v) can be solved with data from three time-compression readings. More accurate values will be obtained with more points using regression analysis. Similarly the three unknowns for radial consolidation (ρ_i, ρ_∞, c_h) can be solved for three or more time-compression points according to Robinson and Allam (1998):

$$\rho = \rho_\infty \left[1 - \exp\left(\frac{-8 c_h t}{r_e^2 \mu} \right) \right] + \rho_i \qquad (2.34)$$

2.8 Combined Vertical and Radial Consolidation Theory

2.8.1 Single Layer Consolidation

In vertical drain consolidation problems the radial component of flow is often much larger than the vertical component. As such consolidation due to vertical flow in the soil is ignored in many cases, especially for long drains. When vertical drainage does becomes significant it must be included in any analysis. Yoshikuni and Nakanodo (1974) presented an early solution to free strain consolidation by vertical and radial drainage. Their solution includes well resistance. Zhu and Yin (2001) have produced design charts on the same problem under ramp loading ignoring well resistance. Both solutions are lengthy, involving double summation series solutions.

Using separation of variables, radial drainage is solved with Bessel functions while the vertical drainage is solved with Fourier sine series. The coupled problem is significantly simplified if the flow in the vertical direction is assumed to occur due to the average hydraulic gradient across a radial cross section. This approach was taken by Tang and Onitsuka (2000) who produced a solution with a single Fourier series. Leo (2004) determined that a closed form solution could be found to the equal strain problem. Leo's (2004) solution under instantaneous or ramp loading used modified Bessel functions. The advantage of a closed form solution (like Terzaghi's one-dimensional equation) is that each term in the series summation is a simple expression rather than the zeros of a transcendental equation, as is the case for Yoshikuni and Nakanodo (1974) and Zhu and Yin (2001).

The solutions mentioned above can be difficult to implement so attempts have been made to consider combined vertical and radial drainage in an approximate manner. The simplest and oldest method is that of Carillo (1942) where the total degree of consolidation is related to the separately considered radial and vertical degrees of consolidation by the following expression:

$$(1-U)=(1-U_v)(1-U_r) \tag{2.35}$$

The above relationship is valid for homogeneous soil conditions; for ramped loading Tang and Onitsuka (2000) and Zhu and Yin (2001) showed than Carillo's solution was not strictly applicable but the discrepancy was small.

Chai et al. (2001) proposed a simplified method for approximating the effect of vertical drains. Vertical drains increase the mass permeability in the vertical

direction. An equivalent vertical permeability (K_{ve}) was derived based on equal average degree of consolidation:

$$K_{ve} = \left(1 + \frac{2.26L^2 k_h}{\mu d_e^2 k_v}\right) k_v \tag{2.36}$$

The approximate degree of consolidation is then given by

$$U_z = 1 - \exp(-3.54) T_v \tag{2.37}$$

where

$$\mu = \ln\left(\frac{d_e}{d_w}\right) + \left(\frac{k_h}{k_s} - 1\right)\ln\left(\frac{d_s}{d_w}\right) - \frac{3}{4} + \frac{\pi 2 l^2 k_h}{3 q_w} \tag{2.38}$$

d_e is the equivalent influence zone diameter; d_w is the equivalent drain diameter; d_s is the smeared zone diameter; k_s and k_h are the smeared and undisturbed horizontal permeability; l is the length of one-way drainage; q_w is the discharge capacity. When calculating the equivalent vertical permeability in each layer of a multi-layered analysis l is taken as the total length of one-way drainage not the height of each layer.

2.8.2 Multi-layered Consolidation

Soil is rarely homogeneous and so to successfully predict consolidation behaviour of real soil, heterogeneity must be modeled. By introducing multiple soil layers the analytical solution to consolidation problems is much more complicated compared to the relatively straight forward solutions mentioned above for single soil layers. Because analytical solutions are tedious to implement, recourse is often made to numerical methods such as the finite difference method (Fox et al., 2003; Nash and Rhyde, 2001; Onoue, 1988b) and finite element method (Li and Rowe, 2001; Zhu

and Yin, 2000; Indraratna and Redana, 2000, Duncan, 1999; Britto and Gunn, 1987). Numerical methods have the advantage of being able to model multiple drains and stress/time dependant soil properties. The analytical solutions that have been developed for multi-layered soil consolidation consider flow in a cylindrical cell. The solutions are quite lengthy but generally involve the following steps:

1. Derive the continuity equation for each soil layer by considering the flow into and out of an infinitesimal soil element. If well resistance is ignored then the continuity equation in each layer is often:

$$\frac{\partial u}{\partial t} = c_v\left(\frac{\partial^2 u}{\partial z^2}\right) + c_h\left(\frac{\partial^2 u}{\partial r^2} + \frac{1}{r}\frac{\partial u}{\partial r}\right) \tag{2.39}$$

2. Using the separation of variables technique, determine the general solution to each of the separated differential equations and the relationship between the separation constants. The general solution for the radial component often utilizes Bessel functions (J_0, Y_0 etc.) while the vertical component uses trigonometric (sin, cos) and sometimes hyperbolic (sinh, cosh) functions.
3. The general solution to the partial differential equation in each layer usually has two unknown constant coefficients which must be determined. Boundary conditions such as equality of pore pressure at layer interfaces, equivalence of volume flow into and out of layer interfaces, and zero pore pressure at a fully drained boundary provide the constraints to solve for the unknowns. By substituting the general solution into each of the boundary condition expressions, a series of equations relating the unknown coefficients and separation constants is revealed. This set of equations is conveniently represented in matrix notation:

$$\mathbf{A}\mathbf{x} = 0 \tag{2.40}$$

where, **A** is a matrix dependant on the separation constant, and **x** is the vector of unknown coefficients. For non-trivial solutions of Equation (2.40) the determinant of **A** must be equal to zero. By varying the separation constant an infinite number of values (eigenvalues) are found which yield a zero determinant for matrix **A**. Substituting each of the eigenvalues into Equation (2.40) a series of unknown coefficients that match each eigenvalue can be determined. By assuming the value of one of the coefficients all other coefficients are determined in relation to the single assumed coefficient.

4. Using the initial condition (often a constant pore pressure value at time zero) the value of the assumed coefficient can be found by Fourier series analysis and treatment of the appropriate othogonality relationships.

The above steps have been followed by various authors in order to study multi-layered consolidation problems. A number of solutions exist for two layer systems. Zhu and Yin (2005b) presented design charts for vertical drainage with two layers. Xie et al. (1999) solved the same problem with partially drained boundaries, while Xie et al. (2002) incorporated small strain theory and nonlinear soil properties where the decrease in permeability is proportional to the decrease in compressibility.

Double layered ground with radial and vertical drainage is studied by Tang and Onitsuka (2001), Wang and Jiao (2004), and Tang (2004). The two layer solutions can be used to study partially penetrating vertical drains. For more than two layers Schiffman and Stein (1970) presented equations for vertical drainage, and Horne (1964) presented equations including radial drainage. More recent work has developed newer techniques for modeling stratified soil. Chen et al. (2005) introduced the differential quadrature method to analyse one-dimensional

consolidation of multiple soil layers. The differential quadrature method approximates the derivates in the continuity equation yielding a series of matrix equations to be solved. Nogami and Li (2002, 2003) use the matrix transfer method in considering radial/horizontal and vertical flow in layered soil with thin sand layers, greatly simplifying the determination of eigenvalues in the vertical direction.

It may not always be convenient to use the complicated analytical solutions or numerical methods. In such cases the degree of consolidation in multi-layered soils can still be approximated. Onoue (1988b) suggested that the multi-layered pore pressure distribution can be approximated by adding the relevant parts of each pore pressure distribution calculated by assuming homogeneous soil conditions with soil properties from each layer over the entire depth of the multiple layers (see Figure 2.16). The degree of consolidation in each layer found and combined to give the layer-thickness-weighted mean. The largest error in this method occurs when the layers are of equal height and there is a large degree of heterogeneity. When $c_{h1}/c_{h2} > 1$ consolidation is overestimated. Consolidation is underestimated for $c_{h1}/c_{h2} < 1$. If $1/10 < c_{h1}/c_{h2} < 10$ then the approximate method is accurate to within 4%.

Please see print copy for Figure 2.16

Figure 2.16 Approximate pore pressure distribution for multi-layered soil (after Onoue, 1988b)

2.9 Application of Vacuum Preloading (Indraratna et al. 2005b)

Indraratna et al. (2005b) presented radial consolidation equations for combined surcharge and vacuum loading (Figure 2.17). The vacuum pressure is assumed to vary in a linear fashion from a value of p_0 at the soil surface to $k_1 p_0$ at the bottom of the drain. The resulting excess pore pressure is described by:

$$\frac{\bar{u}}{\Delta\sigma} = \left(1 + \frac{(1+k_1)p_0}{\Delta\sigma}\right)\exp\left(\frac{-8T_h}{\mu}\right) - \frac{(1+k_1)p_0}{\Delta\sigma} \tag{2.41}$$

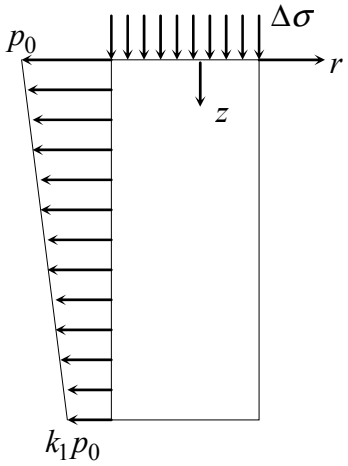

Figure 2.17 Linear variation of vacuum pressure with depth

2.10 Summary

Vertical drains have been widely used to accelerate primary consolidation of soft soils. However, it is difficult to predict the settlements and pore pressures accurately due to the difficulty in estimating the correct values of soil parameters. Particularly important is determination of the coefficient of consolidation, which is central to vertical and radial consolidation problems. Complicating the determination of c_h is the smear zone around vertical drains. Drain installation will result in reduced permeability and increased compressibility adjacent to the drain. The next Chapter provides a more realistic representation of the smear zone compared with the traditional smear zone, which is modeled with reduced permeability, constant with radial distance. The resistance to flow within the drain itself is also an important parameter, but less so with modern prefabricated vertical drains exhibiting high discharge capacity.

Once appropriate soil parameters have been determined they can be used in the numerous analytical solutions available for consolidation problems. Analytical solutions tend to fall into two categories: simple solutions to single soil layers, and complicated solutions for two or more soil layers. When the analytical solutions are inadequate recourse is made to numerical methods such as finite difference of finite element techniques. Powerful analytical solutions are developed in the next Chapter to study vertical drain consolidation. One model considers the change of soil properties with effective stress. Another model, based on the spectral method solution to partial differential equations, provides the ability to analyse multi-layered consolidation problems with vacuum and surcharge loading. Both models developed

in the next Chapter are significant contributions to the vertical drain literature described in this Chapter.

3 THEORETICAL CONSIDERATIONS

3.1 General

This Chapter presents the theoretical basis for three novel contributions to the simulation of soil consolidation problems: (i) treatment of spatially non-constant soil properties in the smear zone of vertical drain problems (radial drainage only); (ii) incorporation of void ratio dependant soil properties and non-Darcian flow in vertical drain problems (radial drainage only); and (iii) the consolidation of multi-layered soil with surcharge and vacuum loading (vertical and radial drainage). Analytical solutions to each consolidation problem are presented based on a unit-cell, equal strain approach to radial drainage.

The variation of smear zone properties is considered in Section 3.2 where the smear zone μ parameter is determined for a linear and parabolic variation of soil properties. The gradual reduction in permeability towards the drain is a more accurate representation of the smear zone than the traditional constant permeability smear zone (Chai and Miura, 1999; Hawlader et al., 2002; Sharma and Xiao, 2000; Hird and Moseley, 2000; Indraratna and Redana, 1998a; Madhav et al., 1993; Bergado et al., 1991). By considering the increased extent of smearing with the linear and parabolic variations (compared to the empirically determined constant permeability smear zone size), the possibility of overlapping smear zones becomes apparent. Overlapping smear zones (investigated with the linear smear zone model) provide some explanation for the apparent lower bound drain spacing, described by Saye (2001), below which no increase in rate of consolidation occurs.

The various μ parameters developed in Section 3.2 may be used in the new consolidation model (presented in Section 3.3) if Darcian flow is assumed. This model investigates three aspects of nonlinearity: non-Darcian flow, a log-linear void ratio-stress relationship, and a log-linear void ratio-permeability relationship. An analytical solution, in the form of an infinite series, is found, which explicitly describes the dissipation of excess pore water pore pressure for normally and overconsolidated soils under instantaneous loading. By using an approximate method to allow for non-constant loading, purely radial drainage problems in which permeability and compressibility changes are important can be analysed.

For problems where the time dependant nature of the soil properties is not important but the spatial variation of properties is, a second new consolidation model (presented in Section 3.4) for multi-layered soil including vertical and radial drainage can be used. Again the new μ parameters developed in Section 3.2 can be used as the model is based on equal strain conditions and Darcian flow. Where the model differs to other analytical methods is in distinctly different and novel use of linearly distributed material properties with depth. This allows an arbitrary distribution of properties (constant with time) to be investigated. By incorporating surcharge and vacuum loading that vary with both depth and time, a wide range of consolidation problems can be analysed.

The two new consolidation models provide an intermediate step between the simplest analytical models (such as Terzaghi, 1948; Hansbo, 1981) and time consuming numerical methods. Together with the more realistic representation of smear effects,

the models described in this Chapter give valuable insight into soil mechanics phenomena.

3.2 Determination of μ Parameter Based on Smear Zone Characteristics and the Associated Soil Properties

3.2.1 General Approach to Equal Strain Radial Consolidation with Darcian Flow

Vertical drains, installed in a square or triangular pattern, are usually modeled analytically by considering an equivalent axisymmetric system. Pore water flows from a soil cylinder to a single central vertical drain with simplified boundary conditions. Figure 3.1 shows a unit cell with an external radius r_e, drain radius r_w, and an initial drainage path length l.

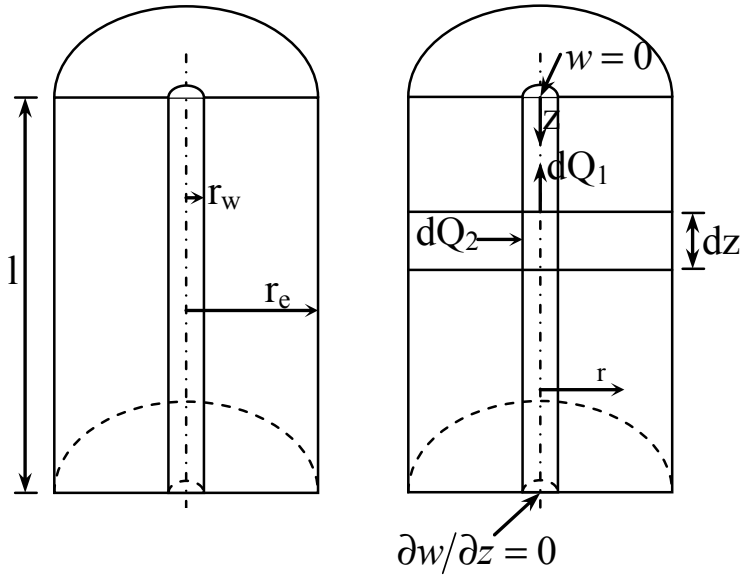

Figure 3.1 Axisymmetric unit cell

Outlined below are the steps involved in calculating the rate of consolidation for radial drainage under equal strain conditions. Of greatest significance is the calculation of the μ parameter which describes the effect of smear zone and drain

spacing properties. In subsequent sections, the general approach is applied to specific soil property and geometry configurations.

STEP 1: Assign soil and geometry parameters.

The soil is subdivided into radial segments and each segment is assigned values of horizontal permeability, k_h, and volume compressibility m_v. The permeability and compressibility need not be constant in each segment though this is traditionally the case.

STEP 2: Determine the radial pore pressure gradient in each soil segment.

The velocity of water flow at radius r (Darcy's law), is given by:

$$\upsilon_r = \frac{k_h(r)}{\gamma_w}\frac{\partial u}{\partial r} \tag{3.1}$$

The rate of fluid flow through the internal face of the hollow cylindrical slice with internal radius r and thickness dz is then determined by:

$$2\pi r \frac{k_h(r)}{\gamma_w}\frac{\partial u}{\partial r} dz \tag{3.2}$$

The rate of volume change in the hollow cylindrical slice with internal radius r, outer radius r_e, and thickness dz is:

$$\pi\left(r_e^2 - r^2\right)\frac{\partial \varepsilon}{\partial t} dz \tag{3.3}$$

For continuity, the volume changes in Equations (3.2) and (3.3) can be equated and rearranged to give the pore pressure gradient in the radial direction as:

$$\frac{\partial u}{\partial r} = -\frac{\gamma_w}{2k_h(r)}\left(\frac{r_e^2}{r} - r\right)\frac{\partial \varepsilon}{\partial t} \tag{3.4}$$

STEP 3: Determine the pore water pressure in the drain.

The pore water pressure in the drain at depth z is designated $w(z)$. For vertical flow in the drain, the change in flow from the entrance to the exit face of the slice with thickness dz (Figure 3.1) is given by:

$$dQ_1 = \frac{\pi r_w^2 k_w}{\gamma_w}\left(\frac{\partial^2 w(z)}{\partial z^2}\right) dzdt \tag{3.5}$$

where, k_w = drain permeability.

The radial flow into the slice is determined from:

$$dQ_2 = \pi\left(r_e^2 - r_w^2\right)\frac{\partial \varepsilon}{\partial t}\, dzdt \tag{3.6}$$

Assuming no sudden drop in pore pressure at the drain-soil boundary (that is, $u = w$ at $r = r_w$), then for continuity,

$$dQ_1 = dQ_2 \tag{3.7}$$

Substituting Equations (3.5) and (3.6) into Equation (3.7) and rearranging gives:

$$\frac{\partial^2 w(z)}{\partial z^2} = \frac{\gamma_w}{q_w}\pi\left(r_e^2 - r_w^2\right)\frac{\partial \varepsilon}{\partial t} \tag{3.8}$$

where, q_w is the discharge capacity of the drain given by:

$$q_w = k_w \pi r_w^2 \tag{3.9}$$

Integrating Equation (3.8) in the z direction with the boundary conditions $w(0) = 0$ and $w(2l) = 0$, reveals the pore water pressure in the drain:

$$w(z) = \frac{r_e^2 \gamma_w}{2q_w}\pi z(2l - z)\left(1 - \frac{1}{n^2}\right)\frac{\partial \varepsilon}{\partial t} \tag{3.10}$$

STEP 4: Determine the pore water pressure in each soil segment.

Equation (3.4) can be integrated in the radial direction with the boundary condition $u = w$ at $r = r_w$, to give the pore pressure at radius r:

$$u = \frac{\partial \varepsilon}{\partial t} f(r) \tag{3.11}$$

where, $f(r)$ is the function of r resulting from the integration. If there are multiple soil segments, then the additional boundary condition of equal pore pressure at the segment interfaces is used to determine the pore pressure in each segment.

STEP 5: Determine the μ parameter.

The average pore water pressure, $\bar{u}$, and the pore pressure distribution with radius are related by the algebraic expression:

$$\pi\left(r_e^2 - r_w^2\right)\bar{u} = \int_{r_w}^{r_e} 2\pi r u \, dr \tag{3.12}$$

Performing the integrations in Equation (3.12) the resulting expression for $\bar{u}$ can usually be rearranged in the following form:

$$\bar{u} = \frac{\gamma_w r_e^2}{2\bar{k}_h} \frac{\partial \varepsilon}{\partial t} (\mu + \mu_w) \tag{3.13}$$

where, $\bar{k}_h$ is a convenient reference value of horizontal permeability (usually that of the undisturbed soil), and μ_w is the contribution of well resistance given by:

$$\mu_w = \frac{\bar{k}_h}{q_w} \pi z (2l - z)\left(1 - \frac{1}{n^2}\right) \tag{3.14a}$$

If well resistance is not included ($q_w \to \infty$) then μ_w is omitted. To give an approximate indication as to how the entire soil layer is affected by well resistance Equation (3.14a) can be averaged over length l to give:

$$\mu_w = \frac{\bar{k}_h}{q_w}\frac{2\pi l^3}{3}\left(1-\frac{1}{n^2}\right) \tag{3.14b}$$

The μ parameter lies at the heart of the equal strain approach. μ is a non-dimensional parameter depending only on the geometry and material property ratios of the soil/drain system. Various expressions for μ are obtained in later sections.

STEP 6: Incorporate the constitutive relationship

The constitutive equation relating strain changes to stress changes is that of Terzaghi's equation for one-dimensional compression:

$$\frac{\partial \varepsilon}{\partial t} = m_{va}\frac{\partial \bar{\sigma}'}{\partial t} = m_{va}\left(\frac{\partial \bar{\sigma}}{\partial t} - \frac{\partial \bar{u}}{\partial t}\right) \tag{3.15}$$

where, $\partial\varepsilon/\partial t$ = volumetric strain rate, $\bar{\sigma}'$ = average effective stress and $\bar{\sigma}$ = average total stress. For the equal strain condition $\bar{\sigma}'$ and $\bar{u}$ are assumed independent of radius. m_{va} is the average value of m_v determined from the following algebraic relationship:

$$\pi\left(r_e^2 - r_w^2\right)m_{va} = \int_{r_w}^{r_e} 2\pi r m_v(r)\, dr \tag{3.16}$$

Substituting Equation (3.15) into Equation (3.13) gives a first order differential equation:

$$\bar{u} = \left(\frac{\partial \bar{\sigma}}{\partial t} - \frac{\partial \bar{u}}{\partial t} \right) \frac{r_e^2}{2c_h} \mu_{m_v} (\mu + \mu_w) \tag{3.17a}$$

where, μ_{m_v} is a the ratio of m_{va} to a reference value of volume compressibility, $\bar{m}_v$, given by:

$$\mu_{m_v} = \frac{m_{va}}{\bar{m}_v} \tag{3.17b}$$

If the soil has constant compressibility then μ_{m_v} is unity. The horizontal coefficient of consolidation, c_h, is now defined relative to the reference values of permeability and volume compressibility:

$$c_h = \frac{\bar{k}_h}{\bar{m}_v \gamma_w} \tag{3.17c}$$

STEP 7: Determine the average pore water pressure.

Note: For brevity, in this step the expression $\mu_{m_v}(\mu + \mu_w)$ from Equation (3.17a) has been replaced by μ^* (i.e. μ_w and μ_{m_v} have been ignored).

The solution of Equation (3.17a) depends on the loading conditions. When a load is applied instantaneously $\partial \bar{\sigma} / \partial t = 0$ and Equation (3.17a) reduces to a first order separable differential equation:

$$\frac{\partial \bar{u}}{\bar{u}} = -\frac{2c_h}{r_e^2 \mu^*} \partial t \tag{3.18}$$

The solution of Equation (3.18) when an instantaneous excess pore pressure of $\bar{u}_0$ is generated at $t = 0$ gives:

$$\bar{u} = \bar{u}_0 \exp\left[\frac{-8T_h}{\mu^*} \right] \tag{3.19}$$

where, the time factor T_h is found from the expression:

$$T_h = \frac{c_h t}{4 r_e^2} \tag{3.20}$$

The average degree of consolidation U_h is defined as:

$$U_h = 1 - \frac{\bar{u}}{\bar{u}_0} \tag{3.21}$$

Substituting Equation (3.19) into Equation (3.21) gives the degree of consolidation for constant loading:

$$U_h = 1 - \exp\left[\frac{-8T_h}{\mu^*}\right] \tag{3.22}$$

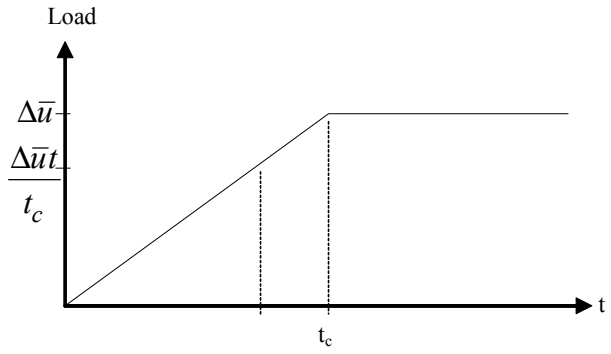

Figure 3.2 Ramp loading

If the total stress is ramped from zero at $t = 0$ to $\Delta\bar{u}$ at $t = t_c$, as in Figure 3.2, then Equation (3.17a) in the ramped zone reduces to:

$$\frac{\partial \bar{u}}{\partial t} + \frac{r_e^2 \mu}{2 c_h} \bar{u} = \frac{\Delta \bar{u}}{t_c} \frac{r_e^2 \mu^*}{2 c_h} \tag{3.23}$$

Solution of Equation (3.23), a first order linear differential equation, gives the average pore pressure during the ramped load:

$$\bar{u} = \frac{\Delta\bar{u}\mu}{8T_c}\exp\left[-\frac{8T_h}{\mu^*}\right]\left(\exp\left[\frac{8T_h}{\mu^*}\right]-1\right) \quad T_h \le T_c \tag{3.24a}$$

When the load becomes constant, the average pore pressure is given by:

$$\bar{u} = \frac{\Delta\bar{u}\mu^*}{8T_c}\exp\left[-\frac{8T_h}{\mu^*}\right]\left(\exp\left[\frac{8T_c}{\mu^*}\right]-1\right) \quad T_h \ge T_c \tag{3.24b}$$

The corresponding expressions for average degree of consolidation are:

$$U_h = 1-\frac{\mu^*}{8T_h}\exp\left[-\frac{8T_h}{\mu^*}\right]\left(\exp\left[\frac{8T_h}{\mu^*}\right]-1\right) \quad T_h \le T_c \tag{3.25a}$$

and,

$$U_h = 1-\frac{\mu}{8T_c}\exp\left[-\frac{8T_h}{\mu^*}\right]\left(\exp\left[\frac{8T_c}{\mu^*}\right]-1\right) \quad T_h \ge T_c \tag{3.25b}$$

The two chief challenges in using the above consolidation equations is the accurate determination of the coefficient of consolidation c_h and the drain/soil parameter μ. The calculation of μ parameter has traditionally been performed assuming a single smear zone of reduced permeability (constant permeability throughout the smear zone). The μ parameter for such a smear zone configuration obtained by Hansbo (1981) is described in Appendix A. Hansbo's μ along with that for an ideal drain (no smear effect) are found to be special cases of a smear zone with multiple soil segments which is also presented in Appendix A. This multi-segment approach can be used to approximate arbitrary distributions of properties in the smear zone. Other expressions for μ can be found by considering smear zone properties that vary in a specific way (in this case higher order polynomials).

3.2.2 Smear Zone with Linear Variation of Permeability

Hansbo's (1981) constant permeability smear zone describes permeability with a zero order polynomial. The next simplest expression for a smear zone is thus a linear

polynomial. The results from following the above steps (section 3.2.1) for such a distribution are described below. The same formulations will be used to consider overlapping smear zones in section 3.2.6.

STEP 1:

Consider radial consolidation of a soil with an undisturbed zone and a smear zone with a linear distribution of permeability as in Figure 3.3.

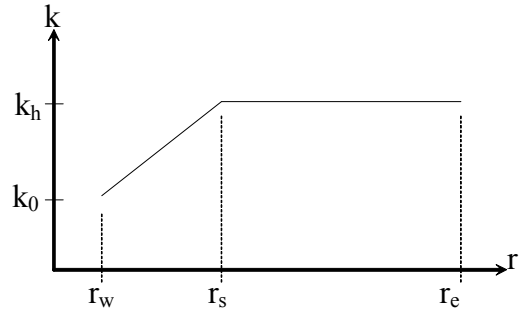

Figure 3.3 Linear distribution of permeability in the smear zone

The linear permeability distribution in the smear zone (Figure 3.3) is determined by two conditions:

$$k_s(r_w) = k_0 \tag{3.26a}$$

and,

$$k_s(r_s) = k_h \tag{3.26b}$$

The linear curve that satisfies the above conditions is:

$$k_s = k_0\left[\frac{A}{r_w}r + B\right] \tag{3.27}$$

where,

$$A = \frac{\kappa - 1}{s - 1} \tag{3.28}$$

$$B = \frac{s - \kappa}{s - 1} \tag{3.29}$$

$$\kappa = \frac{k_h}{k_0} \tag{3.30}$$

It is necessary to consider the special case of $s = \kappa$ where Equation (3.27) reduces to:

$$k_s(r) = \frac{k_0 r}{r_w} \tag{3.31}$$

It is assumed that the volume compressibility also varies linearly in the smear zone. Thus the volume compressibility in the smear zone, m_{vs}, is given by:

$$m_{vs} = m_{v0}\left[\frac{A_\eta}{r_w} r + B_\eta\right] \tag{3.32a}$$

where

$$A_\eta = \frac{\eta - 1}{s - 1} \tag{3.32b}$$

$$\eta = \frac{m_v}{m_{v0}} \tag{3.32c}$$

$$B_\eta = \frac{s - \eta}{s - 1} \tag{3.32d}$$

$$\eta = \frac{m_v}{m_{v0}} \tag{3.32e}$$

STEP 2:

The pore water pressure gradient in smear and undisturbed zones are, respectively:

$$\frac{\partial u_s}{\partial r} = \frac{\gamma_w r_e^2}{2k_h}\frac{\partial \varepsilon}{\partial t}\kappa\left(\frac{1}{Br/r_w} - \frac{A}{B(B + Ar/r_w)} - \frac{r/r_w}{n^2(B + Ar/r_w)}\right) \tag{3.33a}$$

and,

$$\frac{\partial u}{\partial r} = \frac{\gamma_w r_e^2}{2k_h}\frac{\partial \varepsilon}{\partial t}\left(\frac{1}{r} - \frac{r}{n^2 r_w^2}\right) \tag{3.33b}$$

For the case when $s = \kappa$, the pore pressure gradient in the smear zone is:

$$\frac{\partial u_s}{\partial r} = \frac{\gamma_w r_e^2}{2k_h}\frac{\partial \varepsilon}{\partial t} s\left(\frac{1}{r^2/r_w^2} - \frac{1}{n^2}\right) \tag{3.33c}$$

STEP 3:

The pore water pressure in the drain is the same as in Equation (3.10).

STEP 4:

The pore water pressure in smear and undisturbed zones are, respectively:

$$u_s = \frac{\gamma_w r_e^2}{2k_h}\frac{\partial \varepsilon}{\partial t}\kappa\left[\begin{array}{l}\frac{1}{B}\ln\left(\frac{r}{r_w}\right)+\left(\frac{B}{A^2n^2}-\frac{1}{B}\right)\ln\left(B+Ar/r_w\right)\\ +\frac{1-r/r_w}{An^2}+\frac{k_0}{q_w}\pi z\left(2l-z\right)\left(1-\frac{1}{n^2}\right)\end{array}\right] \tag{3.34a}$$

and,
$$u = \frac{\gamma_w r_e^2}{2k_h}\frac{\partial \varepsilon}{\partial t}\left[\begin{array}{l}\ln\left(\frac{r/r_w}{s}\right)-\frac{s^2-r^2/r_w^2}{2n^2}+\frac{k_h}{q_w}\pi z\left(2l-z\right)\left(1-\frac{1}{n^2}\right)\\ +\kappa\left(\frac{1}{B}\ln(s)-\frac{s-1}{An^2}+\left(\frac{B}{An^2}-\frac{1}{B}\right)\ln(\kappa)\right)\end{array}\right] \tag{3.34b}$$

For the case when $s = \kappa$, the pore pressure in the smear and undisturbed zones are, respectively:

$$u_s = \frac{\gamma_w r_e^2}{2k_h}\frac{\partial \varepsilon}{\partial t} s\left[\frac{\left(n^2 - r/r_w\right)\left(r/r_w - 1\right)}{n^2 r/r_w} + \frac{k_0}{q_w}\pi z\left(2l-z\right)\left(1-\frac{1}{n^2}\right)\right] \tag{3.34c}$$

and, $$u = \frac{\gamma_w r_e^2}{2k_h}\frac{\partial \varepsilon}{\partial t}\left[\ln\left(\frac{r/r_w}{s}\right) + s - 1 + \frac{s}{n^2} - \frac{s^2 - r^2/r_w^2}{2n^2} + \frac{k_h}{q_w}\pi z\left(2l-z\right)\left(1-\frac{1}{n^2}\right)\right] \tag{3.34d}$$

STEP 5:

The μ parameter from Equation (3.17) is given by:

$$\mu = \frac{n^2}{n^2-1}\left[\begin{array}{l} \ln\left(\frac{n}{s}\right) - \frac{3}{4} + \frac{s^2}{n^2}\left(1 - \frac{s^2}{4n^2}\right) - \frac{\kappa}{B}\ln\left(\frac{\kappa}{s}\right) + \frac{\kappa B}{A^2 n^2}\left(2 - \frac{B^2}{A^2 n^2}\right)\ln(\kappa) \\ -\frac{\kappa(s-1)}{An^2}\left(2 + \frac{1}{n^2}\left(\frac{A-B}{A}\left(\frac{1}{A} - \frac{s+1}{2}\right) - \frac{(s+1)}{2} - \frac{(s-1)^2}{3}\right)\right) \end{array}\right] \quad (3.35a)$$

Ignoring insignificant terms Equation (3.35a) reduces to:

$$\mu = \ln\left(\frac{n}{s}\right) - \frac{3}{4} + \frac{\kappa(s-1)}{s-\kappa}\ln\left(\frac{s}{\kappa}\right) \quad (3.35b)$$

For the case when $s = \kappa$ the μ parameter is:

$$\mu = \frac{n^2}{n^2-1}\left[\ln\left(\frac{n}{s}\right) - \frac{3}{4} + s - 1 - \frac{s^2}{n^2}\left(1 - \frac{s^2}{12n^2}\right) + \frac{s}{n^2}\left(2 - \frac{1}{3n^2}\right)\right] \quad (3.35c)$$

Ignoring insignificant terms Equation (3.35c) reduces to:

$$\mu = \ln\left(\frac{n}{s}\right) - \frac{3}{4} + s - 1 \quad (3.35d)$$

If the limit of Equation (3.35) is taken as κ approaches unity or s approaches unity, then the μ parameter for the ideal case of no smear is obtained.

STEP 6:

The μ_{m_v} parameter from Equation (3.17) is given by:

$$\mu_{m_v} = 1 + \left(\frac{1-\eta}{\eta}\right)\frac{(s-1)(s+2)}{3\left(n^2-1\right)} \quad (3.36)$$

3.2.3 Smear Zone with Parabolic Variation of Permeability

Following the linear polynomial description of smear zone properties in the previous section, increasing the polynomial order leads to a parabolic variation of smear zone properties. The results from following the steps from section 3.2.1, for such a

distribution are described below. A parabola is the highest order polynomial considered here to describe the variation of smear zone properties; other distributions can be approximated with the multi-segment approach described in Appendix A.

STEP 1:

Consider radial consolidation of a soil with an undisturbed zone and a smear zone with a parabolic distribution of permeability as in Figure 3.4.

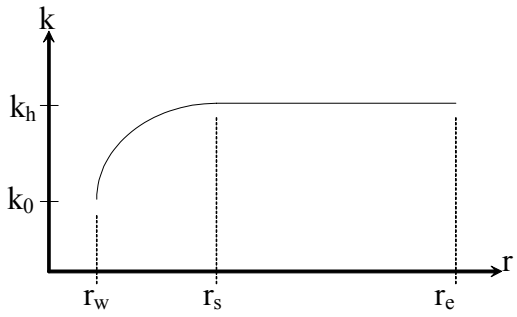

Figure 3.4 Parabolic distribution of permeability in the smear zone

The parabolic permeability distribution in the smear zone (Figure 3.4) is determined by three conditions:

$$k_s(r_w) = k_0 \tag{3.37}$$

$$k_s(r_s) = k_h \tag{3.37b}$$

$$\partial k_s(r_s)/\partial r = 0 \tag{3.37c}$$

The parabolic curve that satisfies the above conditions is:

$$k_s(r) = k_0(\kappa - 1)(A - B + C\,r/r_w)(A + B - C\,r/r_w) \tag{3.38a}$$

where,

$$\kappa = k_h/k_0 \tag{3.38b}$$

$$A = \sqrt{\kappa/(\kappa - 1)} \tag{3.38c}$$

$$B = s/(s-1) \tag{3.38d}$$

$$C = 1/(s-1). \tag{3.38e}$$

STEP 2:

The pore water pressure gradient in the smear and undisturbed zones are, respectively:

$$\frac{\partial u_s}{\partial r} = \frac{\gamma_w r_e^2}{2k_h}\frac{\partial \varepsilon}{\partial t}\frac{A}{2}\left(\begin{array}{l}\dfrac{2A}{\left(A^2-B^2\right)r/r_w} + \left(\dfrac{C}{(A+B)} - \dfrac{(A+B)}{n^2 C}\right)\dfrac{1}{(A+B-Cr/r_w)} \\ -\left(\dfrac{C}{(A-B)} - \dfrac{(A-B)}{n^2 C}\right)\dfrac{1}{(A-B+Cr/r_w)}\end{array}\right) \tag{3.39a}$$

and,
$$\frac{\partial u}{\partial r} = \frac{\gamma_w r_e^2}{2k_h}\frac{\partial \varepsilon}{\partial t}\left(\frac{1}{r} - \frac{r}{n^2 r_w^2}\right) \tag{3.39b}$$

STEP 3:

The pore water pressure in the drain is the same as in Equation (3.10).

STEP 4:

The pore water pressure in smear and undisturbed zones are, respectively:

$$u_s = \frac{\gamma_w r_e^2}{2k_h}\frac{\partial \varepsilon}{\partial t}\frac{A}{2}\left(\begin{array}{l}\left(\dfrac{2A}{\left(A^2-B^2\right)}\ln\left(\dfrac{r}{r_w}\right) - \left(\dfrac{1}{(A+B)} - \dfrac{(A+B)}{n^2C^2}\right)\ln\left(\dfrac{A+B-Cr/r_w}{A+1}\right)\right. \\ \left. -\left(\dfrac{1}{(A-B)} - \dfrac{(A-B)}{n^2C^2}\right)\ln\left(\dfrac{A-B+Cr/r_w}{A-1}\right) + \dfrac{k_0}{q_w}\pi z(2l-z)\left(1-\dfrac{1}{n^2}\right)\right)\end{array}\right) \tag{3.40a}$$

and,
$$u = \frac{\gamma_w r_e^2}{2k_h}\frac{\partial \varepsilon}{\partial t}\left(\begin{array}{l}\ln\left(\dfrac{r/r_w}{s}\right) - \dfrac{s^2 - r^2/r_w^2}{2n^2} + \dfrac{k_h}{q_w}\pi z(2l-z)\left(1-\dfrac{1}{n^2}\right) \\ +\dfrac{A}{2}\left(\begin{array}{l}\dfrac{2A}{\left(A^2-B^2\right)}\ln\left(\dfrac{r}{r_w}\right) - \left(\dfrac{1}{(A+B)} - \dfrac{(A+B)}{n^2C^2}\right)\ln\left(\dfrac{A}{A+1}\right) \\ -\left(\dfrac{1}{(A-B)} - \dfrac{(A-B)}{n^2C^2}\right)\ln\left(\dfrac{A-B+Cr/r_w}{A-1}\right)\end{array}\right)\end{array}\right) \tag{3.40b}$$

STEP 5:

The μ parameter from Equation (3.17) is given by:

$$\mu = \frac{n^2}{n^2-1}\left[\begin{array}{l} \ln(n) - \frac{3}{4} + \frac{s^2}{n^2}\left(1-\frac{s^2}{4n^2}\right) + \frac{B^2}{A^2-B^2}\ln(s) - \frac{A(1+5s)}{2C^3n^4} \\ + \frac{A}{2(A-B)}\left(1-\frac{(A-B)^2}{C^2n^2}\right)^2 \ln\left(\frac{A-1}{A}\right) \\ + \frac{A}{2(A+B)}\left(1-\frac{(A+B)^2}{C^2n^2}\right)^2 \ln\left(\frac{A+1}{A}\right) \end{array}\right] \tag{3.41a}$$

Ignoring insignificant terms, Equation (3.41) reduces to:

$$\begin{aligned} \mu \; = & \ln\left(\frac{n}{s}\right) - \frac{3}{4} + \frac{\kappa(s-1)^2}{\left(s^2-2\kappa s+\kappa\right)}\ln\left(\frac{s}{\sqrt{\kappa}}\right) - \\ & \frac{s(s-1)\sqrt{\kappa(\kappa-1)}}{2\left(s^2-2\kappa s+\kappa\right)}\ln\left(\frac{\sqrt{\kappa}+\sqrt{\kappa-1}}{\sqrt{\kappa}-\sqrt{\kappa-1}}\right) \end{aligned} \tag{3.41b}$$

If the limit of Equation (3.35) is taken as κ approaches unity or s approaches unity, then the μ parameter for the ideal case of no smear is obtained.

STEP 6:

The compressibility parameter μ_{m_v} in Equation (3.17) is given by:

$$\mu_{m_v} = 1 + \left(\frac{1-\eta}{\eta}\right)\frac{(s-1)(s+3)}{6\left(n^2-1\right)} \tag{3.42}$$

3.2.4 Size of Constant, Parabolic, and Linear Smear Zones Producing Equivalent Rate of Consolidation

Laboratory evidence indicates that soil properties in the smear zone vary with distance from the drain (Chai and Miura, 1999; Hawlader et al., 2002; Sharma and

Xiao, 2000; Hird and Moseley, 2000; Indraratna and Redana, 1998a; Madhav et al., 1993; Bergado et al., 1991), and so the linear and parabolic distributions of smear zone properties presented above should give a better description as to the true nature of the smear effect. However, given the difficulty of explicitly measuring the smear zone properties in the field, the constant permeability smear zone of Hansbo (1981) has been used to back calculate the size of the smear zone. Thus, while assuming a constant permeability smear zone of appropriate size may give the correct rate of consolidation (i.e. numerical value of μ) the actual size of the smear zone described will be incorrect. An indication as to the true extent of smearing can be assessed by determining the equivalent size of smear zone required to produce the same μ value using smear zones with constant, linear and parabolic permeability distributions, Equations (3.35), and (3.41). The relative smear zone sizes producing equivalent consolidation to those with constant permeability are presented in Figure 3.5. Figure 3.6 shows the actual distributions of permeability producing equivalent rates of consolidation for different values of $k_h/k_{\text{undisturbed}}$. The three distributions originating from the same value of $k_h/k_{\text{undisturbed}}$ on the y-axis will give identical rates of consolidation. The equivalent smear zone size does not vary greatly for r_e/r_w values greater than 20, so only those for r_e/r_w = 40 are plotted.

Figure 3.5 shows that to produce equivalent consolidation, the parabolic and linear smear zones can be as much as 7 times larger than the constant permeability smear zones. This emphasizes the relative importance of permeability close to the drain. The large equivalent smear zone sizes imply the possibility of overlapping smear zones. Drain spacing ratios of r_e/r_w less than 4 are unlikely so assumed constant

permeability smear zones would never interact. Drain spacing ratios of $r_e/r_w = 20$ are feasible where parabolic and linear smear zones might overlap. Overlapping smear zones are investigated in Section 3.2.6 below.

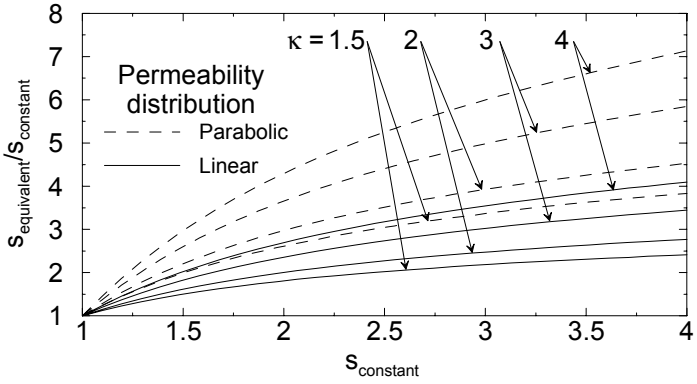

Figure 3.5 Extent of smear zones producing equivalent rate of consolidation ($r_e/r_w = 40$)

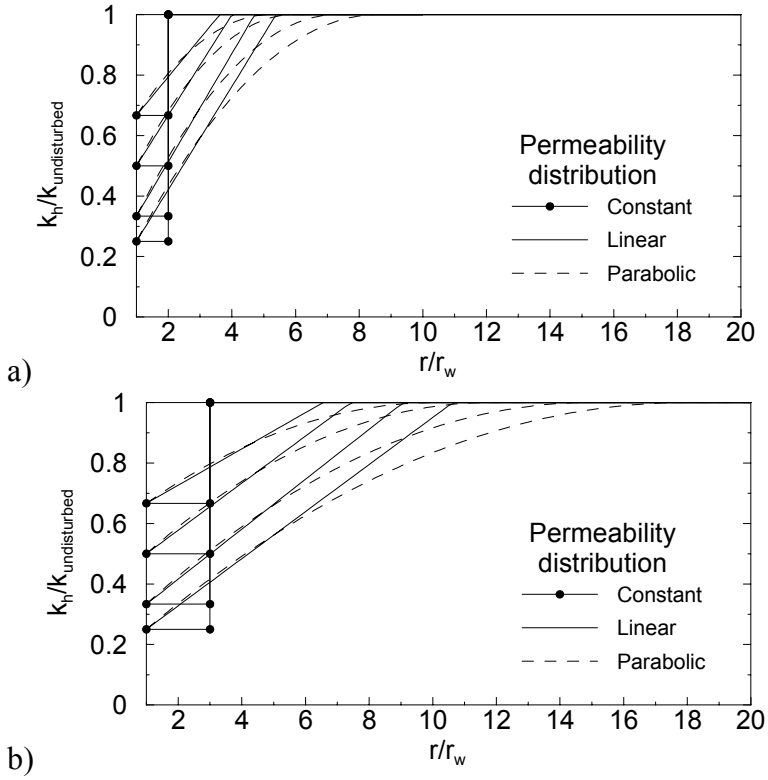

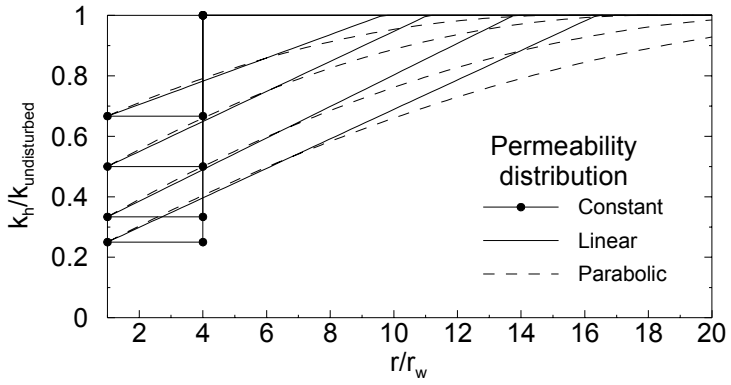

c)

Figure 3.6 Shape of smear zones producing equivalent rate of consolidation (r_e/r_w = 40) with reference to a constant permeability smear zone size of r_s/r_w = a) 2, b) 3, c) 4.

3.2.5 Relative Importance of Compressibility Variations in the Smear Zone

Smear zones are most often described with reference to permeability changes alone, neglecting the effects of compressibility changes. However, smear zone compressibility is important in the light of field trials of vertical drains at different spacing. For smaller drain spacing, the total settlement is higher and values of horizontal consolidation coefficient (back calculated ignoring smear zone compressibility effects) are lower than for widely spaced drains (Saye, 2001; Arulrajah et al., 2004; Bergado et al., 2002). Both findings are consistent with increased compressibility in the smear zone. The effect of smear zone compressibility can be assessed by considering μ_{mv} in Equations (3.36), and (3.42). Figure 3.7 shows μ_{m_v} values for smear zones with constant, linear and parabolic compressibility. Values of μ_{m_v} around 1.2 are feasible for all compressibility distributions, possibly indicating a 20% increase in ultimate settlement. A μ_{m_v} value of 1.2 would also result in a possible 20% decrease in back calculated c_h, if smear zone compressibility was ignored in the calculations. Figure 3.7 deals only

with discrete smear zones; overlapping smear zones are considered in the next section.

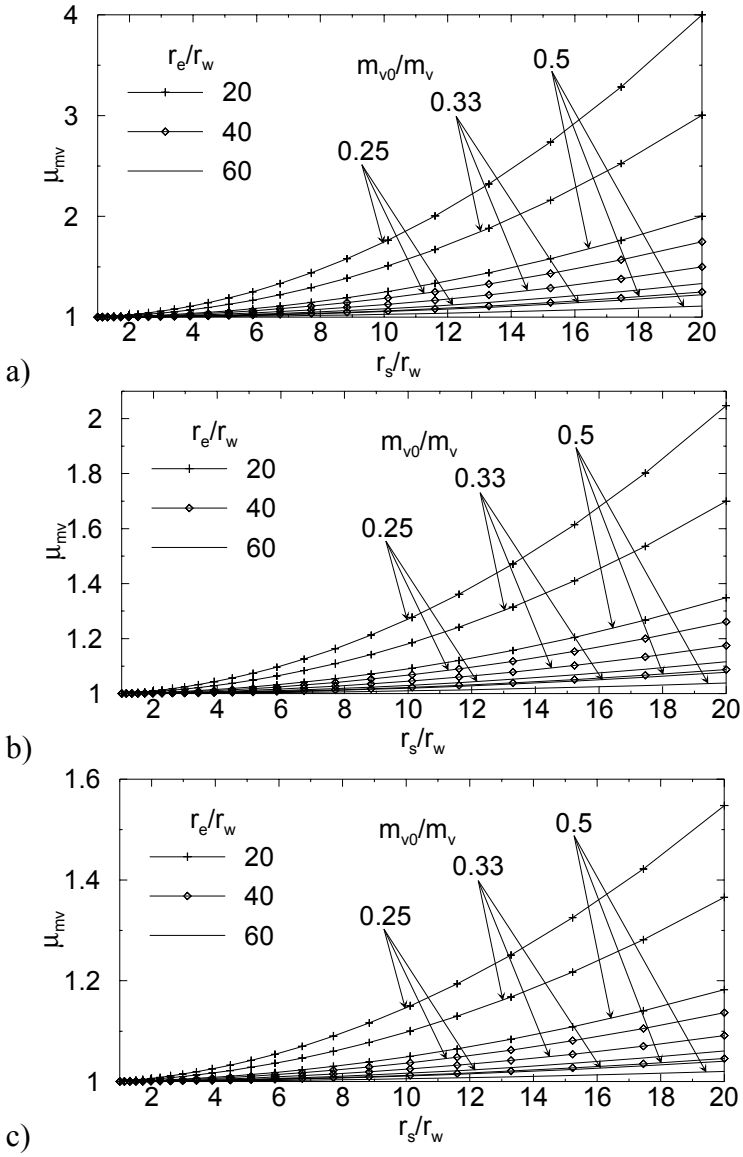

Figure 3.7 Effect of smear zone compressibility for smear zone with a) constant, b) linear, and c) parabolic compressibility

3.2.6 Overlapping Smear Zones

As the costs of PVD and their installation falls, there is a tendency towards ever decreasing drain spacing it an attempt to hasten consolidation (Chu et al., 2004). However, from field experience on multiple Highway projects, Saye (2001) notes that a lower bound drain spacing exists, below which no discernable increase in

consolidation rate occurs. Saye (2001) proposes an empirical relationship between effective consolidation coefficient (c_{he}) and a modified drain spacing parameter for small drain spacing ratios. This empirical relation is given by:

$$\frac{c_{he}}{\text{lab}\, c_v} = 0.066 \exp(0.44 n') \tag{3.43}$$

where, $\text{lab}\, c_v$ is the laboratory determined value of vertical consolidation coefficient, and n' is the ratio of influence radius r_e to equivalent mandrel radius r_m (based on the mandrel perimeter). While Equation (3.43) may provide appropriate properties with which to calculate radial consolidation rates at small drain spacing, the possible mechanisms responsible for a lower bound spacing value are better described with reference to overlapping smear zones as shown in Figure 3.8.

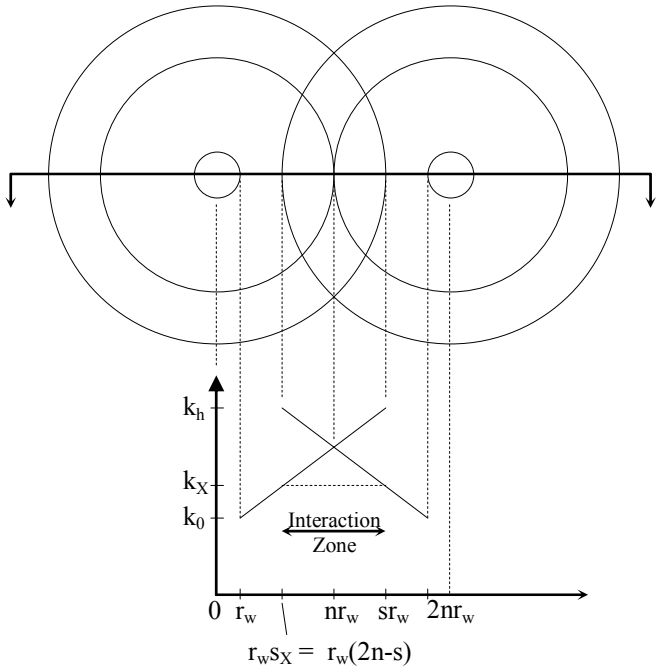

Figure 3.8 Schematic of overlapping smear zones

Owing to the common assumption of a small constant reduced permeability smear zone, such smear zones would rarely interact. More realistic representations of

smear zone permeability such as a linear or parabolic representation suggest larger smear zones which might interact. The novel treatment of linearly varying properties in the smear zone, presented in Section 3.2.2, provides a simple means to assess the effect of overlapping smear zones. With reference to Figure 3.8, two smear zones will interact when the spacing parameter n is less than the smear zone size parameter s. As an idealization, it is assumed the interaction exhibits radial symmetry. It is assumed that in the 'interaction zone' the permeability is constant at a value of k_X, which is the value of permeability where the smear zones begin to overlap, s_X. The problem is now a modified version of the original linearly varying permeability equations. The modified permeability ratio, $\kappa_X = k_X / k_0$, can be found by equating the A parameters of the original and modified smear zones as calculated in Equation (3.27) (because the permeability gradients for both smear zones are the same). This leads to:

$$\kappa_X = 1 + \frac{\kappa - 1}{s - 1}(s_X - 1) \tag{3.44}$$

In the same manner, the new compressibility ratio $\eta_X = m_{vX} / m_{v_0}$ is determined. For the case when $2n - s > 1$, the two smear zones completely overlap and it is assumed the soil properties are constant at values equal to those at the drain/soil interface (that is k_0 and mv_0). With reference to the undisturbed values of soil properties a new modified expression, μ_X, describing the effect of interacting smear zones can be defined as:

$$\mu_X = \begin{cases} \mu[n,s,\kappa]\mu_{\mathrm{m_v}}[n,s,\eta] & n \geq s \\ \dfrac{\kappa}{\kappa_X}\mu_{\mathrm{L}}[n,s_X,\kappa_X]\dfrac{\eta_X}{\eta}\mu_{\mathrm{m_v}}[n,s_X,\eta_X] & 2n-s \geq 1 \text{ AND } s > n \\ \dfrac{\kappa}{\kappa_X}\mu[n]\dfrac{\eta_X}{\eta} & 2n-s < 1 \end{cases} \quad (3.45)$$

where, μ and μ_{m_v} are calculated respectively from Equations (3.35) and (3.36) with the appropriate variables in square brackets. $\mu[n]$ is the μ parameter for an ideal drain (see Appendix A).

Now, by rearranging Equation (3.22), an expression for the time to reach a certain degree of consolidation with interacting smear zones can be obtained:

$$\frac{c_h t}{4r_w^2} = \frac{n^2}{8}\mu_X \ln[1-U_h] \quad (3.46)$$

Figure 3.9 shows the time required to reach 90% consolidation, t_{90}, for various interacting smear zone configurations.

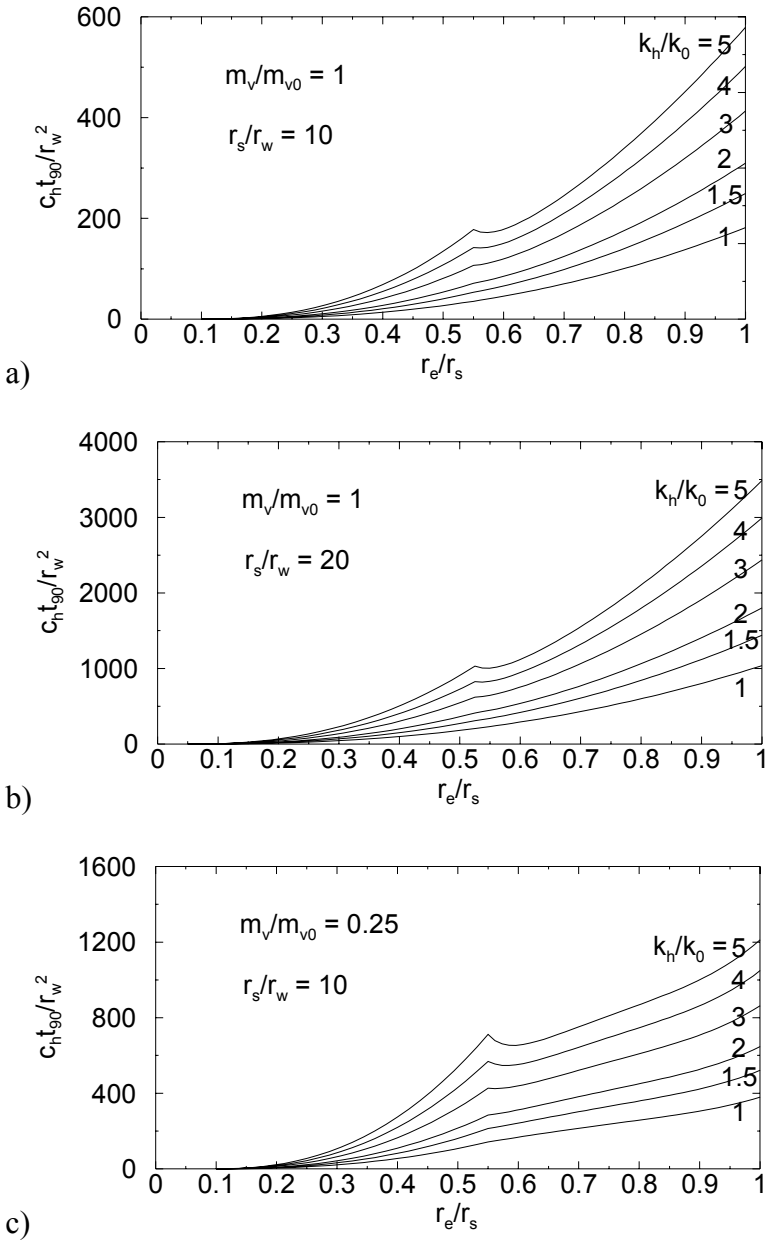

Figure 3.9 Time required for 90% consolidation for overlapping smear zones with linear variation of permeability

Each graph in Figure 3.9 has the same general shape, exhibiting a local minima for high k_h/k_0 ratios when the influence radius is between 0.55 and 0.6 times the smear zone radius. The local minima does not occur when considering small constant permeability smear zones. By changing the m_v/m_{v0} ratio (compare Figure 3.9a

and c) the required consolidation times are increased and the local minima is accentuated. Figure 3.9 suggests that, if not an absolute drain spacing minimum as proposed by Saye (2001), there at least exists a range of drain spacing values across which the time required to reach a certain degree of consolidation does not change. For drain spacing values less than the local minima, the time for consolidation reduces rapidly. This is due to the assumption that once the linear smear zones completely overlap there is no further change in the soil properties; that is a threshold level of disturbance is reached. This assumption is questionable as at an increasingly closer drain spacing the soil may become further remolded, exhibiting properties different to that of the partially remolded smear zone. As such, the local minima in Figure 3.9 may be an absolute minima. In which case, as an approximation, decreasing the equivalent influence radius (by decreasing the drain spacing) beyond a value 0.6 times the linear smear zone radius will not result in faster consolidation times. The phenomena of a lower bound drain spacing only becomes apparent when the radial variation of smear zone properties are considered. This illustrates the importance, at least conceptually, of considering a large smear zone with gradually reducing permeability towards the drain compared with a small constant reduced permeability smear zone.

The μ parameters developed above, including the case of overlapping smear zones, can now be included in the following nonlinear radial consolidation model if Darcian flow is assumed.

3.3 Nonlinear Radial Consolidation

3.3.1 Previous Attempts at Modeling Void Ratio Dependant Material Properties

This section presents analytical solutions for nonlinear radial consolidation under equal strain conditions incorporating smear but ignoring well resistance. Three aspects of nonlinearity are considered: non-Darcian flow, a log-linear void ratio-stress relationship, and a log-linear void ratio-permeability relationship. In non-Darcian flow, the velocity of flow, υ, is related to the hydraulic gradient, i, by the following power law:

$$\upsilon = \tilde{k} i^n \tag{3.47}$$

where $\tilde{k}$ is the coefficient of permeability under non-Darcian conditions, and n is the non-Darcian flow exponent. Void ratio is related to effective stress and permeability by the following relationships:

$$e = e_0 - C_c \log\left(\sigma'/\sigma'_0\right) \tag{3.48}$$

$$e = e_0 + C_k \log\left(\tilde{k}/\tilde{k}_0\right) \tag{3.49}$$

where, e = void ratio, σ' = effective stress, C_c = compressibility index, C_k = permeability index and e_0, σ'_0, $\tilde{k}_0$ = initial values of parameters.

Review of the literature reveals previous attempts to model the corresponding problem with Darcian flow. The excess pore water pressure, $\bar{u}$, under instantaneous loading described by Lekha et al. (1998) is

$$\bar{u} = \sigma'_0 \left[\frac{\Delta\sigma}{\sigma'_0} - \frac{T_h}{\mu} \frac{(1-\beta)}{(2-C_c/C_k)} \left(\left(\beta + \frac{\Delta\sigma}{\sigma'_0} \right)^{(2-C_c/C_k)} - \beta^{(2-C_c/C_k)} \right) \right] \tag{3.50}$$

where,

$$\beta = 1 - \frac{1}{2}\left(1 + \frac{\Delta\sigma}{\sigma_0'}\right) \tag{3.51}$$

Equation (3.50) is a linear function of time factor, T_h, which as T_h approaches infinity leads to infinite negative values of pore water pressure. The excess pore water pressure should decay to zero, thus Equation (3.50) is unsuitable for estimating $\bar{u}$ at large times. Also Equation (3.50) is undefined if $C_c/C_k = 2$. Basak and Madhav (1978) presented a more useful solution with Equation (3.48) but using a linear relationship between permeability and effective stress. Indraratna et al. (2005a) express the excess pore pressure under instantaneous loading as:

$$\bar{u} = \exp\left(-P_{av}\frac{8T_{h0}}{\mu}\right) \tag{3.52a}$$

where,

$$P_{av} = \frac{1}{2}\left(1 + \left(1 + \frac{\Delta\sigma}{\sigma_0'}\right)^{1-C_c/C_k}\right) \tag{3.52b}$$

Equation (3.52) is very similar to the linear solution given by Hansbo (1981), except that the main difference is in the P_{av} parameter. P_{av} represents the average value of consolidation coefficient between the beginning and end values. This averaging of consolidation coefficient over the applied stress increment is implied in Hansbo's (1981) solution. Thus Equation (3.52) simply provides the best choice of consolidation coefficient for use with Hansbo's (1981) equations. Though Indraratna et al. (2005a) recommend using the log-linear void ratio-stress relationship (Equation (3.48)) for settlement calculations, the solution expressed by Equation (3.52) does not reflect the nonlinear processes involved with pore pressure dissipation.

The proposed model presented herein removes these simplifying assumptions. Hansbo's (2001) equal strain solution for radial drainage with non-Darcian flow is extended to include the nonlinear material properties expressed in Equations (3.48) and (3.49). A series solution to the resulting nonlinear partial differential equation is found, explicitly capturing the variation of permeability and compressibility in the consolidation of normally and overconsolidated soil.

3.3.2 Analytical Solution

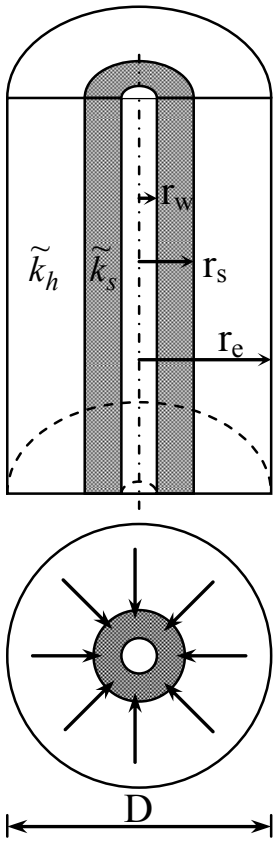

Figure 3.10 Unit cell

Vertical drains, installed in a square or triangular pattern, are usually modeled analytically by considering an equivalent axisymmetric system. Pore water flows from a soil cylinder to a single central vertical drain with simplified boundary conditions. Figure 3.10 shows a unit cell with an external radius r_e, drain radius r_w,

and a smear zone radius of r_s. For simplicity, the material properties in the smear zone are assumed constant. The soil compressibility in the smear zone is assumed equal to that in the undisturbed zone. The velocity of pore water flow in the smear and undisturbed zones are respectively given by:

$$\upsilon = \widetilde{k}_s \left(\frac{1}{\gamma_w} \frac{\partial u'}{\partial r} \right)^n \tag{3.53a}$$

and,

$$\upsilon = \widetilde{k}_h \left(\frac{1}{\gamma_w} \frac{\partial u}{\partial r} \right)^n \tag{3.53b}$$

where, $\widetilde{k}_h$ = undisturbed horizontal permeability for non-Darcian flow, $\widetilde{k}_s$ = horizontal permeability in the smear zone, u = excess pore water pressure in the undisturbed zone, and u' = excess pore water pressure in the smear zone.

The rate of fluid flow through the internal face of the hollow cylindrical slice with internal radius r is:

$$2\pi r \upsilon \tag{3.54}$$

The rate of volume change in the hollow cylindrical slice with internal radius r, outer radius r_e is:

$$\pi \left(r_e^2 - r^2 \right) \frac{\partial \varepsilon}{\partial t} \tag{3.55}$$

where $\partial \varepsilon / \partial t$ is the one-dimensional strain rate. For instantaneous loading the strain rate can be expressed as:

$$\frac{\partial \varepsilon}{\partial t} = -m_v \frac{\partial \overline{u}}{\partial t} \tag{3.56}$$

where, $\overline{u}$ = average excess pore pressure, and m_v = volume compressibility of the soil. The nonlinearity of m_v and $\widetilde{k}$ will be treated later. For continuity, the volume changes in Equations (3.54) and (3.55) can be equated; rearranging the resulting expression using Equation (3.53) and (3.56) the pore pressure gradient in the smear and undisturbed zones is represented by:

$$\frac{\partial u_s}{\partial y} = (r_w\gamma_w)^{1-\frac{1}{n}}\left(-\frac{r_e^2}{2\widetilde{c}_{h0}}\frac{\partial \overline{u}}{\partial t}\right)^{\frac{1}{n}}\left(\frac{\widetilde{c}_{h0}}{\widetilde{c}_h}\right)^{\frac{1}{n}}\left(\frac{\widetilde{k}_h}{\widetilde{k}_s}\right)^{\frac{1}{n}}\left(1-\frac{y^2}{N^2}\right)^{\frac{1}{n}} y^{-\frac{1}{n}} \tag{3.57a}$$

and,

$$\frac{\partial u}{\partial y} = (r_w\gamma_w)^{1-\frac{1}{n}}\left(-\frac{r_e^2}{2\widetilde{c}_{h0}}\frac{\partial \overline{u}}{\partial t}\right)^{\frac{1}{n}}\left(\frac{\widetilde{c}_{h0}}{\widetilde{c}_h}\right)^{\frac{1}{n}}\left(1-\frac{y^2}{N^2}\right)^{\frac{1}{n}} y^{-\frac{1}{n}} \tag{3.57b}$$

where, $N = r_e/r_w$, and a change of variable has been made such that $y = r/r_w$. The coefficient of consolidation under non-Darcian flow can be written as:

$$\widetilde{c}_h = \frac{\widetilde{k}_h}{m_v\gamma_w} \tag{3.58}$$

The value of consolidation coefficient at the start of analysis is denoted $\widetilde{c}_{h0}$.

By using the binomial expansion the terms involving y on the right hand side of Equation (3.57) can be represented by a series:

$$\left(1-\frac{y^2}{N^2}\right)^{\frac{1}{n}} y^{-\frac{1}{n}} = y^{-\frac{1}{n}}\sum_{j=0}^{\infty}\frac{\{-1/n\}_j}{j!}\left(\frac{y}{N}\right)^{2j} \tag{3.59}$$

where, $\{x\}_m$, sometimes called the Pochhammer symbol or rising factorial, is defined by:

$$\{x\}_m = x(x+1)(x+2)...(x+m-1), \quad \{x\}_0 = 1 \tag{3.60}$$

Substituting Equation (3.59) into Equation (3.57) and integrating (with the boundary conditions $u_s = 0$ at $y = 1$, and $u = u'$ at $y = s$ where $s = r_s / r_w$) yields the following pore pressure expressions:

$$u_s(y) = (r_w \gamma_w)^{1-\frac{1}{n}} \left(-\frac{r_e^2}{2\widetilde{c}_{h0}} \frac{\partial \overline{u}}{\partial t} \right)^{\frac{1}{n}} \left(\frac{\widetilde{c}_{h0}}{\widetilde{c}_h} \right)^{\frac{1}{n}} \left(\frac{\widetilde{k}_h}{\widetilde{k}_s} \right)^{\frac{1}{n}} (g(y) - g(1)) \tag{3.61a}$$

and,

$$u(y) = (r_w \gamma_w)^{1-\frac{1}{n}} \left(-\frac{r_e^2}{2\widetilde{c}_{h0}} \frac{\partial \overline{u}}{\partial t} \right)^{\frac{1}{n}} \left(\frac{\widetilde{c}_{h0}}{\widetilde{c}_h} \right)^{\frac{1}{n}} \times \left(g(y) - g(s) + \left(\frac{\widetilde{k}_h}{\widetilde{k}_s} \right)^{\frac{1}{n}} (g(s) - g(1)) \right) \tag{3.61b}$$

where, $g(y)$ is a function given by:

$$g(y) = n y^{1-\frac{1}{n}} \sum_{j=0}^{\infty} \frac{\{-1/n\}_j}{j!((2j+1)n-1)} \left(\frac{y}{N} \right)^{2j} \tag{3.62}$$

The average excess pore pressure satisfies the following algebraic expression:

$$\pi \left(r_e^2 - r_w^2 \right) \overline{u} = 2\pi \int_{r_w}^{r_s} r u_s(r)\, dr + 2\pi \int_{r_s}^{r_e} r u(r)\, dr \tag{3.63a}$$

or in the transformed coordinate system,

$$\overline{u} = \frac{2}{\left(N^2 - 1 \right)} \left(\int_1^s y u_s(y)\, dy + \int_s^N y u(y)\, dy \right) \tag{3.63b}$$

Substituting Equation (3.61) into Equation (3.63) and performing the appropriate integrations gives the excess pore pressure as:

$$\overline{u} = (r_w \gamma_w)^{1-\frac{1}{n}} \left(-\frac{r_e^2}{2\widetilde{c}_{h0}} \frac{\partial \overline{u}}{\partial t} \right)^{\frac{1}{n}} \left(\frac{\widetilde{c}_{h0}}{\widetilde{c}_h} \right)^{\frac{1}{n}} \beta \tag{3.64}$$

with,

$$\beta = \frac{2n}{N^2 - 1} \sum_{j=0}^{\infty} a_j \frac{\{-1/n\}_j}{j!((2j+1)n-1)} \tag{3.65a}$$

$$a_j = \frac{n\left(N^{3-\frac{1}{n}} + s^{3-\frac{1}{n}} \left(\frac{s}{N}\right)^{2j} \left(\left(\frac{\widetilde{k}_h}{\widetilde{k}_s}\right)^{\frac{1}{n}} - 1 \right) - \left(\frac{\widetilde{k}_h}{\widetilde{k}_s}\right)^{\frac{1}{n}} N^{-2j} \right)}{((2j+3)n-1)} + \frac{N^2 - s^2}{2} \left(\left(\frac{\widetilde{k}_h}{\widetilde{k}_s}\right)^{\frac{1}{n}} - 1 \right) s^{1-\frac{1}{n}} \left(\frac{s}{N}\right)^{2j} - \frac{N^2 - 1^2}{2} \left(\frac{\widetilde{k}_h}{\widetilde{k}_s}\right)^{\frac{1}{n}} N^{-2j} \tag{3.65b}$$

The pore pressure at any point in the soil can now be related to the average excess pore water pressure by substituting Equation (3.64) into Equation (3.61). The resulting expressions for pore water pressure in the smear and undisturbed zones are:

$$u_s(y) = \frac{\overline{u}}{\beta} \left(\frac{\widetilde{k}_h}{\widetilde{k}_s}\right)^{\frac{1}{n}} (g(y) - g(1)) \tag{3.66a}$$

$$u(y) = \frac{\overline{u}}{\beta} \left(g(y) - g(s) + \left(\frac{\widetilde{k}_h}{\widetilde{k}_s}\right)^{\frac{1}{n}} (g(s) - g(1)) \right) \tag{3.66b}$$

Usually the expressions for excess pore water pressure would involve explicit functions of time (Hansbo, 1981; Hansbo, 2001), however, as shown below, the solution of Equation (3.64) gives consolidation time as a non-invertible function of $\overline{u}$. Thus after choosing a suitable $\overline{u}$ value the corresponding time at which this average excess pore pressure occurs is determined.

3.3.3 Approximation for Vacuum Loading

Vacuum pressure applied along the drain implies a non-zero pore pressure (negative for vacuum pressure) at the soil drain boundary. The above equations can be

formulated to include vacuum pressure by changing the boundary condition when deriving Equation (3.61). By designating the pore pressure in the drain ($r/r_w = 1$), as the vacuum pressure w, the expressions for pore pressure in Equation (3.64) and (3.66) can be rewritten to include vacuum pressure:

$$\bar{u} = (r_w \gamma_w)^{1-\frac{1}{n}} \left(-\frac{r_e^2}{2\tilde{c}_{h0}} \frac{\partial \bar{u}}{\partial t} \right)^{\frac{1}{n}} \left(\frac{\tilde{c}_{h0}}{\tilde{c}_h} \right)^{\frac{1}{n}} \beta + w \tag{3.67}$$

$$u_s(y) = \frac{\bar{u} - w}{\beta} \left(\frac{\tilde{k}_h}{\tilde{k}_s} \right)^{\frac{1}{n}} (g(y) - g(1)) + w \tag{3.68}$$

$$u(y) = \frac{\bar{u} - w}{\beta} \left(g(y) - g(s) + \left(\frac{\tilde{k}_h}{\tilde{k}_s} \right)^{\frac{1}{n}} (g(s) - g(1)) \right) + w \tag{3.68b}$$

Unfortunately, Equation (3.67) does not have an analytical solution. However, a vacuum load can be modeled by an equivalent surcharge load. For example, a 50 kPa surcharge load and a 20 kPa vacuum load can be simulated by a 70 kPa surcharge. While settlements calculated from the equivalent 70 kPa surcharge may be accurate, the pore pressure values will not correspond to those in the ground. The actual average pore pressure, $\bar{u}$ is obtained from the expression (Note, for vacuum loads $w < 0$):

$$\bar{u} = \bar{u}_c + w \tag{3.69}$$

where, $\bar{u}_c$ is the excess pore water pressure calculated from the combined surcharge load. By substituting Equation (3.69) into Equation (3.68), the pore pressure at radial distance r is found to have the form:

$$u = \frac{\bar{u}_c}{\beta} f(r) + w \tag{3.70}$$

where, $f(r)$ is a function of radial distance described in Equation (3.68). The corresponding form for Darcian flow conditions is:

$$u = \frac{\overline{u}_c}{\mu} f(r) + w \tag{3.71}$$

where, the Darcian parameters μ and $f(r)$ are described in Section 3.2 and Appendix A. If vacuum loads are not included, $w = 0$, then $\overline{u}_c = \overline{u}$. The following section deals with the analytical solution to Equation (3.64) where vacuum loads are not explicitly included. They can be implicitly included with the above technique.

3.3.4 Normally Consolidated Soil

In order to solve Equation (3.64), the consolidation coefficient ($\widetilde{c}_h / \widetilde{c}_{h0}$) must be determined. When considering material nonlinearity, the coefficient of consolidation becomes dependant on the effective stress (under equal strain, the effective stress does not vary radially). The effective stress can be written as:

$$\sigma' = \sigma'_0 + \Delta\sigma + W\Delta\sigma \tag{3.72}$$

where, $\Delta\sigma$ = instantaneous change in total stress, and W is a normalized pore pressure given by:

$$W = \frac{\overline{u}}{\Delta\sigma} \tag{3.73}$$

The consolidation coefficient involves permeability and volume compressibility. Volume compressibility is defined by the relationship:

$$m_v = \frac{1}{1 + e_0} \frac{\partial e}{\partial \sigma'} \tag{3.74a}$$

Differentiating Equation (3.48) to find $\partial e / \partial \sigma'$ and subsequent substitution into Equation (3.74a) yields:

$$m_v = \frac{-0.434 C_c}{\sigma'(1+e_0)} \tag{3.74b}$$

The relative change in volume compressibility with effective stress is thus expressed by:

$$\frac{m_{v0}}{m_v} = \left(\frac{\sigma'}{\sigma'_0}\right) \tag{3.75}$$

Substituting Equation (3.48) into Equation (3.49) gives the relative change in permeability with effective stress given by:

$$\frac{\widetilde{k}}{\widetilde{k}_0} = \left(\frac{\sigma'}{\sigma'_0}\right)^{-C_c/C_k} \tag{3.76}$$

Combining Equations (3.58), (3.72), (3.75), and (3.76), the stress dependency of $\widetilde{c}_h$ is calculated as:

$$\frac{\widetilde{c}_h}{\widetilde{c}_{h0}} = \left(1 + \frac{\Delta\sigma}{\sigma'_0} - \frac{W\Delta\sigma}{\sigma'_0}\right)^{(1-C_c/C_k)} \tag{3.77}$$

Substituting Equation (3.77) into Equation (3.64) gives the differential equation for normally consolidated soil:

$$-\partial\widetilde{T} = \frac{\partial W}{W^n}\left(\frac{\widetilde{c}_h}{\widetilde{c}_{h0}}\right) \tag{3.78}$$

where, $\widetilde{T}$ is a modified time factor defined by:

$$\widetilde{T} = 8\frac{T_{h0}}{\beta^n}\left(\frac{\Delta\sigma}{r_w\gamma_w}\right)^{n-1} \tag{3.79a}$$

$$T_{h0} = \frac{\widetilde{c}_{h0}t}{4r_e^2} \tag{3.79b}$$

Using a power series, expansion of $\widetilde{c}_h/\widetilde{c}_{h0}$ about the point $W = 0$ gives:

$$\frac{\widetilde{c}_{h0}}{W^n \widetilde{c}_h} = \left(1+\frac{\Delta\sigma}{\sigma'_0}\right)^{(1-C_c/C_k)} \sum_{j=0}^{\infty} \frac{\{1-C_c/C_k\}_j}{j!} \left(1+\frac{\sigma'_0}{\Delta\sigma}\right)^{-j} (W)^{j-n-1} \qquad (3.80)$$

Substituting Equation (3.80) into Equation (3.78) and integrating with the initial condition, $W=1$ at $t=0$, results in:

$$\widetilde{T} = -\left(1+\frac{\Delta\sigma}{\sigma'_0}\right)^{-(1-C_c/C_k)} \left[\sum_{j=0}^{\infty} \frac{\{1-C_c/C_k\}_j}{j!(j-n+1)} \left(1+\frac{\sigma'_0}{\Delta\sigma}\right)^{-j} \left(W^{j-n+1}-1\right)\right] \qquad (3.81)$$

For each value of normalized excess pore pressure, $0<W\le 1$, substituted into Equation (3.81) the resulting value of $\widetilde{T}$ is found. The time required to reach the specified degree of consolidation is then found from Equation (3.79). Equation (3.81) is undefined for integer values of n, however, values very close to integer values give the appropriate consolidation times (e.g. use $n=1.0001$ not $n=1$).

When $C_c/C_k=1$, i.e. $\widetilde{c}_h$ does not change during consolidation, Equation (3.81) is numerically equivalent to Hansbo's (2001) non-Darcian radial consolidation equation. For the case of Darcian flow $n=1$, and $\widetilde{T}$ is given by

$$\widetilde{T}_{Darcy} = \frac{8T_{h0}}{\mu} \qquad (3.82)$$

The μ parameter can then be any of those described in Section 3.2 above or Appendix A. When $n=1$ and $C_c/C_k=1$, Equation (3.81) is numerically equivalent to Hansbo's (1981) radial consolidation equation. If $C_c/C_k<1$ then c_h increases over time and the consolidation rate is faster. If $C_c/C_k>1$ then c_h decreases over time and the consolidation rate is slower. The degree to which consolidation is slowed or hastened is controlled by the normalized factor $\Delta\sigma/\sigma'_0$. Taken together

C_c/C_k and $\Delta\sigma/\sigma_0'$ give an indication of the total change in $\widetilde{c}_h$ over the consolidation period as per Equation (3.77). In practice, C_c/C_k ranges between 0.5-2.0 (Berry and Wilkinson, 1969; Mesri and Rokhsar, 1974), with C_k taken from the empirical relation $C_k = 0.5e_0$.

Figure 3.11 gives consolidation curves based on the ratio between the finial and initial consolidation coefficients (c_{hf} and c_{h0}, respectively) for Darcian flow. Though the same change in c_h can be obtained with different C_c/C_k and $\Delta\sigma/\sigma_0'$ values, the resulting difference in degree of consolidation is minimal. The actual values of C_c/C_k and $\Delta\sigma/\sigma_0'$ used in producing Figure 3.11 are given in Table 3.1. Using different parameter values to those in Table 3.1 will result in slightly faster consolidation. Analysis including the nonlinear soil properties is particularly relevant for soils where relatively high values of $\Delta\sigma/\sigma_0'$ will lead to large changes in c_h, and thus potentially large deviations in degree of consolidation compared to calculations based on constant soil property. For c_{hf}/c_{h0} values close to unity, each 10% increase in c_{hf}/c_{h0} decreases the time to reach 90% consolidation by approximately 5% (compared to the ideal case of c_{hf}/c_{h0} = 1). Each 10% decrease in c_{hf}/c_{h0} increases the time to reach 90% consolidation by approximately 10%.

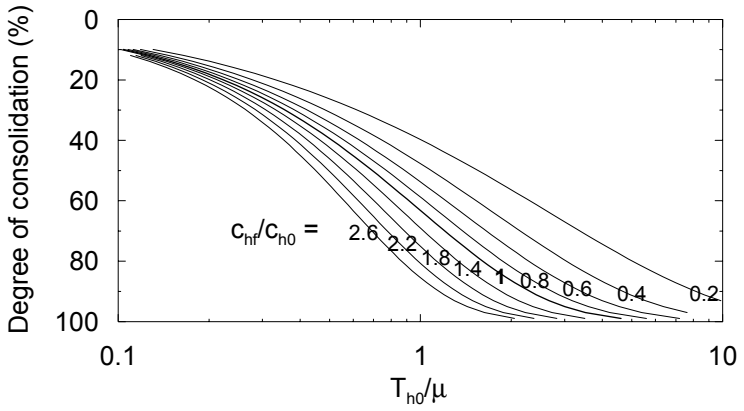

Figure 3.11 Consolidation curves depending on total change in consolidation coefficient

Table 3.1 Parameters used to produce Figure 3.11

C_c/C_k	$\Delta\sigma/\sigma'_0$	c_{hf}/c_{h0}
0.500	5.758	2.600
0.500	3.840	2.200
0.500	2.240	1.800
0.500	0.960	1.400
1.000	1.000	1.000
1.115	6.000	0.800
1.263	6.000	0.600
1.471	6.000	0.400

3.3.4.1 Concise Notation

Similar expressions to that on the right hand side of Equation (3.81) are used in subsequent sections. To avoid writing such large expressions a shorthand notation is used whereby a function, F, depending on parameters, α, θ and W, is described by:

$$F[W,\alpha,\theta] = -\left(1+\frac{\Delta\sigma}{\sigma'_0}\right)^{-(1-\alpha/C_k)} \times \left[\sum_{j=0}^{\infty} \frac{\{1-\alpha/C_k\}_j}{j!(j-n+1)}\left(1+\frac{\sigma'_0}{\Delta\sigma}\right)^{-j}\left(W^{j-n+1}-\theta^{j-n+1}\right)\right] \tag{3.83}$$

For example, Equation (3.81) can now be written in the concise notation as:

$$\widetilde{T} = F[W, C_c, 1] \tag{3.84}$$

3.3.5 Overconsolidated Soil

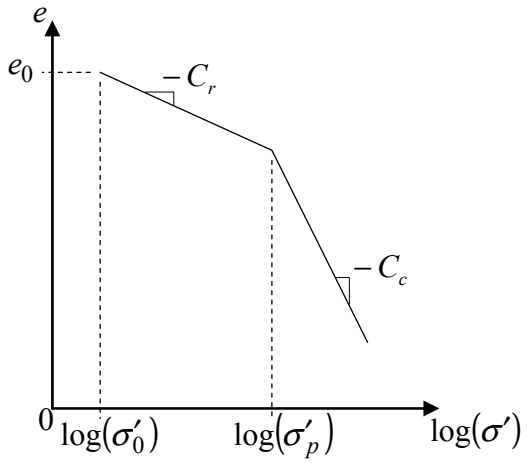

Figure 3.12 Void ratio-stress relationship for overconsolidated soil

The compressibility of soils previously subjected to higher effective stresses (overconsolidated) may increase markedly when the preconsolidation pressure, σ'_p, is exceeded. The void ratio-stress relationship for overconsolidated soil is different to that of Equation (3.48). With reference to Figure 3.12, the compressibility relationships in the recompression zone ($\sigma' \le \sigma'_p$) and the compression zone ($\sigma' > \sigma'_p$) are described, respectively, by:

$$e = e_0 - C_r \log\left(\sigma' / \sigma'_0\right) \tag{3.85a}$$

and,

$$e = e_0 - C_r \log\left(\sigma'_p / \sigma'_0\right) - C_c \log\left(\sigma' / \sigma'_0\right) \tag{3.85b}$$

The change in volume compressibility with effective stress, Equation (3.75), is now given by:

$$\frac{m_{v0}}{m_v} = \left(\frac{\sigma'}{\sigma'_0}\right) \tag{3.86a}$$

and,
$$\frac{m_{v0}}{m_v} = \frac{C_r}{C_c}\left(\frac{\sigma'}{\sigma'_0}\right) \tag{3.86b}$$

The change in permeability with effective stress, Equation (3.76), becomes:

$$\frac{\widetilde{k}}{\widetilde{k}_0} = \left(\frac{\sigma'}{\sigma'_0}\right)^{-C_r/C_k} \tag{3.87a}$$

and,
$$\frac{\widetilde{k}}{\widetilde{k}_0} = \left(\frac{\sigma'_p}{\sigma'_0}\right)^{(C_c-C_r)/C_k}\left(\frac{\sigma'}{\sigma'_0}\right)^{-C_c/C_k} \tag{3.87b}$$

Combining Equations (3.58), (3.72), (3.86), and (3.87), results in the following expressions for the stress dependency of $\widetilde{c}_h$ in the recompression and compression zones:

$$\frac{\widetilde{c}_h}{\widetilde{c}_{h0}} = \left(1 + \frac{\Delta\sigma}{\sigma'_0} - \frac{W\Delta\sigma}{\sigma'_0}\right)^{(1-C_r/C_k)} \tag{3.88a}$$

and,
$$\frac{\widetilde{c}_h}{\widetilde{c}_{h0}} = \frac{C_r}{C_c}\left(\frac{\sigma'_p}{\sigma'_0}\right)^{(C_c-C_r)/C_k}\left(1 + \frac{\Delta\sigma}{\sigma'_0} - \frac{W\Delta\sigma}{\sigma'_0}\right)^{(1-C_c/C_k)} \tag{3.88b}$$

A similar procedure to that used to derive Equation (3.81) is now followed. The power series representation of Equation (3.88a), $\widetilde{c}_h/\widetilde{c}_{h0}$, is substituted into Equation (3.78) and solved with the initial condition, $\widetilde{T} = 0$ $W = 1$, to give:

$$\widetilde{T} = F[W, C_r, 1] \tag{3.89a}$$

where, T_{h0} is calculated using C_r. Equation (3.89a) is valid during recompression, that is when $W \geq W_p$, where W_p corresponds to the preconsolidation pressure. W_p is calculated from:

$$W_p = 1 - \frac{\sigma'_0}{\Delta\sigma}\left(\frac{\sigma'_p}{\sigma'_0} - 1\right) \tag{3.90}$$

The time factor required to reach the preconsolidation pressure, $\widetilde{T}_p$, is determined by substituting W_p into Equation (3.89a), hence,

$$\widetilde{T}_p = F\left[W_p, C_r, 1\right] \tag{3.91}$$

Now the power series representation of Equation (3.88b) is substituted into Equation (3.78) and solved with the initial condition, $W = W_p$ at $\widetilde{T} = \widetilde{T}_p$. The resulting expression for consolidation in the compression phase is:

$$\widetilde{T} = F\left[W, C_c, W_p\right]\frac{C_c}{C_r}\left(\frac{\sigma'_p}{\sigma'_0}\right)^{-(C_c - C_r)/C_k} + F\left[W_p, C_r, 1\right] \tag{3.89b}$$

Equation (3.89b) can be used for normally consolidated soils by putting $C_r = C_c$ and $W_p = 1$. The m_{v0} value in $\widetilde{T}$ should always be calculated using the recompression index, C_r.

3.3.6 Settlements

Primary consolidation settlements, ρ, result from changes in effective stress. Once excess pore water pressures are found (i.e. based on $W = \overline{u}/\Delta\sigma$) then the settlements can be calculated using the following expressions. If the initial and final effective stresses (σ'_0 and $\sigma'_0 + \Delta\sigma$) fall in the recompression zone then settlements are calculated with:

$$\rho = \frac{HC_r}{1 + e_0}\log\left(1 + \frac{\Delta\sigma}{\sigma'_0}(1 - W)\right) \tag{3.92a}$$

where H is the depth of soil. If the initial and final effective stresses fall in the compression zone then settlements are given by:

$$\rho = \frac{HC_c}{1+e_0}\log\left(1+\frac{\Delta\sigma}{\sigma'_0}(1-W)\right) \tag{3.92b}$$

If the initial effective stress is less than the preconsolidation pressure, σ'_p, and the final effective stress is greater than the preconsolidation pressure then settlements in the recompression zone are the same as in Equation (3.92a); settlements in the compression zone are then expressed as:

$$\rho = \frac{H}{1+e_0}\left((C_r - C_c)\log(OCR) + C_c\log\left(1+\frac{\Delta\sigma}{\sigma'_0}(1-W)\right)\right) \tag{3.92c}$$

where, OCR is the overconsolidation ratio defined by:

$$OCR = \frac{\sigma'_p}{\sigma'_0} \tag{3.93}$$

The total primary settlement, ρ_∞, can be calculated by putting $W = 1$ in the above equations.

3.3.7 Degree of Consolidation

The degree of consolidation as determined by pore pressure dissipation is simply given by:

$$U_h = 1 - \frac{\bar{u}}{\Delta\sigma} = 1 - W \tag{3.94}$$

The degree of consolidation based on settlement is written as:

$$U_{hs} = \frac{\rho}{\rho_\infty} \tag{3.95}$$

The relationship between U_{hs} and W depends on the stress history of the soil. With reference to Equation (3.92) U_{hs}, when the stress range is completely in the recompression or compression zones, is related to W by:

$$U_{hs} = \frac{\log\left(1+\frac{\Delta\sigma}{\sigma_0'}(1-W)\right)}{\log\left(1+\frac{\Delta\sigma}{\sigma_0'}\right)} \tag{3.96a}$$

For other cases if $\sigma' \le \sigma_p'$ then:

$$U_{hs} = \frac{\log\left(1+\frac{\Delta\sigma}{\sigma_0'}(1-W)\right)}{(1-C_c/C_r)\log(OCR)+C_c/C_r\log\left(1+\frac{\Delta\sigma}{\sigma_0'}\right)} \tag{3.96b}$$

If $\sigma' > \sigma_p'$ then:

$$U_{hs} = \frac{(1-C_c/C_r)\log(OCR)+C_c/C_r\log\left(1+\frac{\Delta\sigma}{\sigma_0'}(1-W)\right)}{(1-C_c/C_r)\log(OCR)+C_c/C_r\log\left(1+\frac{\Delta\sigma}{\sigma_0'}\right)} \tag{3.96c}$$

The degree of consolidation based on pore pressure and settlement are different. For Equation (3.96a) U_h lags U_{hs} depending on $\Delta\sigma/\sigma_0'$ as shown in Figure 3.13. When determining the degree of consolidation for normally consolidated soils by settlement data, it is important to note that particularly during the middle stages of consolidation, the effective stress in the soil will be less than expected if it is assumed U_h is equal to U_{hs}. For overconsolidated soil a large variety of behaviour can occur, as shown in Figure 3.14, depending on the value of C_c/C_r, OCR and $\Delta\sigma/\sigma_0'$. During the recompression stage, because C_r is low relative to C_c, dissipation of excess pore pressure is fast while the resulting settlements are small compared to the ultimate settlement. This means during recompression U_h will be greater than U_{hs}. During the compression stage, U_{hs} may or may not become

greater than U_h. The wide variety of relationships between U_{hs} and U_h for overconsolidated soil emphasizes the need for accurate determination of the soil stress history and the care needed when specifying construction milestones based on degree of consolidation.

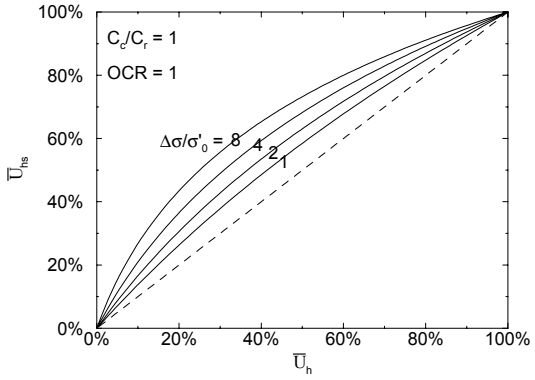

Figure 3.13 Comparison between degree of consolidation based on settlement and pore pressure for normally consolidated soil

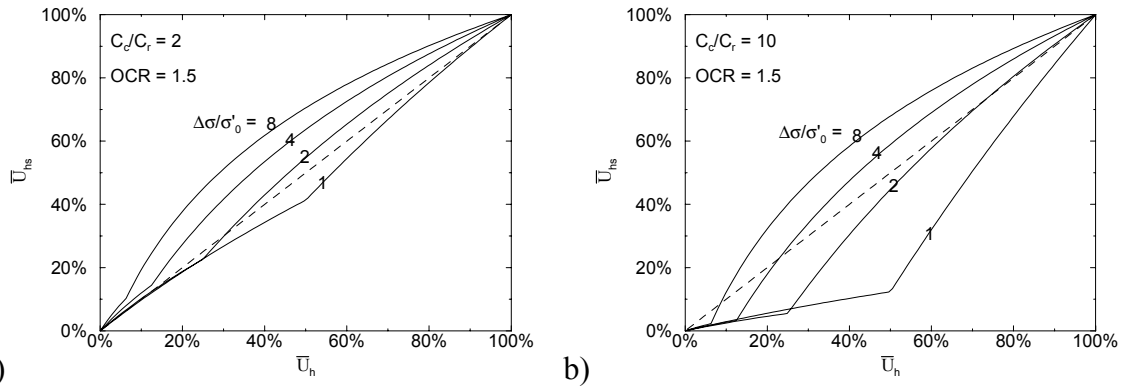

Figure 3.14 Comparison between degree of consolidation based on settlement and pore pressure for overconsolidated soil

3.3.8 Approximation for Arbitrary Loading

The consolidation behaviour expressed by Equation (3.28) is valid only for instantaneous loading. However, arbitrary loading can be simulated by subdividing a continuous loading function into a finite number of instantaneous step loads (see

Figure 3.15). The only restriction is that average excess pore pressure cannot become negative ($u > 0$). For example slightly decreasing loads associated with submergence of fill can be modeled but the swelling associated with preload removal (caused by dissipation of negative pore pressure) cannot be modeled with the consolidation equations presented.

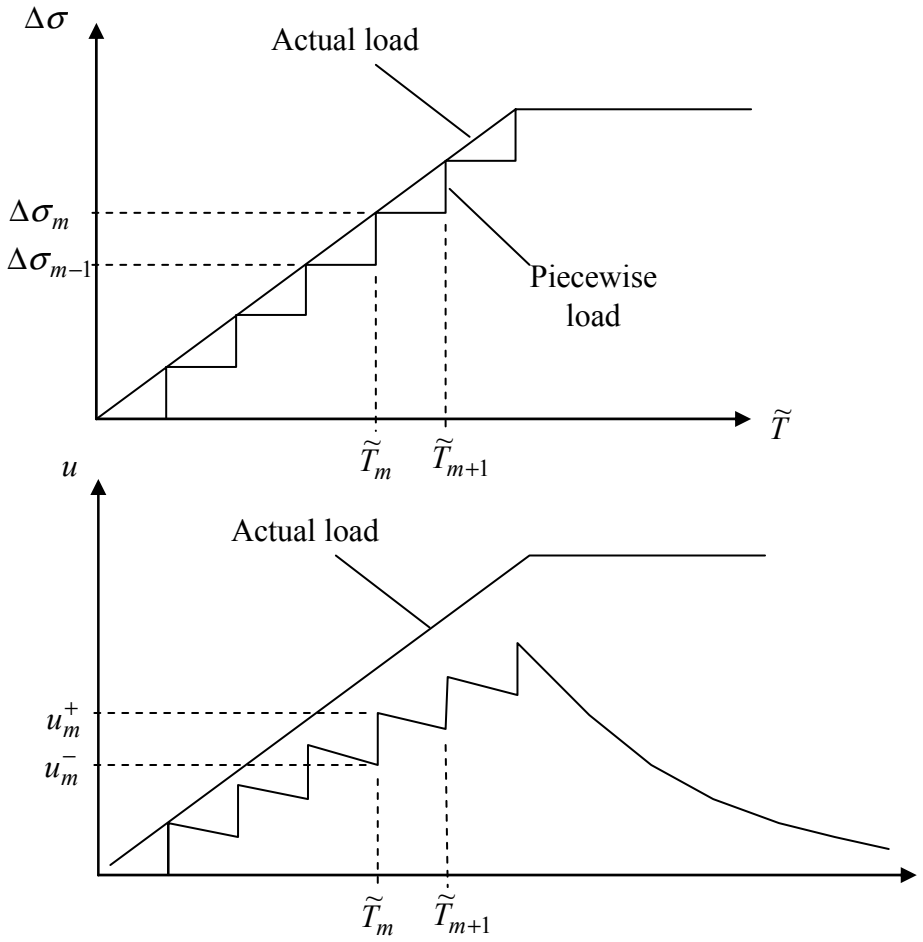

Figure 3.15 Schematic of piecewise loading

For the m^{th} loading stage, as shown in Figure 3.15, at $\widetilde{T}_m$ the load increases from $\Delta\sigma_{m-1}$ to $\Delta\sigma_m$. The loading stage ends at $\widetilde{T}_{m+1}$. The excess pore water pressure at the end of the last increment u_m^- is known (for example in the first loading step $u_m^- = 0$). The pore pressure after the load application, u_m^+, is given by:

$$u_m^+ = u_m^- + \Delta\sigma_m - \Delta\sigma_{m-1} \tag{3.97}$$

The normalized pore pressure at the beginning of the load increment, W_m^+ is then described by:

$$W_m^+ = \frac{u_m^+}{\Delta\sigma_m} \tag{3.98}$$

The initial conditions for solution of Equation (3.78) have now been found: $W = W_m^+$ at $\widetilde{T} = \widetilde{T}_m$. There are three cases to consider in the solution of Equation (3.78). If the preconsolidation pressure has been exceeded in previous loading steps, then the normalized pore pressure in the m^{th} loading step is governed by:

$$\widetilde{T} = \widetilde{T}_m + F\left[W, C_c, W_m^+\right]\frac{C_c}{C_r}\left(\frac{\sigma'_p}{\sigma'_0}\right)^{-(C_c - C_r)/C_k} \tag{3.99a}$$

If the preconsolidation pressure has not been exceeded in previous load steps, then the expressions for normalized pore pressure in the recompression and compression zones are:

$$\widetilde{T} = \widetilde{T}_m + F\left[W, C_r, W_m^+\right] \tag{3.99b}$$

and,
$$\widetilde{T} = \widetilde{T}_m + F\left[W, C_c, W_p\right]\frac{C_c}{C_r}\left(\frac{\sigma'_p}{\sigma'_0}\right)^{-(C_c - C_r)/C_k} + F\left[W_p, C_r, W_m^+\right] \tag{3.99c}$$

The consolidation behaviour can now be described at any point. The following list of steps describes the process of constructing a pore pressure vs. time graph. The process is best automated in a computer program.

1. Approximate the arbitrary loading by a finite number of instantaneous step loads.
2. Convert the loading times to time factor values, $\widetilde{T}$ using Equation (3.79).

3. Calculate W_m^+ using Equations (3.97) and (3.98).
4. In small increments of W calculate $\widetilde{T}$, with Equation (3.99), until $\widetilde{T} > \widetilde{T}_{m+1}$.
5. Calculate u_{m+1}^-. Either use the last W value obtained in step 4, or interpolate between the last two values of W found in step 4.
6. Repeat steps 3 to 5 for each loading stage.
7. Convert the time factor values obtained in above steps to time values using Equation (3.79).

In the steps just described $\Delta\sigma$ changes and in the m^{th} loading stage is equal to $\Delta\sigma_m$. For cases where soil properties vary with depth, the soil profile can be divided into sub-layers and the above process performed for each sub-layer.

3.3.9 Illustrative Example

A pore pressure and settlement analysis has been performed on a soil/drain system with properties given in Table 3.2. The resulting average pore pressure and settlement plots are shown in Figure 3.16.

Table 3.2 Parameters for illustrative example

Parameter	Value	Parameter	Value
r_w (m)	0.07	σ'_0 (kPa)	10
r_e (m)	1.4	σ'_p (kPa)	10, 20, 30
r_s (m)	0.07	n	1.001, 1.3
C_c	0.7	γ_w (kN/m^3)	10
C_r	0.175	e_0	1
C_k	0.875	H (m)	1

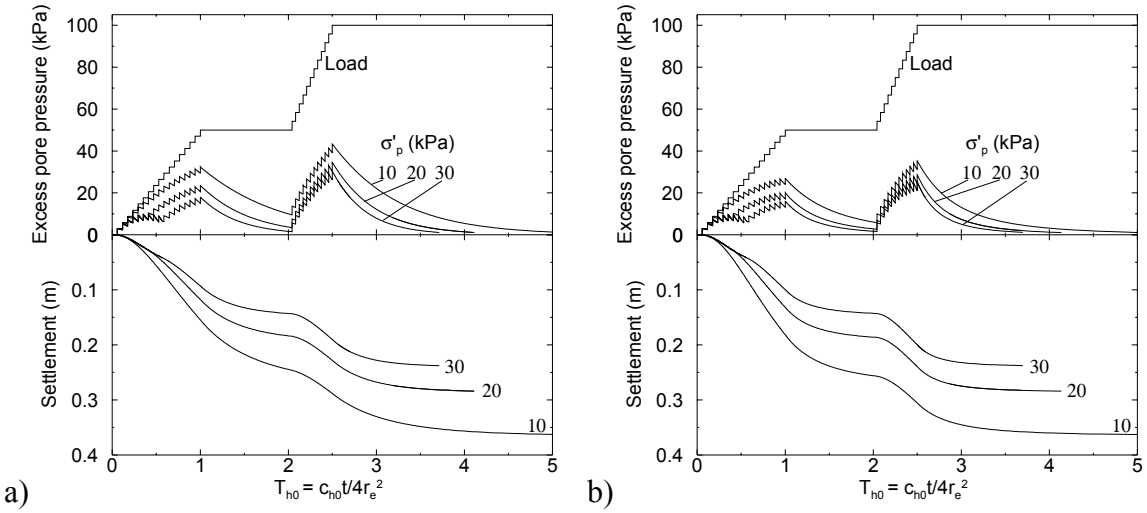

Figure 3.16 Nonlinear radial consolidation for non-Darcian flow exponent a) $n = 1.001$ and b) $n = 1.3$

There are a few salient points to note from Figure 3.16. For the two overconsolidated soils ($\sigma'_p = 20, 30$), the change from recompression to compression can be observed during the first ramp loading stage. At the preconsolidation pressure, the slope of the excess pore pressure plot sharply increases reflecting the slower rate of consolidation during compression. Just prior to the preconsolidation pressure being reached, the dissipation of pore pressure in the highly overconsolidated soil ($\sigma'_p = 30$) actually exceeds that generated by the load application; the pore pressure reduces despite load still being applied. This occurs because $C_r/C_k < 1$ resulting in an increasingly faster consolidation reaching a maximum just prior to the preconsolidation pressure. The difference between the Darcian flow of Figure 3.16a) and the non-Darcian flow of Figure 3.16b) is small for the highly overconsolidated soils. For the normally consolidated soil ($\sigma'_p = 10$), the difference is illustrated during the first ramp loading stage. For non-Darcian flow the pore pressure curve is slightly flatter, because, due to the power law flow

relationship, the higher pore pressures result in faster flow. The settlement plots illustrate the importance of minimizing the disturbance caused by vertical drain installation. Drain installation (see smear zone description in Section 3.2) can to some extent destroy any existing structure in the soil. Hence the preconsolidation pressure may be lowered which, as shown in Figure 3.16, causes greater settlements for the same pressure increase. This examples shows that with the equations presented above, almost any primary consolidation problem involving radial drainage can be modeled (provided the effective stress increases with time). When more than one soil layer is present, the analysis can simply be repeated with different soil properties. However, if vertical drainage is important or the excess pore pressure at some stage becomes negative then a different method, taking these aspects into consideration, should be used. Such a method, for multi-layered soils is described in the Section 3.4 immediately below.

3.4 Multi-layered Consolidation with the Spectral Method

3.4.1 Analytical Solution

A novel use of the spectral method to determine excess pore water pressure during consolidation of multi-layered soil with time constant material properties is presented. A unit cell with combined vertical and radial consolidation under equal strain conditions is considered. The use of linearly distributed material properties with depth allows arbitrary distributions of properties to be modeled. By incorporating surcharge and vacuum loading that vary with both depth and time, a wide range of consolidation problems can be analysed. The spectral method is a meshless technique producing a series solution to the consolidation problem based on

matrix operations. Accuracy can be improved by increasing the number of terms used in the series solution.

3.4.2 Continuity Equation

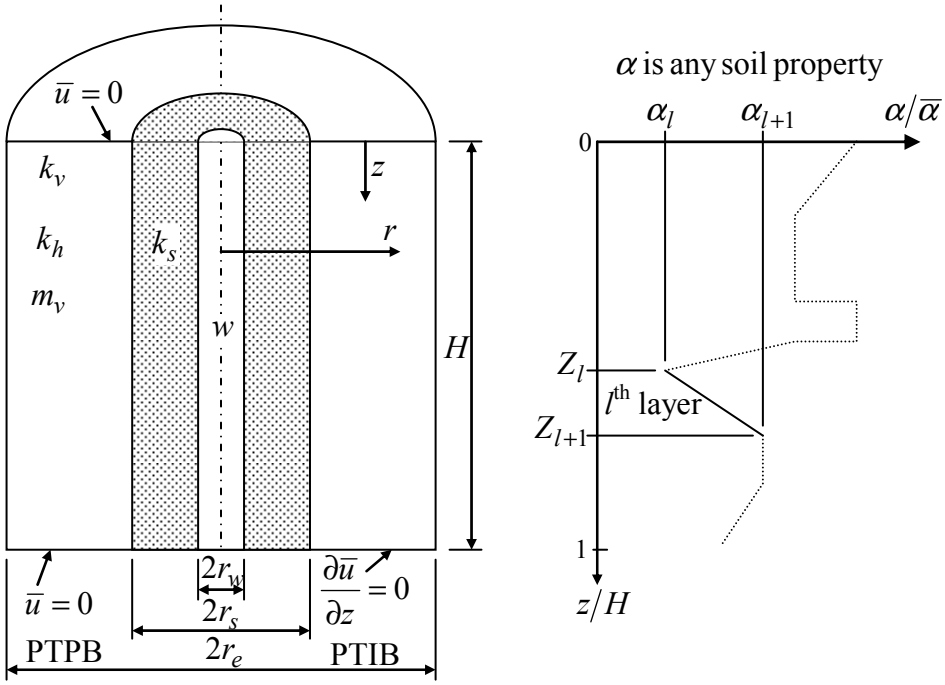

Figure 3.17 Unit cell

The governing partial differential equation for consolidation with vertical and radial drainage, including depth dependant soil properties will now be presented. Figure 3.17 shows a unit cell of height H, and external radius r_e. The radius of the vertical drain and smear zone are r_w and r_s, respectively. Drainage conditions in the vertical direction are either, pervious top and pervious bottom (PTPB), or pervious top and impervious bottom (PTIB). The velocity of flow in the radial direction, v_r, is described by Darcy's law:

$$v_r = -\frac{k_h}{\gamma_w}\frac{\partial u}{\partial r} \tag{3.100}$$

where, k_h = undisturbed horizontal permeability, γ_w = unit weight of water, u = excess pore water pressure, and r = radial coordinate. In the vertical direction, following the approach of Tang and Onitsuka (2000) and Wang and Jiao (2004), Darcy's law is modified to include the average excess pore water pressure at a particular depth, $\bar{u}$. The velocity of flow in the vertical direction, υ_v, is then given by:

$$\upsilon_v = -\frac{k_v}{\gamma_w}\frac{\partial \bar{u}}{\partial z} \tag{3.101}$$

where, k_v is the vertical permeability (k_v in smear and undisturbed zone assumed equal), and z = vertical coordinate. Deformation is assumed to take place solely in the vertical direction under equal-strain conditions (Barron, 1948; Hansbo, 1981), hence:

$$\frac{\partial \varepsilon}{\partial t} = m_v\left(\frac{\partial \bar{\sigma}}{\partial t} - \frac{\partial \bar{u}}{\partial t}\right) \tag{3.102}$$

where, $\partial\varepsilon/\partial t$ = vertical strain rate , m_v = coefficient of volume compressibility (m_v in smear and undisturbed zone assumed equal), and $\bar{\sigma}$ = average total stress. Following Hansbo (1981) approach (modified to include vertical drainage), flow into and out of a cylindrical slice with internal radius r, and external radius r_e is considered. The resulting expressions for pore water pressure gradient in the undisturbed and smear zones are respectively:

$$\frac{\partial u}{\partial r} = \frac{\gamma_w}{2k_h}\left(\frac{r_e^2}{r} - r\right)\left[\frac{\bar{k}_v}{\gamma_w H^2}\left(\frac{\partial}{\partial Z}\left(\frac{k_v}{\bar{k}_v}\right)\frac{\partial \bar{u}}{\partial Z} + \frac{k_v}{\bar{k}_v}\frac{\partial^2 \bar{u}}{\partial Z^2}\right) + \frac{\partial \varepsilon}{\partial t}\right] \tag{3.103a}$$

and,

$$\frac{\partial u_s}{\partial r} = \frac{\gamma_w}{2k_s}\left(\frac{r_e^2}{r} - r\right)\left[\frac{\bar{k}_v}{\gamma_w H^2}\left(\frac{\partial}{\partial Z}\left(\frac{k_v}{\bar{k}_v}\right)\frac{\partial \bar{u}}{\partial Z} + \frac{k_v}{\bar{k}_v}\frac{\partial^2 \bar{u}}{\partial Z^2}\right) + \frac{\partial \varepsilon}{\partial t}\right] \tag{3.103b}$$

where, u_s = excess pore water pressure in the smear zone, k_s = horizontal smear zone permeability, and Z (equal to z/H) is a normalized depth parameter. $\bar{k}_v$ and $\bar{m}_v$ are convenient reference values for the relevant parameters. The average excess pore pressure in the soil cylinder at depth Z is found from the following algebraic expression:

$$\bar{u}\,\pi\left(r_e^2 - r_w^2\right) = \int_{r_w}^{r_s} 2\pi r u_s \, dr + \int_{r_s}^{r_e} 2\pi r u \, dr \tag{3.104}$$

Equation (3.103) is integrated in the r direction (noting k_v, m_v, and σ are independent of r) with the boundary conditions $u(r_s,t) = u_s(r_s,t)$ and $u_s(r_w,t) = w$. The term w is the pore water pressure in the drain which will be negative for vacuum loading. The resulting expressions are combined with Equations (3.102) and (3.104) to give the average pore water pressure at normalized depth Z,

$$\bar{u} = \frac{r_e^2 \gamma_w \mu}{2k_h}\left[\frac{\bar{k}_v}{\gamma_w H^2}\left(\frac{\partial}{\partial Z}\left(\frac{k_v}{\bar{k}_v}\right)\frac{\partial \bar{u}}{\partial Z} + \frac{k_v}{\bar{k}_v}\frac{\partial^2 \bar{u}}{\partial Z^2}\right) + \bar{m}_v \frac{m_v}{\bar{m}_v}\left(\frac{\partial \bar{\sigma}}{\partial t} - \frac{\partial \bar{u}}{\partial t}\right)\right] + w \tag{3.105}$$

The μ parameter can be any of those described in Section 3.2 and Appendix A, or plane strain parameters given by Hird et al. (1992), and Indraratna and Redana (1997).

The analysis so far has involved operations in the horizontal direction. To facilitate ease of computation in the vertical direction, a lumped parameter, η, linked to the contribution of horizontal drainage is introduced, hence,

$$\eta = \frac{k_h}{r_e^2 \mu} \tag{3.106a}$$

The corresponding reference value of η is $\overline{\eta}$. To prevent horizontal drainage within a particular soil layer η is set equal to zero. This is useful for analyzing problems with partially penetrating vertical drains. Soil layers below the penetration depth will have $\eta = 0$ while still allowing vertical drainage. Other than purely numerical methods, existing solutions for partially penetrating drains are only available for two layer systems. The present method can also predict the effect of using both long and short drains in unison. In the lower soil layers where only the longer drains occur, η will be less than in the upper layers where both long and short PVD provide drainage. The treatment of η greatly increases the versatility of the model.

Using the definition of η, Equation (3.105) is now rearranged to give the governing differential equation:

$$\frac{m_v}{\overline{m}_v}\frac{\partial \overline{u}}{\partial t} = -\left[dT_h \frac{\eta}{\overline{\eta}}\overline{u} - dT_v\left(\frac{\partial}{\partial Z}\left(\frac{k_v}{\overline{k}_v} \right)\frac{\partial \overline{u}}{\partial Z} + \frac{k_v}{\overline{k}_v}\frac{\partial^2 \overline{u}}{\partial Z^2} \right) \right] + \frac{m_v}{\overline{m}_v}\frac{\partial \overline{\sigma}}{\partial t} + dT_h \frac{\eta}{\overline{\eta}} w \quad (3.107)$$

where,

$$dT_v = \frac{\overline{c}_v}{H^2} \quad (3.108)$$

$$dT_h = \frac{2\overline{\eta}}{\gamma_w \overline{m}_v} \quad (3.109)$$

$$\overline{c}_v = \frac{\overline{k}_v}{\gamma_w \overline{m}_v} \quad (3.110)$$

Equation (3.107) is a nonhomogeneous partial differential equation with source/sink terms. The source/sink term, $f(Z,t)$, is a function of depth and time, and arises from surcharge and vacuum loading:

$$f(Z,t) = \frac{m_v}{\overline{m}_v}\frac{\partial \overline{\sigma}}{\partial t} + dT_h \frac{\eta}{\overline{\eta}} w \tag{3.111}$$

To solve Equation (3.107) Duhamel's principle (Asmar, 2004) is used: $f(Z,t)$ is replaced by an impulse load applied at time τ and depth ζ, and a 'fundamental solution', $\overline{u}_\delta(Z,t,\zeta,\tau)$, is obtained (with the initial condition $u(Z,0)=0$). The impulse load is then described by:

$$f(Z,t) = \delta(Z-\zeta)\delta(t-\tau) \tag{3.112}$$

where, $\delta(x)$ is the Dirac Delta function which has the following properties:

$$\delta(x) = 0 \quad x \neq 0 \tag{3.113a}$$

$$\int_{-\infty}^{\infty} \delta(x)\, dx = 1 \tag{3.113b}$$

$$\int_{-\infty}^{\infty} g(x)\delta(x-a)\, dx = g(a) \tag{3.113c}$$

Once the fundamental solution is known, the complete solution is given by:

$$\overline{u}(Z,t) = \int_0^{\tau}\int_0^{1} \overline{u}_\delta(Z,t,\zeta,\tau) f(Z,t)\, d\zeta d\tau \tag{3.114}$$

The solution of Equation (3.107) by the spectral method (Boyd, 2000) is described below.

3.4.3 Depth and Time Dependence of Parameters

The soil properties m_v, k_v, and η are assumed to vary with depth (independent of time), in a piecewise linear fashion (Figure 3.17). The variation of any of the three soil parameters, α, in the l^{th} layer, is described by the following:

$$\frac{\alpha_l(Z)}{\overline{\alpha}} = \frac{\alpha_l Z_{l+1} - \alpha_{l+1} Z_l}{\Delta Z} + Z\frac{\Delta\alpha}{\Delta Z} \tag{3.115}$$

where,

$$\alpha_l = \alpha(Z_l)/\overline{\alpha} \tag{3.116}$$

and Δ is an operator in the Z direction such that:

$$\Delta\alpha = \alpha_{l+1} - \alpha_l \tag{3.117}$$

Using a linear variation of material properties is very useful when modeling arbitrary property distributions. For multi-layer consolidation models with constant material properties within a soil layer, modeling a sharp change in a particular parameter involves subdividing a region into many thin layers. With a linear variation of properties, the approximation of the property distribution can be accomplished with far fewer layers.

The surcharge and vacuum loading parameters, $\overline{\sigma}$ and w, are assumed to vary with both depth and time in a piecewise linear fashion (Figure 3.18). The explicit treatment of linearly varying loads is better than many numerical approaches where varying loads are discretised into a number of constant step loads. The variation of $\overline{\sigma}$ and w, in the l^{th} layer and m^{th} loading increment, is described by:

$$\alpha(Z,t) = \alpha_{m,l}\frac{(Z - Z_l)\Delta\alpha_1}{\Delta Z} + \frac{(Z - Z_l)(\Delta\alpha_1 - \Delta\alpha_2) + \Delta Z(\alpha_{m,l} - \alpha_{m+1,1})(t_m - t)}{(t_{m+1} - t_m)\Delta Z} \tag{3.118}$$

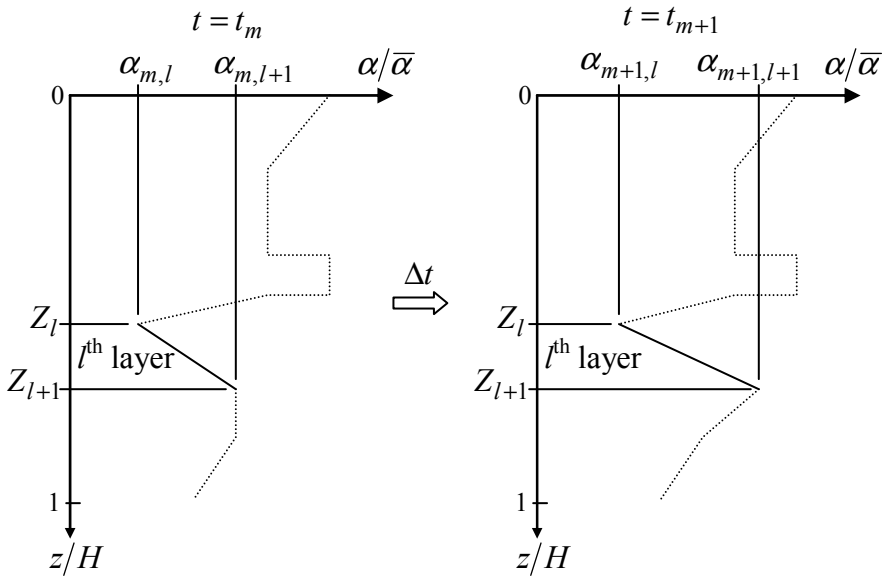

Figure 3.18 Depth and time dependence of surcharge and vacuum loading

3.4.4 Spectral Method

A partial differential equation such as Equation (3.107) can be expressed in a shorthand form as:

$$L\left(\overline{u}\left(Z,t\right)\right) = f\left(Z,t\right) \tag{3.119}$$

where, L is an operator involving partial derivatives. The spectral method involves expressing $u\left(Z,t\right)$ as a truncated series of N terms:

$$\overline{u}\left(Z,t\right) \approx \sum_{j=1}^{N} A_j\left(t\right)\phi_j\left(Z\right) \tag{3.120a}$$

or in matrix notation,

$$\overline{u}\left(Z,t\right) \approx \mathbf{\Phi A} \tag{3.120b}$$

where,

$$\mathbf{\Phi} = \left[\phi_1 \quad \phi_2 \quad \ldots \quad \phi_N\right] \tag{3.121}$$

$$\mathbf{A}^T = \begin{bmatrix} A_1 & A_2 & \dots & A_N \end{bmatrix} \tag{3.122}$$

In the preceding, $\phi_j(Z)$ is a set of linearly independent basis-functions, and $A_j(t)$ are unknown coefficients. The basis functions are generally chosen to satisfy the boundary conditions. In the current analysis, for pervious top and pervious bottom (PTPB) $\bar{u}(0,t)=0$ and $\bar{u}(H,t)=0$, and for pervious top and impervious bottom (PTIB) $\bar{u}(0,t)=0$ and $\partial\bar{u}(H,t)/\partial z=0$. Suitable basis functions are thus:

$$\phi_j(Z) = \sin(M_j Z) \tag{3.123}$$

where,

$$M_j = \begin{cases} j\pi & \text{for PTPB} \\ \dfrac{\pi}{2}(2j-1) & \text{for PTIB} \end{cases} \tag{3.124}$$

The *error*, e_r, of Equation (3.120) that satisfies Equation (3.119) is

$$e_r \approx L(\mathbf{\Phi A}) - f(Z,t) \tag{3.125}$$

The Galerkin procedure requires that the error be orthogonal to each basis function, hence:

$$\int_0^1 e_r \phi_i \, dZ = 0, \text{ for } i = 1,\dots,N \tag{3.126a}$$

Substituting Equation (3.125) into Equation (3.126a) yields:

$$\int_0^1 \phi_i L(\mathbf{\Phi A}) \, dZ - \int_0^1 \phi_i f(Z,t) \, dZ = 0 \tag{3.126b}$$

which is a set of coupled ordinary differential equations for A_j. Substituting Equations (3.107), (3.112), (3.119), and (3.123) into Equation (3.126) and integrating gives the matrix equations:

$$\mathbf{\Gamma A}' = -\mathbf{\Psi A} + \mathbf{\Phi}(\zeta)^T \delta(t-\tau) \tag{3.127}$$

where,

$$\mathbf{A}' = \frac{\partial}{\partial t}\mathbf{A} \tag{3.128}$$

The m_v values of each soil layer contribute to the $\mathbf{\Gamma}$ matrix when the left hand side of Equation (3.107) is integrated over the entire soil depth. The k_v and η values of each soil layer contribute to the $\mathbf{\Psi}$ matrix when the right hand side of Equation (3.107) is integrated. Expressions for calculating the contribution of a layer to the elements of the $\mathbf{\Gamma}$ and $\mathbf{\Psi}$ matrices are given in below in Section 3.4.5. When step changes in soil properties occur an interface layer is introduced. The contribution of an interface layer to $\mathbf{\Gamma}$ and $\mathbf{\Psi}$ can be found by taking the limit as $Z_2 \to Z_1$ in the equations for a finite layer thickness. It is this treatment of layer interfaces that provides a large advantage over traditional approaches. In previous methods, the addition of a new layer required the inclusion of a new domain in the problem space. For each new domain introduced, additional equations for pore pressure, with associated unknown coefficients, are needed. When many layers are analysed, the number of unknown coefficients to solve for can become unwieldy. In the current method, the number of unknown coefficients to solve for, $A_j(t)$ in Equation (3.120a), is fixed at the start of the analysis, regardless of the number of layers used.

To solve the nonhomogeneous system in Equation (3.127), the corresponding homogenous system is solved first, hence:

$$\mathbf{A}' = -\mathbf{\Gamma}^{-1}\mathbf{\Psi A} \tag{3.129}$$

It is expected that excess pore water pressure will decay with time and thus solutions might have the form of:

$$A(t) = v\exp(-\lambda t) \tag{3.130}$$

Upon substitution of Equation (3.130) into Equation (3.129) an eigen problem is revealed:

$$\lambda v = v\boldsymbol{\Gamma}^{-1}\boldsymbol{\Psi} \tag{3.131}$$

where, λ is an eigenvalue value of matrix $\boldsymbol{\Gamma}^{-1}\boldsymbol{\Psi}$, and v is the associated eigenvector. The nature of the problem suggests N distinct eigenvectors, and so $\mathbf{A}$ can be expressed by:

$$\mathbf{A} = \mathbf{v}\mathbf{E}(t)\mathbf{c} \tag{3.132}$$

where, $\mathbf{c}$ is a vector of constant terms, the matrix of eigenvectors, $\mathbf{v}$, is:

$$\mathbf{v} = \begin{bmatrix} v_{11} & v_{12} & \mathrm{K} & v_{1N} \\ v_{21} & v_{22} & \mathrm{K} & v_{2N} \\ \mathrm{M} & \mathrm{M} & \mathrm{O} & \mathrm{M} \\ v_{N1} & v_{N2} & \mathrm{K} & v_{NN} \end{bmatrix} \tag{3.133}$$

and,

$$\mathbf{E}(t) = \begin{bmatrix} \exp(-\lambda_1 t) & 0 & \Lambda & 0 \\ 0 & \exp(-\lambda_2 t) & \Lambda & 0 \\ \mathrm{M} & \mathrm{M} & \mathrm{O} & \mathrm{M} \\ 0 & 0 & \Lambda & \exp(-\lambda_N t) \end{bmatrix} \tag{3.134}$$

Calculating the eigenvalues and eigenvectors of the matrix $\boldsymbol{\Gamma}^{-1}\boldsymbol{\Psi}$ is the most difficult part of the analysis. However, there is a comprehensive literature on eigen problems (Hoffman, 1992) and many software programs exist to solve them. Eigen problems can be easily solved with freeware subroutines for MS Excel (Volpi, 2005) and Fortran (Anderson et al., 1999). Proprietary programs such as Mathematica

(Wolfram Research, Inc., 2004) and Matlab (The MathWorks Inc., 2003) may be used as well. Eigenvalues are also used when using previous solution methods to consolidation problems. These eigenvalues are typically the roots of a non-standard transcendental equation. Determining the equation roots can be more difficult than performing the well known operations of matrix eigenvector and eigenvalue extraction used in the current method. Particular advantage is gained when some existing methods suggest finding roots by plotting the transcendental equation and determining the roots visually (Nogami and Li, 2003).

Using variation of parameters (also called variation of constants), the solution to the nonhomogeneous Equation (3.127) can be found using the initial condition $\mathbf{A}(0)=0$:

$$\begin{aligned}\mathbf{A}(t) &= \mathbf{vE}(t)(\mathbf{vE}(0))^{-1}\mathbf{A}(0)+\mathbf{vE}(t)\int_0^t(\mathbf{vE}(s))^{-1}\boldsymbol{\Gamma}^{-1}\boldsymbol{\Phi}(\zeta)^T\,\delta(s-\tau)\,ds \\ &= \mathbf{vE}(t-\tau)(\boldsymbol{\Gamma}\mathbf{v})^{-1}\boldsymbol{\Phi}(\zeta)^T\end{aligned} \tag{3.135}$$

The fundamental solution to Equation (3.107) with impulse loading is now given by:

$$\bar{u}_{\delta}(Z,t)=\boldsymbol{\Phi}\mathbf{vE}(t-\tau)(\boldsymbol{\Gamma}\mathbf{v})^{-1}\boldsymbol{\Phi}(\zeta)^T \tag{3.136}$$

Equation (3.114) now becomes:

$$\bar{u}(Z,t)=\int_0^{\tau}\int_0^1\boldsymbol{\Phi}\mathbf{vE}(t-\tau)(\boldsymbol{\Gamma}\mathbf{v})^{-1}\boldsymbol{\Phi}(\zeta)^T\left(\frac{m_v}{\overline{m}_v}\frac{\partial\bar{\sigma}}{\partial t}+dT_h\frac{\eta}{\overline{\eta}}w\right)d\zeta\,d\tau \tag{3.137}$$

After substituting Equation (3.118) into Equation (3.137) and integrating the final solution of Equation (3.107) is found to be:

$$\bar{u}(Z,t)=\boldsymbol{\Phi}\mathbf{v}(\boldsymbol{\sigma}+\mathbf{w}) \tag{3.138}$$

The surcharge and m_v values of each layer contribute to the $\boldsymbol{\sigma}$ vector. The vacuum and η values of each layer contribute to the $\mathbf{w}$ vector. Expressions for calculating

the contribution of a layer to the elements of the $\boldsymbol{\sigma}$ and $\mathbf{w}$ vectors are given below in Section 3.4.5.

Care should be taken when including vacuum loading, because due to the formulation, pore pressure will always be zero at $Z = 0$. Thus vacuum loading is applied only along the drain and not across the soil surface. The mathematical problem arises where, if vertical flow is allowed and vacuum is applied along the drain, pore water will flow from the $\bar{u} = 0$ boundary condition at $Z = 0$ into the soil (with negative pore pressure) and then into the drain. This restriction can be overcome by using a thin layer with high horizontal permeability at the soil surface. The mathematical problem will still exist but the unwanted flow into the soil will quickly flow into the drain and not affect the pore pressure at the bottom of the thin layer. The pore pressure at the bottom of the thin layer will approach that of the applied vacuum as required.

The average excess pore pressure between depths Z_l and Z_{l+1} is given by:

$$\begin{aligned}\overline{\bar{u}}(t) &= \int_{Z_l}^{Z_{l+1}} \boldsymbol{\Phi}\mathbf{v}(\boldsymbol{\sigma}+\mathbf{w})/\Delta Z \, dZ \\ &= \overline{\boldsymbol{\Phi}}\mathbf{v}(\boldsymbol{\sigma}+\mathbf{w})\end{aligned} \tag{3.139}$$

where

$$\overline{\boldsymbol{\Phi}} = \begin{bmatrix}\bar{\phi}_1 & \bar{\phi}_2 & \dots & \bar{\phi}_N\end{bmatrix} \tag{3.140}$$

and,

$$\bar{\phi} = -\frac{1}{\Delta Z} CS\left(1, M^1\right) \tag{3.141}$$

where, CS is defined below in Section 3.4.5. There is considerable advantage in having the entire pore pressure distribution across all soil layers defined by one equation, Equation (3.139). All previous methods involve separate equations to describe the pore water pressure in each soil layer. Such equations typically involve combinations of sine and cosine terms, and Bessel functions for free strain radial drainage conditions (Horne, 1964; Nogami and Li, 2003). Thus finding average pore pressure values by integrating across multiple layers is tedious. Using the current method it is equally straight forward to determine average pore pressure values within a soil layer, across some layers, or across all layers.

Equations (3.138) and (3.139) are very concise, showing that soil consolidation can be reduced to a series of matrix operations.

3.4.5 Explicit Equations

In performing the integrations to derive Equation (3.127) many expressions of similar form arise. This is due to repeatedly integrating the product of trigonometric and linear polynomial functions. To present the equations for $\mathbf{\Gamma}$, $\mathbf{\Psi}$, $\boldsymbol{\sigma}$, and $\mathbf{w}$ in a concise manner, a shorthand notation is adopted as described below.

$$SN[\alpha,\beta^k]=\frac{\alpha_{l+1}\sin(\beta Z_{l+1})-\alpha_l\sin(\beta Z_l)}{\beta^k} \tag{3.142}$$

$$CS[\alpha,\beta^k]=\frac{\alpha_{l+1}\cos(\beta Z_{l+1})-\alpha_l\cos(\beta Z_l)}{\beta^k} \tag{3.143}$$

$$M^+=M_j+M_i \tag{3.144}$$

$$M^-=M_j-M_i \tag{3.145}$$

The $\mathbf{\Gamma}$ matrix depends solely on the compressibility of the soil. It is found by consideration of Equation (3.126). Equations (3.107), (3.119), and (3.123) are substituted into Equation (3.126). Collecting terms involving $A'(t)$ gives the element of $\mathbf{\Gamma}$ at row i and column j. Thus the l^{th} soil layer's contribution to $\mathbf{\Gamma}_{ij}$ is:

$$\mathbf{\Gamma}_{ij} = \int_{Z_l}^{Z_{l+1}} \frac{m_v}{\overline{m}_v} \phi_i \phi_j \, dZ \tag{3.146}$$

where, $m_v/\overline{m}_v$ is the linear polynomial in Equation (3.115). Equation (3.146) gives different expressions for the diagonal ($i = j$) and the off diagonal ($i \neq j$) elements of $\mathbf{\Gamma}$. The diagonal elements are calculated with:

$$\mathbf{\Gamma}_{ij} = \frac{1}{2}\left(\frac{\Delta Z}{2}\left(m_{vl} + m_{vl+1}\right) - \frac{\Delta m_v}{\Delta Z} CS\left[1, \left(M^+\right)^2\right] - SN\left[m_v, \left(M^+\right)^1\right]\right), \quad i = j \tag{3.147}$$

The off diagonal elements are given by:

$$\mathbf{\Gamma}_{ij} = \frac{1}{2}\left(\begin{array}{l} \dfrac{\Delta m_v}{\Delta Z}\left(CS\left[1, \left(M^-\right)^2\right] - CS\left[1, \left(M^+\right)^2\right]\right) \\ + SN\left[m_v, \left(M^-\right)^1\right] - SN\left[m_v, \left(M^+\right)^1\right] \end{array}\right), \quad i \neq j \tag{3.147b}$$

In interface layers, $Z_l = Z_{l+1}$, so the limit of Equation (3.147) is taken as $Z_{l+1} \to Z_l$. This limit is zero for both diagonal and off diagonal elements.

The same approach used to find $\mathbf{\Gamma}$ above is also used to determine $\mathbf{\Psi}$. The $\mathbf{\Psi}$ matrix depends on the drainage properties of the soil. The l^{th} soil layer's contribution to $\mathbf{\Psi}_{ij}$ is:

$$\mathbf{\Psi}_{ij} = \int_{Z_l}^{Z_{l+1}} dT_h \frac{\eta}{\overline{\eta}} \phi_j \phi_i \, dZ - \int_{Z_l}^{Z_{l+1}} dT_v \left(\frac{\partial}{\partial Z}\left(\frac{k_v}{\overline{k}_v}\right)\phi_j' \phi_i + \frac{k_v}{\overline{k}_v}\phi_j'' \phi_i \right) dZ \tag{3.148}$$

where, ϕ' and ϕ'' are the first and second derivatives of ϕ. The first integral in Equation (3.148) is due to horizontal drainage, the second is due to vertical drainage. The contribution of vertical and horizontal drainage to the diagonal elements of $\mathbf{\Psi}$ are given respectively by:

$$\mathbf{\Psi}_{ij} = \frac{dT_v M_j^2}{2}\left(\frac{\Delta Z}{2}\left(k_{vl} + k_{vl+1}\right) + \frac{\Delta k_v}{\Delta Z} CS\left[1, \left(M^+\right)^2\right] - SN\left[k_v, \left(M^+\right)^1\right]\right), \quad i = j \tag{3.149a}$$

and,
$$\mathbf{\Psi}_{ij} = \frac{dT_h}{2}\left(\frac{\Delta Z}{2}\left(\eta_l + \eta_{l+1}\right) - \frac{\Delta \eta}{\Delta Z} CS\left[1, \left(M^+\right)^2\right] - SN\left[\eta, \left(M^+\right)^1\right]\right), \quad i = j \tag{3.149b}$$

The off diagonal terms are:

$$\mathbf{\Psi}_{ij} = \frac{dT_v}{2}\left(\begin{array}{l} \dfrac{M_j M_i \Delta k_v}{\Delta Z}\left(CS\left[1, \left(M^-\right)^2\right] + CS\left[1, \left(M^+\right)^2\right]\right) \\ + M_j^2\left(SN\left[k_v, \left(M^-\right)^1\right] - SN\left[k_v, \left(M^+\right)^1\right]\right) \end{array}\right), \quad i \neq j \tag{3.149c}$$

and,
$$\mathbf{\Psi}_{ij} = \frac{dT_h}{2}\left(\begin{array}{l} \dfrac{\Delta \eta}{\Delta Z}\left(CS\left[1, \left(M^-\right)^2\right] - CS\left[1, \left(M^+\right)^2\right]\right) \\ + SN\left[\eta, \left(M^-\right)^1\right] - SN\left[\eta, \left(M^+\right)^1\right] \end{array}\right), \quad i \neq j \tag{3.149d}$$

For interface layers there is no contribution from horizontal drainage. The contribution of vertical drainage is the same for diagonal and off diagonal terms, and is described as:

$$\mathbf{\Psi}_{ij} = -dT_v M_j \Delta k_v \cos\left(M_j Z_1\right)\sin\left(M_i Z_1\right) \tag{3.150}$$

The final element values for $\mathbf{\Gamma}$ and $\mathbf{\Psi}$ are found by summing the contribution of each soil layer.

The loading terms $\boldsymbol{\sigma}$, and $\mathbf{w}$ are found by considering Equation (3.137). The surcharge loading term is defined by the following integral:

$$\boldsymbol{\sigma} = \int_0^{\tau}\int_0^1 \mathbf{E}\left(t-\tau\right)\left(\mathbf{\Gamma v}\right)^{-1}\mathbf{\Phi}\left(\zeta\right)^T \frac{m_v}{\overline{m}_v}\frac{\partial \overline{\sigma}}{\partial t}\, d\zeta\, d\tau \tag{3.151}$$

The vacuum loading term is determined from:

$$\mathbf{w} = \int_0^{\tau} \int_0^1 \mathbf{E}(t-\tau)(\boldsymbol{\Gamma}\mathbf{v})^{-1} \boldsymbol{\Phi}(\zeta)^T \, dT_h \, \frac{\eta}{\overline{\eta}} \, w \, d\zeta \, d\tau \tag{3.152}$$

Performing the integrations in Equation (3.151) and (3.152) for the m^{th} ramp load (described by Equation (3.118)) gives the i^{th} element of $\boldsymbol{\sigma}$ and $\mathbf{w}$ as:

$$\boldsymbol{\sigma}_i = \frac{\Lambda_{1,m,i}}{t_{m+1} - t_m} \sum_{j=1}^{N} (\boldsymbol{\Gamma}\mathbf{v})_{ij}^{-1} \left(\sum_{l=1}^{\#l} \Xi_j \left(\sigma_{m+1,l} - \sigma_{m,l}, \Delta\sigma_{m+1} - \Delta\sigma_m, m_v \right) \right) \tag{3.153}$$

$$\mathbf{w}_i = dT_h \left(\begin{array}{l} \Lambda_{1,m,i} \displaystyle\sum_{j=1}^{N} (\boldsymbol{\Gamma}\mathbf{v})_{ij}^{-1} \left(\sum_{l=1}^{\#l} \Xi_j \left(w_{m,l}, \Delta w_m, \eta \right) \right) \\ + \dfrac{\Lambda_{2,m,i}}{t_{m+1} - t_m} \displaystyle\sum_{j=1}^{N} (\boldsymbol{\Gamma}\mathbf{v})_{ij}^{-1} \left(\sum_{l=1}^{\#l} \Xi_j \left(w_{m+1,l} - w_{m,l}, \Delta w_{m+1} - \Delta w_m, \eta \right) \right) \end{array} \right) \tag{3.154}$$

where $\#l$ is the number of soil layers. Λ and Ξ are further shorthand notation defined by:

$$\Xi_j(\alpha, \beta, \theta) = \frac{1}{M_j} \left(\begin{array}{l} \alpha \left(\dfrac{\Delta\theta}{\Delta Z} SN\left[1, M_j^1\right] - CS\left[\theta, M_j^0\right] \right) + \\ \beta \left(\dfrac{2\Delta\theta}{\Delta Z^2} CS\left[1, M_j^2\right] + \dfrac{1}{\Delta Z} \left(SN\left[\theta, M_j^1\right] + \dfrac{\Delta\theta}{M_j} \sin\left(M_j Z_{l+1}\right) \right) \right) \\ - \theta_2 \cos\left(M_j Z_{l+1}\right) \end{array} \right) \tag{3.155}$$

$$\Lambda_{\theta,m,i} = \begin{cases} \dfrac{\exp[-t\lambda_i]\left(\exp[t_f\lambda_i] - \exp[t_s\lambda_i]\right)}{\lambda_i} & \theta = 1 \\ \dfrac{\exp[-t\lambda_i]\left(\left(1 + (t_m - t_s)\lambda_i\right)\exp[t_s\lambda_i] - \left(1 + (t_m - t_f)\lambda_i\right)\exp[t_f\lambda_i]\right)}{\lambda_i^2} & \theta = 2 \end{cases} \tag{3.156}$$

$$t_s = \min[t, t_m] \tag{3.157}$$

$$t_f = \min[t, t_{m+1}] \tag{3.158}$$

By formulating each ramp loading step with t_s and t_f it is not necessary to determine which is the current loading step, the formulation will make the contribution of loading steps that start after time t equal to zero. For interface layers both $\boldsymbol{\sigma}$ and $\mathbf{w}$ are equal to zero. The start and end times of surcharge and vacuum loading stages need not be the same. The final values for $\boldsymbol{\sigma}$ and $\mathbf{w}$ are found by summing the contribution of each ramp load. For greatest computational efficiency only the Λ functions, Equation (3.156), need be computed at each time step. All other parameters depend only on material properties and loading magnitudes and can thus be initialized at the start of the analysis.

3.5 Verification of Spectral Method Model

To verify the new model, the equations presented above are compared with various analytical solutions taken from the literature.

3.5.1 Multi-Layered Free Strain With Thin Sand Layers (Nogami and Li, 2003)

Nogami and Li (2003) developed a free-strain approach for calculating the excess pore pressure distribution for multi-layered soil with both vertical and radial drainage. An example problem is presented with a soil system consisting of two identical thin sand layers (height h_s) separating three identical clay layers (height h_c). Soil properties are described by the ratios: $k_{\text{sand}}h_s h_c / r_e^2 k_v$ = 5, n = 20, $c_h h_c^2 / c_v r_e^2$ = 1. The average excess pore water pressure calculated with the present approach and that of Nogami and Li (2003) is compared in Figure 3.19. Both methods are in close agreement except for slight deviations in the thin sand layers at low degree of consolidation. The close agreement shows that, as for homogenous

ground (Hansbo, 1981; Barron, 1948), there is little difference between free-strain and equal strain formulations. The current method does not use cumbersome Bessel functions that are associated with free-strain solutions. Also a wider range of problems can be solved with the current method, as the approach of Nogami and Li (2003) does not include vacuum loading or depth dependant surcharge loading.

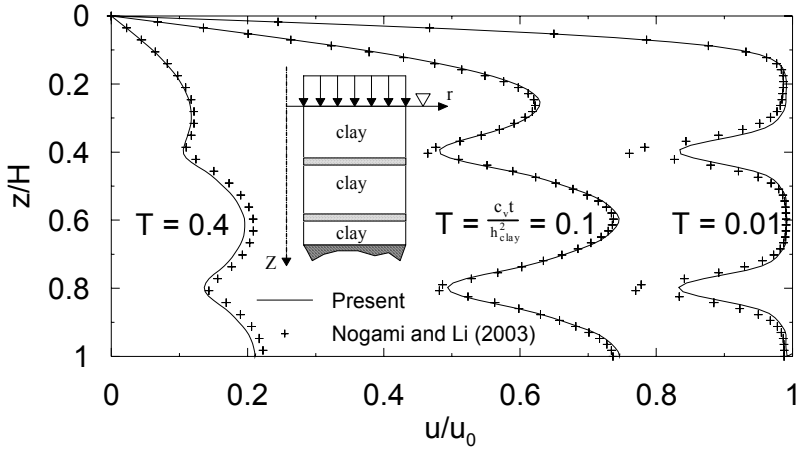

Figure 3.19 Model verification: multi-layer equal-strain vs free-strain

3.5.2 Double Layered Ground With Vertical and Radial Drainage(Nogami and Li, 2003)

Nogami and Li (2003) present the pore pressure distribution during consolidation of a soil system with vertical and radial drainage consisting of two clay layers of equal height h. The material properties of the two clay layers are shown in Table 3.3. The present model requires three layers with the middle one acting as an interface. Comparisons of the pore pressure distributions calculated with each method are shown in Figure 3.20. Any small oscillations in the proposed model result from an insufficient number of terms in the series solution.

Table 3.3 Parameters for double layered ground

Case	n	H/r_w	h_2/h_1	k_{v2}/k_{v1}	c_{v2}/c_{v1}	c_{h2}/c_{h1}
1	10	200	1	2	1	5
2	10	200	1	2	1	1
3	10	200	1	2	1	1/5

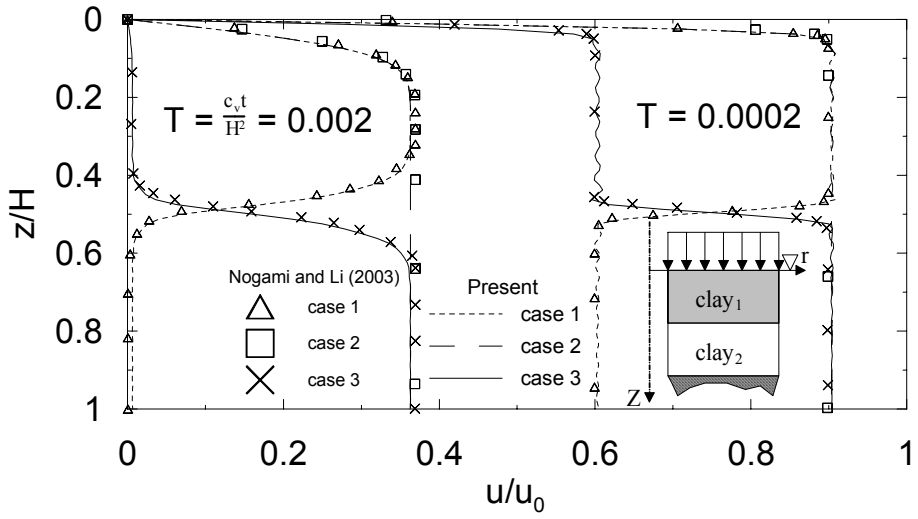

Figure 3.20 Model verification: double layered ground

3.5.3 Linearly Varying Vacuum Loading (Indraratna et al., 2005b)

Indraratna et al. (2005b) describe an analytical solution for consolidation by purely radial drainage with vacuum (negative) pressure varying linearly from p_0 at the top of the drain to zero at the bottom of the drain. A surcharge load σ, is also applied. The excess pore water pressure, averaged over the whole soil layer, is given by:

$$\frac{\overline{\overline{u}}}{\sigma} = \left(1 + \frac{p_0}{2\sigma}\right)\exp(-dT_h) - \frac{p_0}{2\sigma} \tag{3.159}$$

This is compared with the current model for a surcharge load of one and a vacuum pressure at the top of the drain of 0.2, as shown in Figure 3.21. There is no discernable difference in the solutions.

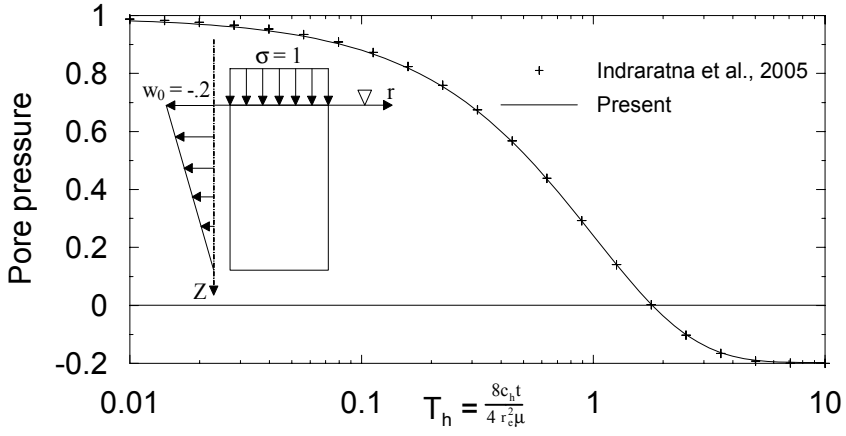

Figure 3.21 Model verification: surcharge and vacuum loading

3.5.4 Multiple Ramp Loading (Tang and Onitsuka, 2001)

Tang and Onitsuka (2001) presented an analytical solution for consolidation by vertical and radial drainage (no smear) for single layer consolidation under multiple ramp loading. The average excess pore water is calculated with the soil/drain properties: $c_v = c_h$, n = 16.7, H/r_e = 2. The surcharge load, initially zero, increases to σ = 0.5 at $dT_h t$ = 0.15, and then increases from σ = 0.5 at $dT_h t$ = 0.3, to σ = 1 at $dT_h t$ = 0.45. Comparisons with the present method are shown in Figure 3.22. There is no discernable difference in the solutions.

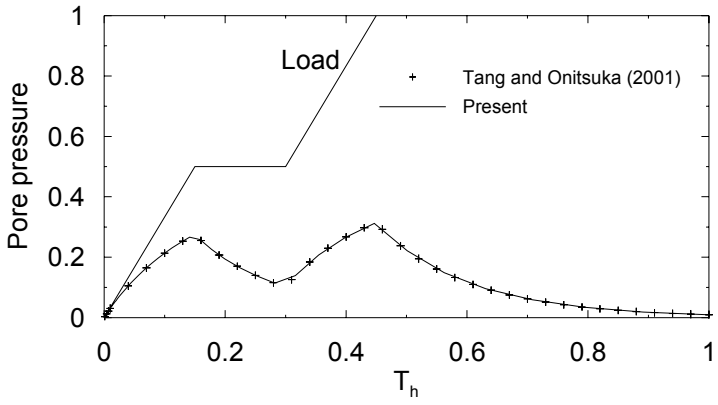

Figure 3.22 Model verification: multiple stage loading

3.5.5 Partially Penetrating Vertical Drains (Runnesson et al., 1985)

Runesson et al. (1985) performed finite element computations for consolidation with partially penetrating vertical drains including vertical and radial drainage. One example presented is for a clay/drain system with the following properties: $h_1/H = 0.5,\ n = 10,\ H^2 c_h / r_e^2\, c_v = 100.$ The degree of consolidation calculated at various depths is compared to those calculated with the present method (Figure 3.23). The differences in the two solutions are acceptable given the approximate nature of the finite element solution.

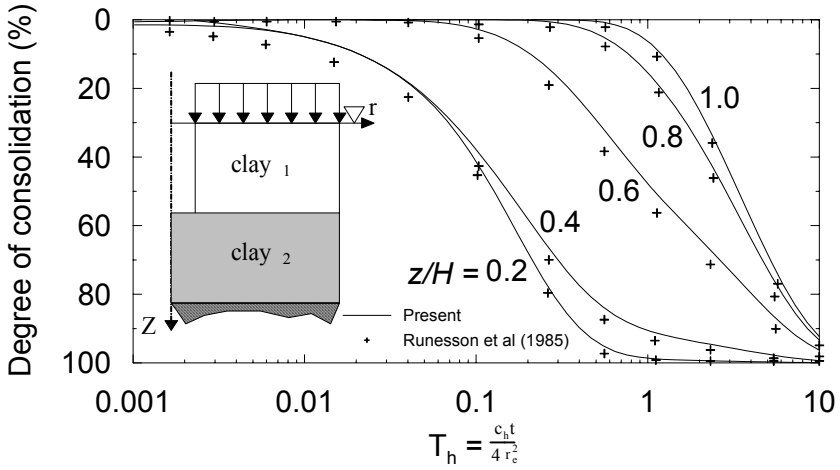

Figure 3.23 Model verification: partially penetrating vertical drains

3.5.6 Vertical Consolidation of Four Layers (Schiffman and Stein, 1970)

Schiffman and Stein (1970) present an analytical solution for one-dimensional consolidation of a layered system. The method is illustrated with an example problem consisting of four layers draining at the top and bottom. The soil properties are given in Table 3.4. The average excess pore water pressure calculated is compared with the present method in Figure 3.24. The differences in the model are very small.

Table 3.4 Soil profile, four layer system

Depth (m)	k_v (m/s)	m_v (m^2/kN)
0 to 3.05	2.78×10^{-11}	6.41×10^{-5}
3.05 to 9.14	8.26×10^{-11}	4.07×10^{-5}
9.14 to 18.29	1.17×10^{-11}	2.03×10^{-5}
18.29 to 24.38	2.94×10^{-11}	4.07×10^{-5}

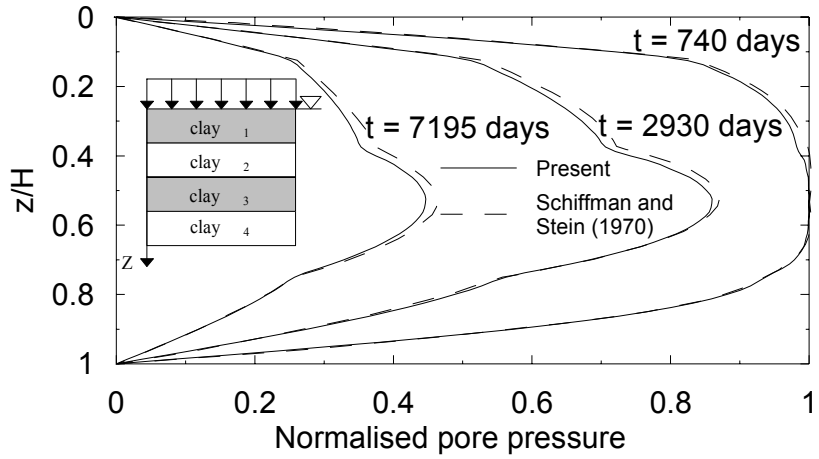

Figure 3.24 Model verification: 4 layer vertical drainage

3.6 Shortcomings of Spectral Analysis

While the spectral method is very useful for analyzing consolidation problems, care must be taken when considering problems where radial drainage dominates. The writer has found that if vertical drainage is ignored ($dT_v = 0$) then some methods of determining the eigenvalues of the solution fail. If this should happen then selecting a small value of dT_v that does not effect the overall solution should allow the eigenvalues to be solved.

Using a series solution can lead to oscillations in the pore pressure profile when discontinuities are modeled. These oscillations are known as Gibbs phenomena (Asmar, 2005). Consider a soil drain system with: $dT_h = 1$, $k_v/\overline{k}_v = 1$, $m_v/\overline{m}_v = 1$, $\eta/\overline{\eta} = 1$. Figure 3.25 shows the pore pressure profile of the soil for consolidation times of $8T_h/\mu$ = 0.01, 0.4, and 1. If vertical drainage is ignored, Figure 3.25(a), then for a homogeneous soil subject to radial drainage only (ignoring vacuum

loading) the pore pressure at any time should be constant with depth. Thus the series solution must approximate a straight line. However, the boundary condition of zero pore pressure at zero depth used to solve the governing equation does not fit this straight line solution; hence the oscillations in Figure 3.25(a). Increasing the number of terms used in the series solution makes the oscillations smaller but does not remove them altogether. For problems with vertical drainage, the pore pressure profile is only a straight line after application of an instantaneous load. As time progresses, the series solution gives a better approximation to the real solution. In Figure 3.25(a), where vertical drainage is neglected, 50 series terms provides an adequate accuracy. Compare this with Figure 3.25(d) where, except for the initial pore pressure distribution, only 3 series terms are needed to give adequate accuracy. The proposed consolidation equations can be used to model radial consolidation problems, but the interpretation of results should take into account the above errors.

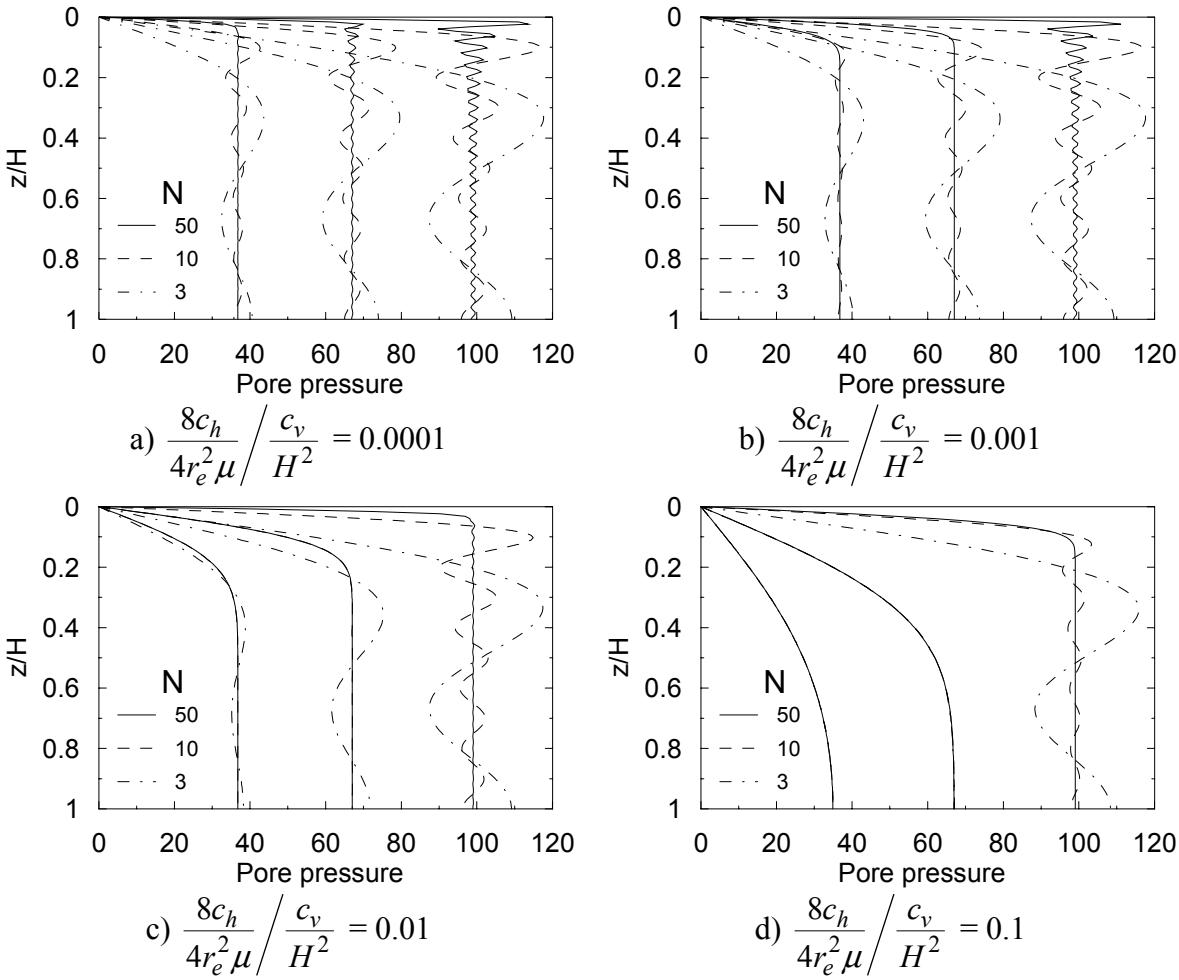

Figure 3.25 Errors associated with series solution

3.7 Vertical Drainage in a Single Layer with Constant c_v (Spectral Method)

By relaxing the assumption of soil homogeneity, the proposed model can be used to investigate some deviations from Terzaghi's one-dimensional consolidation theory. Consider a single layer of soil where k_v and m_v vary linearly such that c_v remains constant throughout. This restriction is ensured when $k_{vT}/k_{vB} = m_{vT}/m_{vB}$, where the subscripts T and B indicate the top and bottom of the soil layer respectively. The effect of the k_{vT}/k_{vB} ratio on consolidation is assessed by calculating the

average degree of consolidation for PTIB and PTPB drainage conditions, under uniform and triangular initial pressure distributions. Consolidation curves are shown in Figures 3.26 and 3.27. The curves for two way drainage (PTPB), regardless of initial pressure distribution, are very similar so only the case of uniform initial pressure distribution is shown.

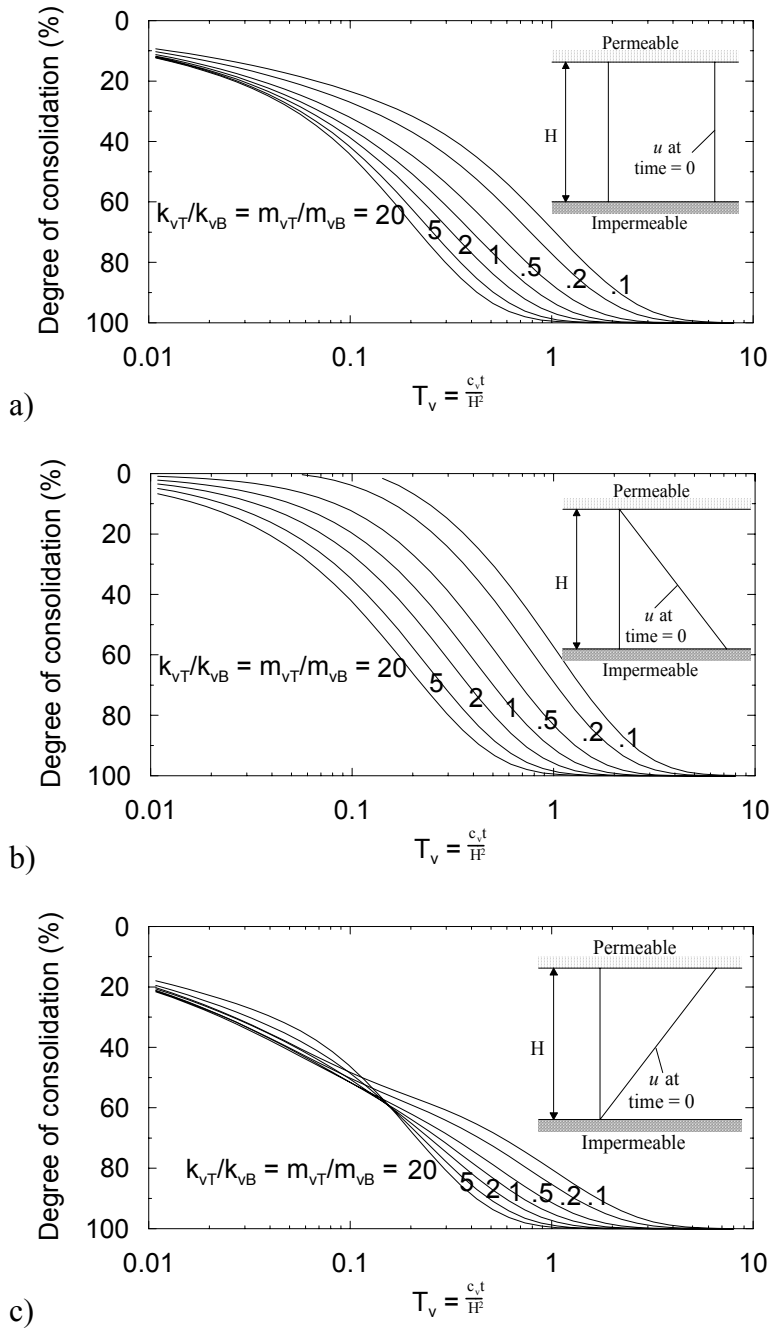

Figure 3.26 Degree of consolidation for pervious top and impervious bottom

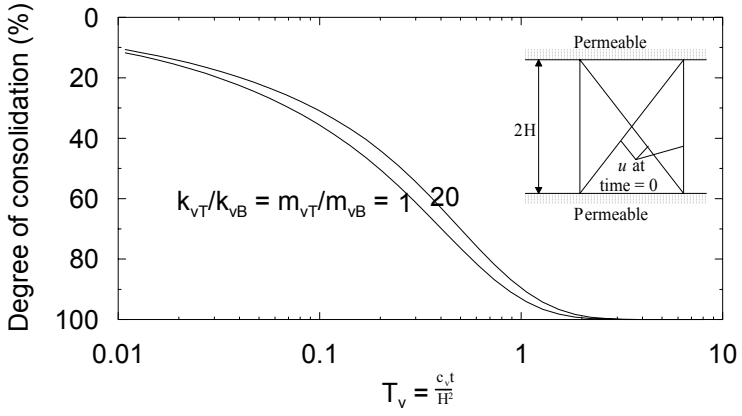

Figure 3.27 Degree of consolidation for pervious top and pervious bottom

As k_v and m_v generally decrease with effective stress, it is expected that $k_{vT}/k_{vB} > 1$ for most soils. As seen from Figure 3.26 such cases exhibit a faster rate of consolidation compared to Terzaghi's theory ($k_{vT}/k_{vB} = 1$). This is consistent with higher strains (higher m_v) near the drainage boundary causing faster consolidation as described by Duncan (1993). Figure 3.26(c) shows an initially slower consolidation rate eventually 'overtaking' the Terzaghi rate. This somewhat surprising result is caused by the inverted triangle pressure distribution: for $k_{vT}/k_{vB} > 1$ there is initially greater flow downward towards the impermeable boundary (see Figure 3.28c). The rate of consolidation for two way drainage is only marginally affected by the k_{vT}/k_{vB} ratio (Figure 3.27). However, once $k_{vT}/k_{vB} > 2$ any change in linear distribution of k_v and m_v will give a slight decrease in consolidation rate. Note that due to symmetry the case $k_{vT}/k_{vB} = x$ is the same as $k_{vT}/k_{vB} = 1/x$.

Not only does a linear variation of k_v and m_v affect the average degree of consolidation it also affects the shape of the pore pressure distribution during consolidation. For k_{vT}/k_{vB} ratios of 0.1, 1, and 10 the pore pressure isochrones corresponding to various degrees of consolidation are plotted in Figures 3.28 and 3.29.

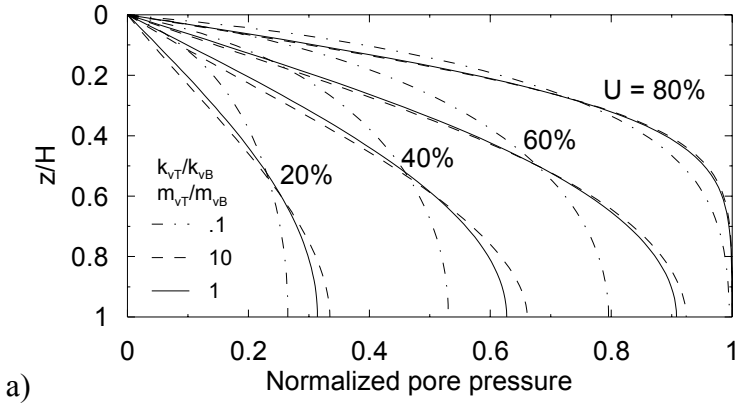

a)

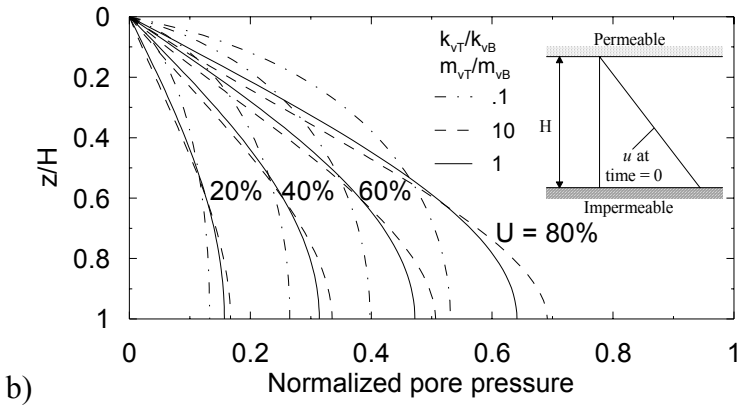

b)

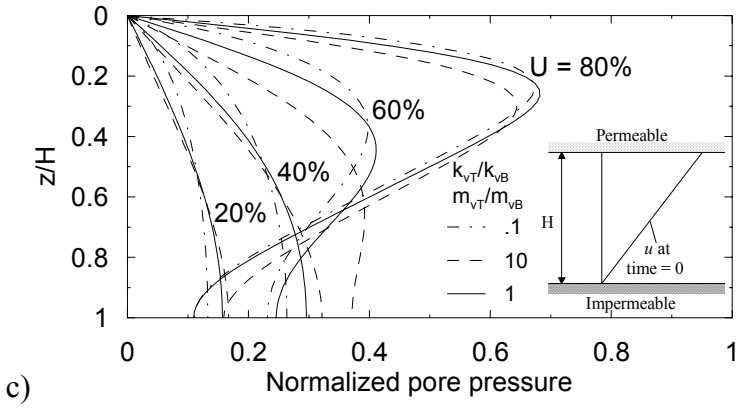

c)

Figure 3.28 Pore pressure isochrones for pervious top and impervious bottom

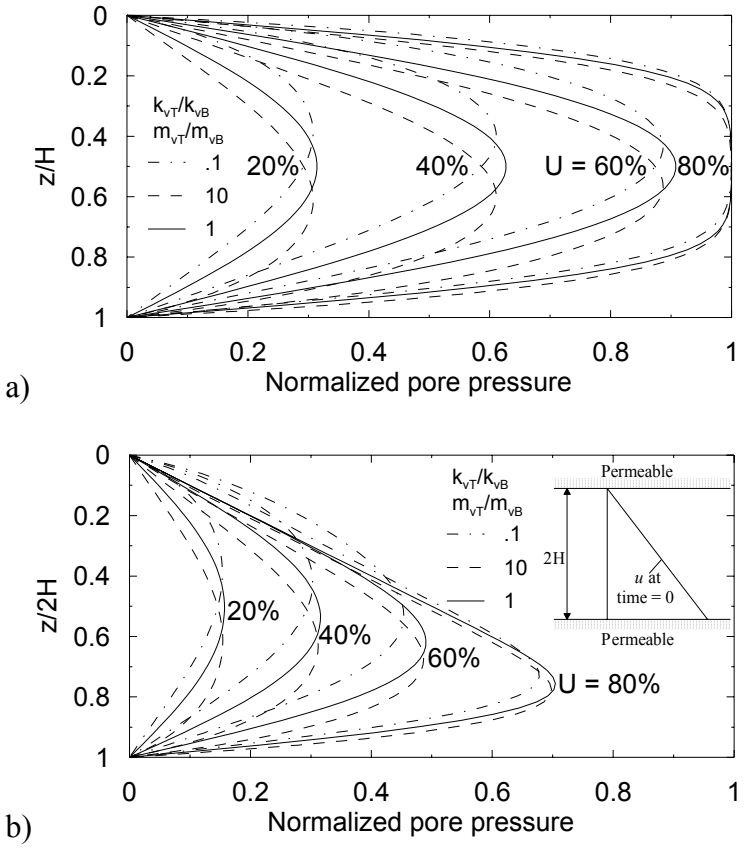

Figure 3.29 Pore pressure isochrones for pervious top and pervious bottom

The above findings are significant for thick clays with PTIB drainage conditions. A change in $k_{vT}/k_{vB} = m_{vT}/m_{vB}$ may lead to significant changes in the rate of consolidation. However, as $k_{vT}/k_{vB} > 1$ leads ultimately to faster consolidation, and is expected in the field, using Terzaghi's analysis ($k_{vT}/k_{vB} = 1$) will simply underestimate the rate of consolidation (a generally safe design approach). The rate of consolidation will also be underestimated when determining consolidation times by comparing the time factors ($T_v = c_v t/H^2$) of two like soils with different drainage lengths (sometimes called the model law of consolidation, (Craig, 1997)). Terzaghi's theory depends only on the time factor. The above analysis shows

consolidation depends also on the parameter $k_{vT}/k_{vB} = m_{vT}/m_{vB}$. Thus, comparing time factors, the rate of consolidation for a thin sample such as an oedometer specimen, where $k_{vT}/k_{vB} \approx 1$, will be different to a thicker specimen such as in the field, where $k_{vT}/k_{vB} \neq 1$.

For PTPB drainage conditions there is little difference between Terzaghi's analysis and the current analysis where k_v and m_v vary with depth. The only significant finding is the altered pore pressure isochrones. With a uniform initial pressure distribution the point of maximum pore pressure will gradually move from mid-height towards the boundary where k_v and m_v are highest. Terzaghi theory predicts maximum pore pressure at mid depth. This is important to note when installing piezometers in the field to gauge the progress of consolidation.

3.8 Consolidation Before and After Drain Installation (Spectral Method)

In many cases vertical drains are installed from a working platform which exerts a load on the soil. Thus there is a period of time before drain installation where consolidation occurs due to drainage in the vertical direction. If the drains are installed at time t_Ω, then for $t \le t_\Omega$ the pore pressure behaviour can be modeled using the above spectral equations by setting dT_h equal to zero. At $t = t_\Omega$ the pore pressure distribution in Equation (3.138) can be rewritten as:

$$\bar{u}(Z, t_\Omega) = \mathbf{\Phi}\boldsymbol{\chi} \tag{3.160}$$

where $\boldsymbol{\chi}$ is the vector $\mathbf{v}(\boldsymbol{\sigma} + \mathbf{w})$ calculated with $dT_h = 0$. Treating the pore pressure distribution in Equation (3.160) as a ramp load applied at t_Ω over an infinitely small

time interval, the pore pressure after drain installation can be determined from Equation (3.137). All matrices are recalculated with the appropriate non-zero value of dT_h. The resulting equation for excess pore pressure is given by:

$$\bar{u}(Z,t) = \mathbf{\Phi v}(\boldsymbol{\sigma} + \mathbf{w} + \boldsymbol{\Omega}) \tag{3.161}$$

where,

$$\boldsymbol{\Omega}_i = \exp(-(t - t_\Omega)\lambda_i)\sum_{j=1}^{N}(\mathbf{\Gamma v})_{ij}^{-1}\left(\sum_{l=1}^{\#l}\sum_{k=1}^{\#\chi}\Gamma_{ikl}\boldsymbol{\chi}_k\right) \tag{3.162}$$

and $\#\chi$ is the number of series terms used in the previous time increment. The number of series terms used before and after drain installation need not be the same. As the loading steps before drain installation are included in the χ vector, the time values used in calculating the vectors $\boldsymbol{\sigma}$ and $\mathbf{w}$ are need to be modified. Equations (3.157) and (3.158) thus modified are:

$$t_s = \min[t, \max[t_m, t_\Omega]] \tag{3.163}$$

$$t_f = \min[t, \max[t_{m+1}, t_\Omega]] \tag{3.164}$$

The above process of updating the material properties at a certain time can be used to perform a piecewise nonlinear analysis. By dividing the consolidation process into a discrete number of time steps, material properties, though constant during any particular time interval, can be varied across the time steps. Particular points in the soil system (layer interfaces and some intermediary points) are chosen where the material properties at the end of each time increment will be determined. Between these points the material properties vary linearly with depth. The pore pressure distribution is calculated at the end of a time step and the properties at the pertinent points are updated.

The time stepping process can be applied, not just for material properties, but for soil system geometry as well. At each time step total height and layer depths may be updated to allow for large strain effects. Surcharge loading can be altered to reflect submergence of fill. These modifications increase the computation time of the analysis. Even ignoring geometry updates, a small number of time increments will greatly increase the computational cost of analysis as the $\mathbf{\Gamma}$ and $\mathbf{\Psi}$ matrices, and the eigenvalues and eigenvectors must be calculated at each time step. The time consuming piecewise nonlinear approach is briefly investigated in Appendix B. It adds to the wide class of problems that can be studied with the above spectral method.

3.9 Summary

This Chapter has presented three new contributions to the solution of consolidation problems. Section 3.2 developed new expressions for the μ parameter central to equal strain radial consolidation under Darcian flow conditions. The new expressions, based on a linear and parabolic variation of soil properties in the radial direction (Equations 3.35 and 3.41), give a more realistic representation of the extent of smear. The equations presented for overlapping linear smear zones (Equation 3.45) provide some explanation for the phenomena of a minimum drain spacing, below which no increase in the rate of consolidation is achieved. It appears this minimum influence radius is 0.6 times the size of the linear smear zone. The new μ parameters may be used in the two new consolidation models presented in Sections 3.3 and 3.4.

Section 3.3 presents analytical solutions to nonlinear radial consolidation problems. The equations (Equations 3.84 and 3.89) are valid for both Darcian and non-Darcian flow and can capture the behaviour of overconsolidated and normally consolidated soils. For nonlinear material properties, consolidation may be faster or slower when compared to the cases with constant material properties. The difference depends on the compressibility/permeability ratios (C_c/C_k and C_r/C_k), the preconsolidation pressure (σ'_p) and the stress increase ($\Delta\sigma/\sigma'_0$). If $C_c/C_k < 1$ or $C_r/C_k < 1$ then the coefficient of consolidation increases as excess pore pressures dissipate and consolidation is faster. If $C_c/C_k > 1$ or $C_r/C_k > 1$ then the coefficient of consolidation decreases as excess pore pressures dissipate and consolidation becomes faster. For the case where $C_c/C_k = 1$ the solution is identical to Hansbo (2001). The equations presented give an analytical solution to nonlinear radial consolidation that can be used to verify purely numerical methods. With the approximation for arbitrary loading the almost any vertical drain problem where vertical drainage is negligible and effective stresses always increase can be analysed.

Section 3.4 developed a novel solution to multi-layered consolidation problems. The model includes both vertical and radial drainage where permeability, compressibility and vertical drain parameters vary linearly with depth. The ability to include surcharge and vacuum loads that vary with depth and time allows for a large variety of consolidation problems to be analysed. The powerful model can also predict consolidation behaviour before and after vertical drains are installed.

While this Chapter has verified the new models against existing analytical models, the following two Chapters use particular case histories for verification. Chapter 4 considers large-scale laboratory consolidation experiments performed at the University of Wollongong. Chapter 5 compares the new models to particular field trials found in the literature.

4 LABORATORY VERIFICATION

4.1 General

This Chapter applies the theoretical developments of the previous Chapter to laboratory experiments performed at the University of Wollongong. Three sets of experiments are analysed with the multi-layered spectral method model and the nonlinear radial consolidation model: a) consolidation with multi-stage surcharge loading; b) normally consolidated soil with surcharge loading and stress dependant permeability and compressibility; c) consolidation under combined vacuum and surcharge loading. The first experiment involved extensive determination of smear zone permeability, justifying the use of a parabolic distribution of permeability in the smear zone.

4.2 Laboratory Testing of Vertical Drain Consolidation

Laboratory testing with large-scale consolidation apparatus have proved useful in analysing the behaviour of vertical drains installed in soft clay. Equipment generally consists of a single drain installed in a cylinder of soil, with the ability to apply a surcharge load and monitor settlement and pore pressure values at certain points within the cell. Bergado et al. (1991) used a transparent PVC cylinder (455 mm internal diameter, 920 mm height , 10 mm wall thickness). The cylinder was filled with soft remolded Bangkok clay and a PVD (Ali drain - 4 mm × 60 mm) was installed using the 6 mm × 80 mm mandrel. Indraratna and Redana (1995) used a large-scale consolidometer (450 mm × 950 mm) to investigate the effect of smear due to the installation of prefabricated vertical drains and sand compaction piles. The extent of the smear zone, was investigated by determining the coefficient of permeability (calculated from conventional oedometer tests on horizontal and

vertical specimens) at several locations within the cell. Sharma and Xiao (2000) also conducted a series of large-scale tests to study the behaviour around vertical drains installed in soft clay using remolded kaolin clay.

For vacuum application without PVD, a small-scale test was built by Mohamedelhassan and Shang (2002). A 70 mm diameter by 25 mm high soil sample was used in the tests to measure the excess pore water pressure, settlement, and change in volume. The results indicate that under one-dimensional conditions, the vacuum pressure compared to a surcharge pressure of the same magnitude is almost identical. Small-scale tests were also conducted by Hird and Moseley (2000) and Hird and Sangtian (2002) to investigate smearing of finely stratified soils with PVD installation. Alternate clay and sand layers were assembled to a height of 150-170 mm into a cell 252 mm in diameter. The novel sample preparation consisted of clay layers wire-cut from an extruded clay cylinder, and sand layers of appropriate thickness frozen to maintain structural integrity during sample assembly. Hird and Sangtian (2002) reported that the effect of smear on such stratified soils was only severe when $k_{\text{sand}}/k_{clay} > 100$.

Other laboratory studies involving the University of Wollongong consolidometer are outlined in the following section.

4.3 The University of Wollongong Large-scale Consolidometer

The large-scale consolidometer at the University of Wollongong (Figure 4.1) is a 450 mm diameter, 950 mm high steel cylinder with the ability to monitor the pore pressure and settlement response of soils under load. Since 1995 the consolidometer

has been used by University of Wollongong researchers to study various aspects of vertical drain consolidation. Research has been conducted in the following areas:

- Redana (1999) conducted consolidation tests on circular sand drains and prefabricated vertical drains. By taking horizontal and vertical cored samples, the nature of smearing was investigated by determining the change in permeability in the smear zone compared to the undisturbed zone. The smear zone around PVD was found to be elliptical in shape, with horizontal permeability decreasing towards the drain, approaching the value of vertical permeability at the soil drain interface (Indraratna and Redana, 1995; Indraratna and Redana, 1998a; Indraratna and Redana, 1998b).
- Bamunawita (2004) assessed the combined effect of vacuum and surcharge loading on PVD. Indraratna at al. (2002) and Indraratna at al. (2004) identified a drop in vacuum pressure along the drain and confirmed a plane-strain permeability matching procedure for modeling vertical drains beneath embankments.
- Sathananthan (2005a) verified a cavity expansion model for predicting the pore water pressure and associated smear generated during mandrel installation of PVD (Sathananthan and Indraratna, 2005b). Also studied was the correlation between permeability and moisture content in the smear zone.
- Rujikiatkamjorn (2006) studies combined surcharge and vacuum loading as well as semi-log stress/permeability-void ration relationships for vertical drain consolidation (Indraratna et al., 2005a).

Figure 4.1 Large-scale consolidometer

4.3.1 General Testing Procedure

Figure 4.2 shows a schematic picture of the large-scale consolidometer. The cylindrical cell consists of two stainless steel sections bolted together along the two joining flanges. The internal diameter of the cell is 450 mm and the height is 950 mm. Top and bottom drainage can be facilitated by placing a geotextile on the cell base and clay surface. If only radial drainage is required the permeable geotextile is replaced by an impervious plastic sheet. The clay is thoroughly mixed with water to ensure full saturation and the resulting slurry is placed in the consolidation cell in

layers approximately 20 cm thick. Soil need not fill the entire cell as an internal 'riser' can be used to transfer loads from the loading piston to the shortened sample. The ring friction expected with such a large height/diameter ratio (1.5 - 2) is almost eliminated by using an ultra-smooth Teflon membrane around the cell boundary (friction coefficient less than 0.03). Surcharge loading with a maximum capacity of 1200 kN can be applied by an air jack compressor system via a rigid piston of 50 mm thickness. Vacuum loading with a maximum capacity of 100 kPa can be applied through the central hole of the rigid piston. A LVDT (Linear Variable Differential Transformer) transducer is placed on top of the piston to monitor surface settlement. Pore water pressures are monitored by strain gauge type pore pressure transducers installed trough small holes in the steel cell at various positions in the soil. Transducers are easily located on the cell periphery or, can be placed within the clay by using small diameter stainless steel tubes. The LVDT and pore pressure transducers are connected to a PC based data logger.

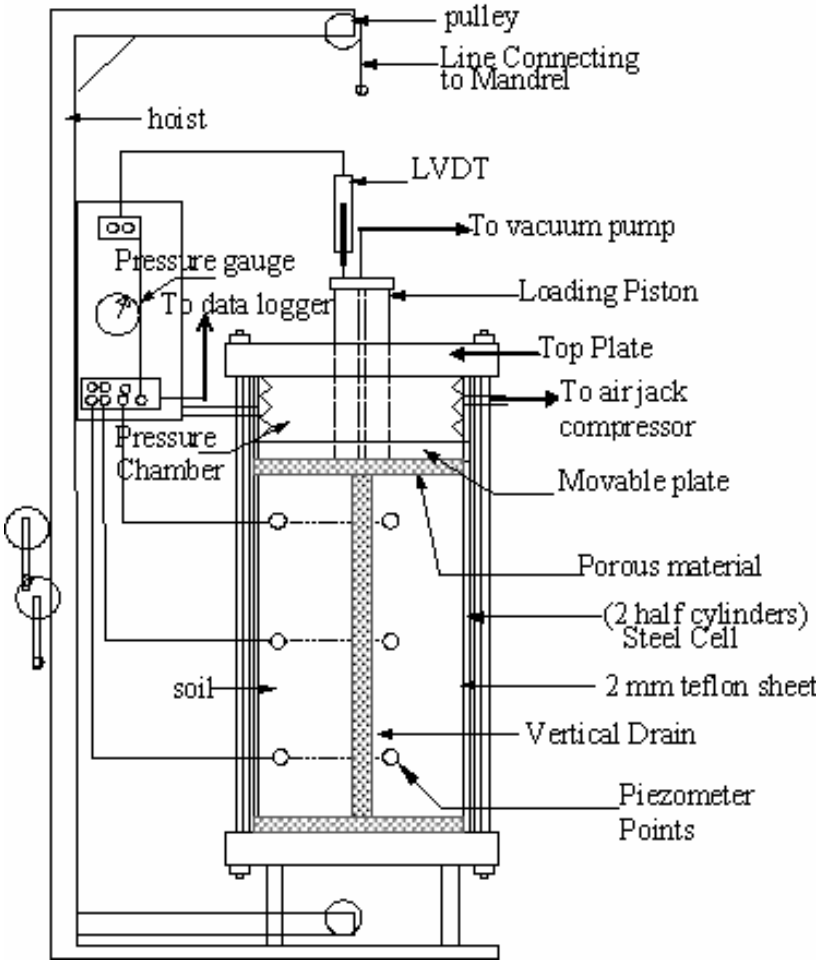

Figure 4.2 Schematic of large-scale consolidation apparatus

The soil is subjected to an initial preconsolidation pressure (usually σ'_p = 20 kPa), until the settlement rate becomes negligible. The load is then removed and a single vertical drain, with the aid of a guide, is installed using a rectangular steel mandrel. Sand compaction piles may be installed with a circular pipe mandrel. Depending on the purpose of the test, vertical and horizontal samples may be cored to investigate the effect of drain installation on soil properties. Once the drain has been installed the required loading sequence is applied to the sample.

4.3.2 Verification of Smear Zone with Parabolic Variation of Permeability

The purpose of this test, conducted by Redana (1999), was to determine the permeability changes associated with smearing. Soil properties, testing procedures, settlement and pore pressure data for the laboratory test described below are described fully in Indraratna and Redana (1998a) and Indraratna and Redana (1998b). The relevant data (summarized below) from this test is reanalysed here with a parabolic smear zone. Predicted and measured settlement data are compared.

The soil consisted of reconstituted alluvial clay from Moruya (40 to 50% clay sized particles (<2μm), 40% saturated water content, 70% liquid limit, 30% plastic limit, 17 kN/m^3 saturated unit weight). The soil was subjected to an initial preconsolidation pressure, σ'_p = 35 kPa. The vertical drain (Flowdrain 75mm × 4mm) was installed using a rectangular steel mandrel (80mm × 10mm). Subsequently the surcharge pressure was increased to 50 kPa, 100 kPa and 200 kPa (3 stage loading).

In order to measure the disturbance of the soil due to insertion of the mandrel, small horizontal and vertical specimens were cored from the tested consolidometer sample. These samples were subject to one-dimensional consolidation using conventional (50 mm diameter) oedometers. The variation of permeability with distance from the drain, shown in Figures 4.3 and 4.4, fits very well with the parabolic equation described in Equation (3.38).

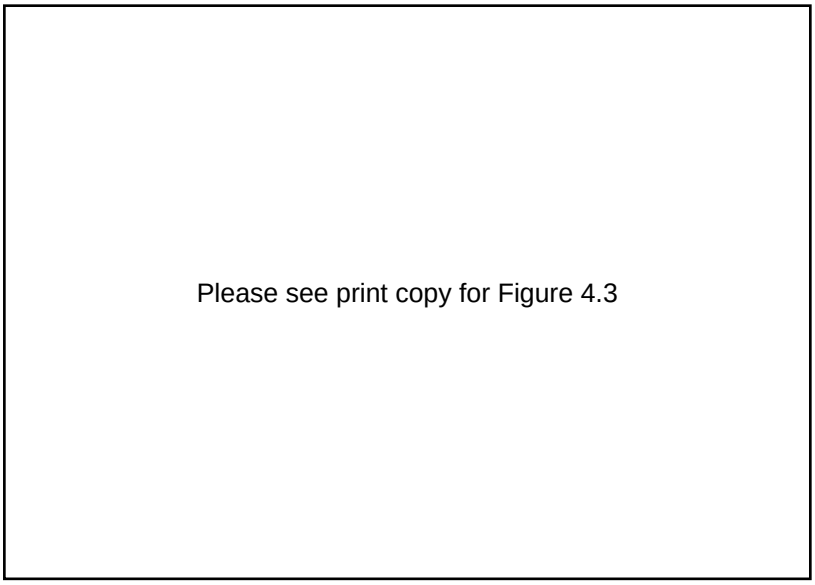

Figure 4.3 Horizontal permeability along radial distance from drain in large-scale consolidometer (original data from Indraratna and Redana, 1998a)

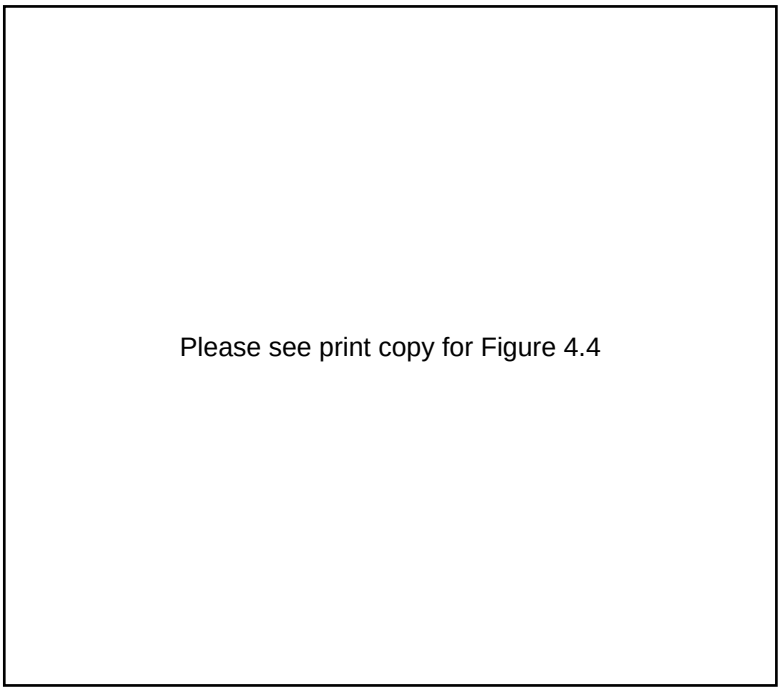

Figure 4.4 Ratio of horizontal to vertical permeability along radial distance from drain in large-scale consolidometer (original data from Indraratna and Redana, 1998a)

The measured soil properties are as follows: compression index $C_c = 0.34$, recompression index $C_r = 0.14$, vertical coefficient of consolidation $c_v = 1.5 \times 10^{-8}$ m^2/s (c_v in smear and undisturbed zone assumed equal), vertical coefficient of permeability $k_v = 2.25 \times 10^{-10}$ m/s, and the horizontal permeability distribution is shown in Figure 4.3. The high C_r/C_c ratio exceeding 0.4 is due to remolding, and a similar value for remolded Winipeg clay was determined by Graham and Li (1985). The equivalent radius of the band drain (after Rixner et al., 1986) is $r_w = (75 + 4)/4 = 20$ mm. The fitted parabolic curve in Figure 4.4 is described by $k_h/k_0 = 1.6$ (at $r = r_w$, k_0 is assumed equal to k_v), $r_e/r_w = 11.25$, and $r_s/r_w = 8.4$. These parameters give $k_h = 3.60 \times 10^{-10}$ m/s, $k_0 = 2.25 \times 10^{-10}$ m/s, $\mu = 2.25$, and $c_h = 2.4 \times 10^{-8}$ m^2/s. The initial void ratio was taken as $e_0 = 0.95$.

Measured settlements are compared with the settlements calculated from pore pressure predictions based on the two new consolidation models presented in the previous chapter: consolidation using the spectral method, and nonlinear radial consolidation. Owing to the short vertical drainage length, the well resistance can be ignored. For the nonlinear radial consolidation model only Darcian flow was considered (i.e. $n = 1.001$). This is reasonable considering that the small influence radius ($r_e = 225$ mm) would result in high hydraulic gradients which may exceed the critical gradient for power law flow. As drainage in the vertical direction is allowed, the nonlinear model must be modified to account for the resulting vertical consolidation. The vertical degree of consolidation was considered by Terzaghi's one-dimensional equation:

$$U_z = 1 - \sum_{m=0}^{\infty} \frac{2}{M} \exp\left[-M^2 T_z\right] \tag{4.1}$$

where $M = \pi(2m+1)/2$, m = 1,2,…, and $T_z = c_v t/l^2$ is the vertical time factor. Consolidation by vertical and horizontal drainage are combined with Carillo's (1942) relationship:

$$(1-U) = (1-U_z)(1-U_h) \tag{4.2}$$

The material properties quoted above are average values calculated for use with the spectral method, where, in calculating excess pore pressure, soil properties do not change. Thus for the nonlinear model the following soil properties were assumed to be: C_k = 0.45 and c_{h0} = 3.36 × 10^{-8} m/s.

Settlement curves are shown in Figure 4.5. Both methods of prediction provide a good match with measured settlement data, especially during the third loading stage. During the first loading stage the spectral method slightly underestimates settlement while the nonlinear model slightly overestimates settlement. This may be due to some uncertainty as to the stress state at the start of the test. Also shown in Figure 4.5 are the corresponding settlement plots with constant permeability throughout the smear zone, for the ideal drain (no smear: r_s/r_w = 1) and an assumed upper bound for maximum smear (r_s/r_w = 6) (see Appendix A for μ formula). k_h/k_0 is the same as for the parabolic case, i.e. 1.6.

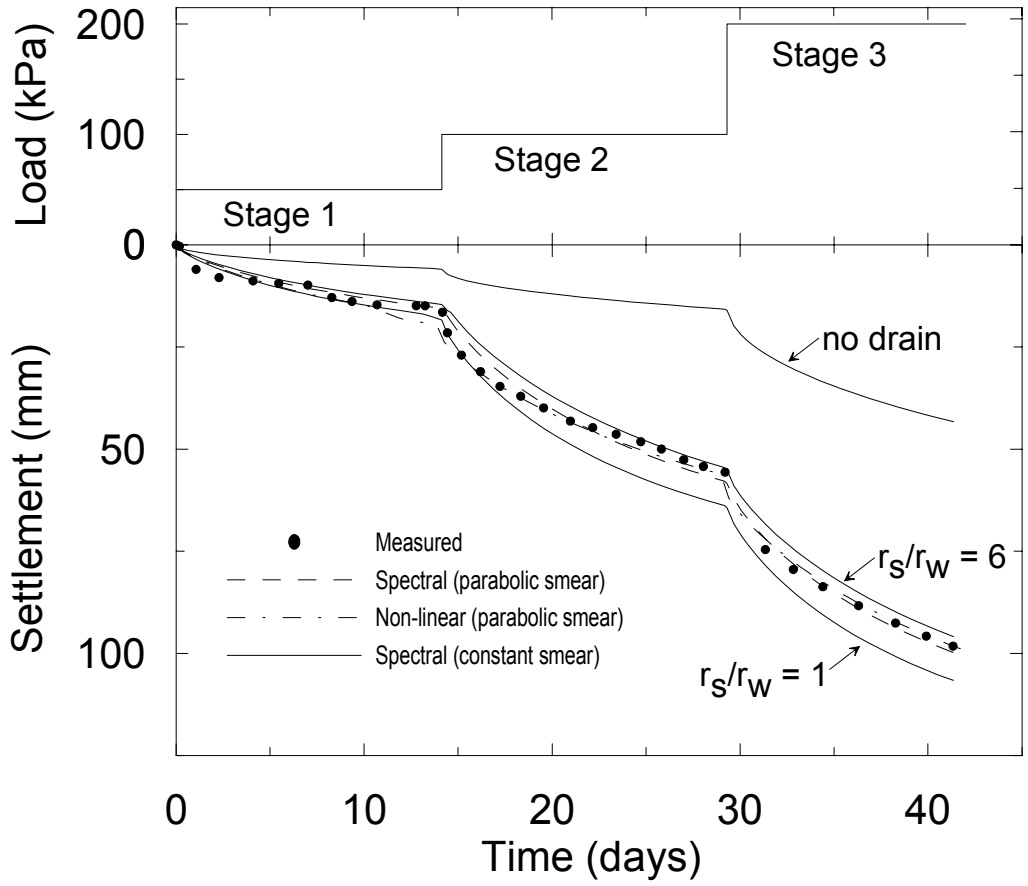

Figure 4.5 Predicted and measured settlement for large-scale consolidometer

The writers spectral solution with parabolic permeability decay, $r_s/r_w = 8.4$, and Hansbo (1981) with constant permeability are identical only in the case of Hansbo's $r_s/r_w = 2.62$. This shows that the extent of smearing is much greater than that assumed when considering a smear zone with constant reduced permeability smear zone. Figure 4.5 confirms that the effects of smear can be assessed by using existing assumptions about the size of a constant permeability smear zone with a radius of 1.6 to 4 times the equivalent drain or mandrel radius (Hansbo, 1981; Indraratna and Redana, 1998a). However, more meaningful interpretations of the extent of smear can be made using the proposed parabolic change of lateral permeability within the smear zone, justifiable based on laboratory observations.

By using the measured parabolic permeability distribution, which gives good agreement with the model analysis as shown in Figure 4.5, the need for assuming a constant smear zone radius and the consequent uncertainty in the analysis are reduced. It is acknowledged that μ is easier to calculate for constant properties, but in soils where the rate of consolidation is dependant on the properties of the smear zone, the parabolic smear zone model provides enhanced reliability, in spite of the more rigorous computational procedure.

4.3.3 Verification of Nonlinear Consolidation Model

The purpose of this test, conducted by Rujikiatkamjorn (2006), was to verify the radial consolidation model of Indraratna et al. (2005a). The model of Indraratna et al. (2005a) determines the best value of c_h to use in Hansbo's (1981) consolidation equation with reference to C_c, C_k and the stress range. It should be noted that the spectral method of Chapter 3 will give the same pore pressure values as Indraratna et al. (2005a) theory if the appropriate value of c_h is used. Detailed testing procedures are described in Indraratna and Redana (1998a) and Indraratna and Redana (1998b).

The soil consisted of reconstituted alluvial clay from Moruya (40 to 50% clay sized particles (<2μm), 45% saturated water content, 17% plastic limit, 17 kN/m^3 saturated unit weight). The soil was similar to that used in Section 4.3.2 with greater emphasis placed on accurately determining soil properties, particularly the value of C_c and C_k. Figure 4.6 shows the soil test results from which the compressibility and permeability parameters were determined. In two separate tests, the soil was

subjected to an initial preconsolidation pressure, σ'_p = 20 kPa and 50 kPa for five days. The load was removed, a 100 mm × 4 mm band drain centrally installed, and the preconsolidation loads reapplied. Drainage in the vertical direction was prevented. Once settlements became negligible, the load was increased by 30 kPa and 50 kPa, respectively (i.e. $\Delta\sigma$ = 30, 50). Settlements were monitored after this point with the soil consolidating in the compression range. The properties of the soil/drain system are given in Table 4.1. Only for the purpose of analysis, Darcian flow was considered (i.e. n = 1.001). The degree of consolidation based on settlement is calculated and compared with laboratory data, the proposed model, and Indraratna et al. (2005a)). The comparison of the three approaches is shown in Figure 4.7.

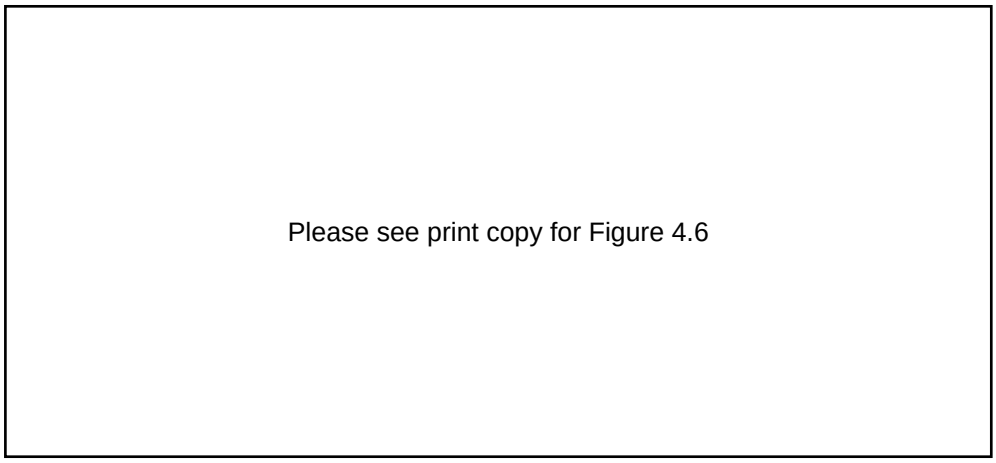

Figure 4.6 Typical $e - \log(\sigma')$ and $e - \log(k_h)$ for Moruya Clay (Rujikiatkamjorn, 2006)

Table 4.1 Parameters used in analysis (Indraratna et al., 2005a)

Please see print copy for Table 4.1

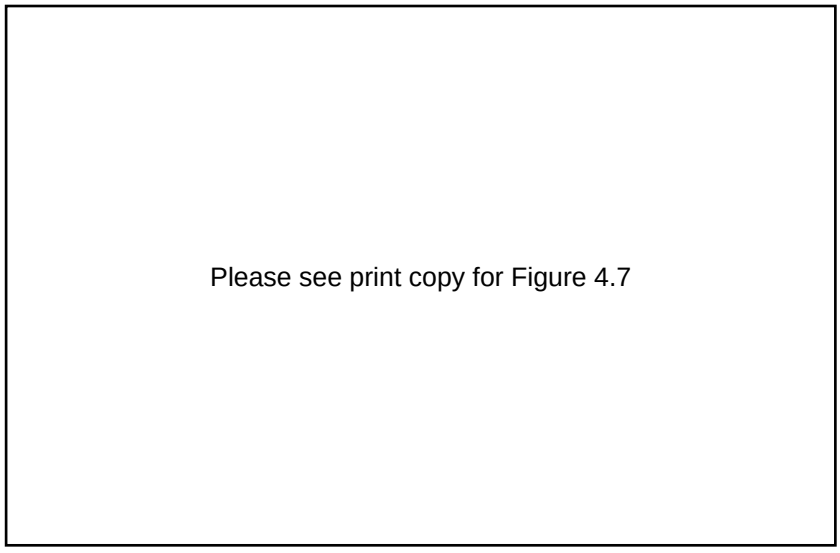

Figure 4.7 Comparison between proposed nonlinear model and Indraratna et al. (2005a)

Figure 4.7 shows good agreement between the measured and predicted values of degree of consolidation for both the proposed nonlinear equations and Indraratna et al. (2005a). As mentioned above, in this case, the method of Indraratna et al. (2005a)

(Equation 3.52) will give the same results as the spectral method (Equation 3.139). The proposed equations give a slightly better match in the early stages of consolidation; the difference is less for Test 2 than for Test 1. As the consolidation coefficient is increasing during consolidation ($C_c/C_k < 1$), by using an average value of c_h as in Indraratna et al. (2005a), settlement would be expected to be over predicted in the initial stages of consolidation, which is shown in Figure 4.7. The combination of $C_c/C_k = 0.64$ and $\Delta\sigma/\sigma'_0$ =1.5 and 1, produce ratios of final to initial consolidation coefficient of 1.39 and 1.28, respectively, for Test 1 and Test 2. Chapter 3 showed that for such values of c_{hf}/c_{h0}, the difference between the nonlinear equations and Hansbo (1981) equation are small. This explains the small difference between the analysis based on the proposed relationship and that of Indraratna et al. (2005a).

4.3.4 Verification of Combined Surcharge and Vacuum Loading

This purpose of this test, performed by Bamunawita (2004), was to investigate soil consolidation under combined vacuum and surcharge loading conditions. The test results are described fully in Indraratna et al. (2004). The relevant data (summarized below) from this test is reanalysed here with the proposed consolidation equations.

The soil consisted of reconstituted alluvial clay from Moruya (40 to 50% clay sized particles (<2μm), 40% saturated water content, 70% liquid limit, 30% plastic limit, 18.1 kN/m^3 saturated unit weight). Drainage was provided at the top of the soil. The soil was subjected to an initial preconsolidation pressure of σ'_p = 20 kPa. The load was then removed and a single prefabricated vertical drain (100 mm × 3 mm) was

installed using a rectangular steel mandrel. After drain installation a 100 kPa vacuum was applied at the top of the cell and the surcharge pressure was increased in two stages to 50 kPa and 100 kPa. The vacuum pressure was subsequently removed and reapplied. Pore pressure measurements indicated that the vacuum pressure along the drain decreases approximately linearly with depth to 70 kPa at the bottom of the cell.

The measured soil properties are as follows: compression index $C_c = 0.34$, recompression index $C_r = 0.12$, vertical coefficient of permeability $k_v = 1.1 \times 10^{-10}$ m/s, and undisturbed horizontal permeability $k_h = 2.5 \times 10^{-10}$ m/s. The equivalent radius of the band drain (after Rixner et al., 1986) is $r_w = (100 + 3)/4 = 26$mm. The radius of smear zone was assumed to be four times the equivalent drain radius, with a constant horizontal permeability equal to the vertical permeability. Given the above parameters, $\mu = 3.06$ and the vertical and horizontal coefficients of consolidation are taken as $c_v = 5.7 \times 10^{-9}$ m^2/s and $c_h = 13.2 \times 10^{-9}$ m^2/s. The initial void ratio was taken as $e_0 = 0.95$.

The spectral consolidation model allows for direct input of vacuum load that varies with depth and surface application of vacuum by way of a dummy layer with high horizontal permeability (see Chapter 3). For the nonlinear radial consolidation model vacuum loading (assumed constant with depth at 100 kPa) was modeled using an equivalent surcharge load. As in Section 4.3.2 above, drainage in the vertical direction was incorporated into the nonlinear radial consolidation model with

Carillo's (1942) relationship. The assumed initial parameters for nonlinear analysis are: $C_k = 0.45$ and $c_{h0} = 3.6 \times 10^{-8}$ m/s.

The calculated and measured settlements are shown in Figure 4.8. The cause for the large instantaneous settlement at the start of the second surcharge loading stage, and the otherwise good settlement match, is unknown. The settlements calculated with the spectral method approach show an appropriate response to vacuum removal and reloading illustrating the applicability of the proposed consolidations equations in modeling such phenomena. The nonlinear equations adjusted for vacuum loading and vertical drainage show significant deviations form the measured settlement when the vacuum loading is removed. This discrepancy arises more from the inclusion of vertical drainage than the treatment of vacuum as an equivalent surcharge load. Care should be taken when modeling the change of vacuum loads with the nonlinear consolidation equations.

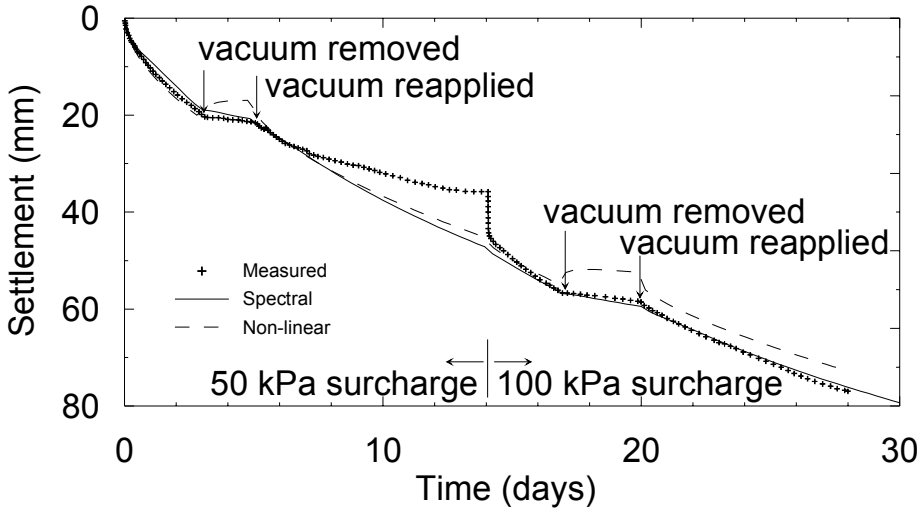

Figure 4.8 Settlement of large-scale consolidation cell with vacuum and surcharge loading

4.4 Summary

This Chapter has verified the proposed theoretical models presented in the previous Chapter against large-scale laboratory consolidation tests. The parabolic permeability distribution in the smear zone provides a good match with the permeability distribution measured in the large-scale consolidometer at the University of Wollongong. The spectral method model and the nonlinear radial consolidation model can be used to predict the behaviour of soil under surcharge and vacuum loading. In particular, the spectral method approach provides excellent predictions for changing vacuum loads. This will also be demonstrated in the next Chapter, where the new consolidation models will be applied to selected case histories in the field.

5 CASE HISTORY VERIFICATION

5.1 General

This Chapter applies the theoretical developments of Chapter 3 to two field case histories. The first case history is the trial embankments constructed for the Second Bangkok International Airport. Both the spectral method and nonlinear radial consolidation models are used compare predicted and measured values of pore pressure and settlement. The second case history illustrates the versatility of the spectral method in modeling ground subsidence due to ground water pumping in the Saga Plain, Japan.

5.2 Second Bangkok International Airport (Bergado et al., 1998)

As part of the Second Bangkok International Airport (30 km east of Bangkok, Thailand) a series of test embankments was constructed to assess the behaviour of the thick compressible subsoil. The surface settlement and excess pore water pressure at the middle of two embankments, TV1 and TV2, incorporating vacuum loading and vertical drains are analysed here. Both embankments have previously been analysed using the finite element method (Bergado et al., 1998; Indraratna et al., 2004; Indraratna et al., 2005b).

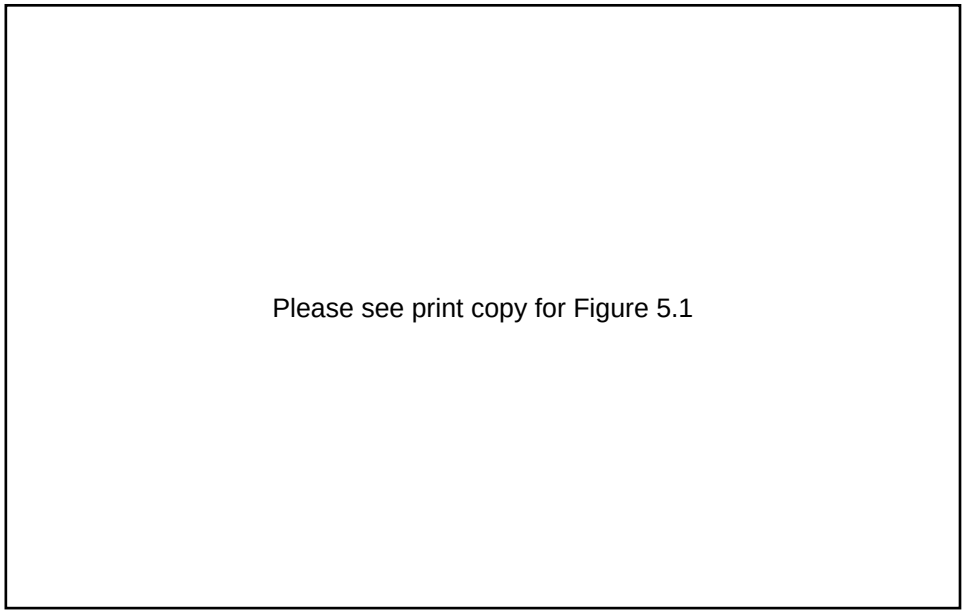

Figure 5.1 Site plan for the test embankments at Second Bangkok International Airport (Bamunawita, 2004)

Figure 5.1 shows the site plan for the two embankments. Figures 5.2 and 5.3 show the soil properties obtained from borehole and oedometer tests. The subsoil can be divided into five sub-layers: weathered clay (0-2 m), very soft clay (2-8.5 m), soft clay (8.5-10.5 m), medium clay (10.5-13 m), and stiff to hard clay (13-15m). The modified Cam-clay properties of each layer used in previous finite element analyses are given in Table 5.1. Each embankment covers an area of $40\,\text{m} \times 40\,\text{m}$. For embankment TV1, PVD ($r_w = 0.05\text{m}$, 15 m long at 1 m triangular spacing) were installed from a working platform comprising 0.3 m of sand. Drainage at the surface was provided by a hypernet drainage system. To facilitate vacuum application, a geomembrane liner was placed above the drainage layer and sealed with a bentonite trench surrounding the embankment. A 60 kPa vacuum was applied and the embankment height was subsequently raised in stages to a height of 2.5 m (the unit

weight of surcharge fill was 18 kN/m^3). TV2 was similarly constructed but with a 0.8 m working platform, 12 m PVD, and a drainage system of geotextiles and perforated and corrugated pipes.

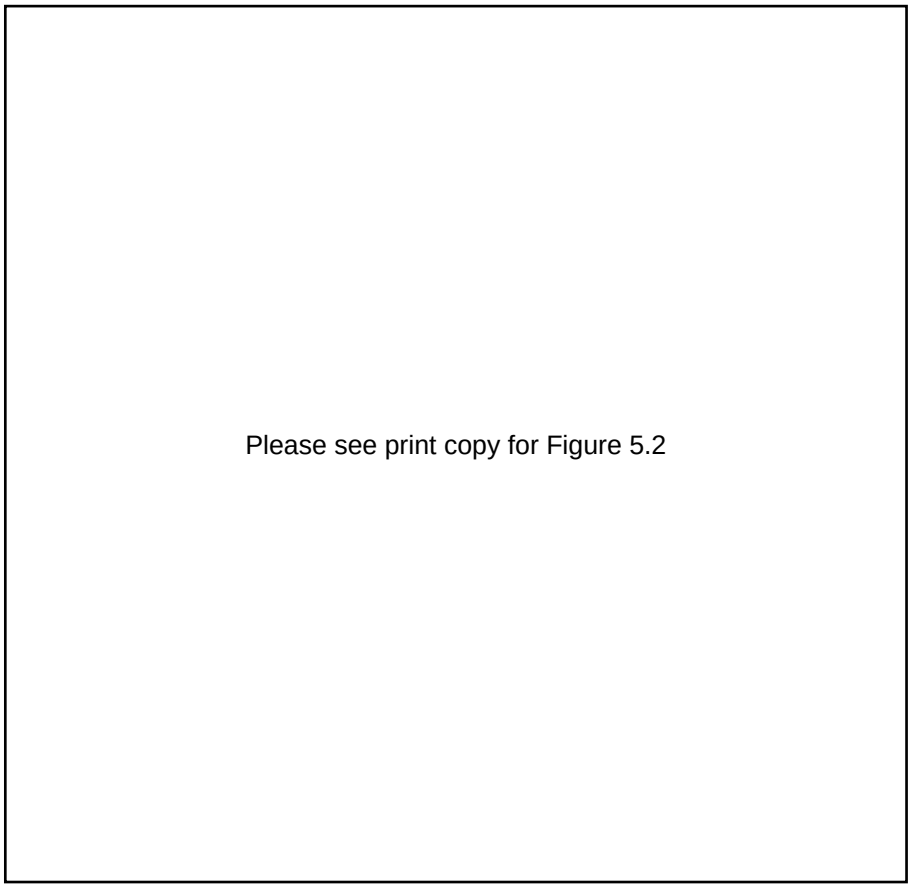

Figure 5.2 General soil properties for SBIA test embankments (after Sangmala, 1997)

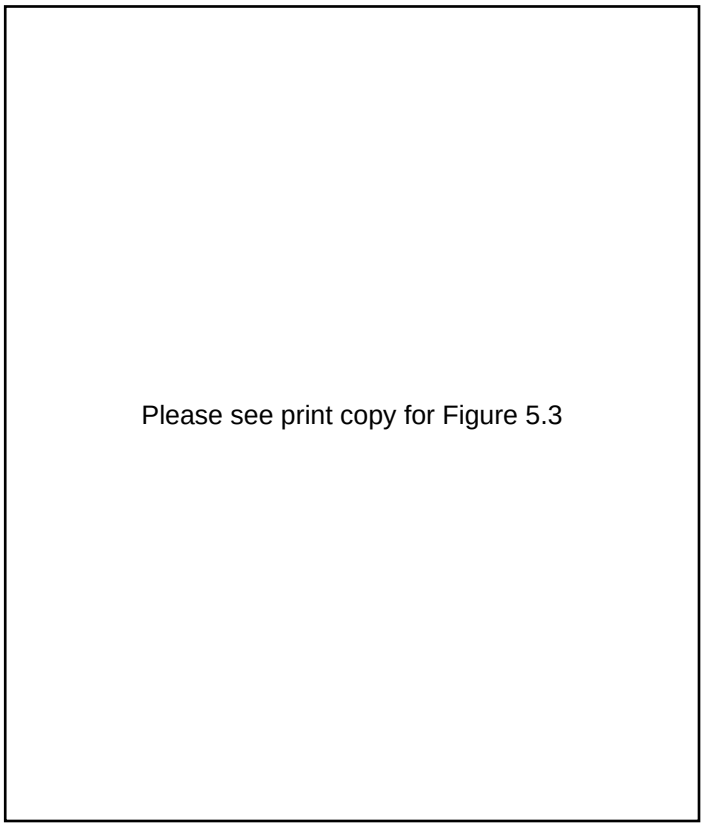

Figure 5.3 Compression properties for SBIA test embankments (after Sangmala, 1997)

Table 5.1 Modified Cam-clay parameters for SBIA test embankments (Indraratna et al., 2004)

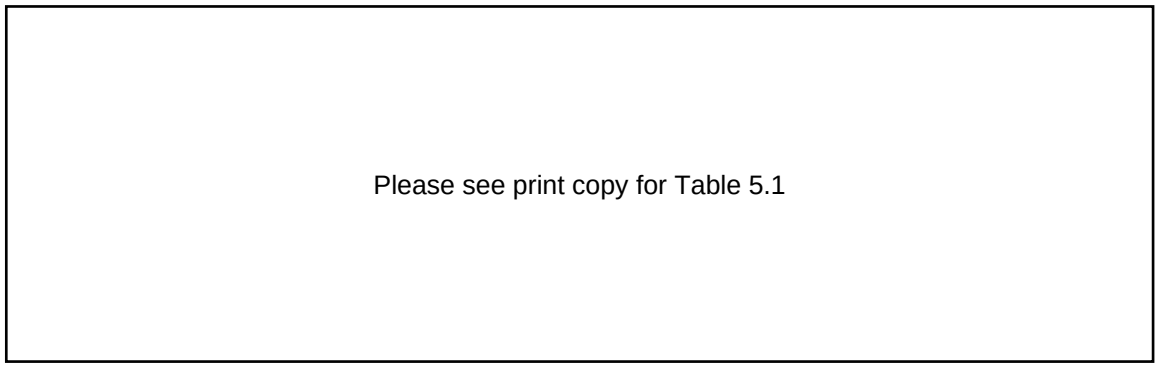

5.2.1 Spectral Method Parameters

The spectral method model was developed in Chapter 3 and is used here to analyse the two trial embankments. To model the PVD a smear zone with radius 6 times the effective drain radius and a horizontal permeability equal to the undisturbed vertical

permeability was assumed. This results in a μ value of approximately 3.95 for all layers. For the spectral method approach the properties at the top of the very soft clay were used as reference values, with $\bar{c}_v$ = 0.005 m^2/day, $\bar{c}_h$ = 0.01 m^2/day, $\bar{\eta}$ = 0.02. The relevant parameters for the other layers used in the calculation of excess pore pressure are then given relative to the reference values in Tables 5.2 and 5.3. In calculating the $k_v/\bar{k}_v$ parameter the permeability coefficients in each layer are taken from Table 5.1. As the vertical drain configuration and smear zone properties are assumed to be identical in each layer the relative value of the vertical drain parameter $\eta/\bar{\eta}$ will depend only on the permeability values, and thus have the same value as the $k_v/\bar{k}_v$ parameter. The compressibility parameter $m_v/\bar{m}_v$ chosen is based on the void ratio change expected from an effective stress increase of 50 kPa using the Cam-Clay compressibility properties in Table 5.1). The initial effective stress and overconsolidation ratio required for such a void ratio change calculation are interpolated from Figure 5.2 and 5.3 respectively. In each analysis the soil below the PVD was ignored.

To calculate surface settlements, the excess pore pressure at 30 points (see Tables 5.4 and 5.5) in the soil system was determined using the proposed spectral consolidation equations. The strain at each point was calculated using the excess pore pressure values and the compression characteristics given in Tables 5.4 and 5.5. The resulting strain profile was numerically integrated to give settlement values at various depths. The applied surcharge load, found from the unit weight of embankment fill, was multiplied by a load factor (see Figure 5.4) to account for load variation with depth. Piezometer readings indicate that the constant total vacuum pressure applied by the

vacuum pump did not fully transfer to the soil, hence the assumed vacuum variation over time in Figure 5.5. Loss of vacuum may be caused by air leaks in the system. Also Indraratna et al. (2005b) suggest that vacuum pressure can vary linearly with depth within the PVD. In this analysis vacuum pressure was assumed to vary from the value in Figure 5.5 at the soil surface to zero at the bottom of the drain.

Table 5.2 Soil properties for spectral method modeling of TV1 pore pressure

Depth (m)	Normalised depth (Z)	$k_v/\overline{k}_v$	$m_v/\overline{m}_v$	$\eta/\overline{\eta}$
-3.00*	0.00	1.00	0.37	50.00
0.00*	0.17	1.00	0.37	50.00
0.00	0.17	2.36	0.37	2.36
2.00	0.28	2.36	0.41	2.36
2.00	0.28	1.00	1.00	1.00
8.50	0.64	1.00	0.49	1.00
8.50	0.64	0.47	0.34	0.47
10.50	0.75	0.47	0.59	0.47
10.50	0.75	0.20	0.35	0.20
13.00	0.89	0.20	0.25	0.20
13.00	0.89	0.05	0.08	0.05
15.00	1.00	0.05	0.09	0.05

* dummy layer for surface vacuum application

Table 5.3 Soil properties for spectral method modeling of TV2 pore pressure

Depth (m)	Normalised depth (Z)	$k_v/\overline{k}_v$	$m_v/\overline{m}_v$	$\eta/\overline{\eta}$
-3.00*	0.00	1.00	0.37	50.00
0.00*	0.20	1.00	0.37	50.00
0.00	0.20	2.36	0.37	2.36
2.00	0.33	2.36	0.41	2.36
2.00	0.33	1.00	1.00	1.00
8.50	0.77	1.00	0.49	1.00
8.50	0.77	0.47	0.34	0.47
10.50	0.90	0.47	0.59	0.47
10.50	0.90	0.20	0.35	0.20
12.00	1.00	0.20	0.26	0.20

* dummy layer for surface vacuum application

Table 5.4 Soil properties for spectral method modeling of TV1 settlement

Depth (m)	Normalised depth (Z)	σ'_0	σ'_p	e_0	C_c	C_r
0.00	0.17	5.00	58.00	1.01	0.69	0.07
0.54	0.20	5.09	57.36	1.06	0.69	0.07
1.07	0.23	6.49	47.71	1.78	0.69	0.07
1.61	0.26	8.18	41.29	2.35	0.69	0.07
2.14	0.29	11.07	47.71	2.29	1.61	0.18
2.68	0.32	13.86	50.39	2.29	1.61	0.18
3.21	0.35	16.43	45.57	2.42	1.61	0.18
3.75	0.38	19.10	41.50	2.45	1.61	0.18
4.29	0.40	21.89	38.29	2.37	1.61	0.18
4.82	0.43	24.61	39.89	2.39	1.61	0.18
5.36	0.46	27.29	44.71	2.46	1.61	0.18
5.89	0.49	29.83	43.84	2.58	1.61	0.18
6.43	0.52	32.32	40.89	2.72	1.61	0.18
6.96	0.55	34.76	46.77	2.91	1.61	0.18
7.50	0.58	37.20	54.00	3.11	1.61	0.18
8.04	0.61	39.64	66.32	2.99	1.61	0.18
8.57	0.64	42.06	76.79	2.89	1.15	0.12
9.11	0.67	44.42	75.18	2.92	1.15	0.12
9.64	0.70	46.81	74.00	2.84	1.15	0.12
10.18	0.73	49.27	74.00	2.45	1.15	0.12
10.71	0.76	51.96	75.61	2.19	0.69	0.07
11.25	0.79	54.99	79.63	2.12	0.69	0.07
11.79	0.82	57.94	86.21	2.07	0.69	0.07
12.32	0.85	60.84	95.05	2.03	0.54	0.05
12.86	0.88	63.69	95.86	2.02	0.30	0.03
13.39	0.91	66.53	92.64	2.01	0.23	0.02
13.93	0.94	69.82	92.00	2.01	0.23	0.02
14.46	0.97	73.22	92.00	2.01	0.23	0.02
15.00	1.00	73.45	92.00	2.01	0.23	0.02

Table 5.5 Soil properties for spectral method modeling of TV2 settlement

Depth (m)	Normalised depth (Z)	σ'_0	σ'_p	e_0	C_c	C_r
0.00	0.20	5.00	58.00	1.01	0.69	0.07
0.43	0.23	5.00	58.00	1.01	0.69	0.07
0.86	0.26	5.93	51.57	1.49	0.69	0.07
1.29	0.29	7.04	43.86	2.07	0.69	0.07
1.71	0.31	8.76	42.57	2.34	0.69	0.07
2.14	0.34	11.07	47.71	2.29	1.61	0.18
2.57	0.37	13.34	51.36	2.27	1.61	0.18
3.00	0.40	15.40	47.50	2.37	1.61	0.18
3.43	0.43	17.46	43.64	2.47	1.61	0.18
3.86	0.46	19.66	40.86	2.44	1.61	0.18
4.29	0.49	21.89	38.29	2.37	1.61	0.18
4.71	0.51	24.07	38.93	2.37	1.61	0.18
5.14	0.54	26.21	42.79	2.43	1.61	0.18
5.57	0.57	28.33	45.61	2.50	1.61	0.18
6.00	0.60	30.33	43.25	2.61	1.61	0.18
6.43	0.63	32.32	40.89	2.72	1.61	0.18
6.86	0.66	34.28	45.32	2.87	1.61	0.18
7.29	0.69	36.23	51.11	3.03	1.61	0.18
7.71	0.71	38.18	58.93	3.06	1.61	0.18
8.14	0.74	40.13	68.79	2.97	1.61	0.18
8.57	0.77	42.06	76.79	2.89	1.15	0.12
9.00	0.80	43.95	75.50	2.92	1.15	0.12
9.43	0.83	45.84	74.21	2.94	1.15	0.12
9.86	0.86	47.79	74.00	2.68	1.15	0.12
10.29	0.89	49.76	74.00	2.37	1.15	0.12
10.71	0.91	51.96	75.61	2.19	0.69	0.07
11.14	0.94	54.38	78.82	2.14	0.69	0.07
11.57	0.97	56.79	82.68	2.09	0.69	0.07
12.00	1.00	59.10	89.75	2.06	0.69	0.07

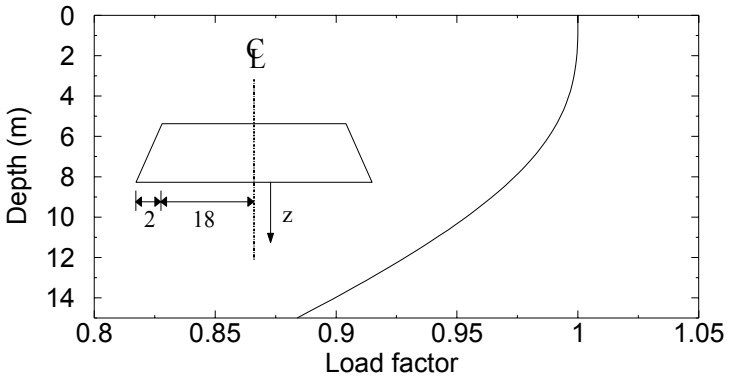

Figure 5.4 Variation of load with depth at embankment centerline

5.2.2 Nonlinear Radial Consolidation Model Parameters

The approximate method for the nonlinear radial consolidation model under arbitrary loading was developed in Chapter 3 and is used here to analyse the two trial embankments. Vertical drainage was ignored due to the dominant nature of the radial drainage. Variations in surcharge and vacuum loading with depth and time are identical to the spectral method parameters above; as are the drain properties. The excess pore pressure and settlement in embankment TV1 was calculated for 16 sub-layers with soil properties described in Table 5.6. Embankment TV2, with a shorter PVD length of 12 m, was modeled by omitting the bottom three sub layers. Vacuum pressure in the drain was simulated by an equivalent surcharge load.

Table 5.6 Soil properties for nonlinear radial consolidation modeling of embankment TV1

Layer	Sub layer thickness (m)	k_{h0} (m/s)	C_c	C_r	σ'_0 (kPa)	σ'_p (kPa)	e_0
1	1	9.03×10^{-9}	0.37	0.06	3	58	1.8
2	1	9.03×10^{-9}	0.37	0.06	9	58	1.8
3	1	3.81×10^{-9}	1.6	0.08	14.5	45	2.8
4	1	3.81×10^{-9}	1.6	0.08	19.5	45	2.8
5	1	3.81×10^{-9}	1.6	0.08	24.5	45	2.8
6	1	3.81×10^{-9}	1.6	0.08	29.5	45	2.8
7	1	3.81×10^{-9}	1.6	0.08	34.5	45	2.8
8	1	3.81×10^{-9}	1.6	0.08	39.5	45	2.8
9	0.5	3.81×10^{-9}	1.6	0.08	43.25	45	2.8
10	1	1.81×10^{-9}	1.7	0.05	47	70	2.4
11	1	1.81×10^{-9}	1.7	0.05	52	70	2.4
12	1	7.68×10^{-10}	0.95	0.03	57.5	80	1.8
13	1	7.68×10^{-10}	0.95	0.03	63.5	80	1.8
14	0.5	7.68×10^{-10}	0.95	0.03	68	80	1.8
15	1	1.80×10^{-10}	0.88	0.01	73.5	90	1.2
16	1	1.80×10^{-10}	0.88	0.01	81.5	90	1.2

5.2.3 Comparison of Settlement and Excess Pore Pressure

The calculated and measured centre-line surface settlements for the two embankments, along with the surcharge and assumed vacuum loading stages, are shown in Figure 5.5. Figure 5.6 compares the calculated and measured settlements at 3, 6, and 9 m depths for embankment TV2. Both the spectral method and nonlinear approaches provide an adequate match for the development of settlements given the uncertainty in vacuum application. The nonlinear radial consolidation model slightly overestimates settlements in the early stages of loading. The increased consolidation rate is associated with consolidation in the recompression range which is generally much faster due to higher soil stiffness. The spectral method, with constant soil properties, tends to average the effects of recompression and compression, and so does not exhibit the fast initial consolidation rate. The fact that the spectral method,

with average properties that do not explicitly capture rapid recompression, gives a better match with the measured settlement response suggests that the preconsolidation pressure in the field may be lower than expected. This may be caused by soil disturbance associated with vertical drain installation.

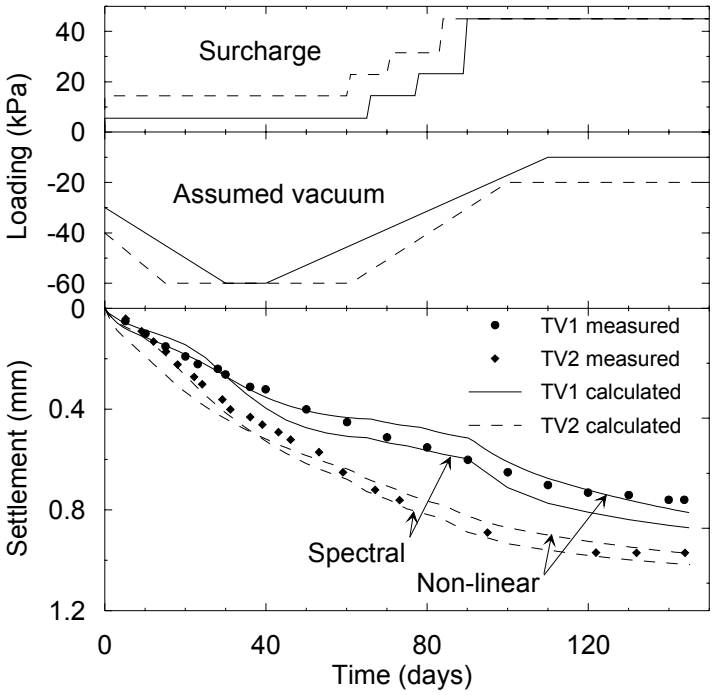

Figure 5.5 Centerline surface settlement plots for SBIA test embankments

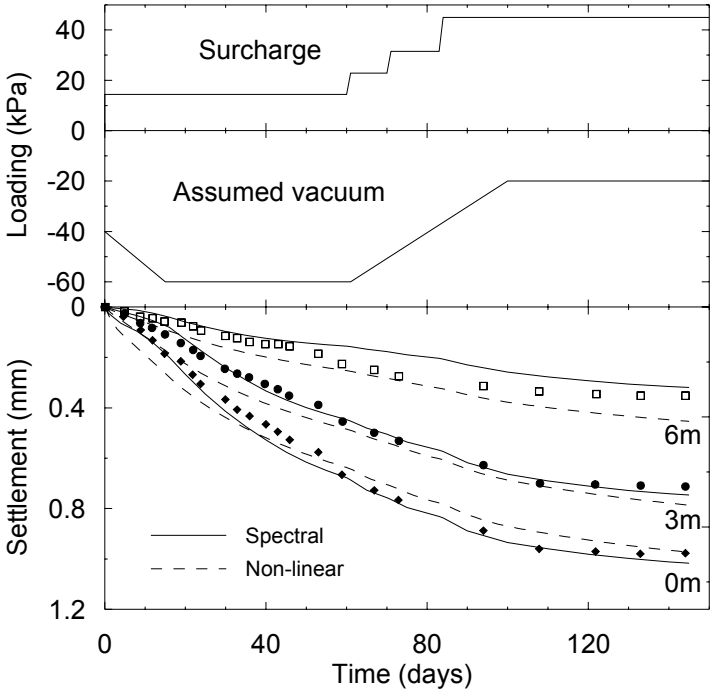

Figure 5.6 Centerline settlement at various depths for embankment TV2

The absence of recompression behaviour is supported by the pore pressure measurements shown in Figures 5.6 and 5.7. The swift pore pressure dissipation expected during the recompression phase, as calculated by the nonlinear approach, is not reflected in the measured pore pressure values. The spectral method gives a slightly better pore pressure match during the early stage of consolidation. A more accurate match might be achieved for both settlement and pore pressure prediction if the assumed vacuum loading is altered, though it would be difficult to predict the loss of vacuum pressure in the field before construction. At least with the present models, the effects of possible loss of vacuum, and its variation with depth, can be assessed.

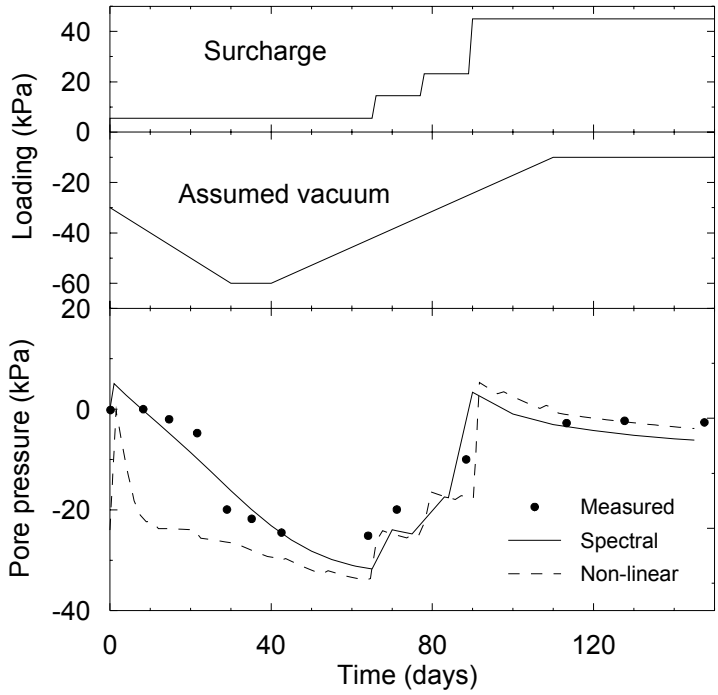

Figure 5.7 Excess pore pressure 3 m below centerline of embankment TV1

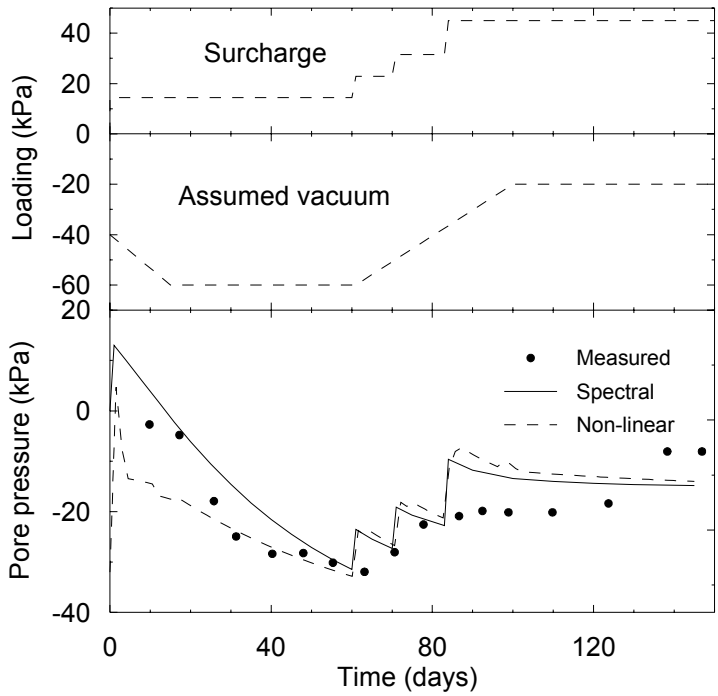

Figure 5.8 Excess pore pressure 3 m below centerline of embankment TV2

5.2.4 Comparison With Previous Finite Element Method Studies

As mentioned above, the finite element method (FEM) has been used previously to model the settlement and pore pressure response beneath the Second Bangkok International Airport test embankments. Figure 5.9 compares the centerline settlements of Figure 5.6 (embankment TV2) with the finite element results of Bergado et al. (1998) and Indraratna et al. (2005b). The Excess pore pressures from Figure 5.8 (embankment TV2) are compared with Indraratna et al. (2005b) in Figure 5.10. The figures are inconclusive as to which modeling method is the best as each of the four models (Spectral method, nonlinear radial consolidation, and two finite element models) give a fairly good settlement match with measured values. Figures 5.9 and 5.10 at least show that the new spectral method and nonlinear radial consolidation model are useful in modeling the centerline behaviour beneath an embankment. If accurate prediction is required away from the centerline (e.g. modeling slope stability and heave at the embankment toe) or if fully coupled analysis with more complex constitutive models need to be performed then multi-drain analysis with methods such as finite elements must be used.

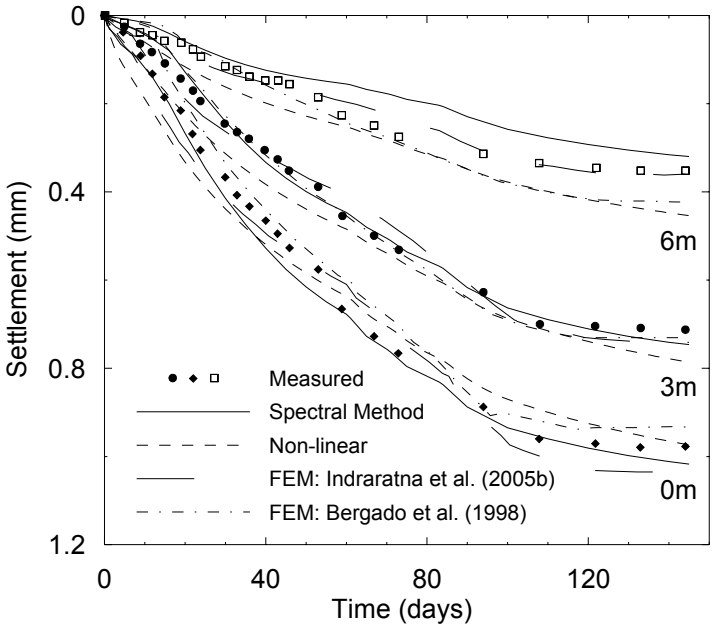

Figure 5.9 Centerline settlement for embankment TV2 including previous finite element models

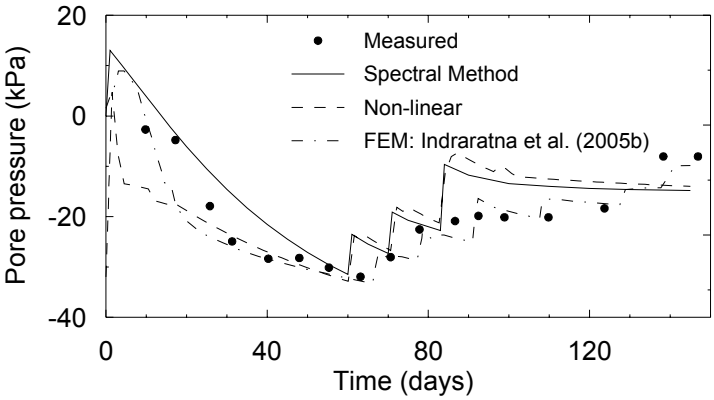

Figure 5.10 Excess pore pressure below TV2 inclduing a prevous finite element model

5.3 Land Subsidence Due to Seasonal Pumping of Groundwater in Saga Plain, Japan (Sakai, 2001)

The Saga Plain on the Japanese island of Kyushu suffers from subsidence due to seasonal changes in groundwater level. Groundwater pumping in summer for agriculture, and winter recharge causes changes in effective stress, resulting in consolidation. Sakai (2001) describes the monitoring of land subsidence in the Saga Plain. The area is reclaimed from the Ariake Sea, consisting of 10-30 m of

compressible marine clay underlain by a sandy aquifer. A series of observation wells were installed in the Shiroishi district in 1996 to investigate the changes in groundwater level and associated subsidence settlements at various depths down to 90 m (Sakai, 2001). The changing groundwater level in one of the observation wells (27.5 m depth) is converted to excess pore water pressure and used with the proposed spectral method consolidation model to match the compression of the overlying 26 m of clay. As subsidence is due only to vertical flow in the clay layers the nonlinear radial consolidation model is not applicable.

By using a dummy layer with high horizontal permeability at the bottom of the soil system, the changes in excess pore pressure caused by groundwater pumping can be simulated with the proposed spectral method consolidation model. An appropriate vacuum load is specified at this dummy layer, while not allowing horizontal drainage in the clay layer. The soil properties in the Shiroishi district are shown in Figure 5.11. For pore pressure calculations, a single layer with uniform properties (c_v = 0.067 m^2/day) was used to model the 26 m of marine clay. The groundwater level recorded at the 27.5 m deep observation well was converted to excess pore pressure values (see Figure 5.12) and applied to the bottom of the clay by way of a 3 m thick dummy layer. To establish an initial pore pressure distribution, it was assumed that for 4 months prior to the start of observations, the applied modeled vacuum was equal to the first measured value of excess pore pressure. As for the Second Bangkok International Airport example, settlements were calculated by integrating the strain profile after pore pressure values have been determined. The properties for settlement calculations are given in Table 5.7. The relative settlement between the ground level and the observation well at 27.5 m depth is shown in

Figure 5.12. The discrepancy during the early months of analysis may be due to the largely unknown pore pressure distribution in the soil. Following this initial period, the calculated settlements match well with those measured. This example illustrates that consolidation caused by arbitrary changes in excess pore water pressure can be modeled with the proposed spectral method consolidation equations.

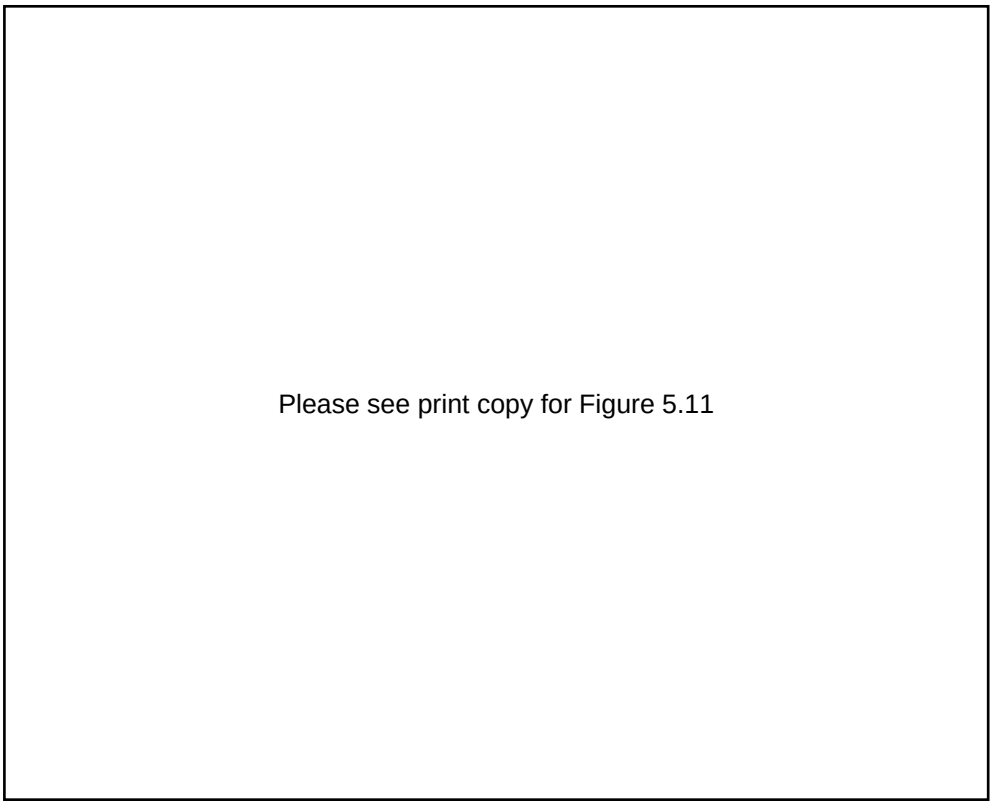

Figure 5.11 Soil properties at Shiroishi (after Sakai, 2001)

Table 5.7 Soil properties for settlement modeling of Shiroishi ground subsidence

Depth (m)	Normalised depth (Z)	C_c	C_r	e_0	σ'_0 (kPa)	σ'_p (kPa)
0.00	0.00	1.60	0.16	4.00	5.00	10.00
0.92	0.03	1.57	0.16	3.89	8.83	16.33
1.83	0.06	1.53	0.15	3.77	12.67	22.67
2.75	0.09	1.50	0.15	3.66	16.50	29.00
3.67	0.12	1.47	0.15	3.55	20.33	35.33
4.58	0.15	1.43	0.15	3.43	24.17	41.67
5.50	0.18	1.40	0.14	3.32	28.00	48.00
6.42	0.21	1.37	0.14	3.21	31.83	54.33
7.33	0.24	1.33	0.14	3.09	35.67	60.67
8.25	0.27	1.30	0.14	2.98	39.50	67.00
9.17	0.30	1.27	0.13	2.87	43.33	73.33
10.08	0.33	1.23	0.13	2.75	47.17	79.67
11.00	0.36	1.20	0.13	2.64	51.00	86.00
11.92	0.39	1.17	0.13	2.53	54.83	92.33
12.83	0.42	1.13	0.12	2.41	58.67	98.67
13.75	0.45	1.10	0.12	2.30	62.50	105.00
14.67	0.48	1.07	0.12	2.19	66.33	111.33
15.58	0.51	1.03	0.11	2.07	70.17	117.67
16.50	0.54	1.00	0.11	1.96	74.00	124.00
17.42	0.57	0.97	0.11	1.85	77.83	130.33
18.33	0.60	0.93	0.11	1.73	81.67	136.67
19.25	0.63	0.90	0.10	1.62	85.50	143.00
20.17	0.66	0.87	0.10	1.51	89.33	149.33
21.08	0.69	0.83	0.10	1.39	93.17	155.67
22.00	0.72	0.80	0.10	1.28	97.00	162.00
22.92	0.75	0.77	0.09	1.17	100.83	168.33
23.83	0.78	0.73	0.09	1.05	104.67	174.67
24.75	0.81	0.70	0.09	0.94	108.50	181.00
25.67	0.84	0.67	0.09	0.83	112.33	187.33
26.58	0.87	0.63	0.08	0.71	116.17	193.67
27.50	0.90	0.60	0.08	0.60	120.00	200.00

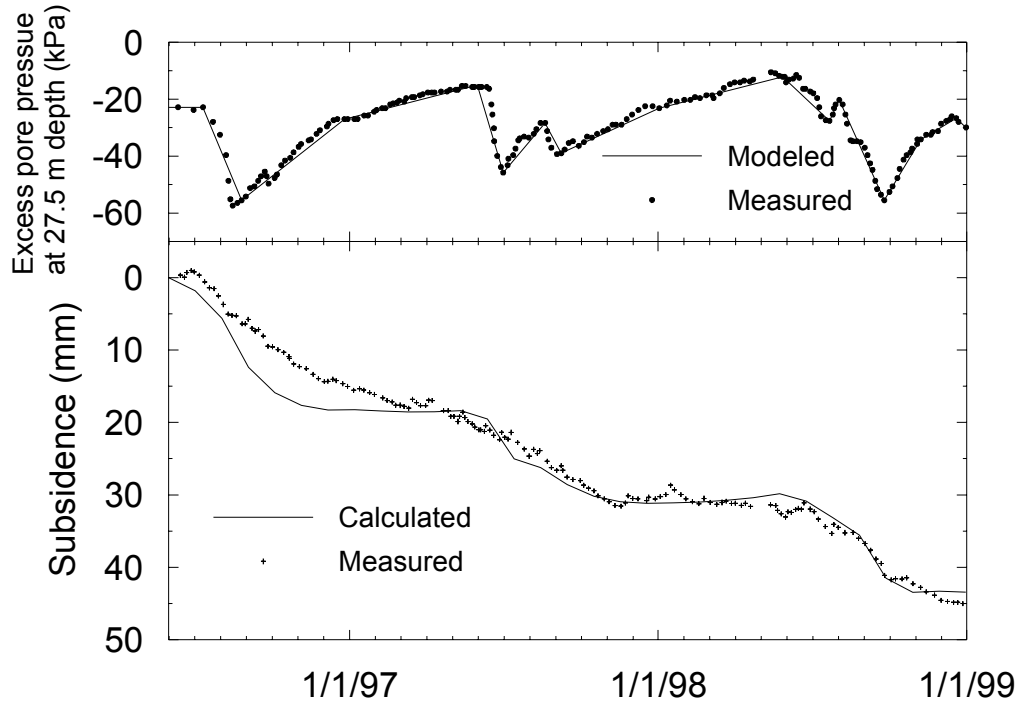

Figure 5.12 Compression of 26 m of marine clay

5.4 Summary

This Chapter confirmed that the two new consolidation models developed in Chapter 3, (a) spectral method model and (b) nonlinear radial consolidation model, can be used to predict settlement and pore pressure behaviour beneath the centre-line of an embankment subjected to vacuum loading. The spectral model conveniently describes the entire pore pressure distribution across multiple layers, while for the nonlinear radial consolidation model analysis must be completed for a series of sub-layers. Two case histories were analysed: trial embankments at the Second Bangkok International Airport, and ground subsidence in the Saga Plain, Japanese.

The next and final Chapter summarises the work presented so far in this thesis and provides recommendations for future work.

6 CONCLUSIONS AND RECOMMENDATIONS

6.1 General Summary

After a comprehensive review of vertical drain literature (Chapters 1 and 2), Chapter 3 developed three new contributions to the solution of consolidation problems: (i) a more realistic representation of the smear zone where soil properties vary gradually with radial distance from the vertical drain; (ii) a nonlinear radial consolidation model incorporating void ratio dependant soil properties; and (iii) a solution to multi-layered consolidation problems with vertical and horizontal drainage using the spectral method. Each model is verified against existing analytical solutions (Chapter 3) and laboratory experiments conducted at the University of Wollongong (Chapter 4). The nonlinear radial consolidation model and the spectral method are verified against two trial embankments involving surcharge and vacuum loading at the Second Bangkok International Airport, Thailand (Chapter 5). The versatility of the spectral method model is further demonstrated by analysing ground subsidence associated with ground water pumping in the Saga Plain, Japan (Chapter 5). Specific outcomes from the three models are described below.

6.2 Representation of Smear Zone

1. A number of researchers have noted that the disturbance in the smear zone increases towards the drain (Chai and Miura, 1999; Hawlader et al., 2002; Sharma and Xiao, 2000; Hird and Moseley, 2000; Indraratna and Redana, 1998a; Madhav et al., 1993; Bergado et al., 1991). Figure 6.1 below, shows the horizontal permeability distribution in a large-scale laboratory test varying in a parabolic fashion. Despite such observations the smear effect is

conventionally modeled using a smear zone of small size with reduced horizontal permeability, constant with radial distance from the drain.

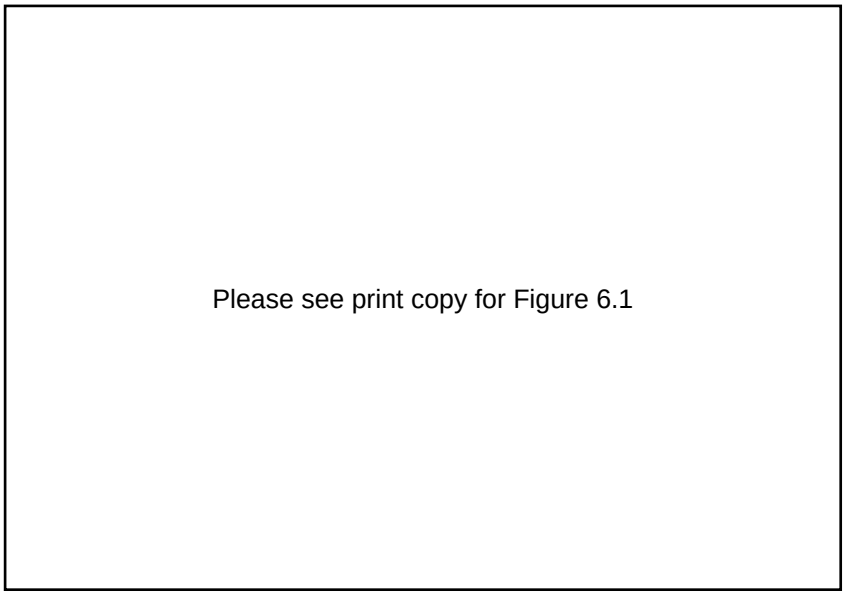

Figure 6.1 Horizontal permeability along radial distance from drain in large-scale consolidometer (original data from Indraratna and Redana, 1998a)

2. A more realistic representation of smear effect is found by modeling the gradual decrease in horizontal permeability towards the drain. Analytical expressions of the μ parameter used in Hansbo's (1981) radial consolidation equations are derived for linear and parabolic variations of smear zone permeability. The new μ expressions involve the same number of soil/geometry parameters as Hansbo's (1981) original constant permeability μ. With the ratio of undisturbed permeability to permeability at the drain soil interface designated κ, the new μ parameters based on permeability are:

$$\mu = \ln\left(\frac{n}{s}\right) - \frac{3}{4} + \frac{\kappa(s-1)^2}{\left(s^2 - 2\kappa s + \kappa\right)}\ln\left(\frac{s}{\sqrt{\kappa}}\right) - \frac{s(s-1)\sqrt{\kappa(\kappa-1)}}{2\left(s^2 - 2\kappa s + \kappa\right)}\ln\left(\frac{\sqrt{\kappa}+\sqrt{\kappa-1}}{\sqrt{\kappa}-\sqrt{\kappa-1}}\right) \quad \text{(parabolic)} \tag{6.1}$$

$$\mu = \begin{cases} \ln\left(\frac{n}{s}\right) - \frac{3}{4} + \frac{\kappa(s-1)}{s-\kappa}\ln\left(\frac{s}{\kappa}\right), & s \neq \kappa \\ \ln\left(\frac{n}{s}\right) - \frac{3}{4} + s - 1, & s = \kappa \end{cases} \quad \text{(linear)} \tag{6.2}$$

3. Based on equivalent consolidation rates, linear smear zone radii are approximately 2 to 4 times larger than the equivalent constant permeability smear zone radii. Parabolic smear zone radii are 4 to 7 times larger than the equivalent constant permeability smear zone radii.
4. The detrimental effect of increased smear zone compressibility, traditionally ignored, on the rate of consolidation may become important when considering the larger smear zones associated with a linear and parabolic variation of soil properties.
5. Larger smear zones may overlap. The μ expressions presented for overlapping linear smear zones provide some explanation for the phenomena of a minimum drain spacing, below which no increase in the rate of consolidation is achieved. It appears this minimum influence radius is 0.6 times the size of the linear smear zone. Figure 6.2 below, gives an example of the local minimum drain spacing associated with the theoretical consolidation curves for overlapping smear zones.

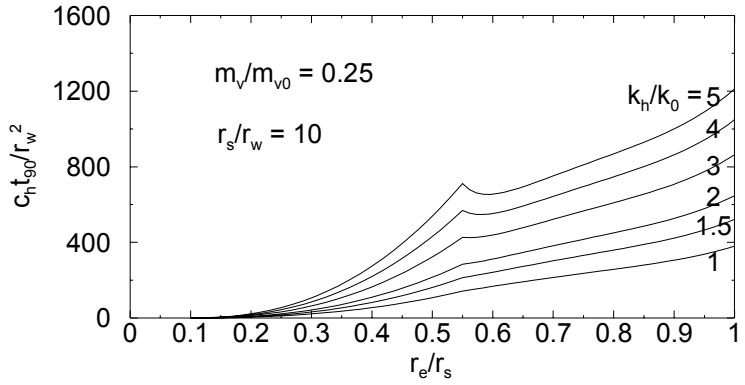

Figure 6.2 Time required for 90% consolidation for overlapping smear zones with linear variation of permeability

6.3 Nonlinear Radial Consolidation Model

1. The pertinent points of the nonlinear radial consolidation model are:
    a. Radial drainage only.
    b. Equal strain, one-dimensional deformation.
    c. Semi-log void ratio-stress relationship.
    d. Semi-log void ratio-permeability relationship.
    e. Non-Darcian flow.
    f. Inclusion of overconsolidated and normally consolidated soil behaviour.
    g. A closed form series solution is produced.
2. For nonlinear material properties, consolidation may be faster or slower when compared to the cases with constant material properties. The difference depends on the compressibility/permeability ratios (C_c/C_k and C_r/C_k), the preconsolidation pressure (σ'_p) and the stress increase ($\Delta\sigma/\sigma'_0$). If $C_c/C_k < 1$ or $C_r/C_k < 1$ then the coefficient of consolidation increases as

excess pore pressures dissipate and consolidation is faster. If $C_c/C_k > 1$ or $C_r/C_k > 1$ then the coefficient of consolidation decreases as excess pore pressures dissipate and consolidation becomes faster. For the case where $C_c/C_k = 1$ the solution is identical to Hansbo (2001). For normally consolidated soils the change in consolidation times depends approximately on the ratio of final to initial consolidation coefficient ($\tilde{c}_{hf}/\tilde{c}_{h0}$) as shown in Figure 6.3 below. For overconsolidated soils an increased number of soil parameters leads to a large variety of possible soil behaviour. The new equations can explicitly capture the retarded consolidation rates as the preconsolidation pressure is exceeded.

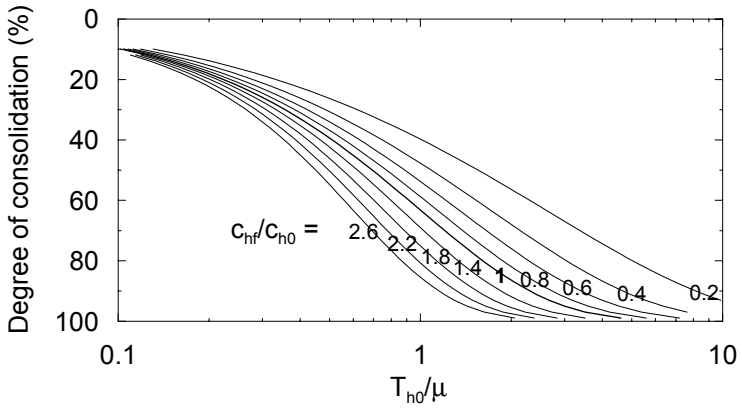

Figure 6.3 Consolidation curves depending on total change in consolidation coefficient

3. The introduction of soil nonlinearity produces discrepancies between the degree of consolidation based on pore pressure dissipation (U_h) and settlement (U_{hs}). For normally consolidated soils U_h lags U_{hs} depending on the stress ratio $\Delta\sigma/\sigma'_0$. For heavily overconsolidated soils U_h will only

lag U_{hs} in the latter stages of consolidation. Given the large variety of behaviour it becomes imperative to know the stress history of the soil.

4. The equations presented give an analytical solution to nonlinear radial consolidation that can be used to verify purely numerical methods.
5. By including an approximation for arbitrary loading almost any vertical drain problem where vertical drainage is negligible and effective stresses always increase can be analysed.

6.4 Multi-layered Spectral Method Model

1. The pertinent points of the multi-layered spectral method model are:
    a. Equal strain, one-dimensional deformation.
    b. Vertical and radial drainage.
    c. Multiple soil layers where permeability, compressibility, and vertical drain parameter vary in a linear fashion within each layer.
    d. Combined vacuum and surcharge loading that vary with both depth and time.
    e. Ability to control pore pressure boundary conditions by using dummy layers of high permeability to apply specified vacuum loads.
    f. Use of the spectral method to solve the governing equations. A single expression, calculated with common matrix operations, gives the pore pressure profile across all soil layers. Accuracy is improved by increasing the number of terms in the series solution.
    g. For the analytical solution soil properties are constant with time.
    h. Ability to use the pore pressure solution at any time as the initial condition for a separate analysis. This technique allows the analysis

of consolidation before and after vertical drain installation and piecewise constant treatment of time varied soil properties (see Appendix B).

2. The versatility and general nature of the spectral method model is demonstrated by accurate simulation of the following existing analytical models:
    a. Multi-layered free strain with thin sand layers (Nogami and Li, 2003)
    b. Double layered ground with vertical and radial drainage (Nogami and Li, 2003)
    c. Linearly varying vacuum loading (Indraratna et al., 2005b)
    d. Multiple ramp roading (Tang and Onitsuka, 2001)
    e. Partially penetrating vertical drains (Runnesson et al., 1985)
    f. Vertical consolidation of four layers (Schiffman and Stein, 1970)
3. The use of soil properties that vary in a linear fashion allows for, not only existing problems to be analysed but, new behaviour to be analysed. In this way one-dimensional consolidation with constant coefficient of consolidation is found to vary with the variation of permeability and compressibility within the soil (see Figure 6.4 below). This is significant for thick soil deposits with pervious top impervious bottom drainage conditions. Ratios of top permeability to bottom permeability greater than one, $k_{vT}/k_{vB} > 1$, leads to faster consolidation, and is expected in the field, and so using Terzaghi's analysis ($k_{vT}/k_{vB} = 1$) will simply underestimate the rate of consolidation (a generally safe design approach). When comparing time factors, the rate of consolidation for a thin sample such as an oedometer specimen, where

$k_{vT}/k_{vB} \approx 1$, will be different to a thicker specimen such as in the field, where $k_{vT}/k_{vB} \neq 1$.

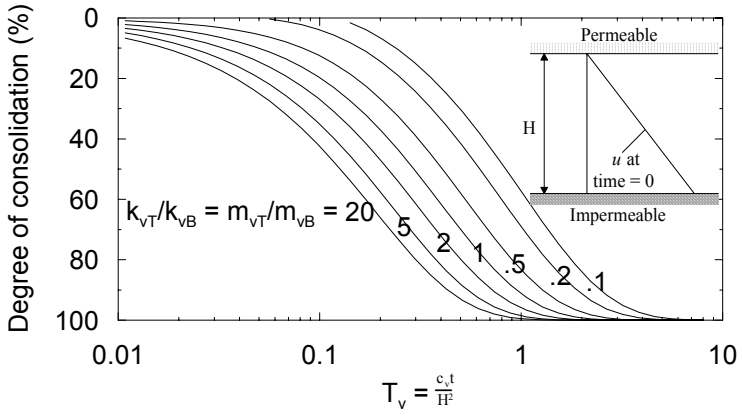

Figure 6.4 Consolidation curves for constant c_v

6.5 Recommendations for Future Research

Future work extending the work of this thesis could include the following aspects:

1. The new smear zone formulations presented in this thesis are based on laboratory evidence. There is little information available as to measured smear zones in the field. Back-calculated values of the coefficient of consolidation, c_h, based on any of the smear zone formulations may successfully model the consolidation behaviour for a particular case, but different values of c_h might be obtained for different drain spacings, indicating inadequacy in the smear zone formulations. It would be very beneficial to have a total description of smear whereby back-calculated values of c_h at different drain spacing values would reveal the same undisturbed consolidation coefficient. The complete smear zone description would have to consider the increased ultimate settlements associated with close drain spacings.

2. It is plausible that the spectral method model presented in this thesis could be improved by:
    a. Including well resistance
    b. Including electro-osmosis
    c. Explicitly modeling pore pressure boundary conditions rather than using dummy layers of high permeability to apply specified values of vacuum.
3. The nonlinear spectral method presented briefly in Appendix B should be further explored to determine the effect on consolidation of soil properties changing with time/stress etc.
4. The spectral method is a powerful method for accurate solution of linear partial differential equations and might be used in other areas of geotechnical engineering. Of immediate application is the study of one-dimensional diffusion of aqueous solutes in saturated porous media, which is directly analogous to the consolidation equations presented in this thesis (Shakelford and Lee, 2005).

7 REFERENCE LIST

Abeiera, H., N. Miura, D. Bergado and Nomura (1999). "Effects of using elecrto-conductive PVD in the consolidation of reconstituted Ariake clay." *Canadian Geotechnical Journal*, 30(2), 67-83.

Aboshi, H. and H. Monden (1963). "Determination of the horizontal coefficient of consolidation of an alluvial clay." Proc. *4th Australian-New Zealand Conference on Soil Mechanics and Foundation Engineering*,

Almeida, M.S.S. and C.A.M. Ferreira (1993). "Field in situ and laboratory consolidation parameters of a very soft clay." Proc. *Predictive Soil Mechanics, Worth Memorial Symposium*, London, 73-93.

American Society of Testing Materials (1993). *Annual Book of ASTM Standards: Soil and Rock; dimension Stone; Geosynthetics.* Philadelphia, USA, American Society of Testing and Materials.

American Society of Testing Materials (1993). *Annual book of ASTM standards: soil and rock; dimension stone; seosynthetics.* Philadelphia, USA, American Society of Testing and Materials.

Anderson, E. and et al. (1999). *LAPACK Users' Guide*. Philadelphia, Society for Industrial and Applied Mathematics.

Anderson, E.e.a. (1999). *LAPACK Users' Guide*. Philadelphia, Society for Industrial and Applied Mathematics.

Arulrajah, A., H. Nikraza and M.W. Bo (2004). "Factors affecting field instrumentation assessment of marine clay treated with prefabricated vertical drains." *Geotextiles and Geomembranes*, 22, 415-437.

Asaoka, A. (1978). "Observation procedure of settlement prediction." *Soil and Foundations, Japanese Geotechnical Society*, 18(4), 87-101.

Asmar, N.H. (2004). *Partial differential equations with fourier series and boundary value problems*. Upper Saddle River, NJ, Pearson Prentice Hall.

Athanasiu, C., A. Bye and J.A. Finstad (1999). "Design of required surcharge and time for pre-consolidation with vertical drains for ground improvement at New Bangkok International Airport." Proc. *European Conference on Soil Mechanics and Geotechnical Engineering*, 1451-1458.

Atkinson, M.S. and P.J.L. Eldred (1981). "Consolidation of soil using vertical drains." *Geotechnique*, 31(1), 33-43.

Bamunawita, C. (2004). "*Soft clay foundation improvement via prefabricated vertical drains and vacuum preloading*". PhD thesis, University of Wollongong, Wollongong, New South Wales, Australia.

Barron, R.A. (1948). "Consolidation of fine-grained soils by drain wells." *Transactions, ASCE*, 113, 718-742.

Basak, P. and M.R. Madhav (1978). "Analytical solutions of sand drain problems." *Journal of Geotechnical Engineering, ASCE*, 104(1), 129-135.

Bergado, D.T., H. Asakami, M.C. Alfaro and A.S. Balasubramaniam (1991). "Smear effects of vertical drains on soft Bangkok clay." *Journal of Geotechnical Engineering, ASCE*, 117(10), 1509-1530.

Bergado, D.T., A.S. Balasubramaniam, R.J. Fannin and R.D. Holtz (2002). "Prefabricated vertical drains (PVDs) in soft Bangkok Clay: a case study of the new Bangkok International Airport project." *Canadian Geotechnical Journal*, 39(2), 304-315.

Bergado, D.T., J.C. Chai, Miura, N. and A.S. Balasubramaniam (1998). "PVD improvement of soft Bangkok clay with combined vacuum and reduced sand embankment preloading." *Geotechnical Engineering Journal, Southeast*

Asian Geoechnical Society, 29(1), 95-122.

Bergado, D.T., R. Manivannan and A.S. Balasubramaniam (1996). "Proposed criteria for discharge capacity of prefabricated vertical drains." *Geotextiles and Geomembranes*, 14(9 Sep), 481-505.

Berry, P.L. and W.B. Wilkinson (1969). "The radial consolidation of clay soils." *Geotechnique*, 19(2), 253-284.

Bjerrum, L. (1967). "Engineering geology of Norwegian normally-consolidated marine clays as related to settlement of buildings." *Geotechnique*, 17(2), 81-118.

Bo, M.W. (2003). *Soil improvement: prefabricated vertical drain techniques*. Singapore, Thomson.

Boyd, J. (2000). *Chebyshev and Fourier spectral methods*. New York, DOVER Publications, Inc.

Britto, A.M. and M.J. Gunn (1987). *Critical state soil mechanics via finite elements*. Chichester, England, Ellis Horwood, Ltd.

Cao, L.F., M.F. Chang, C.I. Teh and Y.M. Na (2001). "Back-calculation of consolidation parameters from field measurements at a reclamation site." *Canadian Geotechnical Journal*, 38, 755-769.

Carillo, N. (1942). "Simple two and three dimensional cases in the theory of consolidation of soils." *Journal of Mathematics and Physics*, 21(1), 1-5.

Chai, J.C., J.P. Carter and S. Hayashi (2005). "Ground deformation induced by vacuum consolidation." *Journal of Geotechnical and Geoenvironmental Engineering, ASCE*, 131(12), 1552-1561.

Chai, J.C., N. Miura, S. Sakajo and D. Bergado (1995). "Behaviour of vertical drain improved subsoil under embankment loading." *Soil and Foundations,*

Japanese Geotechnical Society, 35(4), 49-61.

Chai, J.C., S.L. Shen, N. Miura and D.T. Bergado (2001). "Simple method of modeling PVD-improved subsoil." *Journal of Geotechnical and Geoenvironmental Engineering, ASCE*, 127(11), 965-972.

Chai, J.-C. and N. Miura (1999). "Investigation of factors affecting vertical drain behaviour." *Journal of Geotechnical and Geoenvironmental Engineering, ASCE*, 125(3), 216-226.

Chen, R.P., W.H. Zhou, H.Z. Wang and Y.M. Chen (2005). "One-dimensional nonlinear consolidation of multi-layered soil by differential quadrature method." *Computers and Geotechnics*, 32, 358-369.

Choa, V. (1989). "Drains and vacuum preloading pilot test." Proc. *12th International Conference on Soil Mechanics and Foundation Engineering*, Rio de Janeiro, Brazil, 1347-1350.

Christopher, B.R. and R.D. Holtz (1985). Geotextile Engineering Manual, U.S. Federal Highway Administration.

Chu, J., M.W. Bo and V. Choa (2004). "Practical considerations for using vertical drains in soil improvement projects." *Geotextiles and Geomembranes*, 22(1-2 February/April), 101-117.

Craig, R.F. (1997). *Soil Mechanics*. London, E & FN SPON.

de Jager, W.F.J. and J.P. Oostveen (1990). "Systematic quality control of vertical drains." Proc. *4th International Conference on Geotextiles, Geomembranes and Related Products*, The Hague, 321-326.

den Hoedt, G.D. (1981). "Laboratory testing vertical drains." Proc. *10th International Conference on Soil Mechanics and Foundation Engineering*, Stockholm,

Duncan, J.M. (1993). "Limitations of conventional analysis of consolidation

settlement." *Journal of Geotechnical Engineering, ASCE*, 119, 1333-1359.

Duncan, J.M. (1999). "Applying the finite element method to practical use in geotechnical engineering." *Civil Engineering Practice*, 14(2), 75-80.

Eriksson, U., S. Hansbo and B.-A. Torstensson (1999). "Soil improvement at Stockholm-Arlanda Airport." *Ground Improvement*, 4(2), 73-80.

Esrig, M.I. (1968). "Pore pressures, consolidation, and electokinetics." *Journal of Soil Mechanics and Foundations Division, Proc. ASCE*, 94(SM4), 899-921.

Fellenius, B.H., J.C. Brodhur and S. Hansbo (1981). "Discussion and Closure: Consolidation of clay by band-shaped prefabricated drains." *Ground Engineering*, 39-44.

Fellenius, B.H. and N.G. Castonguay (1985). The efficiency of band shaped drains - a full scale laboratory study, National Research Council of Canada and the Industrial Research Assistance Programme, 54.

Fox, P.J. and J.D. Berles (1997). "CS2: a piecewise-linear model for large strain consolidation." *International Journal for Numerical and Analytical Methods in Geomechanics*, 21, 435-475.

Fox, P.J., M.D. Nicola and D.W. Quigley (2003). "Piecewise-linear model for large strain radial consolidation." *Journal of Geotechnical and Geoenvironmental Engineering, ASCE*, 129(10), 940-950.

Fox, P.J. and T. Qiu (2004). "Model for large strain consolidation with compressible pore fluid." *International Journal for Numerical and Analytical Methods in Geomechanics*, 28, 1167-1188.

Graham, J. and E.C. Li (1981). "Comparison of natural and remolded plastic clay." *Journal of Geotechnical and Geoenvironmental Engineering, ASCE*, 111(7), 865-881.

Han, J. and S.L. Ye (2002). "A theoretical solution for consolidation rates of stone column-reinforced foundations accounting for smear and well resistance effects." *International Journal of Geomechanics*, 2(2), 135–151.

Hansbo, S. (1979). "Consolidation of clay by band-shaped prefabricated drains." *Ground Engineering*, 12(5), 16-25.

Hansbo, S. (1981). "Consolidation of fine-grained soils by prefabricated drains." Proc. *10th International Conference Soil Mechanics and Foundation Engineering*, Stokholm, 677-682.

Hansbo, S. (1987a). Fact and fiction in the field of vertical drainage. Prediction and performance in geotechnical engineering. C. Joshi Ramesh and J. Griffiths Fred. Rotterdam, Netherlands, A. A. Balkema**,** 61-72.

Hansbo, S. (1987b). "Design aspects of vertical drains and lime column installation." Proc. *9th Southeast Asian Geotechnical Conference*, 1-12.

Hansbo, S. (1997). "Aspects of vertical drain design: Darcian or non-Darcian flow." *Geotechnique*, 47(5), 983-992.

Hansbo, S. (2001). "Consolidation equation valid for both Darcian and non-Darcian flow." *Geotechnique*, 51(1), 51-54.

Hausmann, M.R. (1990). *Engineering principles of ground modification*. New York, McGraw-Hill.

Hawlader, B., G. Imai and B. Muhunthan (2002). "Numerical study of the factors affecting the consolidation of clay with vertical drains." *Geotextiles and Geomembranes*, 20, 213-239.

Hird, C.C. and V.J. Moseley (2000). "Model study of seepage in smear zones around vertical drains in layered soil." *Geotechnique*, 50(1), 89-97.

Hird, C.C., I.C. Pyrah and D. Russell (1992). "Finite element modeling of vertical

drains beneath embankments on soft ground." *Geotechnique*, 42(3), 499-511.

Hird, C.C. and N. Sangtian (2002). "Model study of seepage in smear zones around vertical drains in layered soil; further results." *Geotechnique*, 52(5), 375-378.

Hoffman, J.D. (1992). *Numerical methods for engineers and scientists*. New York, McGraw-Hill.

Holtz, R.D., M. Jamiolkowski, R. Lancellotta and S. Pedroni (1988). "Behaviour of bent prefabricated vertical drains." Proc. *12th International Conference Soil Mechanics and Foundation Engineering*, Rio De Janeiro, 1657-1660.

Holtz, R.D., M. Jamiolkowski, R. Lancellotta and S. Pedroni (1989). "Behaviour of bent prefabricated vertical drains. Proc." Proc. *12th International Conference on Soil Mechanics and Foundation Engineering*, Rio De Janeiro, 1657-1660.

Holtz, R.D., M. Jamiolkowski, R. Lancellotta and S. Pedroni (1991). *Prefabricated vertical drains: design and performance, CIRIA ground engineering report: ground improvement*. UK, Butterworth-Heinemann Ltd.

Hong, H.P. and J.Q. Shang (1998). "Probabilistic analysis of consolidation with prefabricated vertical drains for soil improvement." *Canadian Geotechnical Journal*, 35(4 Aug), 666-677.

Horne, M.R. (1964). "The consolidation of a stratified soil with vertical and horizontal drainage." *International Journal of Mechanics and Science*, 6, 187-197.

Indraratna, B., A.S. Balasubramaniam and S. Balachandran (1992). "Performance of test embankment constructed to failure on soft marine clay." *Journal of Geotechnical Engineering, ASCE*, 118(1), 12-33.

Indraratna, B., A.S. Balasubramaniam and N. Sivaneswaran (1997). "Analysis of settlement and lateral deformation of soft clay foundation beneath two full-

scale embankments." *International Journal for Numerical and Analytical Methods in Geomechanics*, 21(9 Sep), 599-618.

Indraratna, B., C. Bamunawita and H. Khabbaz (2004). "Numerical modeling of vacuum preloading and field applications." *Canadian Geotechnical Journal*, 41, 1098-1110.

Indraratna, B., C. Bamunawita, I.W. Redana and G. McIntosh (2002). "keynote paper: Modeling of prefabricated vertical drains in soft clay and evaluation of their effectiveness in practice." Proc. *4th International Conference on Ground Improvement Techniques*, Malaysia, 47-62.

Indraratna, B. and I.W. Redana (1995). "Large-scale, radial drainage consolidometer with central drain facility." *Australian Geomechanics*, 29, 103-105.

Indraratna, B. and I.W. Redana (1998a). "Laboratory determination of smear zone due to vertical drain installation." *Journal of Geotechnical and Geoenvironmental Engineering, ASCE*, 124(2 Feb), 180-185.

Indraratna, B. and I.W. Redana (1998b). "Development of the smear zone around vertical band drains." *Ground Improvement*, 2, 180-185.

Indraratna, B. and I.W. Redana (1999). "Closure: Plane strain modeling of smear effects associated with vertical drains." *Journal of Geotechnical Engineering, ASCE*, 123(5), 474-478.

Indraratna, B. and I.W. Redana (2000). "Numerical modeling of vertical drains with smear and well resistance installed in soft clay." *Canadian Geotechnical Journal*, 37(1), 132-145.

Indraratna, B., C. Rujikiatkamjorn and I. Sathananthan (2005a). "Radial consolidation of clay using compressibility indices and varying horizontal permeability." *Canadian Geotechnical Journal*, 42, 1330-1341.

Indraratna, B., I. Sathananthan, C. Rujikiatkamjorn and A.S. Balasubramaniam (2005b). "Analytical and numerical modeling of soft soil stabilized by prefabricated vertical drains incorporating vacuum preloading." *International Journal of Geomechanics*, 5(2), 114-124.

Jamiolkowski, M., R. Lancellotta and W. Wolski (1983). "Precompression and speeding up consolidation." Proc. *8th European Conference on Soil Mechanics and Foundation Engineering*, Helsinki, 1201-1226.

Johnson, S.J. (1970). "Precompression for improving foundation soils." *Journal of Soil Mechanics and Foundation Engineering, ASCE*, 96(SM1).

Karunaratne, G.P., H.K. Jong and S.H. Chew (2004). "New electrically conductive geosynthetics for soft clay consolidation." Proc. *GeoAsia2004 (3rd Asian Regional Conference on Geosynthetics -Now and Future of Geosynthetics in Civil Engineering)*, Seoul, Korea, 277-284.

Kjellman (1948). "Accelerating consolidation of fine grain soils by means of cardboard wicks." Proc. *2nd International Conference Soil Mechanics and Foundation Engineering*, 302-305.

Koda, E., A. Szymanski and W. Wolski (1989). "Behaviour of Geodrains in organic subsoil." Proc. *11th International Conference on Soil Mechanics and Founbdation Engineering*, Rio de Janeiro, 1377-1380.

Koerner, R.M., Ed. (1987). *Soft soil stabilization using geosynthetics*. London, Elsevier Applied Science.

Kremer, R., W. de Jager, A. Maagdenberg, I. Meyvogel and J. Oostveen (1982). "Quality standards for vertical drains." Proc. *2nd International Conference on Geotextile*, Las Vegas, 319-332.

Kremer, R., J. Oostveen, A.F. Van Weele, W. de Jager and I. Meyvogel (1983). "The

quality of vertical drainage." Proc. *8th European Conference on Soil Mechanics and Foundation Engineering*, Helsinki., 721-726.

Ladd, C.C. (1991). "Stability evaluation during staged construction." *Journal of Geotechnical Engineering*, 117(4), 540–615.

Lau, K.W.K. and J.W. Cowland (2003). "Geosynthetically enhanced embankments for the Shenzhen River." *Geotechnical Special Publication #103, ASCE*, 140-161.

Lawrence, C.A. and R.M. Koerner (1988). "Flow behaviour of kinked strip drains." *Geotechnical Special Publication #18, ASCE*, 22-39.

Lefebvre, G. and F. Burnotte (2002). "Improvements of electroosmotic consolidation of soft clays by minimizing power loss at electrodes." *Canadian Geotechnical Journal*, 39, 399-408.

Lekha, K.R., N.R. Krishnaswamy and P. Basak (1998). "Consolidation of clay by sand drain under time-dependent loading." *Journal of Geotechnical and Geoenvironmental Engineering, ASCE*, 124(1), 91-94.

Leo, C.J. (2004). "Equal strain consolidation by vertical drains." *Journal of Geotechnical and Geoenvironmental Engineering, ASCE*, 130(3), 316-327.

Li, A.L. and R.K. Rowe (2001). "Combined effects of reinforcement and prefabricated vertical drains on embankment performance." *Canadian Geotechnical Journal*, 38(6), 1266-1282.

Lo, D. (1998). "Vertical drain performance: myths and facts." *Transactions, Hong Kong Inst. Eng*, 5(1), 34-50.

Long, R.P. and A. Covo (1994). "Equivalent diameter of vertical drains with an oblong cross section." *Journal of Geotechnical Engineering, ASCE*, 120(9 Sept), 1625-1630.

Madhav, M.R., N. Miura and T. Igarashi (2002). "Development and human settlement in Saga and Shiroishi Plains by reclamation." *Lowland Technology International*, 4(1), 37-45.

Madhav, M.R., Y.-M. Park and N. Miura (1993). "Modelling and study of smear zones around band shaped drains." *Soils and Foundations*, 33(4), 135-147.

Matyas, E.L. and L. Rothenburg (1996). "Estimation of total settlement of embankments by field measurements." *Canadian Geotechnical Journal*, 33, 834-841.

Mesri, G. (1975). "New design procedure for stability of soft clays: discussion." *Journal of Geotechnical and Geoenvironmental Engineering, ASCE*, 101(4), 409-412.

Mesri, G. and Y.K. Choi (1985). "Settlement analysis of embankments on soft clays." *Journal of Geotechnical Engineering, ASCE*, 111(4), 441-464.

Mesri, G. and A. Rokhsar (1974). "Theory of consolidation for clays." *Journal of Geotechnical Engineering, ASCE*, 100(8), 889-904.

Mohamedelhassan, E. and J.Q. Shang (2002). "Vacuum and surcharge combined one-dimensional consolidation of clay soils." *Canadian Geotechnical Journal*, 39, 1126-1138.

Morris, P.H. (2005). "Analytical solutions of linear finite- and small-strain one-dimensional consolidation." *International Journal for Numerical and Analytical Methods in Geomechanics*, 29, 127-140.

Nagaraj, T.S., N.S. Pandiam and P.S.R. Narasimha Raju (1994). "Stress-statepermeability relations for overconsolidated clays." *Geotechnique*, 44(2), 349-352.

Nash, D.F.T. and S.J. Ryde (2001). "Modeling consolidation accelerated by vertical

drains in soils subject to creep." *Geotechnique*, 51(3), 257-273.

Nogami, T. and M. Li (2002). "Consolidation of system of clay and thin sand layers." *Soil and Foundations, Japanese Geotechnical Society*, 42(4), 1-11.

Nogami, T. and M. Li (2003). "Consolidation of clay with a system of vertical and horizontal drains." *Journal of Geotechnical and Geoenvironmental Engineering, ASCE*, 129(9), 838-848.

Onoue, A. (1988a). "Consolidation by vertical drains taking well resistance and smear into consideration." *Soil and Foundations, Japanese Geotechnical Society*, 28(4), 165-174.

Onoue, A. (1988b). "Consolidation of multi-layered anisotropic soils by vertical drains with well resistance." *Soil and Foundations, Japanese Geotechnical Society*, 28(3), 75-90.

Onoue, A., N.H. Ting, J.T. Germaine and R.V. Whitman (1991). "Permeability of disturbed zone around vertical drains." Proc. *ASCE Geotechnical Engineering Congress*, Colorado, 879-890.

Pradhan, T.B.S., G. Imai, T. Murata, M. Kamon and S. Suwa (1993). "Experiment study on the equivalent diameter of a prefabricated band-shaped drain." Proc. *11th Southeast Asian Geotechnical Conference*, 391-396.

Redana, I.W. (1999). "*Effectiveness of vertical drains in soft clay with special reference to smear effect*". PhD thesis, University of Wollongong, Wollongong, New South Wales, Australia.

Richart, F.E.J. (1957). "A review of the theories for sand drains." *Journal of Soil Mechanics and Foundation Engineering, ASCE*, 83(SM 3), 1301-1338.

Rixner, J.J., K. S.R. and A.D. Smith (1986). Prefabricated Vertical Drains, Vol. I, II and III: Summary of Research Report-Final Report. Washington D.C, Federal

Highway Admin.

Robinson, R. and M. Allam (1998). "Analysis of consolidation data by a non-graphical matching method." *Geotechnical Testing Journal*, 21(2), 14-143.

Rujikiatkamjorn, C. (2006). "*Analytical and numerical modeling of soft clay foundation improvement via prefabricated vertical drains and vacuum preloading*". PhD thesis, University of Wollongong, Wollongong, New South Wales, Australia.

Runesson, K., S. Hansbo and N.E. Wiberg (1985). "The efficiency of partially penetrating vertical drains." *Geotechnique*, 35(4), 511-516.

Sakai, A. (2001). "Land subscidence due to seasonal pumping of groundwater in Saga Plain, Japan." *Lowland Technology International*, 3(1), 25-40.

Sangmala, S. (1997). "*Efficiency of drainage syatems of vacuum preloading with surcharge on PVD improved soft Bangkok clay*". ME thesis, Asian Institute of Technology, Bangkok, Thailand.

Sathananthan, I. (2005a). "*Modeling of vertical drains with smear installed in soft clay*". PhD thesis, University of Wollongong, Wollongong, New South Wales, Australia.

Sathananthan, I. and B. Indraratna (2005). "Laboratory evaluation of smear zone and correlation between permeability and moisture content." *Journal ofGeotechnical and Geoenvironmental Engineering, ASCE*, (in press).

Sathananthan, I. and B. Indraratna (2005b). "Laboratory Evaluation of Smear Zone and Correlation between Permeability and Moisture Content." *Journal of Geotechnical and Geoenvironmental Engineering, ASCE*, (in press).

Saye, S.R. (2001). "Assessment of soil disturbance by the installation of displacement sand drains and prefabricated vertical drains." *Geotechnical*

Special Publication #119, ASCE, 325-362.

Schiffman, R.L. and J.R. Stein (1970). "One-dimensional consolidation of layered systems." *Journal of Soil Mechanics and Foundation Engineering, ASCE*, 96(4), 1499–504.

Shackelford, C.D. and J.-M. Lee (2005). "Analyzing diffusion by analogy with consolidation." *Journal of Geotechnical and Geoenvironmental Engineering, ASCE*, 131(11), 1345-1359.

Shang, J.Q. (1998). "Electroosmosis-enhanced preloading consolidation via vertical drains." *Canadian Geotechnical Journal*, 35(3), 491-499.

Sharma, J.S. and D. Xiao (2000). "Characterization of a smear zone around vertical drains by large-scale laboratory tests." *Canadian Geotechnical Journal*, 37(6), 1265-1271.

Shogaki, T., Moro, M. H., M., M. Kaneko, K. Kogure and T. Sudho (1995). "Effect of sample disturbance on consolidation parameters of anisotropic clays." Proc. *International Symposium on Compression and Consolidation of Clayey Soils*, Hiroshima, Japan, 561-566.

Su, J.Q. and Z. Wang (2003). "The two-dimensional consolidation theory of electro-osmosis." *Geotechnique*, 53(8), 759-763.

Tang, X.W. and K. Onitsuka (2000). "Consolidation by vertical drains under time-dependent loading." *International Journal for Numerical and Analytical Methods in Geomechanics*, 24(9), 739-751.

Tang, X.W. and K. Onitsuka (2001). "Consolidation of double-layered ground with vertical drains." *International Journal for Numerical and Analytical Methods in Geomechanics*, 25(14), 1449-1465.

Tatsuoka, F., I. M., B.H. Di and R. Kuwano (2002). "Time-dependent deformation

characteristics of geometerials and their simulation." *Soils and Foundations*, 42(2), 106-132.

Tavenas, F., P. Jean, P. Leblond and S. Leroueil (1983). "The permeability of natural soft clays; Part II, Permeability characteristics." *Canadian Geotechnical Journal*, 20(4), 645-660.

Terzaghi, K. (1943). *Theoretical Soil Mechanics*. New York, John Wiley and Sons.

The MathWorks Inc. (2003). MATLAB. Natick, Massachusetts, The MathWorks Inc.

Van Zanten, R. (1986). "The guarantee of the quality of vertical drainage systems." Proc. *3rd International Conference on Geotextiles*, Vienna, 651-655.

Vaziri, H.H. and H.A. Christian (1994). "Application of Terzaghi's consolidation theory to nearly saturated soils." *Canadian Geotechnical Journal*, 31, 311-317.

Volpi, L. (2005). MATRIX - Matrix and Linear Algebra addin for EXCEL. Piombini, Italy, Foxes Team.

Wang, X.-S. and J.J. Jiao (2004). "Analysis of soil consolidation by vertical drains with double porosity model." *International Journal for Numerical and Analytical Methods in Geomechanics*, 28, 1385-1400.

Welker, A.L., R.B. Gilbert and J.J. Bowders (2000). "Using a reduced equivalent diameter for a prefabricated vertical drain to account for smear." *Geosynthetics International*, 7(1), 47-57.

Wolfram Research Inc. (2004). Mathematica. Illinois, Wolfram Research, Inc.

Xiao, D. (2001). "*Consolidation of soft clay using vertical drains*". PhD thesis, Nanyang Technological University, Singapore.

Xie, K.H. and C.J. Leo (2004). "Analytical solutions of one-dimensional large strain

consolidation of saturated and homogeneous clays." *Computers and Geotechnics*, 31, 301-314.

Xie, K.-H., X.-Y. Xie and X. Gao (1999). "Theory of one-dimensional consolidation of two-layered soil with partially drained boundaries." *Computers and Geotechnics*, 24, 265-278.

Xie, K.-H., X.-Y. Xie and W. Jiang (2002). "A study on one-dimensional nonlinear consolidation of double-layered soil." *Computers and Geotechnics*, 29, 151-168.

Yang, L.-A., T.-S. Tan, S.-A. Tan and C.-F. Leung (2002). "One-dimensional self-weight consolidation of a lumpy clay fill." *Geotechnique*, 52(10), 713-725.

Yoshikuni, H. and H. Nakanodo (1974). "Consolidation of Fine-Grained Soils by Drain Wells with Finite Permeability." *Soil and Foundations, Japanese Geotechnical Society*, 14(2), 35-46.

Zeng, G.X. and K.H. Xie (1989). "New development of the vertical drain theories." Proc. *12th International Conference Soil Mechanics and Foundation Engineering*, 1435-1438.

Zeng, G.X., K.H. Xie and Z.Y. Shi (1987). "Consolidation analysis of sand drained ground by FEM." Proc. *8th Asian Regional Conference on SMFE*, Kyoto, 139-142.

Zhang, L. (1999). "Settlement patterns of soft soil foundations under embankments." *Canadian Geotechnical Journal*, 36, 774-781.

Zhou, W., H.P. Hong and J.Q. Shang (1999). "Probabilistic design method of prefabricated vertical drains for soil improvement." *Journal of Geotechnical and Geoenvironmental Engineering, ASCE*, 125(8), 659-664.

Zhu, G. and J.-H. Yin (1998). "Consolidation of soil under depth-dependent ramp

load." *Canadian Geotechnical Journal*, 35(2 Apr), 344-350.

Zhu, G. and J.-H. Yin (2005a). "Consolidation of a soil layer subsequent to cessation of deposition." *Canadian Geotechnical Journal*, 42, 678-682.

Zhu, G. and J.-H. Yin (2005b). "Solution charts for the consolidation of double soil layers." *Canadian Geotechnical Journal*, 42, 949-956.

Zhu, G. and J.H. Yin (2000). "Elastic visco-plastic consolidation modeling of clay foundation at Berthierville test embankment." *International Journal for Numerical and Analytical Methods in Geomechanics*, 24(5), 491-508.

Zhu, G. and J.H. Yin (2001). "Consolidation of soil with vertical and horizontal drainage under ramp load." *Geotechnique*, 51(4), 361-367.

APPENDIX A: μ PARAMETER FOR PIECEWISE CONSTANT PROPERTIES

A.1 Multi-segment Smear Zone

This Appendix develops the μ parameter for a smear zone consisting of multiple segments each of which has different but constant soil properties. The resulting equation can be used to model smear zones with arbitrary soil property distributions in the radial direction. Hansbo's (1981) μ parameters for an ideal drain and a single smear zone of constant permeability are found to be special cases of the more general multi-segment approach described below.

The steps followed to determine μ are those in Chapter 3.

STEP 1:

Any radial distribution of permeability and volume compressibility can be approximated by dividing the soil into m segments as in Figure A.1. m_v and k_h are constant within each segment. To enable the use of index notation the inner radius r_w and outer radius r_e have been replaced with r_0 and r_m respectively.

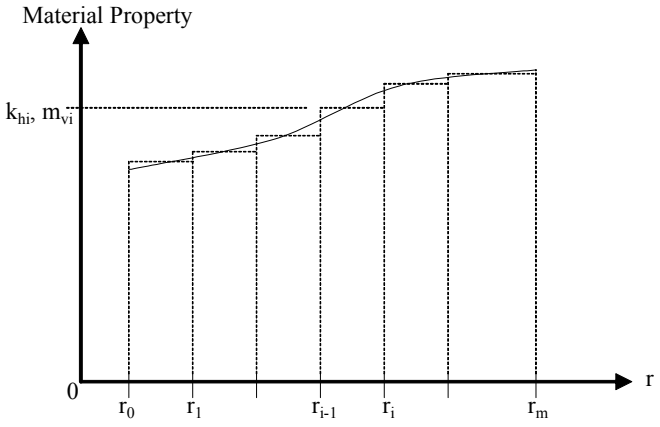

Figure A.1 Discretised radial properties

STEP 2:

The pore pressure gradient in the i^{th} segment is:

$$\frac{\partial u_i}{\partial r} = \frac{\gamma_w r_m^2}{2\bar{k}_h}\frac{\partial \varepsilon}{\partial t}\kappa_i\left[\frac{1}{r} - \frac{r}{n^2 r_0^2}\right] \tag{A.1a}$$

where,

$$\kappa_i = \frac{\bar{k}_h}{k_{hi}} \tag{A.1b}$$

$$n = \frac{r_m}{r_0} \tag{A.1c}$$

The permeability ratio, κ_i, is calculated with respect to a convenient reference value, $\bar{k}_h$ (usually that of the undisturbed soil).

STEP 3:

The pore water pressure in the drain is the same as those in Chapter 3.

STEP 4:

Using the boundary conditions $u(r_0) = w$ and $u_i(r_i) = u_{i+1}(r_i)$, equation (A.1) is integrated in the r direction for each segment to give the pore pressure in the i^{th} segment:

$$u_i = -\frac{r_m^2}{2c_h}\frac{\partial \bar{u}}{\partial t}\left[\begin{array}{l}\kappa_i\left(\ln\left(\frac{r}{r_{i-1}}\right) - \frac{1}{2}\left(\frac{r^2}{n^2 r_0^2} - \frac{s_{i-1}^2}{n^2}\right) + \psi_i\right) \\ \frac{k_{hi}}{q_w}\pi z(2l - z)\left(1 - \frac{1}{n^2}\right)\end{array}\right] \tag{A.2a}$$

where,

$$s_i = \frac{r_i}{r_0} \tag{A.2b}$$

and,
$$\psi_i = \frac{1}{\kappa_i}\sum_{j=1}^{i-1}\kappa_j\left[\ln\left(\frac{s_j}{s_{j-1}}\right)-\frac{1}{2}\left(\frac{s_j^2}{n^2}-\frac{s_{j-1}^2}{n^2}\right)\right] \tag{A.2c}$$

STEP 5:

By calculating the average pore water pressure the μ parameter is revealed as:

$$\mu = \frac{n^2}{n^2-1}\sum_{i=1}^{m}\kappa_i\left[\begin{array}{l}\dfrac{s_i^2}{n^2}\ln\left(\dfrac{s_i}{s_{i-1}}\right)-\dfrac{1}{2}\left(\dfrac{s_i^2}{n^2}-\dfrac{s_{i-1}^2}{n^2}\right)\\ -\dfrac{\left(s_i^2-s_{i-1}^2\right)^2}{4n^4}+\psi_i\left(\dfrac{s_i^2}{n^2}-\dfrac{s_{i-1}^2}{n^2}\right)\end{array}\right] \tag{A.3}$$

The well resistance parameter μ_w is the same as in Chapter 3.

STEP 6:

The compressibility parameter μ_{m_v} in is given by:

$$\mu_{m_v} = \frac{n^2}{n^2-1}\sum_{i=1}^{m}\frac{1}{\eta_i}\frac{s_i^2-s_{i-1}^2}{n^2} \tag{A.4a}$$

where,

$$\eta_i = \frac{\overline{m}_v}{m_{vi}} \tag{A.4b}$$

A.2 Ideal Drain (No Smear)

STEP 1:

Hansbo's (1981) formulation for an ideal drain is a special case of the multiple segment solution presented in section A.1. For an ideal drain $m=1$, $\kappa_1=1$, $\eta_1=1$, $s_1=n$ and $s_0=1$.

STEP 2:

The pore water pressure gradient in the radial direction is:

$$\frac{\partial u}{\partial r} = \frac{\gamma_w r_m^2}{2k_h}\frac{\partial \varepsilon}{\partial t}\left(\frac{1}{r} - \frac{r}{n^2 r_w^2}\right) \tag{A.5}$$

STEP 3:

The pore water pressure in the drain is the same as in Chapter 3.

STEP 4:

The pore water pressure in the soil is:

$$u = \frac{\gamma_w r_m^2}{2k_h}\frac{\partial \varepsilon}{\partial t}\left[\ln\left(\frac{r}{r_w}\right) - \frac{1}{2}\left(\frac{r^2}{n^2 r_w^2} - \frac{1}{n^2}\right) + \frac{k_h}{q_w}\pi z(2l - z)\left(1 - \frac{1}{n^2}\right)\right] \tag{A.6}$$

STEP 5:

The μ parameter is given by:

$$\mu = \frac{n^2}{n^2 - 1}\left[\ln(n) - \frac{3}{4} + \frac{1}{n^2} - \frac{1}{4n^4}\right] \tag{A.7a}$$

Because n^2 is usually much greater than unity the terms in equation (A.7a) with high powers of n in the denominator are insignificant and can be ignored. The resulting simplified expression for μ is

$$\mu = \ln(n) - \frac{3}{4} \tag{A.7b}$$

STEP 6:

The μ_{m_v} parameter is unity.

A.3 Smear Zone with Constant Reduced Permeability

STEP 1:

Hansbo's (1981) formulation for a smear zone with constant reduced permeability and an undisturbed zone is a special case of the multiple segment solution presented in section A.1. For a single smear zone $m = 2$, $\kappa_1 = k_h / k_h' = \kappa$, $\kappa_2 = 1$, $\eta_1 = \eta_2 = 1$, $s_0 = 1$, $s_1 = r_s / r_w = s$ and $s_2 = r_e / r_w = n$. The formulation given by Hansbo (1981) is altered slightly to include the case where the smear zone compressibility is different to the undisturbed compressibility ($\eta_1 = m_v / m_v' = \eta$ and $\eta_2 = 1$).

STEP 2:

The pore water pressure gradient in smear and undisturbed zones are, respectively,

$$\frac{\partial u_s}{\partial r} = \frac{\gamma_w r_m^2}{2k_h} \frac{\partial \varepsilon}{\partial t} \kappa \left(\frac{1}{r} - \frac{r}{n^2 r_w^2} \right) \tag{A.8a}$$

and

$$\frac{\partial u}{\partial r} = \frac{\gamma_w r_m^2}{2k_h} \frac{\partial \varepsilon}{\partial t} \left(\frac{1}{r} - \frac{r}{n^2 r_w^2} \right) \tag{A.8b}$$

STEP 3:

The pore water pressure in the drain is the same as Chapter 3.

STEP 4:

The pore water pressure in the smear and undisturbed zones are, respectively,:

$$u_s = \frac{\gamma_w r_m^2}{2k_h} \frac{\partial \varepsilon}{\partial t} \left[\kappa \left(\ln\left(\frac{r}{r_w} \right) - \frac{1}{2} \left(\frac{r^2}{n^2 r_w^2} - \frac{1}{n^2} \right) \right) + \frac{k_h'}{q_w} \pi z (2l - z) \left(1 - \frac{1}{n^2} \right) \right] \tag{A.9a}$$

and, $$u = \frac{\gamma_w r_m^2}{2k_h}\frac{\partial \varepsilon}{\partial t}\left[\begin{array}{l}\ln\left(\frac{r}{sr_w}\right) - \frac{1}{2}\left(\frac{r^2}{n^2 r_w^2} - \frac{s^2}{n^2}\right) + \kappa\left(\ln(s) - \frac{1}{2}\left(\frac{s^2}{n^2} - \frac{1}{n^2}\right)\right) \\ + \frac{k_h}{q_w}\pi z(2l - z)\left(1 - \frac{1}{n^2}\right)\end{array}\right] \quad \text{(A.9b)}$$

STEP 5:

The μ parameter is given by:

$$\begin{array}{l}\mu_s = \frac{n^2}{n^2-1}\left(\ln\frac{n}{s} + \kappa \ln s - \frac{3}{4}\right) + \frac{s^2}{n^2-1}\left(1 - \frac{s^2}{4n^2}\right) + \\ + \frac{\kappa}{n^2-1}\left(\frac{s^4-1}{4n^2} - s^2 + 1\right)\end{array} \quad \text{(A.10a)}$$

Ignoring insignificant terms equation (A.10a) reduces to:

$$\mu_s = \ln\frac{n}{s} - \frac{3}{4} + \kappa \ln s \quad \text{(A.10b)}$$

STEP 6:

The μ_{m_v} parameter from is given by:

$$\mu_{m_v} = 1 + \left(\frac{1-\eta}{\eta}\right)\frac{(s-1)(s+1)}{\left(n^2-1\right)} \quad \text{(A.11)}$$

APPENDIX B: Nonlinear Spectral Method

B.1 General

In Chapter 3, using the spectral method, a technique for determining the pore pressure response before and after the installation of vertical drains was developed. The material parameters are updated at the time of drain installation to allow horizontal drainage. The process of updating the material properties at a certain time can be used to perform a piecewise nonlinear analysis. By dividing the consolidation process into a discrete number of time steps, material properties, though constant during any particular time interval, can be varied across the time steps. This Appendix briefly explores some of the possibilities of employing this method. The technique is first verified against the analytical nonlinear radial consolidation model presented in Chapter 3. The vertical consolidation behaviour of normally consolidated clay and cyclic loading is then considered.

B.2 Constitutive Model

While the time stepping process allows for any relationship between soil properties and effective stress, the constitutive model chosen here (for ease of implementation) is the same as used elsewhere in this thesis; namely the semi-log void ratio stress relationships governed by the compression index C_c and recompression index C_r. The equations for void ratio-stress/permeability given in Chapter 3 are modified to include an evolving maximum effective stress ($\sigma'_{\max}$), thus allowing unloading/cyclic loading to be analysed.

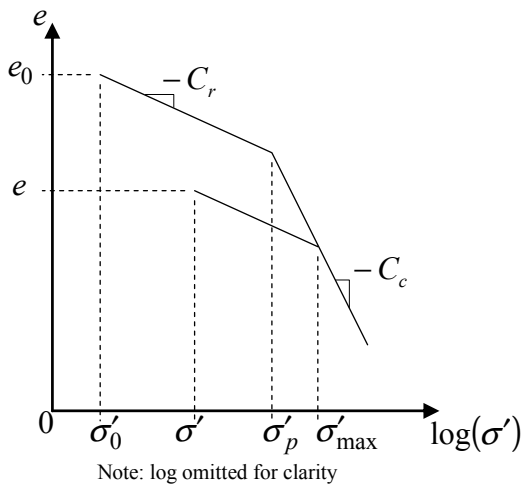

Figure B.1 Void ratio-stress relationship for evolving maximum effective stress

With reference to Figure B.1 the void ratio e for two cases must be considered. The recompression zone is defined by $\sigma' < \sigma'_{\max}$ where initially $\sigma'_{\max} = \sigma'_p$. The compression zone occurs when $\sigma' \geq \sigma'_{\max}$. The void ratio in the recompression and compression zones are given respectively by:

$$e = e_0 + (C_c - C_r)\log(\sigma'_{\max}/\sigma'_p) - C_r \log(\sigma'/\sigma'_0) \tag{B.12a}$$

and,

$$e = e_0 + (C_c - C_r)\log(\sigma'_{\max}/\sigma'_0) - C_c \log(\sigma'/\sigma'_0) \tag{B.12b}$$

Once the maximum effective stress is exceeded $\sigma'_{\max}$ is updated to reflect the new maximum stress.

The change in volume compressibility, relative to initial values, before and after $\sigma'_{\max}$ is exceeded, is now given respectively by:

$$\frac{m_{v0}}{m_v} = \left(\frac{\sigma'}{\sigma'_0}\right) \tag{B.13a}$$

and,
$$\frac{m_{v0}}{m_v} = \frac{C_r}{C_c}\left(\frac{\sigma'}{\sigma'_0}\right) \tag{B.13b}$$

The relative change in permeability is given by:

$$\frac{k}{k_0} = \left(\frac{\sigma'_p}{\sigma'_{\max}}\right)^{(C_c - C_r)/C_k}\left(\frac{\sigma'}{\sigma'_0}\right)^{-C_r/C_k} \tag{B.14a}$$

$$\frac{k}{k_0} = \left(\frac{\sigma'_p}{\sigma'_0}\right)^{(C_c - C_r)/C_k}\left(\frac{\sigma'}{\sigma'_0}\right)^{-C_c/C_k} \tag{B.14b}$$

The material input parameters for the spectral method as described in Chapter 3 are given relative to a convenient reference value. That is $k_v/\bar{k}_v$, $m_v/\overline{m}_v$ and $\eta/\overline{\eta}$. If the initial input parameters are given as $k_{v0}/\bar{k}_v$, $m_{v0}/\overline{m}_v$ and $\eta_0/\overline{\eta}$ then the input parameters can easily be updated during the analysis by multiplying by equation (B.13) and (B.14). Thus the updated input parameters for each time step are given by:

$$\frac{k_v}{\bar{k}_v} = \frac{k_{v0}}{\bar{k}_v}\frac{k}{\bar{k}_0} \tag{B.15a}$$

$$\frac{m_v}{\overline{m}_v} = \frac{m_{v0}}{\overline{m}_v}\frac{m_v}{m_{v0}} \tag{B.15b}$$

$$\frac{\eta}{\overline{\eta}} = \frac{\eta_0}{\overline{\eta}}\frac{k}{\bar{k}_0} \tag{B.15c}$$

Settlement calculations can be performed with reference to equation (B.12). The settlement during recompression and compression are given by:

$$\rho = \frac{H}{1+e_0}\left((C_c - C_r)\log\left(\sigma'_{\max}/\sigma'_p\right) - C_r\log\left(\sigma'/\sigma'_0\right)\right) \tag{B.16a}$$

$$\rho = \frac{H}{1+e_0}\left((C_c - C_r)\log(\sigma'_{\max}/\sigma'_0) - C_c \log(\sigma'/\sigma'_0)\right) \qquad \text{(B.16b)}$$

It should be noted that in deriving equations (B.13) and (B.16) the specific volume of the soil, $1+e_0$, was assumed constant. Thus the above equations are only suitable for small strain.

B.3 Initial Effective Stress Distribution

For consolidation problems where the initial stress and void ratio profiles with depth are not known, they must be approximated for input into the model. For an idealized soil the initial void ratio and stress distributions should be consistent with the constitutive model described in equation (B.12). for determining the initial stress profile the parameters in equation (B.12) take on new meaning: $\sigma'_0 = \sigma'_{00}$ = effective stress at the soil surface; $\sigma'_p = \sigma'_{0p}$ = preconsolidation stress at the surface; $\sigma' = \sigma'_{0z}$ = effective stress at depth z; $\sigma'_{\max} = \sigma'_{zp}$ = preconsolidation stress at depth z; $e_0 = e_{00}$ = initial void ratio at the surface; $e = e_{0z}$ = initial void ratio at depth z. Assuming fully saturated soil, the initial effective stress distribution is found using the differential form of static effective stress given by:

$$\frac{\partial \sigma'_{0z}}{\partial z} = \frac{(G_s - 1)}{1+e_{0z}}\gamma_w \qquad \text{(B.17)}$$

where, G_s = specific gravity of soil solids. Knowing the distribution of preconsolidation stress with depth, equation (B.12) is substituted into equation (B.17). The resulting equation is numerically integrated to give the initial effective stress profile in the overconsolidated zone. The integration is continued in the z direction until the soil becomes normally consolidated. This depth is z_n and the

corresponding stress and void ratio at $z = z_n$ are σ'_{0n} and e_{0n}. In the normally consolidated zone, equation (B.17) can be solved and the effective stress is found to satisfy the following relationship:

$$\sigma'_{0z} = \sigma'_{0n} + \frac{(G_s - 1)}{1 + e_{0n}} \gamma_w (z - z_n) + \frac{C_c}{1 + e_{0n}} \left[\sigma'_{0z} \left(\log\left(\frac{\sigma'_{0z}}{\sigma'_{0n}} \right) - 0.434 \right) + 0.434 \sigma'_{0n} \right] \quad \text{(B.18)}$$

Thus, if the initial void ratio and initial effective stress at the top of the soil layer are known, along with the preconsolidation pressure profile, then the initial effective stress and void ratio profiles can readily be determined from equations (B.12), (B.17) and (B.18).

B.4 Verification

To verify the nonlinear approach an analysis is performed and compared with the analytical solution for nonlinear radial consolidation presented in Chapter 3 (using Darcian flow). An idealized soil is subject to radial drainage only. The material properties are given in Table B.1. For the purpose of analysis the depth of soil was considered to be 41/20 m deep and 20 series terms were used. The pore pressure and settlement of a 1 m segment was determined between the normalized depths of 20/41 and 40/41. The fractional depth values were chosen to minimize the errors associated with the spectral method (see Chapter 3) when considering radial drainage alone. Figure B.2 shows the pore pressure and settlement plots for the two analysis methods. The difference between the analytical solution and the nonlinear spectral method are very small, demonstrating the efficacy of the nonlinear spectral method.

Table B.1 Parameters for verification example

Parameter	C_c	C_r	C_k	σ'_0 (kPa)	σ'_p (kPa)	e_0	H (m)
Value	0.7	0.175	0.875	10	10,20,30	1	1

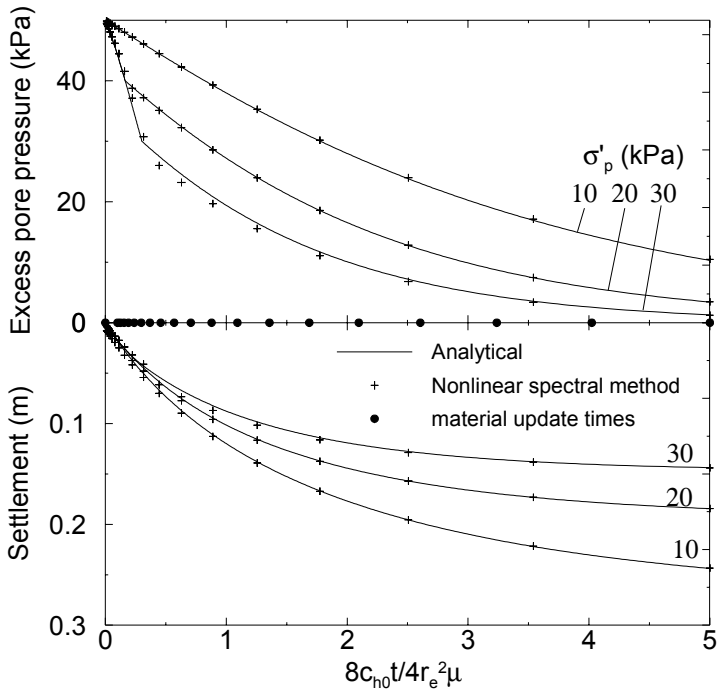

Figure B.2 Verification of nonlinear spectral method

B.5 Vertical Consolidation of Normally Consolidated Soil

With the nonlinear spectral method it is possible to study consolidation that deviates from Terzaghi's one-dimensional assumptions. Consider a normally consolidated clay subject to vertical drainage alone. Initial stress and void ratio distributions are described by Equation (B.18). Initial permeability distribution is described by Equation (B.14). Initial virgin compressibility distribution is then given by:

$$m_{v0} = \frac{0.434 C_c}{(1+e_0)\sigma'} \tag{B.19}$$

Using the properties given in Table B.2 as a base, a rudimentary parametric study is conducted to assess the effect of changing: drainage condition (pervious/impervious bottom); C_c/C_k ; soil depth; surface effective stress; void ratio; applied stress. Consolidation curves are presented in Figures B.3 to B.5. Note that the time factor T_v is calculated from initial stress at top of soil layer.

Table B.2 Default parameters for normally consolidated vertical consolidation parametric study

Parameter	C_k	σ'_{00} (kPa)	e_{00}	γ_w (kN/m^3)	G_s
Value	0.4	10	2	10	2.73

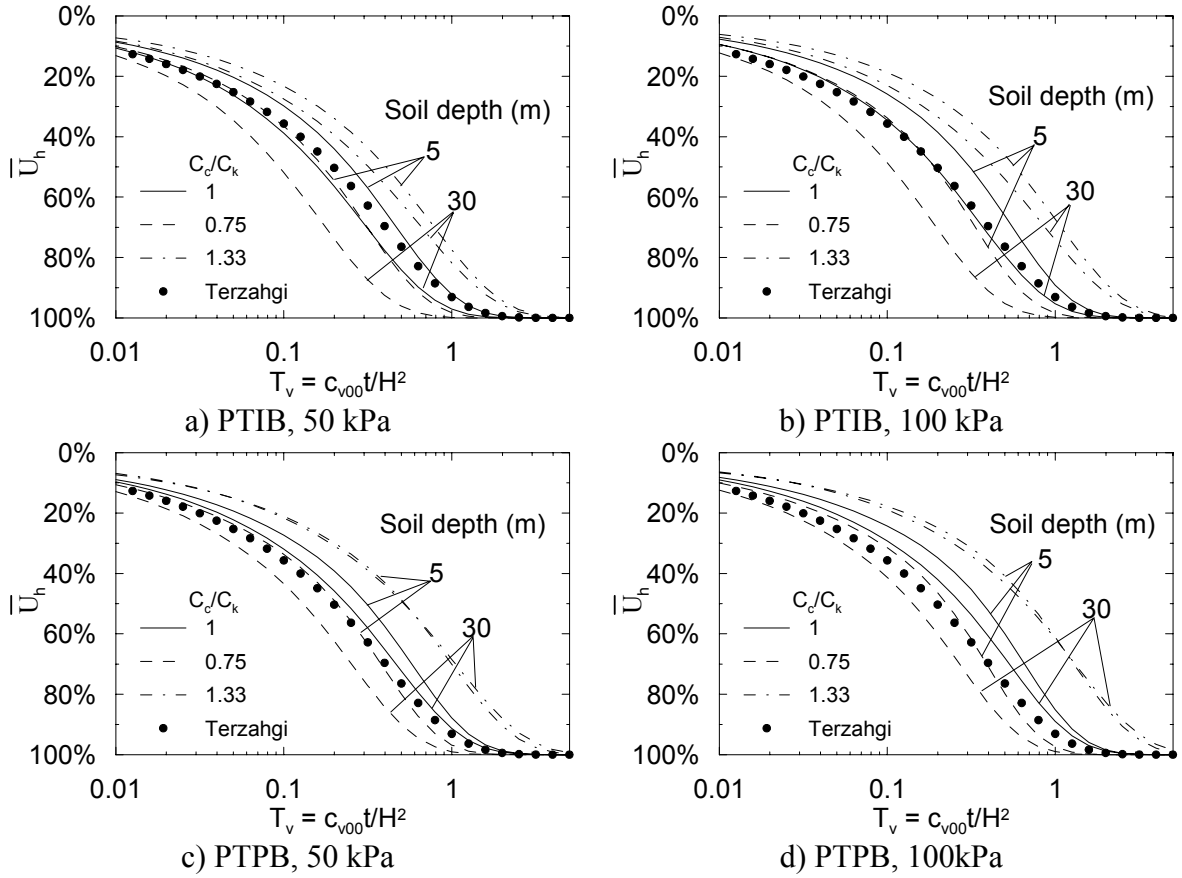

Figure B.3 Effect of varying soil depth

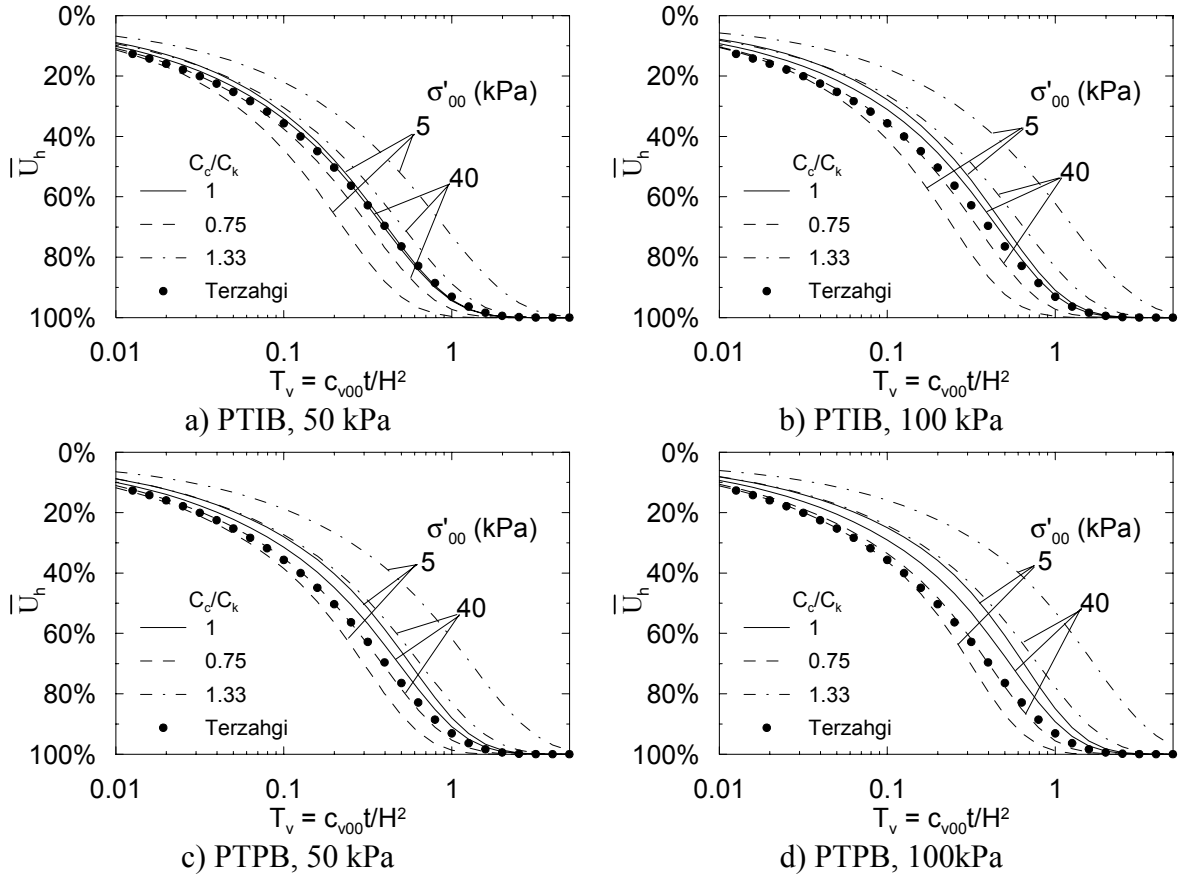

a) PTIB, 50 kPa b) PTIB, 100 kPa

c) PTPB, 50 kPa d) PTPB, 100kPa

Figure B.4 Effect of varying initial surface stress

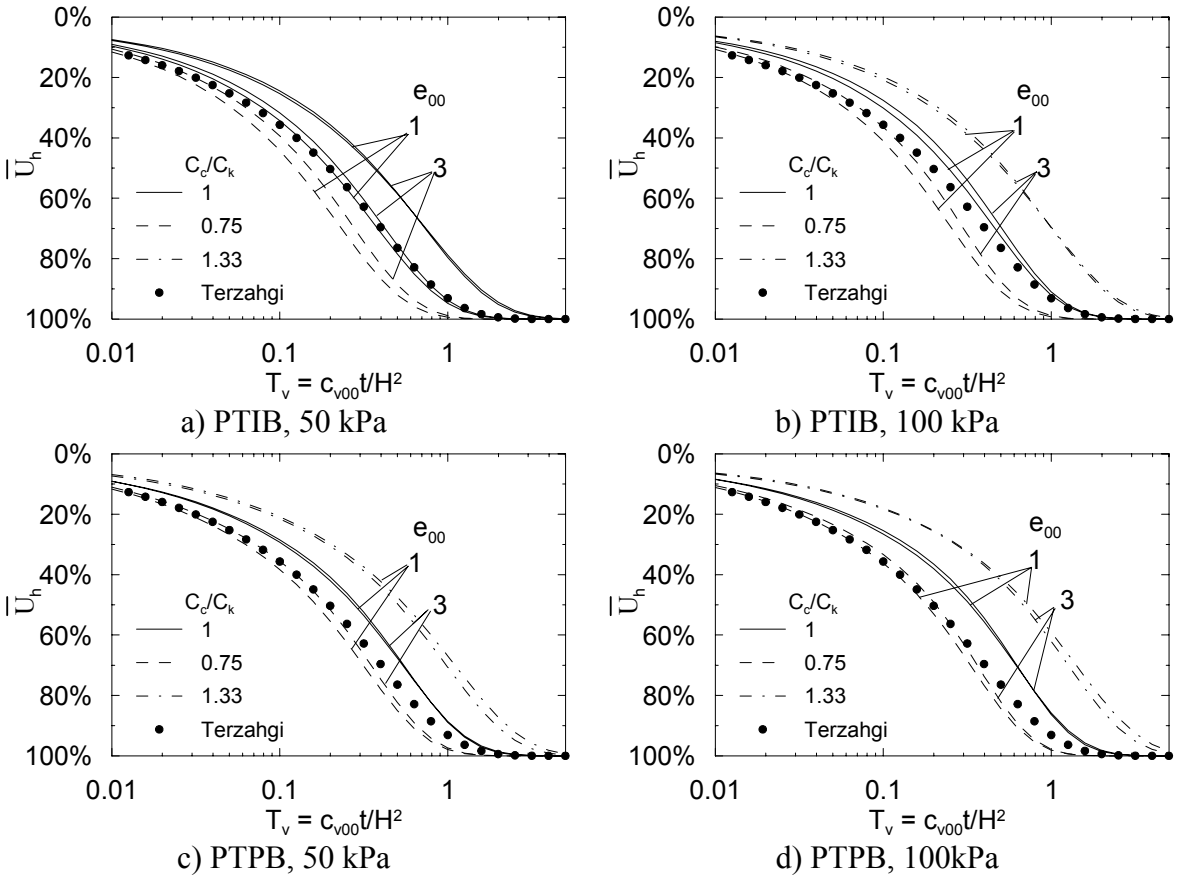

Figure B.5 Effect of varying initial surface void ratio

Figures B.3 to B.5 show that the most important parameter in producing deviation form Terzaghi's one-dimensional consolidation is the ratio of compression index to permeability change index, C_c/C_k. For $C_c/C_k < 1$ consolidation is usually faster. In Chapter 3, the nonlinear radial consolidation model reduced to Hansbo's (1981) solution when $C_c/C_k = 1$ (decrease in permeability is the same as decrease in compressibility). In the same manner it may be expected that if $C_c/C_k = 1$ in the current one-dimensional analysis then Terzaghi's solution would be obtained. This is not the case due to the rapid decrease in permeability close to the drainage boundary. All pore water has to travel through this zone of reduced permeability and hence, for $C_c/C_k = 1$ conditions consolidation may be slower than that predicted by

Terzaghi theory. The effects caused by changes in C_c/C_k are less pronounced for two-way drainage than for one-way drainage.

Other deviations from Terzaghi's consolidation curves are related to the stress range experienced by the soil. The large changes in permeability and compressibility will occur from a low starting value of effective stress. Thus shallow soil layers with low overburden exhibit the greatest differences when compared to Terzaghi consolidation. While the above conclusions provide some guidelines for consolidation analysis, given the large number of parameters involved, it would be prudent to perform calculations for particular cases encountered in design.

B.6 Cyclic Loading

A load that varies linearly with depth and cyclically with time can be described by the sinusoidal loading function given by:

$$\sigma = \left(A_l + \frac{Z - Z_l}{\Delta Z}\left(A_{l+1} - A_l\right)\right)\sin\left(\omega t + \varphi\right) \tag{B.20}$$

where, A_l = amplitude at depth Z_l, ω = angular frequency and φ = phase. The angular frequency is related to the natural frequency f, and wave period P by the relationship:

$$\omega = 2\pi f = \frac{2\pi}{P} \tag{B.21}$$

By substituting equation (B.20) into the spectral equations from Chapter 3 the average pore pressure under surcharge, vacuum and cyclic loading is given by:

$$\bar{u}\left(Z,t\right) = \mathbf{\Phi v}\left(\boldsymbol{\sigma} + \mathbf{w} + \boldsymbol{\Omega} + \boldsymbol{\Theta}\right) \tag{B.22}$$

For the m^{th} cyclic load, the i^{th} element of the cyclic loading vector ($\boldsymbol{\Theta}$) is described as:

$$\boldsymbol{\Theta}_i = \frac{\omega_m \Lambda_{3,m,i}}{\lambda_i^2 + \omega_m^2} \sum_{j=1}^{N} (\boldsymbol{\Gamma}\mathbf{v})_{ij}^{-1} \left(\sum_{l=1}^{\#l} \Xi_j \left(A_{m,l}, \Delta A_m, m_v \right) \right) \tag{B.23}$$

Equation (B.23) is very similar in for to the expressions for $\boldsymbol{\sigma}$ and $\mathbf{w}$ given in the last chapter. The Λ term in equation (B.23) is given by:

$$\begin{aligned} \Lambda_{3,m,i} = {} & \lambda_i \cos(\omega_m t + \varphi_m) + \omega_m \sin(\omega_m t + \varphi_m) \\ & - \exp\left[-(t - t_\Omega)\lambda_i \right] \left(\lambda_i \cos(\omega_m t_\Omega + \varphi_m) + \omega_m \sin(\omega_m t_\Omega + \varphi_m) \right) \end{aligned} \tag{B.24}$$

B.6.1 Illustrative Example

Using the cyclic loading terms given above a nonlinear analysis may be conducted. A normally consolidated soil with properties given in Table B.3 and property distributions described in Section B.2 is subjected to cyclic loading. Four cases are considered:

- With and without ideal vertical drains ($r_e = 1.5$, $n = 30$, $\mu =$) under a cyclic load constant with depth, with amplitude = 10kPa $P = 0.2 dT_{v00}$, $\varphi = -\pi/2$, plus 10 kPa constant surcharge
- With and without drains under constant surcharge of 20 kPa.

Settlement plots for each case are shown in Figure B.6, illustrating that vertical drains accelerate the dissipation of pore water pressure and hence, increase the rate of settlement. The elastic rebound that occurs during each cyclic load shows that the nonlinear spectral method proposed here is sensitive enough to study such problems. Consideration of cyclic loading is important for applications such as railway tracks

constructed over soft ground. Vertical drains increase dissipation of pore pressure thus reducing lateral spreading caused during the undrained loading.

Table B.3 Soil properties for cyclic loading example

Parameter	C_c	C_r	C_k	σ'_{00} (kPa)	e_{00}	γ_w (kN/m^3)	G_s
Value	0.3	0.05	0.4	30	2	10	2.7

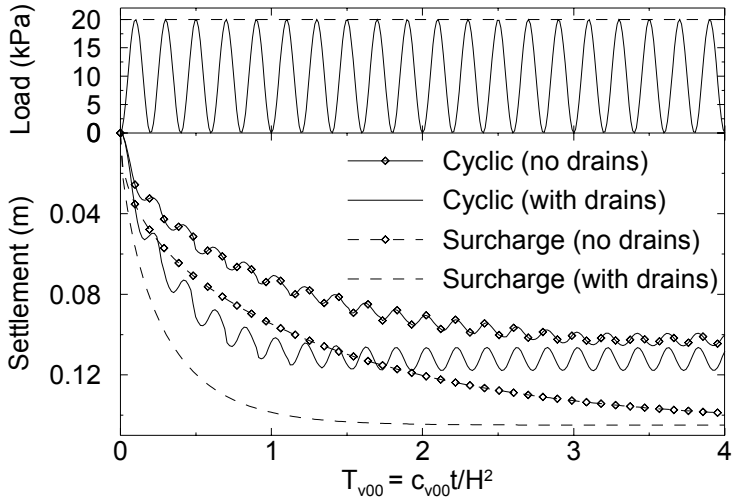

Figure B.6 Settlement under cyclic loading